PREPRINTS

FOURTH INTERNATIONAL MEETING ON STATISTICAL CLIMATOLOGY

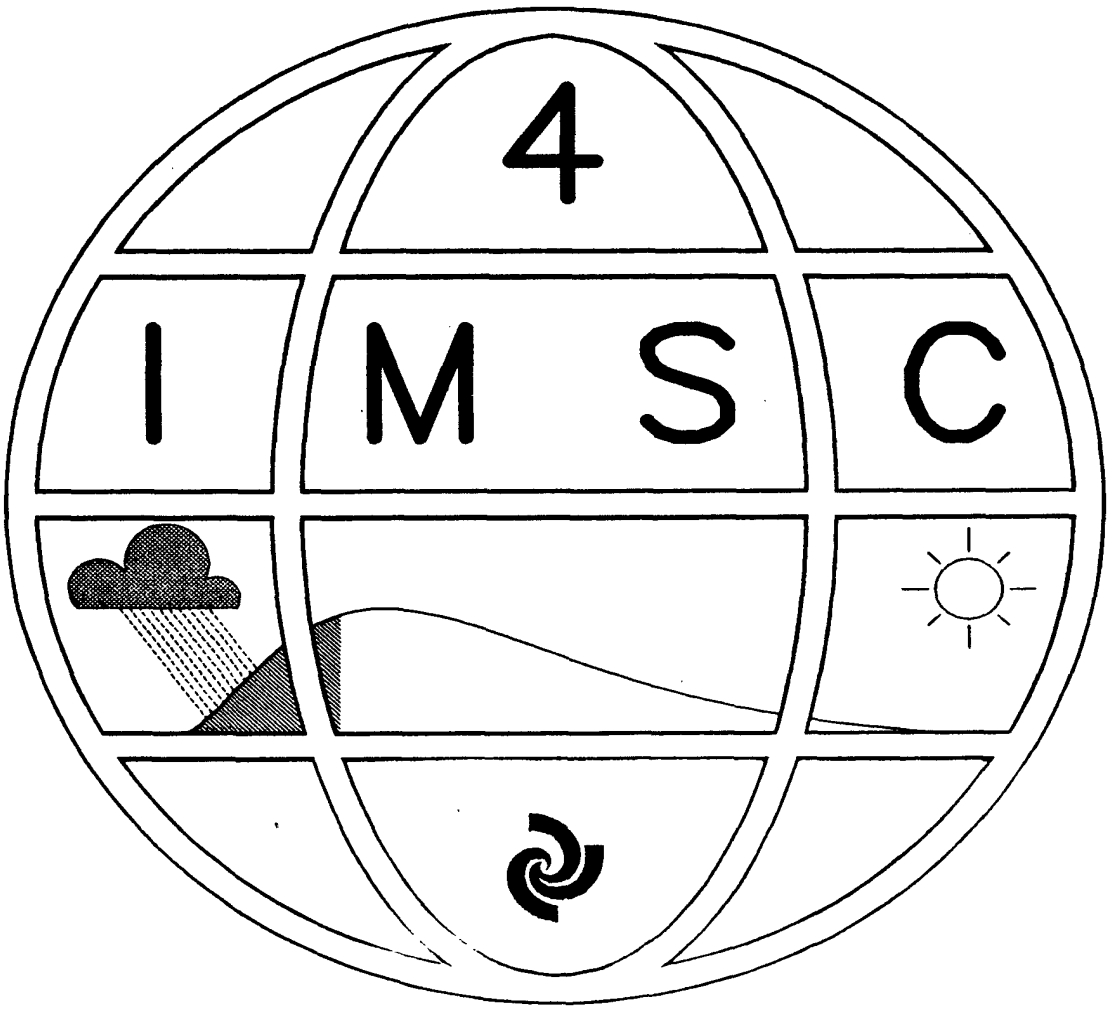

27 – 31 MARCH, 1989

ROTORUA, NEW ZEALAND

Daily Programme

March		Morning	Afternoon	Evening
Sunday	26		Registration	Icebreaker/Social 5.50 for 6pm Sponsored by Stats Assn & Met Soc Welcome by Mayor of Rotorua
Monday	27	Session 1	Session 2	Maori Welcome and Hangi at THC International
Tuesday	28	Session 3	Session 4	4IMSC Dinner 7-9pm Guest Speaker Prof Whittle
Wednesday	29	Session 5	Local tours (Lake Taupo/Kiwifruit coast etc)	own arrangements
Thursday	30	Session 6	Session 7 Luncheon meeting for Steering/Organizing Committees	Thawstopper!
Friday	31	Session 8 and closure midday Farewell luncheon? Begin short tour south to Wellington		

4IMSC Session Programme: Priority will be given to papers read by authors

0845 Opening:Mr J.S. Hickman, Past-Pres. WMO RAV

Monday am

Chair: *Alastair J. Scott*

0855-0930 D. Vere-Jones
Quality control of precipitation measurements
0930-0950 H. Madsen
Accuracy of 'now-cast' winds
0950-1010 S.J. Reid
Statistical analysis of turbulence
0110-1030 J. Urbančič

- *morning break*

Chair: *James McGregor*

Homogeneity of a long series of observations
1100-1120 R. Sneyers
Inhomogeneities in precipitation time series
1120-1140 B. Sevruk
Marine stratocumulus spatial structure
1140-1200 R.F. Cahalan
Modelling ocean whitecap coverage
1200-1220 I.G. O'Muircheartaigh
Detection of the CO_2 effect
(poster) A.J. Coops

Monday pm

Chair: *Peter J. Lamb*

POP analysis of Rossby waves
1330-1355 H. von Storch
Procrustes target analysis
1355-1420 M.B. Richman
Analysis of pentad precipitation vibration
1420-1445 Y-F. Liu
Whither 5IMSC?
1445-1500 A.H. Murphy

- *afternoon break*

Chair: *John W. Kidson*

Models for cloud-free viewing climatologies
1530-1550 D.G. Grantham
Satellite-derived cloud climatology
1550-1610 A.J. Gorman
Distribution of solar radiation from cloud fields
1610-1630 P.K. Love
Wave cloud climatology from AVHRR data
1630-1650 J. McGregor
Sampling errors in satellite rainfall climatology
1650-1710 T.L. Bell
Variations of rainfall and OLR over India
1710-1730 R.H. Kripalani

1830 Hangi & Concert THC

Tuesday am

Chair: *Kevin E. Trenberth*

Critical review of two decades of teleconnection studies
0830-0910 R.E. Livezey
Search for teleconnections
0910-0930 B.G. Brown
Solar-atmospheric relationships
0930-0950 D.J. Shea
Teleconnection between Arctic ice and 500 hPa gph
0950-1010 Z-F. Fang

- *morning break*

Chair: *Neil D. Gordon*

ENSO and rainfall variability
1030-1050 N. Nicholls
Prediction of SO extremes with POP
1050-1110 J-S. Xu
Spectrum of univariate time series
1110-1130 P-S. Chu
Non-linear time series models of ENSO indicies
1130-1150 F.W. Zwiers
Assessments of the anthropogenic greenhouse effect
1150-1210 C-D. Schönwiese
Current climate lead to global change
1210-1230 F. Kogan

Tuesday pm

Chair: *Peter J. Thomson*

Detecting shifts trends and periodicities
1330-1410 C.F. Ansley
Detecting periodicities obscured by noise
1410-1430 F.M. Fujioka
Temperature trends at the South Pole
1430-1450 K.E. Trenberth
Location of linear trends in climatic data
1450-1510 V.T. Radionhin

- *afternoon break*

Chair: ??

Early instrumental climate data for the S Hemisphere
1530-1610 P.D. Jones
Wind rose similarity after 140 years
1610-1630 A. Court
Quality/value relationships for climate forecasts
1630-1650 A.H. Murphy
Valuing climate forecast information
1650-1710 S.T. Sonka
Economic decisions on climatically variable areas
1710-1730 E.E. Zhukovsky

1900 4IMSC Dinner:Professor Peter Whittle

Wednesday am

Chair: *Oskar Essenwanger*

Estimating dimension and predictability
0850-0930 K. Fraedrich

Climate prediction via a diffusion model
0930-0955 S.W. Goulter

Multiple recurrence analysis
0955-1020 F.W. Zwiers

• *morning break*

Chair: *Neville Nicholls*

Prediction of mean monthly temperature
1040-1100 T. Ueno

Forecasting seasonal monsoon rainfall
1100-1120 S.V. Singh

Effects of missing data on circulation statistics
1120-1140 K.E. Trenberth

Deterministic chaos model
1140-1200 A.M. Selvam

Thursday am

Chair: *Francis W. Zwiers*

Cluster analysis of climate variables
0830-0855 K. Wolter

Cluster analysis to identify persistent states
0855-0920 J.W. Kidson

Nearest neighbour analysis of tornadoes
0920-0945 K.K. Leiker

Analysis of species distributions wrt climate
0945-1010 N.D. Mitchell

Climatic stability in zones of Karnataka
(reserve) B.P. Ratnam

• *morning break*

Chair: *Martin A.J. van Montfort*

Clustering of high values in climatological series
1030-1110 M.R. Leadbetter

Applications of theory of EV's
1110-1130 R.W. Katz

Bayesian error update of distributions
1130-1150 A.R. Boehm

Box-Jenkins assessment of climate change
1150-1210 R.C. Balling

Framework for interpreting rainfall models
1210-1230 K.J.A. Revfeim

Thursday pm

Chair: *Edward S. Epstein*

Statistical problems of climate monitoring
1330-1355 G.V. Gruza

Identification of time varying transfer function
1355-1420 H. Madsen

Statistical analysis of Hong Kong temperatures
1420-1445 E.H. Koo

Types of agweather situations
1445-1510 R.E. Nield

• *afternoon break*

Chair: *Shyam V. Singh*

Interannual climate variability in the global tropics
1530-1555 C.F. Ropelewski

Low frequency tropical convective disturbances
1555-1620 B. Wang

Composite climatology of mesoscale rainfall
1620-1645 E.I. Tollerud

Study of easterly tropical wave disturbances
1645-1710 O.S.R.U. Bhanu Kumar

Friday am

Chair: *Hans von Storch*

Comparing multiple regression and factor analysis
0830-0855 O. Essenwanger

Time series modelling based on mean GF
0855-0920 H. Cao

Modes of growing season precipitation
0920-0945 P.J. Lamb

Statistical character of decadel climate in China
0945-1010 Y-T. Liu

(reserve)

• *morning break*

Chair: *Alistair I. McKerchar*

Rainfall as a fractal process
1030-1050 T. Beer

Precipitation climatology from frequency of 'wet-days'
1050-1110 E.S. Epstein

Precipitation patterns based on law of leaks
1110-1130 L. le Barbe

Distribution functions for rainfall totals
1130-1150 V-T-V Nguyen

Daily rainfall by self adjusting distribution function
1150-1210 M. Molina

1215 Closure: Prof A.H. Murphy, Convenor Steering Committee

FOREWORD

4IMSC was sponsored by the World Meteorological Organisation, Canadian Airlines International and the New Zealand Meteorological Service. Notices and publicity were provided by the American Meteorological Society. Travel support for unfunded participants was given by External Aid Division of the NZ Ministry of External Relations and Trade and three private sponsors in New Zealand.

The meeting was held at Quality Inn, Rotorua NZ, from 27-31 March 1989. An international Steering Committee of Prof A.H. Murphy (USA, Convenor), Dr N. Nicholls (Australia), Dr R. Sneyers (Belgium), Dr F. Zwiers (Canada), Dr G.V. Gruza (USSR) and Dr I. Rodriguez-Iturbe (Venezuela) provided guidance for the 4IMSC host committees.

Planning and running of 4IMSC was carried out by K.J.A. Revfeim (Convenor, Organizing Committee), S.W. Goulter (Convenor, Programme Committee), C.S. Thompson, and J. Sansom with some assistance from other staff of the New Zealand Meteorological Service.

Procedures, notices, programme layout and standard correspondence (invitations to lead speakers, chairpersons etc.) were processed using LaTeX software. Likely participants were invited to submit abstracts on $3\frac{1}{2}$" or $5\frac{1}{4}$" computer disk. After testing the viability of this form accepted papers were requested on disk as an alternative to normal text. The latter remained an optional form although requiring additional labour to scan using an optical character reader. The experience of preparing the Pre-print volume and Proceedings in this manner will be produced as a separate publication that may be useful for running international or national meetings taking advantage of electronic communication and processing facilities. It may well be profitable (in both senses of the word) to keep IMSC to the forefront of this technology.

EDITORIAL

This Pre-print volume is issued as a draft of the Proceedings of 4IMSC. All papers submitted as text or on disk before 10 March 1989 have been included. Other papers expected to be read have been included as ABSTRACTS in the form submitted for programme selection.

Paper headings have been reformatted from LaTeX article style to improve space utilization. Some editorial changes to submitted text and formula layout have been made. Authors are asked to carefully read their paper as processed by us and any required amendments should be addressed to the Convenor, Programme Committee (form supplied in 4IMSC satchel), and preferably handed in at Rotorua before the closure of 4IMSC.

The Registration fee does not include the price of the full Proceedings which will be offered for sale around June 1989. Participants at Rotorua and authors of submitted papers (whether they are able to attend or not) may order the Proceedings at half the full sale price which is expected to be around NZ$100 (i.e. half price NZ$50 including packing and postage). Nett sale proceeds will be invested to provide initial funding for 5IMSC.

Contents

Quality control of precipitation measurements in Denmark

Henning Madsen
Danish Meteorological Institute

Abstract

Manual quality control of precipitation measurements is taken care of in Denmark by means of experienced meteorologists. Over the past years more accurate statistical means has been developed in terms of statistical models for the variation of daily precipitation (1,2). These models assess the variation, in a site specific and temporal frame work (parametric structure) and make use of spatial correlations after remioval of the systematic influence of the site - and temporal effects. The paper discusses semi-automatic quality control procedures in the light of this model and outline a competing procedure based upon calculations of median point values for a given area, which is less sensitive to outliers than quality control procedures based upon a full parametric statistical model, where the estimation of parameters induce biased controls.

References

Allerup, P., and Madsen, H., 1983: A statistical model for precipitation data with application to interpolation problems. *Proc. 2IMSC*, Lisbon.

Allerup, P., and Madsen, H., 1986: Variation of spatial correlation patterns in Denmark. *Proc. 3ICSC*, Vienna.

The accuracy of now-cast winds

S.J. Reid
New Zealand Meteorological Service

Introduction

The need for grid-point wind data for numerical models has led to an examination of the degree to which different types of observing method can produce a truly representative wind for an area. Wylie et al. (1985) have found that that differences between low-level wind observations from land stations which are within 100km of each other have average speed standard deviations of 3 m/s and average direction differences of 45°. The differences represent an intrinsic noise level in the data source due in part to local windflow irregularities.

For many practical purposes it is necessary to predict winds at specific points using the results of synoptic analyses and predictions and from physical extrapolations of wind observations. Gemmill et al. (1988) have tested several methods of determining surface winds from large-scale analyses. They found RMS differences between predicted wind speeds and observed values over the sea of about 4 m/s. It appears that these differences can also be regarded as resulting from the noise in the point observations.

Tennekes (1988) has argued for an increased emphasis on the predictability of atmospheric phenomena. The purpose of the present paper is to find an expression for the error in the wind direction and speed for specific points in the now-cast case. A knowledge of the accuracy with which a value can be given is important for users of the information to determine what margin needs to be allowed for differences from expected values. The degree of error with which winds may be given is a criterion which may be used to determine the need for more stations.

Differences between wind speeds and directions at adjacent stations

Procedure for obtaining differences

Differences between simultaneous wind speeds and directions have been obtained for pairs of neighbouring stations in New Zealand. The data used are mainly wind speeds and directions at hourly intervals, read from a chart record by visually averaging over 10-minute periods through the excursions of the pen trace. This averaging period is a compromise between the need to smooth out local variations of the wind which have little information about the large- scale state of the atmosphere and the need to provide timely information.

The averaging procedure almost certainly is one source of uncertainty in the data. If it is assumed that the reading errors amount to one gradation on the charts of the main operational anemographs then the direction values have uncertainties of $\pm 10°$ and the speeds have uncertainties of $\pm 2kt$ (approximately $\pm 1m/s$).

The speed and direction differences and differences squared have been added together in classes representing different times of day, seasons, and various ranges of speed and direction. Means and standard deviations have been obtained for each class as well as for all classes combined. A computer programme tabulates these quantities for 4 periods over the day, 4 seasons over the year and for 6 speed and 8 direction categories. Because individual speed and direction values generally fall into different categories at the 2 stations, a major station is designated and the speed and direction classes are defined for values at this station.

Characteristics of differences

The pairs of stations used are listed in Table 1. In the following tables each pair is designated by a single number and this is given in the first column of Table 1. The horizontal and vertical separations between the stations are given in the fourth and fifth columns. The actual locations of the stations are not important and the data are indicative of relationships rather than of regional characteristics. The major station in pair 9 uses triangulation data from balloon soundings to obtain wind speed and direction data at the 900m level and the reading error in the data is of a different nature to the other winds.

Table 1: List of Station Pairs

Station pair	Major Station A	Minor Station B	Separations Horiz(km)	Vert.(m)
1	Wellington Airport	Kelburn	6.0	120
2	Wellington Airport	Wn Apt Sth	0.6	5
3	Wellington Airport	Wn Apt Nth	1.2	5
4	Wellington Airport	Somes Is	9.0	50
5	Kaukau Top	Wellington Airport	11.0	550
6	Kaukau Top	Kaukau Middle	0.0	61
7	Kaukau Top	Kaukau Lower	0.0	96
8	Ohakea	Palmerston Nth	26.0	5
9	Ohakea 900m	Ohakea	1.0	900

Some values of the mean direction difference are given in Table 2. These are for all directions and all times combined but for individual speed classes at the major station (station A or the first named in each pair). The data cannot be obtained for one of the station pairs because there were only speed records for one of the stations. The direction differences are mostly less than 20°. For pair 9 larger values do occur and are fairly consistently negative as might be expected with the turning of wind in the boundary layer. The wind at the major station of this pair can be regarded as a free air value.

Table 2: Mean direction differences in degrees between the pairs of stations listed in Table 1.

Station Pair	Speed class station A (knots) 1-3	4-10	11-16	17-21	22-27	28+
1	8	15	17	17	19	16
2	2	0	1	1	0	0
3	13	16	19	19	18	19
4	-13	-10	-7	-2	1	-2
5	-1	-2	-10	-14	-14	-15
6	-	-	-	-	-	-
7	-20	-5	-4	-3	-2	1
8	3	8	7	5	7	8
9	14	-24	-26	-14	-24	-13

Values of the mean speed differences are given in Table 3. In the lowest speed category (1-3 kt)

differences are negative except for 2 station pairs where speeds as low as this at the major station did not occur. The negative sign indicates that overall the speeds at the minor station are higher than at the major station. For the class in which the speeds at the major station are 28 knots or more the mean differences are all positive and show that the speeds at the minor station are consistently less. This is clearly a regression effect in the original sense of the term (Brooks and Carruthers, 1953, p 219). Reid (1987) has evaluated correlation coefficients using this type of data.

Table 3: Mean speed differences in knots between the pairs of stations listed in Table 1.

Station Pair	Speed class station A (knots)					
	1-3	4-10	11-16	17-21	22-27	28+
1	-0.2	1.2	1.7	3.3	5.7	9.5
2	-1.6	-1.5	-2.4	-2.4	-1.4	0.6
3	-1.4	0.0	0.4	1.3	2.1	4.0
4	-2.6	0.2	2.2	4.6	6.6	9.4
5	-2.1	2.5	6.8	9.4	11.1	15.3
6	-	1.6	2.6	3.2	3.8	4.9
7	-	1.0	2.2	3.4	3.9	6.7
8	-2.0	0.5	1.3	2.6	4.7	6.7
9	-0.8	1.6	7.0	9.3	15.2	22.3

Values of the standard deviation of the direction difference are given in Table 4. There is a clear tendency for the magnitude to decrease as the wind speed increases. This is consistent with an increasing variability of direction as the speed decreases as might be expected. There also seems to be an increase with the vertical separation of the stations.

Table 4: Standard deviation of direction differences in degrees between the pairs of stations listed in Table 1.

Station Pair	Speed class station A (knots)					
	1-3	4-10	11-16	17-21	22-27	28+
1	54	43	26	24	20	17
2	36	24	16	14	13	14
3	40	31	21	20	17	16
4	49	42	30	25	27	22
5	79	74	52	36	29	22
6	-	-	-	-	-	-
7	-	40	26	20	18	15
8	56	45	31	22	17	17
9	75	79	60	54	47	22

Table 5 presents the standard deviations of the speed differences. The tendency for the magnitude to change systematically with wind speed is less marked for this data. Although the values in the right-hand column are generally larger than in the other columns, in almost half the rows there is no clear trend. In view of the large range of wind speeds contributing to the differences it is more useful to consider the differences as absolute magnitudes rather than as proportions of the speeds.

Table 5: Standard deviation of speed differences in knots between the pairs of stations listed in Table 1.

Station Pair	Speed class station A (knots)					
	1-3	4-10	11-16	17-21	22-27	28+
1	3.3	3.9	4.5	6.0	4.5	5.4
2	2.3	2.4	3.0	3.8	3.6	3.7
3	3.1	2.9	2.8	3.3	3.7	4.2
4	4.3	4.1	4.0	4.5	5.3	6.8
5	3.9	4.6	4.8	4.9	4.9	6.3
6	-	5.1	5.9	5.5	6.0	6.1
7	-	5.1	4.6	4.0	4.1	5.0
8	5.0	4.6	5.1	5.2	4.8	6.3
9	2.9	4.1	5.1	6.3	6.2	8.8

The 2 sets of mean differences provide a means of predicting wind speeds and directions at station B given data for station A. The 2 sets of standard deviations provide a basis for placing error estimates on the predicted data. A practical application of this is if station B is established for only a short time and after its removal prediction of the winds at B is continued using values for station A and subtracting the mean of the differences. The standard deviation of the differences is an estimate of the standard error of the speeds and directions obtained from this procedure. There is a problem in determining to what extent the differences should be confined to specific classes of speed, direction, time of day, and season because the accuracy of the differences is likely to depend on having an adequate sample of data.

Standard deviations and correlation coefficients

Brooks and Carruthers (1953) give the following expression for the standard error (se) of a difference (or the standard deviation):

$$\text{se} = \sqrt{(\sigma_1^2 + \sigma_2^2 - 2r\sigma_1\sigma_2)} \qquad (1)$$

where σ_1 and σ_2 are the standard deviations of the wind speeds at stations A and B and r is the correlation coefficient.

The se is the square root of the sum of the separate variances of the speeds from stations A and B less twice the product of the two standard deviations mutiplied by r. If $r = 1$ and $\sigma_1 = \sigma_2$ then se = 0. This corresponds in practice to identical wind speeds. However, in the more normal practical situation where $\sigma_1 \neq \sigma_2$ then
se> 0 and if $r < 1$ then se is larger still.

In Table 6, below, the standard deviation of the differences obtained using data in all speed ranges is given for the pairs of stations used in Tables 1 - 5. The standard deviations for the speeds at each station have been evaluated separately and r has been calculated using a rearrangement of equation 1. The data show that the magnitude of the standard deviation has a complex relationship with the correlation coefficient.

If it is assumed that the reading errors for obtaining the wind speeds are such that $\sigma_1 = 2$ kt and $\sigma_2 = 2$ kt then because r=0 for reading errors the se of the difference $\approx$ 3kt. This is about the observed value for station pairs 2 and 3 and it is probable that the 3 anemometers on Wellington Airport do

Table 6: Observed standard deviations for the station pairs and the correlation coefficients calculated from them using equation 1.

Station pair	Standard deviation (all obs) kt	Correlation coefficient
1	5.1	0.75
2	3.2	0.92
3	3.4	0.90
4	5.5	0.72
5	7.0	0.84
6	6.0	0.88
7	5.0	0.91
8	5.2	0.63
9	10.1	0.54

have mean wind speeds which are within the observing error of each other. A similar calculation for wind direction gives values of the se of the difference about 14°. This is similar to observed values in the highest wind speed range for the majority of the station pairs and suggests that wind direction has little intrinsic noise at high wind speeds. On the other hand it does appear very noisy at low speeds.

The accuracy of now-cast winds

In this section the general problem of how accurately the wind speed and direction at some point of interest can be specified is discussed. It is envisaged that the wind flow is known in some macroscopic sense so that the errors associated with the primary source of wind information do not enter the consideration. This situation is important in practice for predicting winds from a synoptic chart or regression model. Similarly there could be a smoothed wind field based on wind observations from anemometer stations.

Wind speed

Supposing that the wind speed at the major station (A) is a prediction for the speed at point (B). It is reasonable that the statistical properties (ie. mean and standard deviation) of the 2 sets of speeds should be identical, then $\sigma_1 = \sigma_2$. The equation (1) is simplified but has a factor of 2 which can be removed if it is argued that there is no uncertainty in the wind speed at station A because it is fully determinate. The equation reduces to:

$$\text{se} = \sigma\sqrt{(1-r)} \qquad (2)$$

where σ is the standard deviation of the wind speed at the point of interest and r is the correlation coefficient between it and the macroscopic wind.

For many practical purposes the standard deviation may be obtained by assuming that the speed distribution has a simple form eg. the Weibull distribution: $P(V > v) = \exp\{-(v/c)^k\}$ where P is the probability of speeds above some threshold of v, the wind speed, and c and k are constants. In many cases $k \approx 2$ and $\sigma \approx 0.52\bar{v}$, the mean speed, and the se can be estimated simply from the mean speed at the point of interest and information about the correlation coefficient, r.

The most important factor determining the error is the mean speed at the point of interest. This may be estimated from known values in similar terrain, by the use of wind-flow models or by short-term measurements.

An uncertainty in r has less impact on the error calculation than if σ is poorly known, because of the square root. Also the parameter will in many cases be known between pairs of stations with similar separation in similar terrain. It should be observed that the values of r obtained above are degraded to some extent by reading errors of the anemometers. In many practical situations the effect on the se will be small.

The correlation coefficient, r, may be regarded as a function of the separation distance between the stations. Wylie et al. (1985) provide a nomogram which can used for stations separated by horizontal distances of hundreds of km. For smaller separations it is reasonable that r should increase roughly inversely with the separation distance. The data in Table 6 do not seem consistent with this expected relation and it appears that the vertical separation may also influence the correlation coefficient. The nature of the land surface between stations may also influence r because hilly country disrupts the regular flow of the air and it is reasonable to expect smaller correlation coefficients in rougher country.

The se of the wind speed calculated using equation (2) is based on statistical properties of the wind at a point. The se can be applied to speeds which are given for that place at particular times because the se of the speed is only weakly dependent on its actual magnitude.

Wind direction

The variation with speed of the se of the difference between wind directions at pairs of stations means that it is not possible to give a single error which applies to all predictions of direction. Rather it is necessary to give separate values applying to ranges of speed.

Another difficulty is that the circular distribution of wind directions means that it is not possible in general to calculate a simple correlation coefficient. One possible exception may be where winds at nearby stations are confined to small ranges of direction and the peaked distribution can be considered to be unbounded so that all pairs of direction data can be regressed against each other and the equations given above may be applied to the data.

For station pairs 1 to 7 the winds are almost exclusively from directions around south and north. The shape of the distribution has been approximated as a normal distribution and the correlation coefficients have been calculated for some of the direction and speed ranges. There is a tendency for the calculation procedure to give negative values of$r$ and this appears to be due to the assumed nature of the distribution. There are many more data in the tails of the distribution than is given by the normal curve because of large irregular direction differences at low wind speeds. If these low speed differences are avoided by confining the calculations to the high wind speed ranges small positive correlation coefficients are found.

It appears from the above that the standard error of the wind direction for wind speeds above about 5m/s may be estimated using the equation (2) with $r = 0$. The appropriate value of σ to use is the observed spread about the predominant direction. This may be determined by land features in some cases. For wind directions away from the predominant direction peaks, the error may be obtained from the standard deviation between appropriate pairs of stations. The value should be chosen on the basis of the horizontal and vertical distances between stations, the complexity of the terrain and the wind speed.

For wind speeds of 5m/s or less, observed wind direction differences have high standard deviations. If it is assumed that the wind direction is completely decoupled from the predicted value, differences between observed and predicted directions form a rectangular distribution from -180°to +180°and the value of σ is 104°.

Conclusions

The standard error of a now-cast wind speed at a specified place can be expressed as a single number (eg. ± 3 m/s) so that for low speeds the error may exceed the speed but at high wind speeds the same absolute value applies. The value is approximate but for practical applications is most useful in a simple form. It can be calculated from the standard deviation of the speed at the point of interest (obtainable from an estimation of the mean wind speed) and the correlation coefficient between the speeds predicted and observed (this is clearly not available without measurement but can probably be estimated in many cases with sufficent accuracy).

It appears to be more difficult to specify an error for the wind direction because at low speeds very high levels of uncertainty are apparent, decreasing to rather low values at high wind speeds. Also it does not appear to be possible to provide a useful expression for the correlation coefficient between wind directions. It appears to be necessary to take an empirical approach in this case. It is possible that there may be more useful information in the accuracy with which wind direction changes can be specified in time.

References

Brooks, C.E.P., and N.Carruthers, 1953: Handbook of Statistical Methods in Meteorology, *London: Her Majesty's Stationery Office.*

Gemmill, W.H., T.W.Yu and D.M.Feit, 1988: A Statistical Comparison of Methods for Determining Ocean Surface Winds, *Weather and Forecasting*, **3** , 153-160.

Reid, S.J., 1987: The accuracy of mountain-top winds estimated from free air data, *J Wind Eng. Ind. Aerodyn.*, **26** , 179-193.

Tennekes, H., 1988: The Outlook: Scattered Showers, *Bulletin American Meteorological Society*, **692** , 368-372.

Wylie, D.P., B.B.Hinton, M.R.Howland and R.J.Lord, 1985: Autocorrelation of Wind Observations, *Monthly Weather Review*, **113** , 849-857.

The statistical analysis of turbulence in the Bora

J. Urbančič
Jožef Institute, Ljubljana, Yugoslavia

Abstract

Turbulence analysis (especially turbulence flux computations) is a task which cannot be done with certainty. In the power spectrum the "gap" between turbulent motion and medium or large scale motions tends to disappear somewhat higher above the ground. This fact makes it difficult to distinguish turbulent motion from other types. The bora wind seems to be a "difficult example" where strong turbulence appears in a stable air layer. The paper discusses the strategy of solving the problem to obtain results with reasonable certainty.

On the homogeneity of long series of observations

R. Sneyers
Royal Meteorological Institute, Ave Circulaire 3, B-1180 Brussels, Belgium

Abstract Homogenizing of series of observations is a general problem in the case of long series. The proposed solution consists in reducing the elements of the heterogeneous parts of the series in such a way that their probability in the final series be preserved.

The method is developed in the case where the distribution of the elements is normal or defined by two parameters : one for position and one for scale, the estimators of which are linear. The method of estimation of the parameters is related to short series in correlation with longer series.

Moreover, the problem of testing the homogeneity of a series of observations is briefly reviewed.

Introduction

A homogeneous series of observations is a series made up continously at the same unchanged instrument in a site which also has remained unchanged. The advantage of having homogeneous series at disposal is that if the statistical properties of the series are stable it will be possible to estimate the probability (or return period) associated with each element of the series and if not, to characterize the change of climate responsible for the instability of the series. Now that the monitoring of climate has become a major problem for climatologists, the assessment of the homogeneity of long series of observations appears as a fundamental question.

The fact that long series of observations are seldom obtained with the same instrument at the same unchanged location shows the difficulty of this question, the solution of which remains in the examination of simultaneous observations, when they exist, or in the comparison of the series with another correlated series, the homogeneity of which is well known.

The first case generally concerns observations of the same kind, e.g. rainfall measured simultaneously at two raingauges; the second case may involve observations of a different kind such as daily sunshine and the corresponding daily amplitude of the air temperature variation.

However, both cases are related to the problem of estimation when the time series are correlated.

Time Series Homogenizing

Heterogeneities are introduced in the time series when there is a change of instrument or of site or of both instrument and site. In these circumstances two situations are possible :

a) simultaneous observations with different instruments and or sites are available, which implies that the two time series are overlapping;

b) the time series is uninterrupted but simultaneous observations have not been made.

Case of existing simultaneous observations

Let the first observations x extend from dates t_1, to t_2, and the following observations y extend from dates t_3 to t_4 with $t_1 < t_3 < t_2 < t_4$.

The homogenizing of the series will be realized if it is possible to substitute for the observations estimated values of y having the same probability in the series of y as have the values of x in the series of x, the probability being considered over the period t_3 to t_4 .

If x and y are independently distributed with distributions defined by two population parameters μ and σ, the one for position and the other for scale, and if they have the same reduced variate u, we

will have :

$$x = \mu_1 + u_1\sigma_1 \text{ and } y = \mu_2 + u_2\sigma_2 \tag{1}$$

where u_1 and u_2 are the values of u determining the probability associated with x or y.

The homogeneity will thus be realized if we substitute for x the value of y corresponding to $u_2 = u_1$. from which it follows :

$$\frac{x - \mu_1}{\sigma_1} = \frac{y - \mu_2}{\sigma_2} \text{ or } y = \mu_2 + \sigma_2/\sigma_1 (x - \mu_1) \tag{2}$$

The problem reduces thus to the computation of adequate estimates for μ_1, μ_2, σ_1 and σ_2 .

Two cases may be considered according to whether the distribution of u is the standard normal distribution or to whether the population parameters have efficient linear estimators (i.e. the parameters of the double exponential distribution).

If x and y have normal distributions, let $\hat{\mu_1}$, $\hat{\mu_2}$, $\hat{\sigma_1}$, and $\hat{\sigma_2}$, be the moment estimates of the means μ_1, μ_2 and the standard deviations σ_1 and σ_2 given by the series of simultaneous observations made from t_3 to t_2, and let μ_2^* and σ_2^* be the estimates of μ_2 and σ_2 given by the series of observations of y from t_3 to t_4 . Optimal estimates for μ_1 and σ_1 are then given by the relations(cf Sneyers, 1975, p.116 and Sneyers, 1969) :

$$\mu_1^* = \hat{\mu_1} - \hat{\rho}\frac{\hat{\sigma_1}}{\hat{\sigma_2}}(\hat{\mu_2} - \mu_2^*) \text{ and } \sigma_1^* = \hat{\sigma_1}(\sigma_2^*/\hat{\sigma_2})^k \tag{3}$$

where $\hat{\rho}$ is the estimate of the correlation coefficient (supposed to be > 0) given by the simultaneous observations, and $k = \hat{\rho}^2$

When the population parameters have linear estimators, the relations (3) become:

$$\sigma_1^* = \hat{\sigma_1}(\sigma_2^*/\hat{\sigma_2})^{\hat{\rho^2}} \text{ and } \mu_1^* = \hat{\mu_1} - \hat{\rho_1}(\sigma_1^*/\sigma_2^*)(\hat{\mu_2} - \mu_2^*) \tag{4}$$

Two particular cases may be considered according to whether $\sigma_1 = \sigma_2$ or $\mu_1 = \mu_2 = 0$.

The scale parameters are equal

In this case, from (2), we have :

$$y = x + (\mu_2 - \mu_1) \tag{5}$$

and the optimal estimates of $\mu_2 - \mu_1$ become from (3) and (4) (normal case and linear case) :

$$\mu_2^* - \mu_1^* = \mu_2^*(1 - \hat{\rho}) + \hat{\rho}\hat{\mu_2} - \hat{\mu_1} \tag{6}$$

If $\rho = 1$, or if $t_2 = t_4$, we have :

$$\mu_2^* - \mu_1^* = \hat{\mu_2} - \hat{\mu_1} \tag{7}$$

which is the formula given by the so called difference method (Δ -method).

With var $\hat{\mu_1}$ = var $\hat{\mu_2}$ the error of estimation for (6) is given by :

$$var(\mu_2^* - \mu_1^*) = (1 - \rho)^2 var\mu_2^* + \left(1 - \rho^2\right) var\hat{\mu_2} \tag{8}$$

For (7), we have :

$$var(\hat{\mu_2} - \hat{\mu_1}) = 2(1 - \rho) var\hat{\mu_2} \tag{9}$$

The position parameters are zero

This occurs when the two distributions are normal with zero means or when we have gamma distributions with the same shape parameter.

We have then with (2):

$$\frac{x}{\sigma_1} = \frac{y}{\sigma_2} \text{ or } y = \frac{\sigma_2}{\sigma_1} x \tag{10}$$

Moreover, the estimate Q^* of the quotient $Q = \sigma_2/\sigma_1$ is then with (3) and (4) :

$$Q^* = \sigma_2^*/\sigma_1^* = \sigma_2^{*2(1-k)} \hat{\sigma_2}^k / \hat{\sigma_1} \tag{11}$$

with $k = \hat{\rho^2}$ or $\hat{\rho}$ according to whether the distribution is normal or to whether the estimators of the parameters are linear.

Having then $\text{var}\hat{\sigma_1}/\sigma_1^2 = \text{var}\hat{\sigma_2}/\sigma_2^2$ and $\text{cov}\,(\hat{\sigma_1}, \hat{\sigma_2}) / (\sigma_1\sigma_2) = k\text{var}\,(\hat{\sigma_1}) / \sigma_1^2$, the variance of the error of estimation of Q^* is given by :

$$varQ^*/Q^2 = (1-k)^2\, var\sigma_2^*/\sigma_2^2 + \left(1-k^2\right) var\hat{\sigma_2}/\sigma_2^2 \tag{12}$$

If $t_2 = t_4$, the estimate (11) of Q becomes (Q - method) :

$$Q^* = \frac{\hat{\sigma_2}}{\hat{\sigma_1}} \tag{13}$$

and the variance of the error of estimation is then given by:

$$varQ^*/Q^2 = 2\,(1-k)\, var\hat{\sigma_2}/\sigma_2^2 \tag{14}$$

The two series do not overlap ($t_3 = t_2 + 1$)

If it can be established that x as well as y are pure random variates all over the whole period of observations t_1 to t_4, μ_1, and σ_1, can then be estimated from the series extending from t_1 to t_2 and μ_2 as well as σ_2 from the series extending from t_3 to t_4 . Relations (2) have then to be applied.

When this is not the case, the homogeneity of the complete series can be tested if there exists a homogeneous series of observations z extending from t_1 to t_4 in correlation with x and y.

If (x, y) is the complete series of observations of x and y , this can be done by computing the regression of the series (x, y) on the series z and by testing the randomness of the residuals of the regression, randomness signifying homogeneity.

With a non random residual, whenever the regression is given by the relation :

$$(x, y) = a + bz + e \tag{15}$$

where a and b are constants and e the residual, the series (x, y) will be first corrected for the change in the mean of the residual e.

If $(x, y)'$ is the corrected series, a new regression will lead to a relation of the form :

$$(x, y)' = a' + b't + e' \tag{16}$$

which will make it possible to correct $(x, y)'$ for the variation of the variance of e':

Testing the homogeneity of series of observations

The homogeneity of a series of observations can generally not be ascertained directly by applying a test of randomness, since a homogeneous series may contain non random effects due to the instability of the climate. On the contrary, when a series of observations can be compared with a series known to be homogeneous, its homogeneity can be verified by testing the randomness of some residual derived from the two series by the method of differences or of quotients, or by regression.

The question which arises is to use the most appropriate tests of randomness to put in evidence the kind of heterogeneity which is most likely to appear, i.e. change in the mean, change in the variance, or change in both the mean and the variance. of course, tests against specified alternatives have to be preferred to omnibus tests for obvious reasons of power.

To begin with, a first choice has to be made between parametric and non-parametric (distribution free) tests.

Parametric tests, based on the assumption of normality, are generally more powerful than distribution free tests; on the other hand, distribution free tests have a wider applicability and in certain cases have a power very near to the power of the corresponding parametric test. It follows that when possible, distribution free tests have to be chosen.

For what concerns the residuals, some caution has to be taken in the case where these residuals are computed from a regression. Actually, when the real residuals are random, the computed (estimated) residuals being linear functions of the real residuals (cf. Kendall, 1976, p.163), they lose this random character.

For the choice of appropriate tests of randomness, reference should be made to the general discussion gwen in Kendall, 1976 , p.21 , to the principles advocated in Sneyers, 1975, where the randomness is tested through a distribution free test against autocorrelation associated with a trend test applied in his progressive onward and backward version, to the synthesis on parametric tests on cumulative deviations from the mean (cusums) made in Buishand, 1982, and to a distribution free version of these tests developed in Pettitt, 1979 . For residuals from a regression, the test against autocorrelations should be replaced by the Durbin-Watson test for which tables are given in Kendall, 1976. For this purpose, it should be noted that in the case of one regressor, the ordinary autocorrelation test remains practically valid.

Trend tests and cusum tests are powerful against alternatives of instability of the mean. When the series have been corrected for eventual changes in the mean, the stability of the variance can be tested by applying the foregoing tests to the series of squares of the deviations from the mean.

Conclusion

A general theory has been developed to solve the problem of correcting meteorological series for heterogeneities. For this, it was necessary to make some assumptions. The application of this theory to the series of Brussels-Uccle begnning in 1833, 1878 or 1887 have shown the importance of verifying these assumptions.

Of course, the methods described above are not only applicable to monthly data but also to daily data, though in this case the variances of the error of estimation of the parameters of the distribution are modifieded due to autocorrelation in the series of consecutive daily observations. Moreover, the method of regression may be generalized as advocated by Michalczewski.

This generalization should however follow the scheme given in 2.2 by correcting the heterogeneous parts, first for the mean and afterwards for the variance.

References

Buishand, T.A., 1982: Some Methods for Testing the Homogeneity of Rainfall Records. *J. Hydrol.*, 58, 12-27.

Kendall, Sir Maurice, 1976: Time-Series. Charles Griffin and Co. Ltd., 2nd edition, 198p.

Michalczewski, J., 1986: Filling Gaps and Removing Heterogeneities in Series of Warsaw's Daily Mean Temperatures. (case study). Personal communication.

Pettitt, A.N., 1979: A Non-parametric Approach to the Change-point Problem. *Appl. Statist.* **28**(2), 126-135.

Sneyers, R., 1969: Notes sur la notion d'independance climatologique, *Revue de Statistique Appliquée.* **17**, 4, 45-53.

Sneyers, R., 1975: Sur l'analyse statistique des series d'observations, *Organ. Mét. Mond. Note Technique* no **143**, 192p.

Inhomogeneities in precipitation time series

B. Sevruk
Federal Institute of Technology, Zurich, Switzerland

Introduction

The problem of inhomogeneous precipitation time series is more serious than generally accepted. Due to frequent changes in this century of gauge sites, measurement technique standards and observers, the precipitation time series show multiple inhomogeneities and consequently, they are hardly suitable to be used to compute the 'climatical norms' and to study precipitation trends or made conclusions concerning global precipitation. Since through the empirical adjustment factors the homogeneity relative to the adjacent gauge sites can be restored, the systematic error of precipitation measurement, which is the real culprit of inhomogeneities cannot be eliminated unless the specific correction procedures are applied to precipitation time series from different types of precipitation gauges. Moreover, the correction of systematic measurement error helps not only to reduce the effects of notoriously different exposure of gauge sites in a particular national network but also eliminates the effect of different precipitation measurement standards as used in different countries. Thanks to it, the leaps of isohyets at the borders of countries disappear and the global compatibility of precipitation time series could be established. Thus the application of corrections open new ways in dealing with inhomogeneities. It makes the studies of global precipitation all the more conclusive.

The purpose of this paper is to analyse the effect of systematic measurement error on inhomogeneities due to exchange of different types of precipitation gauge. The results of precipitation intercomparison measurements at one site in Switzerland are presented and analysed with the aim to show that the adjustment factors for inhomogeneities of liquid precipitation data depend on wind speed and precipitation structure. In contrast to the previous studies by Shver (1965 and 1984) in the USSR, who used long-term data to derive adjustment factors between precipitation time series of two types of manual gauges in terms of climatical regions, mean annual wind speed and six classes of site protection, the data used in this study consist of actual hourly averages of wind speed and precipitation intensity. The actuality of the intercomparison is stressed by the fact that the one gauge is manual of the 'classic' Hellmann type and the other is the recording, 'modern' heated tipping-bucket gauge, which is progressively used worldwide in the automatic meteorological stations. This is also the case in Switzerland where during the last decade, 70 gauges of this type have been uniformly distributed over the country and compared with the older one. The paper shows the problems arising from such an exchange of precipitation gauges and indicates ways to solve them.

The literature on the subject of systematic error of precipitation measurement was reviewed by Sevruk (1982). Recent references could be found in Sevruk (1986a, 1987). Legates and Willmott (1989) show the global distribution of magnitude of systematic error in precipitation measurement. A review on homogeneity tests applied to precipitation data was presented by Buishand (1982) and Alexandersson (1986). Both authors point out that inhomogeneities in precipitation time series exist in Holland and in Sweden but were not systematically dealt with as yet. Such investigation have been made only in the USSR as shown by Shver (1965, 1984). Camuffo (1984) analysed the longest preserved precipitation time series in the world at Padua, Italy. Bradley et al. (1987) studied precipitation fluctuations over northern hemisphere since mid-19th century and found evidence of inhomogeneities. Further references are listed in bibliography at the end of this paper.

Methods

The automatic ASTA and the Hellmann gauges were installed in an open site at the Geneva Airport. The annual precipitation is approximately 1100 mm and the proportion of snow in total annual precipitation is 12%. The distance between the gauges was 1.6 m and the height of orifice of both gauges was 1.5 m above ground. The gauges differ slightly in their outer form. Their height is 0.48 vs. 0.46 m. However, the orifice rim of the ASTA gauge is essentially larger because it contains the heating system. In addition, it is solid and almost perpendicular to the inner walls of the gauge collector, having only two small inside steps. On the other hand, the orifice rim of the Hellmann gauge is not only considerably thinner but has a completely different form. It is open and it hangs inside, over the gauge orifice, like a console. None of the gauges were equipped with a windshield, but the bird protection ring was used on the ASTA gauge. The orifice area of both gauges is the same (200 cm^2). For pictures of gauges see Sevruk et al. (1989a) and for the description of the gauge site and for the results of preliminary analysis of daily data see Spiess (1987).

Simultaneously with the hourly precipitation amount of the ASTA gauge, wind speed was also recorded. The Hellmann gauge was measured manually each 12 h. The form of precipitation was registered at each observation. The hourly data set was available for the 4-yr period, 1981-1984. These data were sub-divided according to the season, whereas the summer included months from May through October and the winter from December to February. For each half-day, the average of the hourly values of wind speed during the precipitation period was computed. In addition, the fraction of low intensity precipitation was estimated in per cent of total semi-daily precipitation. The threshold value was 0.3 mm h^{-1}.

In the first step, the mean monthly systematic error due to wind was corrected for the Hellmann gauge using procedure as developed by Sevruk (1986b). The aim was to see the correction estimates for the systematic error of the ASTA gauge. For this gauge no correction procedure is available as yet . In this case, the 6-yr period, 1980-1985 was considered. In the second step, the semi-daily difference (in [mm]), between non-corrected precipitation amounts of both gauges was correlated with the corresponding Hellmann gauge precipitation amount, separately for the winter and summer seasons,days with snow excluded. Additionally, the differences were sub-divided according to wind speed smaller or greater than 2.3 m s^{-1}. The resulting correlation coefficients were plotted against the fraction of low intensity precipitation. All in all, 740 half-days were included in the analysis (winter 221, summer 519).

Results

Figure 1 shows the seasonal pattern of percentage difference relative to the Hellmann gauge values together with the variables wind speed and proportion of snow. Both variables appear to affect the magnitude of difference but the effect of the proportion of snow is very pronounced. Since the average annual difference amounts to 14%, in the summer it is 11% and in the winter as much as 16%. The Hellmann gauge showed always more precipitation. In the case of the corrected Hellmann gauge precipitation values, the respective differences are 29% per year, 22% in the summer and 36% in the winter.

Figure 2 shows the plots of correlation coefficients against the fraction of low intensity precipitation. As is seen from the figure, the correlation coefficients are less sensitive to wind speed mainly in the summer, but they increase considerably with the increasing fraction of low intensity precipitation. Generally, this dependency is slightly less pronounced in the summer than in the winter.

Discussion

The large deficit of measured precipitation of the automatic ASTA gauge is partly due to the big orifice rim and to the bird protection ring as used on this gauge at Geneva Airport. This was confirmed in a special investigation of the Hellmann and the ASTA gauges in a wind tunnel, carried out by Sevruk et al. (1989a,b).

The fact that the effect of wind speed smaller or greater than 2.3 m $s^{-}1$ on the difference is smaller than that of the fraction of low intensity precipitation could be explained by the relative small range of wind speed at the Geneva Airport as shown in Figure 2. Yet this phenomenon indicates the important role of low intensity precipitation to estimate adjustment factors of inhomogeneous precipitation time series, a fact unnoticed in many studies as yet. The threshold value of 0.3 mm h^{-1} was a suitable one for Geneva Airport, but it could be expected that for different locations other values will show better results, depending on the range of wind speed and the structure of liquid precipitation . However, the type of precipitation gauge seems to be also an important factor. For instance, Bogdanova (1966) analysing the systematic error of precipitation measurement of the Tretyakov gauge (USSR) recommended a threshold value of 0.03 mm min^{-1}, which is considerably more than the 0.3 mm h^{-1} as used in this study.

Conclusions

The appearance of inhomogeneities in precipitation time series due to exchange of different types of precipitation gauges is a consequence of various magnitudes of systematic error of precipitation measurement of given gauges, particularly the wind-caused loss. Therefore, adjustment procedures should be based rather on the physics of phenomenon, i.e. on variables as used in respective correction models of systematic error and not on statistics alone. In the case of wind-caused loss of liquid precipitation such variables are wind speed and a parameter of structure of precipitation. The latter could be expressed by the fraction of low intensity precipitation in total precipitation amount of a particular time interval used. For the semi-daily precipitation amounts at the Geneva Airport in Switzerland the threshold value of low intensity precipitation was 0.3 mm h^{-1}.

References

Alexandersson, H., 1986: A homogeneity test applied to precipitation data. *J. Climatol. 6 (6). 661-675.*

Bogdanova, E. G.,1966: Investigation of precipitation measurement losses due to the wind (in Russian). *Trans. Voyeykov Main Geophys. Observ. 195, 40-62.*

Bradley, R.S., H.F. Diaz, J.K. Eischeid, P.D. Jones, P.M. Kelly and C.M. Goodess, 1987: Precipitation fluctuations over northern hemisphere land areas since the mid-19th century. *Science, 237, 171-175.*

Buishand, T.A., 1982: Some methods for testing the homogeneity of rainfall records. *J. Hydrol., 58, 11-27.*

Camuffo, D., 1984: Analysis of the series of precipitation of Padua, Italy. *Clim. Change 6, 57-77.*

Legates, D.R. and C.J. Willmott, 1989: Mean seasonal and spatial variability in global precipitation. *J. Climatol., 1989 (in press).*

Sevruk, B. (ed.), 1986a: Correction of precipitation measurements. *Proc. ETH/WMO/IAHS, International Workshop on the Correction of Precipitation Measurements, 1-3. April 1985, Zurich ETH. Zrcher Geographische Schriften, ETH Zrich No 23, 289pp.*

Sevruk, B., 1986b: Correction of precipitation measurements: Swiss experience. *In: B. Sevruk (ed.): Proc. ETH/WMO/IAHS, International Workshop on the Correction of Precipitation Measurements. 1-3. April 1985, Zurich ETH. Zrcher Geographische Schriften, ETH Zrich No 23, 289pp.*

Sevruk, B., 1987: Point precipitation measurements: why are they not corrected? *In: Proc. of the Rome Symposium: Water for the Future; Hydrology in Perspective. Internat. Assoc. Hydrol. Sci. publ., No. 164, 477-486.*

Sevruk, B., J.-A. Hertig and R. Spiess, 1989a: The effect of a precipitation gauge orifice rime on the wind field deformation as investigated in a wind tunnel. *Atm. Envir., (in press).*

Sevruk, B., J.-A. Hertig and R. Spiess, 1989b: Wind field deformation above precipitation gauge orifices. *In: Proc. Internat. Assoc. Hydrol. Scie., Scie. Assembly, Baltimore, 7 p. (in press).*

Shver, Z.A., 1965: Investigation of results of observations of raingauge and precipitation gauge (in Russian). *Gidrometeorologicheskoe Izdatelstvo, Leningrad, 170 p.*

Shver, Z.A., 1984: Regularities in distribution of precipitation amount over continents (in Russian). *Gidrometeoizdat, Leningrad, 285p.*

Spiess, R., 1987: Comparison of precipitation values from automatic and conventional meteo-stations (in German) (unpublished). *Swiss Federal Institute of Technology ETH Zentrum, Zurich, Switzerland, Diplomarbeit*

Bibliography

Artemyeva, N.P. and A.A. Ivanova, 1980: Problem of checking and analysing the internal homogeneity of a long series of hydrological information. *Soviet Hydrol.: Select Pap., 19, 156-159.*

Brunet-Moret, Y., 1980: Retour sur l'homogénéisation des pluies annuelles par vecteur regional. *La Météorologie VIe Série n°' 20-21 Mars-Juin, 61-63.*

Jones, P.D., 1985: Comment on 'Homogeneity analysis of rainfall series: An application of the use of a realistic rainfall model'. *J. Climatol., 5(3), 337-341*

Karl, Th.R. and C.N. Williams Jr. 1987: An approach to adjusting climatological time series for discontinuous inhomogeneities. *J. Climate. Appl. Meteor., 26(12), 1744-1763.*

L'Hote, Y., 1986: Verification of rainfall data quality and homogeneity through the method of annual rainfall indices vector. *In: B. Sevruk (ed.): Correction of precipitation measurements. Zrcher Geographische Schriften, ETH Zrich, No. 23, 263-268.*

Thompson, C.S. 1984: Homogeneity analysis of rainfall series: An application of the use of a realistic rainfall model. *J. Climatol., 4(6), 609-619*

Thompson C.S. and K.J.A. Revfeim, 1985: Comment on 'Homogeneity analysis of rainfall series: An application of the use of a realistic rainfall model '. *J. Climatol., 5(6), 579-581.*

Marine stratocumulus spatial structure

Robert F. Cahalan[1], M. Nestler[2], W. Ridgway[3], W.J. Wiscombe[1] T. Bell[1]
[1]Laboratory for Atmospheres, Goddard Space Flight Center, Greenbelt; [2]Science Applications Research, Lanham; [3]Applied Research Corporation, Landover, MD, USA

Introduction

Many theoretical studies have shown the sensitivity of cloud radiative properties to their spatial structure, ranging from the seminal work of McKee and Cox (1974) and Stephens (1976) to more recent work by Harshvardan and Weinman (1982), Welch and Wielicki (1985), and others. As Harshvardan and Randall (1985) have pointed out, current general circulation models, because of their reliance on plane-parallel assumptions, are in the embarrassing situation of having to use unrealistically small liquid water amounts to produce realistic albedos. Stephens (1985) has emphasized that the mean albedo is not a function of mean liquid water alone, but depends upon its spatial distribution. Lovejoy (1982) suggested that cloud spatial distributions may be modelled as self-similar fractals, and has more recently generalized to multifractals (Schertzer and Lovejoy, 1988). Rhys and Waldvogel (1986) and others have shown that cloud fractal dimensions undergo abrupt changes at certain scales, and Cahalan and Joseph (1989) found that these characteristic scales depend upon cloud type.

Marine stratocumulus are perhaps closest to plane-parallel, being largely confined between the lifting condensation level and the strong subtropical inversion. In a recent study of marine stratocumulus, using data from FIRE (summarized by Albrecht et al.), Cahalan and Snyder (1989, hereafter CS) found a change in the stratocumulus wavenumber spectrum from a -5/3 power to a -3 power at a scale determined by the cloud thickness, a few hundred meters. This is consistent with two- dimensional homogeneous turbulence (Kraichnan, 1967), in which energy injected at a particular scale (e.g. the cloud thickness) cascades to lower wavenumbers with a -5/3 power law, while the enstropy cascades to higher wavenumbers with a -3. Observations by commercial aircraft (Gage and Nastrom, 1986) show a -3 at low wavenumbers, presumably from baroclinic forcing at a few thousand km, changing at a few hundred kilometers to a -5/3, which we suggest is associated with convective forcing at the cloud thickness scale. In the following we briefly summarize the stratocumulus observations, then present a simple model for the observed structure.

Observed Stratocumulus Structure

Much of our knowledge of stratocumulus horizontal structure is based upon observations of cloud reflectivity (see e.g. Cahalan and Joseph, 1989; for vertical structure see Boers and Betts, 1988). A more basic question is how the cloud liquid water is distributed, since the reflectivity can be computed from the distribution of liquid water, traditionally by specifying microscopic properties like drop sizes, and macroscopic properties like optical depth, etc.. The radiation field provides a kind of low-pass spatial filter, so that there may be small-scale variations of liquid water to which the LANDSAT data are completely insensitive (Cahalan, 1988b). [At the same time, the mesoscale structure of stratocumulus liquid water, which leads to the power-law wavenumber spectrum described below, is to some extent mirrored in the reflectivity data, which follows the same power-law (CS).] These liquid water variations are not included in our usual plane-parallel computations, and will be an important input to more realistic radiative transfer models.

Vertically integrated liquid water was measured at 1 minute intervals over a three-week period during FIRE (see CS for details). The histogram of this data is shown in figure 1a on a log-linear scale, with a lognormal fit plotted for comparison. The lognormal roughly follows the data, while differing in detail. The "shoulders" seen to each side of the observed central peak are a reminder that

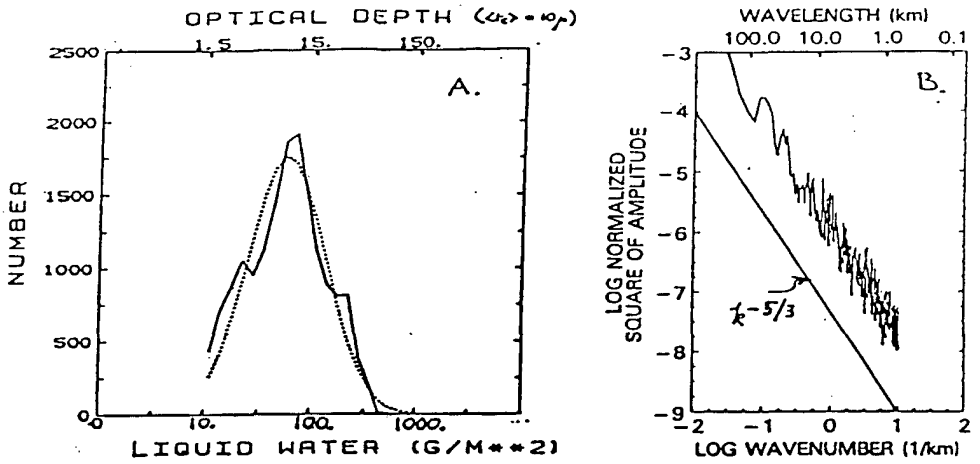

Figure 1: (a) Probability distribution of vertically integrated stratocumulus liquid water in mm plotted on a log-linear scale, along with a lognormal fit. The equivalent optical depth scale shown at the top assumes a 10 micron effective radius. (b) Wavenumber spectrum of integrated liquid water computed from time series assuming 5 m/s frozen turbulence.(CS)

individual days often show a bimodal distribution. The liquid water wavenumber spectrum (fig.1b) was estimated from the frequency spectra computed from several one-day time series of one-minute averages of total vertically integrated liquid water measured at San Nicolas Island during FIRE. Results were translated from frequency to wavenumber assuming frozen turbulence with a 5 m/s mean advection. The least-squares fit from about 400 km down to about 400 m gives $S(k) \sim k^{-5/3}$ (see Cahalan and Snider, 1989). By contrast, fair weather cumulus show a much flatter spectrum over the same scales (CS).

This is the classic Kolmogorov result for the wavenumber spectrum of any component of the velocity field, and is also the spectrum expected for a "passive scalar", i.e. a scalar field whose variations in space and time are due only to advection. This suggests that the total integrated liquid water in stratocumulus clouds fluctuates with the vertical velocity, being large in updrafts and small in downdrafts. This kind of behavior has been observed in fine-resolution numerical simulations (MacVean and Nicholls, 1988), though they do not reproduce the highly irregular fractal structure described above. Correlations of vertical velocity and liquid water will be of much interest as more of the FIRE data is analyzed.

Fractal Stratocumulus Streets

In this section we first describe a technique for analyzing wavenumber spectra which is especially convenient for cascade models. We then consider two simple multiplicative cascade models which give spatial distributions of liquid water which are fractal in one horizontal dimension, and uniform in the other horizontal direction and in the vertical. Both models give lognormal-like probability densities of optical depth. However, the range of optical depths in the first model is unbounded as the resolution increases, while the second model has both an upper and lower bound. The first model also produces a wavenumber spectrum flatter than k^{-1}, while the second model may be tuned to reproduce the observed $k^{-5/3}$.

Spectral analysis preliminaries

Consider a stochastic function of position $f(x)$, which is homogeneous over some domain L_0, and let $f'(x)$ be the deviation from the mean, so that $\langle f'(x) \rangle = 0$, where the angular brackets indicate an ensemble average. The associated lag covariance function is then given by

$$c(x) = \langle f'(x_0)\, f'(x_0 + x) \rangle. \tag{1}$$

The power spectrum may be computed from the covariance by Fourier transform, so that

$$S(k) = \int_{-\infty}^{\infty} dx\, e^{-ikx}\, c(x). \tag{2}$$

A simple approach to analyzing the spectrum, which turns out to be particularly convenient for multiplicative cascade models, is Lorenz' "poor man's spectral analysis" (Lorenz, E. N., 1979). We consider averages of $f(x)$ over successively smaller subdivisions of the domain:

$$\overline{f}_n(x) = \frac{1}{L_n} \int_0^{L_n} dx\, f(x), \tag{3}$$

where each interval, L_n, is half as big as the previous:

$$L_n = \frac{L_0}{2^n}. \tag{4}$$

The variance of $\overline{f}_n$ is then

$$\begin{aligned} V_n &= \langle (\overline{f}_n)^2 \rangle \\ &= \frac{1}{L_n^2} \int_0^{L_n} dx_1 \int_0^{L_n} dx_2\, \langle f(x_1)\, f(x_2) \rangle \\ &= \frac{1}{L_n^2} \int_0^{L_n} dx_1 \int_0^{L_n} dx_2\, c(x_1 - x_2) + \langle f \rangle^2 \\ &= \frac{1}{L_n^2} \int_0^{L_n} dx_1 \int_0^{L_n} dx_2 \int_{-\infty}^{\infty} \frac{dk}{2\pi}\, e^{ik(x_1 - x_2)}\, S(k) + \langle f \rangle^2 \\ &= \int_{-\infty}^{\infty} \frac{dk}{2\pi}\, |\mathcal{F}(kL_n)|^2\, S(k) + \langle f \rangle^2, \end{aligned} \tag{5}$$

where

$$\mathcal{F}(kL_n) = \frac{1}{L_n} \int_0^{L_n} dx\, e^{ikx} = \frac{e^{ikL_n} - 1}{ikL_n}, \tag{6}$$

so that

$$|\mathcal{F}(z)|^2 = \frac{\sin^2(z/2)}{(z/2)^2} \tag{7}$$

To remove the mean in (5), we consider the **variance increment** defined as

$$\Delta V_n \stackrel{\text{def}}{=} V_n - V_{n-1}, \tag{8}$$

which gives the variance on scales L_n about the means over twice that scale. Using (5), (8) becomes

$$\Delta V_n = \int_{-\infty}^{\infty} \frac{dk}{2\pi}\, S(k)\, \mathcal{D}(kL_n), \tag{9}$$

with

$$\mathcal{D}(z) \stackrel{\text{def}}{=} |\mathcal{F}(z)|^2 - |\mathcal{F}(2z)|^2 = \left[\frac{\sin^2(z/2)}{z/2}\right]^2. \tag{10}$$

According to (9) ΔV_n is simply a filtered version of the spectrum $S(k)$, with the band-pass filter function $\mathcal{D}(kL_n)$ isolating power in the wavenumber interval centered on

$$k_n \stackrel{\text{def}}{=} \frac{\pi}{L_n}. \tag{11}$$

Inserting into (9) a power-law wavenumber spectrum,

$$S(k) \sim k^{-\alpha}, -1 < \alpha < 2, \tag{12}$$

the effect of the filter on the spectrum gives $k_n^{-\alpha}$, and an additional factor of k_n comes from the dk, so that

$$\Delta V_n \sim k_n^{1-\alpha} \sim L_n^{\alpha-1} \sim 2^{n(1-\alpha)}. \tag{13}$$

In other words, if we observe a variance increment as in (13), then the spectrum must have the power-law given by (12). Taking the natural log of both sides of (13), we find that the spectral exponent α may be determined by

$$\alpha = 1 - \frac{\ln(\Delta V_n)}{n \ln 2} \tag{14}$$

Simple cascade models

We consider a stratocumulus cloud confined between the lifting condensation level and the inversion height, and initially having a uniform distribution of liquid water with optical depth given by

$$\tau_0 = 10. \tag{15}$$

We consider an infinitely long slab of horizontal width L_0, and divide it into two slabs of width $L_0/2$. A fraction of the liquid water is transferred from one half to the other, with the direction chosen at random. The optical depth in one half is then increased by some fraction, say f_1 (due to increased density — thickness is assumed unchanged), and the other half is correspondingly optically thinner. This may be written

$$\tau_1^{(\pm)} = (1 \pm f_1)\tau_0. \tag{16}$$

where the superscript on the left side of (16) indicates whether the brighter or darker half is being considered.

To continue the process, each half is itself divided in half, and a fraction of liquid water, f_2, is transferred, again in a random direction, so that

$$\tau_2^{(\pm)} = (1 \pm f_2)\tau_1. \tag{17}$$

After iterating for $n+1$ steps, there are 2^{n+1} segments, each with an optical depth of the form

$$\tau_{n+1}^{(\pm)} = \prod_{k=1}^{n}(1 \pm f_k)\tau_0. \tag{18}$$

Any of the possible combinations of signs in (18) may be found somewhere among the 2^{n+1} segments. An upper bound on the optical depth of the optically thickest segment may be found from

$$\prod_{k=1}^{n}(1 + f_k) < \prod_{k=1}^{n} \exp(f_k) = \exp(\sum_{k=1}^{n} f_k) \tag{19}$$

The fractions f_n are assumed to be stictly between 0 and 1, and we consider two models:

$$f_n = f, \text{ (singular model)} \tag{20}$$

where f is constant, and

$$f_n = fc^n. \text{(bounded model)} \tag{21}$$

where f and c are both constants between 0 and 1. The upper bound given by (19) diverges for the singular model, and it can be shown in this case that the liquid water becomes concentrated on a fractal set of singularities as $n \to \infty$. The upper bound for the bounded model is $\exp(fc/(1-c))\tau_0$ and provides a good estimate of τ_{max}.

From the variance increment defined in equation (8) we may compute the spectral exponent of both the singular model and the bounded model using (14). The computation is aided by the fact that the optical depth averaged over L_n is a constant independent of n, since liquid water is being conserved. Thus we may write

$$\begin{aligned} V_n &= \langle [\prod_{k=1}^{n} (1 \pm f_k)\tau_0]^2 \rangle \\ &= \prod_{k=1}^{n} \langle (1 \pm f_k)^2 \rangle \langle \tau_0^2 \rangle. \end{aligned} \tag{22}$$

While the optical depth is different for each segment in a given realization, the statistics are the same for all segments. If we let

$$\mu_k \stackrel{\text{def}}{=} \langle (1 \pm f_k)^2 \rangle, \tag{23}$$

then (22) may be written

$$V_n = [\prod_{k=1}^{n} \mu_k] \langle \tau_0^2 \rangle. \tag{24}$$

so that the variance increment becomes

$$\Delta V_n = [\prod_{k=1}^{n-1} \mu_k](\mu_n - 1)\langle \tau_0^2 \rangle. \tag{25}$$

For each of the models we obtain

$$\mu_k = 1 + f^2, \text{ (singular model)} \tag{26}$$

and

$$\mu_k = 1 + f^2 c^{2k}. \text{(bounded model)} \tag{27}$$

so that the variance increment in (25) behaves for large n as

$$\Delta V_n \sim (1 + f^2)^n, \text{ (singular model)} \tag{28}$$

and

$$\Delta V_n = \left[\prod_{k=1}^{n-1} (1 + f^2 c^{2k})\right] f^2 c^{2n} \langle \tau_0^2 \rangle. \text{(bounded model)} \tag{29}$$

Finally, using (14) we obtain

$$\alpha = 1 - \frac{\ln(1 + f^2)}{\ln 2}, \text{ (singular model)} \tag{30}$$

and

$$\alpha = 1 - 2\frac{\ln c}{\ln 2}. \text{(bounded model)} \tag{31}$$

where we used the fact that the factor in square brackets in (29) becomes independent of n for large n. Note that as $f \to 1$ the exponent of the singular model goes to zero, giving a flat (white noise)

spectrum, while as $f \rightarrow 0$ the spectrum steepens to k^{-1}. No value of f allows the singular model to fit the observed $\alpha = 5/3$ spectrum shown in figure 1b. The exponent of the bounded model is independent of f, and if we choose $c = 2^{-1/3}$ we obtain $\alpha = 5/3$. The probability density is quite sensitive to the value of c, and often has considerable structure. However, when $c = 2^{-1/3}$ it is close to lognormal, and qualitatively agrees with figure 1a.

Conclusions

The simple 2-parameter model presented here gives a reasonable fit to two important properties of vertically integrated stratocumulus liquid water : the lognormal-like probability density, and the power-law wavenumber spectrum. The model is being used to determine the radiative properties of fractal clouds, and investigate the limits of plane-parallel theory. Each cascade step redistributes liquid water in an initially plane-parallel cloud while cloud height and mean optical depth are held fixed at each step. Redistribution invariably decreases the mean albedo from the plane parallel case, since the albedo of optically thick regions saturates as optical depth is increased. The albedo of each homogeneous region may be computed from the thickness of each region independently only when the horizontal optical depth is large compared to the photon mean free path. The albedo of a region comparable in horizontal optical depth to the photon mean free path depends upon radiation from the sides. The mean albedo is insensitive to variations in optical depth on horizontal scales much smaller than the photon mean free path. Further development of these concepts will be closely tied to realistic simulations of the turbulent structure of boundary-layer clouds observed during FIRE.

References

Albrecht, B.A., D.A. Randall, and S. Nicholls, 1988: Observations of marine stratocumulus clouds during FIRE, *Bull. Amer. Meteor. Soc., 69, 618-626.*

Boers, R., and A.K. Betts, 1988: Saturation point structure of marine stratocumulus clouds, *J. Atmos. Sci., 45, 1156-1175.*

Cahalan, R.F. 1988a: LANDSAT observations of fractal cloud structure, in *Scaling, Fractals and Nonlinear Variability in Geophysics, D. Schertzer and S. Lovejoy, ed., Kluwer, in press.*

Cahalan, R.F. 1988b: Overview of fractal clouds, in *Advances in Remote Sensing Retrieval Methods, A. Deepak Publishing, in press.*

Cahalan, R.F., and J.H. Joseph, 1989: Fractal statistics of cloud fields, *Mon. Wea. Rev., 117, 257-268.*

Cahalan, R.F., and J.B. Snider, 1989: Marine stratocumulus structure during FIRE, submitted to *Remote Sensing of the Environment.*

Gage, K.S. and G.D. Nastrom, 1986: Theoretical interpretation of atmospheric wavenumber spectra of wind and temperature observed by commercial aircraft during GASP, *J. Atmos. Sci., 43, 729-740.*

Harshvardhan and D.A. Randall, 1985: Comments on "The parameterization of radiation for numerical weather prediction and climate models", *Mon. Wea. Rev., 113, 1832-1833.*

Harshvardan and J.A. Weinman, 1982: Infrared radiative transfer through a regular array of cuboidal clouds, *J. Atmos. Sci., 39, 431-439.*

Kraichnan, R.H., 1967: Inertial ranges in two-dimensional turbulence, *Phys. Fluids, 10, 1417-1423.*

Lorenz, E.N., 1979: Forced and free variations of weather and climate, *J. Atmos. Sci., 36, 1367-1376.*

Lovejoy, S., 1982: Area-perimeter relation for rain and cloud areas, *Science, 216, 185-187.*

MacVean, M.K., and S. Nicholls, 1988: A fine-resolution, two-dimensional numerical study of a cloud-capped boundary layer, *Proceedings of the 10th International Cloud Physics Conference, Bad-Hamburg, FRG, August 15-20, pp. 425-427.*

McKee, T.B. and S.K. Cox, 1974: Scattering of visible radiation by finite clouds, *J. Atmos. Sci., 31, 1885-1892.*

Rhys, Franz S., and A. Waldvogel, 1986: Fractal shape of hail clouds, *Phys. Rev. Lett., 56, 784-787.*

Schertzer, D., and S. Lovejoy, 1988: Multifractal simulations and analysis of clouds by multiplicative processes, *Atmos. Res., 21, 337-361.*

Stephens, G.L., 1976: The transfer of radiation through vertically non-uniform stratocumulus clouds, *Cont. Phys. Atmos., 49, 237-253.*

Stephens, G.L., 1985: Reply (to Harshvardan and Randall), *Mon. Wea. Rev., 113, 1834-1835.*

Welch, R.M. and B.A. Wielicki, 1985: A radiative parameterization of stratocumulus cloud fields, *J. Atmos. Sci., 42, 2888-2897.*

Statistical calibration: an application to the problem of estimation of wind speed

I.G. O'Muircheartaigh
University College, Galway, Ireland

E.C. Monahan
University of Connecticut, Avery Point, CT, USA

Introduction

It is well known that the extent of whitecap cover on the surface of a sea is greatly influenced by the surface windspeed (Monahan (1971), Toba and Chaen (1973), Wu (1979), Monahan and O Muircheartaigh (1980)). Other variables, such as sea surface temperature, are also important, but windspeed action appears to play the dominant role. Whitecap cover can be remotely sensed while windspeed cannot, so it is tempting to utilize the relationship between windspeed and whitecaps to infer reasonable values for the surface windspeed. To do so requires that the natural causative relation of "whitecaps — wind speed", quantitatively estimated from field data as a statistical regression of (some measure of) whitecap coverage on windspeed, be reversed. It turns out that the "natural" way of solving the problem, namely by regressing whitecap cover on windspeed and then inverting that regression relation, actually produces results that are inferior to those from some other procedures. Since the indirect remote sensing of windspeed is of operational interest, and since similar problems may well arise in different remote sensing, and other areas we present illustrative statistical data analyses of a number of whitecap-windspeed data sets in this paper.

The general problem of which the present case is a particular application is that of making inferences about the unknown $P \times 1$ vector X from a single random observed $Q \times 1$ response vector Y. The relationship between Y and X is "calibrated" with experimental data $(X_i, Y_i), i = 1, 2, \ldots, n$, where Y_i, X_i are $Q \times 1$ and $P \times 1$ vectors, respectively. The case $P = Q = 1$ has been extensively discussed in the literature, and reference will be made below to several basic contributions to calibration methods for this case. The case when at least one of P, Q is greater than one is the subject of a comprehensive paper by Brown (1982).

A brief outline of the paper is as follows: In section 2 we describe several different plausible methods of point estimation in univariate calibration. The methods described are subsequently applied to six data sets, and their performance evaluated in Section 3. Some general conclusions and comments are advanced in Section 4.

The Univariate Problem

The simplest version of the calibration problem is the case where $P = Q = 1$, and where the calibration curve is linear in both the parameters and the independent variable. The situation of interest may therefore be described as follows: given two random variables X, Y with the relationship:

$$Y = \alpha + \beta X + \varepsilon \tag{1}$$

where, more classically, $\varepsilon \sim N(0, \sigma^2)$, and given n independent pairs of observations (X_i, Y_i) on (X, Y) and a new observation y_0 on Y, how do we predict or estimate the corresponding value of $X = x(y_0)$? Numerous methods have been suggested, and their performances evaluated. Four of the methods, in particular, have been applied to six different data sets for the purposes of this paper. The methods in question are:

(i) The *"classical"* method: Estimate α, β in equation (1) by least squares, and then for $Y = y_0$ the predicted value of X is

$$X_C = (y_0 - \hat{\alpha})/\hat{\beta}, \quad \hat{\beta} \neq 0$$

(ii) Krutchkoff (1967) suggested another estimator obtained by rewriting (1) as

$$X = \gamma + \delta Y + \varepsilon$$

and obtaining least square estimators $\hat{\gamma}, \hat{\delta}$ of γ, δ; the predicted value of X, given $Y = y_0$, will then be

$$X_I = \hat{\gamma} + \hat{\delta} y_0$$

so denoted because it is known as the inverse estimator.

(iii) Lwin and Maritz (1980) proposed an alternative estimator based on the fact that, for this particular problem the predictor of X_0 is given by

$$X^*(y_0) = E\{X \mid Y = y_0\}$$

as a minimum mean-squared error (provided α, β and σ^2 are all known). By using consistent estimators of α, β and σ and by approximating the marginal distribution of X with the corresponding empirical distribution function, Lwin and Maritz showed that the estimator

$$X_E = \sum_{i=1}^{n} x_i f\{(y_0 - \hat{\alpha} - \hat{\beta} x_i) \mid \hat{\sigma}\} / \sum_{i=1}^{n} f\{(y_0 - \hat{\alpha} - \hat{\beta} x_i) \mid \hat{\sigma}\}$$

will, subject to easily satisfied regularity conditions, tend to the optimal estimator $X^*(Y_0)$ in mean square, where f is the error density function (presumed known, otherwise estimated).

(iv) An alternative version of the estimator X_E is derived by assuming that the distributions of X and Y/X are $N(\mu_x, \sigma_x^2)$ and $N(\alpha + \beta X, \sigma_y^2)$, respectively. Then, it is easily shown (O'Muircheartaigh and Gaver (1986)) that the empirical Bayes estimator of X, given $Y = y$, is

$$X_{EB} = [\hat{\sigma}_x^2 \hat{\beta}(y - \hat{\alpha}) + \bar{x}\hat{\sigma}_y^2]/[\hat{\beta}^2 \hat{\sigma}_x^2 + \hat{\sigma}_Y^2]$$

that this estimator has a number of significant properties, viz.,

(a) the estimator X_C tends to this estimator (when X and Y are highly correlated)

(b) this estimator is virtually identical to X_I (for any reasonably large sample size). This latter property provides some heuristic justification for using the inverse estimator X_I. We have, therefore, four different univariate estimators to be compared: (i) the classical predictor X_C

(ii) the inverse predictor X_I

(iii) the empirical predictor X_E

(iv) the empirical Bayes estimator X_{EB}

Evaluation of Univariate Predictors

The data

The performance of each of the above predictors was evaluated by applying it to the following eight data sets:

- Data set 1: Monahan (1971)
- Data set 2: Toba and Chaen (1973)

- Data set 3: JASIN experiment (1978) (Monahan et. al., (1981))
- Data set 4: STREX experiment (1981) (Monahan et. al., (1981))
- Data set 5: MIZEX experiment (1983)
- Data set 6: MIZEX experiment (1984)

Each data set consists of measurements of instantaneous oceanic whitecap coverage (Y) and wind speed (X), and the object of the exercise is the prediction of X_0, given a new observation y_0. The data sets also contain records of air temperature and water temperature at the observation site.

An initial inspection of the data suggested lognormal distributions for both X and Y and a log transformation gave an acceptable fit to a Normal distribution. Data points for which whitecap coverage was 0.0 were excluded from the analysis for several reasons, but particularly because it seemed reasonable to assume that a zero whitecap coverage gave no additional information in relation to wind speed over and above the conditional distribution of wind speed given zero whitecap coverage.

The number of data points used from the respective sets were $54, 36, 52, 84, 21$ and 38.

Cross-validation of estimative performance

For each data set, we excluded one data point at a time and obtained each of the three estimators based on the remaining data. We then predicted the x-value of the excluded point, given the y-value of the point, using each of the four estimators. This provided four values for each point in each data set. Finally, for each of the four estimators and for each data set, we calculated the mean bias (MB) and the mean-squared prediction error (MPSE) defined as follows for a given data set:

$$MB = \sum_{i=1}^{n}(x_i - \hat{x}_i)/n$$

$$MPSE = \sum_{i=1}^{n}(x_i - \hat{x}_i)^2/n$$

where n is the number of points in the data set.

Results

The results are presented in Tables 1 and 2.

Table 1. Bias of estimators

	Data sets					
Estimator	1	2	3	4	5	6
X_C	0.001	0.001	-0.001	-0.002	0.017	-0.001
X_I	0.001	-0.004	-0.004	0.000	-0.002	-0.001
X_E	0.001	-0.004	-0.001	0.001	-0.003	-0.001
X_{EB}	0.001	-0.004	-0.001	0.000	-0.002	-0.001

Table 1 shows that, in terms of bias, there is essentially no bias for any of the estimators for any data set, with the possible exception of estimator X_C for data set 5.

Table 2. Mean squared prediction error

Estimator	Data sets 1	2	3	4	5	6
X_C	0.121	0.144	0.125	0.108	0.255	0.228
X_I	0.071	0.085	0.074	0.063	0.093	0.085
X_E	0.072	0.086	0.076	0.065	0.092	0.087
X_{EB}	0.071	0.085	0.074	0.063	0.093	0.085

This table shows that in terms of average squared prediction error, the classical predictor is once again uniformly the poorest, having mean prediction error in the range two to three times that of any of the other estimators. The remaining estimators all have mean-squared error of the same order of magnitude, and indeed the homogeneity of these mean-squared prediction errors is a feature of the results, suggeseting that, purely in terms of predictive performance there is not a great difference between the latter three estimators. Some simulation studies (O'Muircheartaigh and Gaver (1986)) lend support and some qualification to this result.

Summary and Conclusions

This paper is an attempt to evaluate a number of wind-retrieval algorithms (statistical calibration methods) based on the relationship between wind-speed and instantaneous whitecap coverage, as determined from several data sets. We find that the inverse regression method and the almost equivalent empirical Bayes procedure suggested here are uniformly superior to the intuitively more appealing classical regression method. It would seem that the empirical Bayes method suggested here possesses the double benefit of being both an intuitively reasonable method, and giving (close to) optimal predictive performance.

References

Brown, P.J. (1982) Multivariate Calibration, *J.R. Statist. Soc.*, B, **44**, 287.

Krutchkoff, R.G. (1967) Classical and inverse regression methods of calibration. *Technometrics*, **9**, 425.

Lwin, T., and Maritz, J.S. (1980). A note on the problem of statistical calibration. *Appl. Statist.*, **29**, 135.

Monahan, E.C. (1971). Oceanic whitecaps. *J. Phys. Oceanography*, **1**, 139.

Monahan, E.C., Bowyer, P.A., Doyle, D.M., Fitzgerald, M.P., O' Muircheartaigh, I.G., Spillane, M.C. and Taper J.J. (1981). Whitecaps and the marine atmosphere. *Technical Report 3*, University College, Galway, Ireland.

O'Muircheartaigh I.G. and Gaver D.P. (1986). Estimation of sea-surface wind-speed from whitecap cover: statistical approaches compared empirically and by simulation. *Int. J. Remote Sensing*, **7**, No. 8, 985.

Toba, Y. and Chaen, M. (1973). Quantitative expression of the breaking of wind waves on the sea surface. *Rec. Oceanogr. Works Japan*, **12**, 1.

Principal oscillation pattern analysis of extra-tropical Rossby waves

H. von Storch and F. Gallagher
Max Planck Institüt fuer Meteorologie, Hamburg, FRG

Abstract

We introduce the "Principal Oscillation Pattern" (POP) analysis as a valuable tool to filter regularly evolving patterns from a data set. For that purpose, a multicomponent first order autoregressive process is fitted to the time series to be analyzed. The eigenvectors of the estimated system matrix are called POPs. They may be regarded either as one standing or two oscillating patterns depending on the eigenvalues, which may by real or complex. The decay time and the oscillation period can be inferred from the eigenvalue.

To demonstrate the merits of the proposed analysis technique, we consider Southern Hemisphere extratropical waves. For that purpose a zonal wavenumber analysis is done for a multi-year time series of daily 500 mb height fields of the Southern Hemisphere. The meridional distribution of cosine and sine coefficients of a given zonal wavenumber is analysed with the POP technique.

For zonal wavenumbers 5 to 9, two modes are found, which travel uniformly eastward. One mode has maximum intensity north of the 45°S-jet with longer periods (5 to 7.5 days) and decay times (3-6 days) and weak meridional momentum trransport. The other mode has maximum intensity south of the 45°S-jet, periods of 4.5 to 5.5 days and decay times of 1-3 days.

The result are found to be consistent with the result obtained with the more standard standard frequency wavenumber analysis.

Procrustes target analysis: Theory and applications

M.B. Richman
Climate and Meteorology Section, State Water Survey, Champaign IL, USA

Introduction

With the advent of increasingly higher-speed computers and commensurately sophisticated mathematical/statistical software, eigenanalyses of climatological data sets have become commonplace in the literature. To date, nearly all applications have been exploratory. Indeed, this is a strength of eigentechniques – they yield two simultaneous displays, typically functions of space and time, which have optimal data reduction properties (unrotated) and can be linearly transformed to emphasize regional or temporal anomalies for physical interpretation (rotated) . As such, eigentechniques have become one of the preferred multivariate tools for classification and dissection of large meteorological data sets and model output (e.g. , Barnston and Livezey, 1987; Kang and Lau, 1986 ; Lorenc, 1984; Pitcher and Geisler, 1987; Volmer et al. , 1984; wnite, 1988, Appendix D) . Frequently, we desire to relate the output of eigenanalyses to external variables for diagnostic or predictive purposes. Two representative examples of this type of approach are Walsh and Richman. (1981) who sought relationships between Pacific ocean SST eigenvectors and North American temperature anomalies and Lau and Lau (1986) who attempted to relate their velocity potential eigenvectors to the 40-50 day oscillation. Although some physical insight has been gained by relating eigenvectors to other fields, the purely exploratory nature of eigentechniques such as Principal Component Analysis (PCA) and Empirical Orthogonal Functions (EOF) will rarely yield modes of variation optimally associated with specific patterns of interest in secondary fields.

There are other multivariate techniques at our disposal to more accurately relate two sets of spatial patterns or time series. In order to accomplish this, we move away from purely exploratory techniques, to invoke a "quasi- confirmatory" analysis tool, Procrustes Target Analysis (PTA) . PTA provides for the incorporation of interesting a priori information, perhaps based on first principles, knowledge engineering, or some previous exploratory research, such that a set of eigenvectors are linearly transformed to be optimally related to this given information. In doing so, it yields a least-squares fit between two matrices, yet allows for the same simultaneous displays as other eigentechniques – a feature which enhances it's utility. The object of this paper is to (1) introduce and showcase PTA as an analysis tool and (2) provide examples of spatial and temporal applications.

Methods

Since PTA is a specific type of linear transformation of a group of PCs, it is useful to examine "typical" (hypothetical) flow charts of its operationalization (Fig. 1). PTA is termed quasi-confirmatory for two reasons@ (i) the analysis can yield results which differ from the initial a priori values we desire to fit and (ii) either the temporal or spatial display (PTA scores in Fig. 1) is unknown prior to the analysis. Hence, it lies somewhere in the middle of a continuum ranging from purely exploratory at one extreme to confirmatory at the other. Inspection of the flow charts reveal similarity to a standard PCA, with an important exception, the inclusion of a new input matrix, called the "target". Each box of Fig. 1, different from a standard PCA, will now be explored below in more detail.

The target matrix

This matrix is where the a priori information of interest is placed. The coefficients of the target can be as simple as a sequence of binary values (as will soon be illustrated) , specific coefficients based on

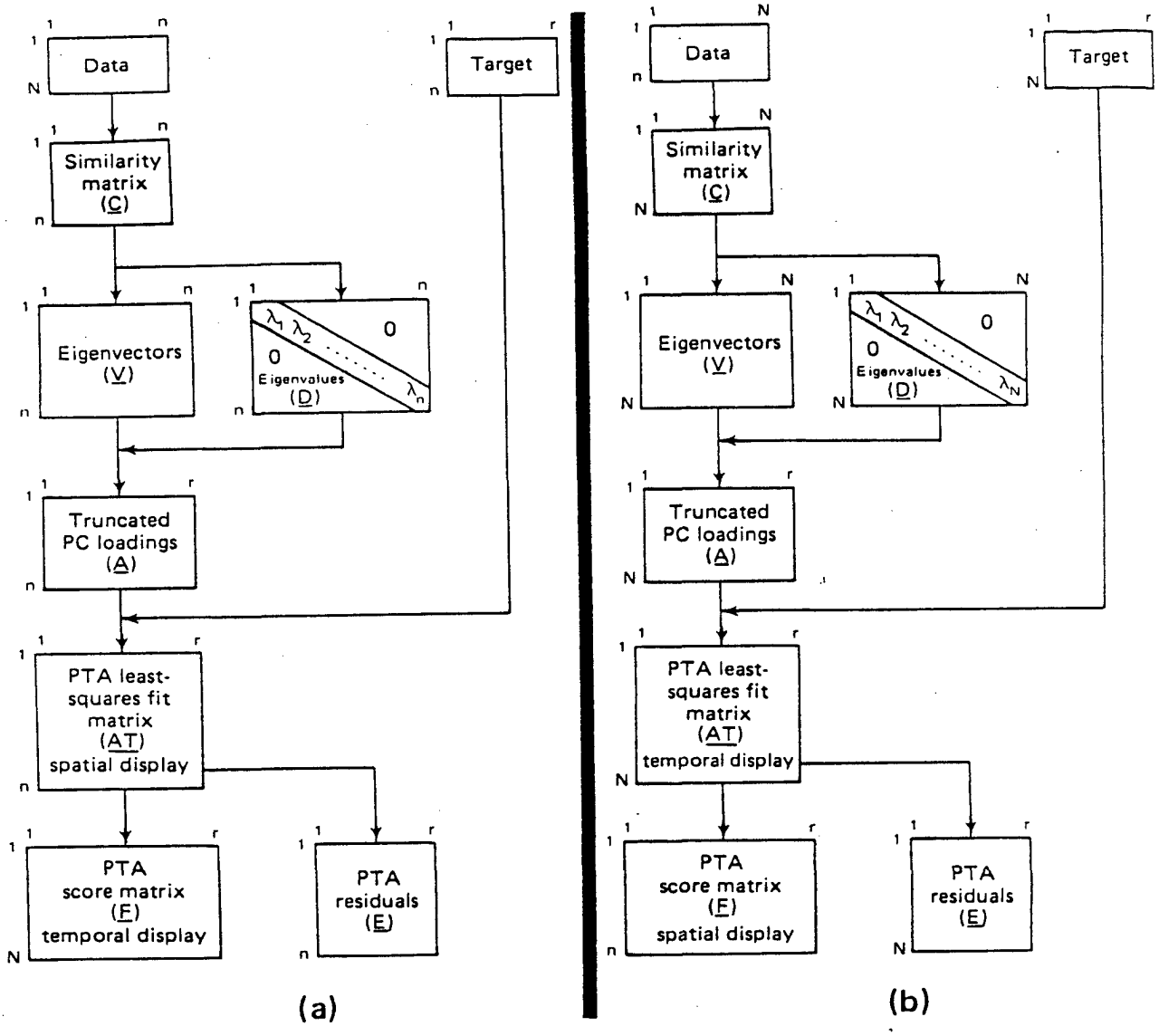

Figure 1: Two hypothetical flow diagrams for Procrustes Target Analysis (PTA) used in (a) S-mode analyses and (b) T-mode analyses.

prior analyses or a proxy time series of an external variable (such as the Southern Oscillation Index) . Since this matrix is fit, in a least-square sense, to the unrotated PC loadings (A) , it is useful to restrict the range of the relative magnitudes of the target coefficients to be similar to those in A. This is partly a function of the type of similarity matrix used in Fig. 1 (i.e. , correlation, covariance or cross-products).

The eigenanalysis

The component model is used in order to express much of the spatial or. temporal variability of C in terms of a more compact number of component- loading vectors which can then be rotated to maximal agreement with the target matrix. Only a brief description of the model as applied will be presented. The basic PTA equation in matrix form is

$$Z = FA^{\mathrm{T}} \tag{1}$$

where Z is the data matrix; F, the principal components or principal component scores; and A, the component loadings. A linear transformation can be applied to A such that

$$B = AT \tag{2}$$

where the matrix T transforms A into B under some constraint (see Richman, 1986). We will capitalize on this extensively; however, the matrix A has several properties which aid in its interpretation. These are its orthogonality (columns of a_j) and its relationship to the eigenvectors V: $A = VD^{1/2}$ where $D^{1/2}$ is the diagonal matrix of the square roots of the corresponding eigenvalues.

Typically, A is truncated at some point $r < n$ according to eigenvalue magnitude or eigenvalue separation characteristics.

The Procrustes Target Analysis

Since the criteria of interest (as stated in 2a above) serve as a known

target based on some prior knowledge or guess, a PTA is applied to determine to what degree such spatial or temporal patterns exist. Once B and A are obtained, only a T is needed, as shown in (2) , to find the maximal fit from

the data to the target. The solution to finding the correct T without rank restriction is as follows:

Let A and B be nxr matrices with $n \geq r$. We wish to find a transformation matrix T such that

$$\mathrm{trace}(B - AT)^{\mathrm{T}}(B - AT) = \mathrm{trace}(E^{\mathrm{T}}E) \tag{3}$$

is a minimum under the restraint that $\mathrm{diag}(T^{\mathrm{T}}T) = I$. Browne (1967) provides a numerical solution to the columns of T which will be summarized. A solution for the individual columns of T can be found: let t_m be the m-th column of T. Since At_m represents the approximation of the mth column b_m of the matrix B, the column vector t_m can be searched for, such that

$$g = \mathrm{trace}(b_m - At_m)^{\mathrm{T}}(b_m - At_m) \tag{4}$$

is at a minimum under the restraint $t_m^{\mathrm{T}}t_m - 1 = 0$. When all r columns of t_m $m = 1, \ldots, r$ of T are found, corresponding to the b_m of B, the T is found.

In order to minimize g under the restraint $t_m^{\mathrm{T}}t_m - 1 = 0$,

$$\frac{\partial g}{\partial t_m} - \frac{\partial}{\partial t_m}\theta\left(t_m^{\mathrm{T}}t_m - 1\right) = 0 \tag{5}$$

where θ is a Lagrangian multiplier. Taking the derivatives of (5) and setting the result equal to zero, yields

$$A^{\mathrm{T}} A t_m - \theta t_m = A^{\mathrm{T}} b_m \tag{6}$$

This solution can be simplified by applying an initial orthogonal transformation to t and diagonalizing $A^{\mathrm{T}} A$. This is accomplished by an $r x r$ orthonormal matrix P, such that

$$p^{\mathrm{T}} \left(A^{\mathrm{T}} A \right) P = D_c \tag{7}$$

where D_c is the diagonal matrix of eigenvalues $(c_l, ..., C_r)$ of $A^{\mathrm{T}} A$ and P, the corresponding eigenvectors such that $P^{\mathrm{T}} P = P P^{\mathrm{T}} = I$ Then define an $r \times 1$ column vector $w = P^{\mathrm{T}} t_m$ or $t_m = P w$ and premultiply (6) by P^{T}, using the previously given relationships to arrive at

$$D_c w - \theta w = (D - \theta I)\, w = u \tag{8}$$

where u is a $rx1$ column vector equal to $P^{\mathrm{T}} A^{\mathrm{T}} b_m$ The transformation of (6) to (8) is equivalent to rotating A to principal axis form. Since $t_m = P w$,

$$w^{\mathrm{T}} w = t_m^{\mathrm{T}} P P^{\mathrm{T}} t_m = t_m^{\mathrm{T}} I t_m = 1 \tag{9}$$

and (4) takes on the form

$$g = \mathrm{trace}(b_m - APW)^{\mathrm{T}} (b_m - APW) = 0 \tag{10}$$

Equations (8) and (9) can be rewritten as

$$w_i = u_i / (c_i - \theta) \sum_{i=1}^{r} w_i^2 - 1 = 0 \tag{11}$$

Browne (1967) notes that this form leaves $(r + 1)$ equations with $r + 1$ unknowns , θ, $w_1, ..., W_r$; however, a more convenient form with one equation and one unknown can be found by substituting (11) into (12)

$$h(\theta) = 0 \tag{12}$$

where

$$h(\theta) = \sum_{i=1}^{r} u_i^2 / (c_i - \theta)^2 - 1 \tag{13}$$

Browne (1967, p. 128) illustrates an example showing that the function h (8) tends to - 1 as θ tends to $+\infty$ or $-\infty$ and tends to $+\infty$ as θ approaches each c_i. One of the real roots of $h(\theta)$ corresponds to the absolute minimum of g and can be found via some numerical procedure (i.e. , Newton's method for finding the roots of a polynomial equation) which yields the w_i in (11) , and the vector t_m from (9) can then be found, and hence T.

The matrix AT is the least squares fit to B:

$$B = AT + E \tag{14}$$

where E constitutes the residuals (Richman, 1986, pp. 316-317). These matrices AT and E are both plotted (temporally or spatially) and examined for fit to B.

Once the matrix AT is found, standard calculation of the PTA scores (identical to PC scores) can performed by a variety of techniques. A least squares fit is shown. Defining $G = AT$, then following (1) ,

$$F = Z \left(G^{\mathrm{T}} G \right)^{-1} G^{\mathrm{T}} (15) \tag{15}$$

The matrix F contains the time series (S-mode) or spatial patterns (T-mode) associated with the fit to the target B as shown in Fig. 1. This can be mapped to indicate where or when the targeted conditions occurred, depending on if a T- or S-mode analysis is used.

Application

Several applications will now be explored, illustrating the potential utility of PTA. The first, based on Richman and Easterling (1988) , will be a T-mode analysis of climate fluctuations thought to negatively impact corn production in the Midwest portion of the United States, One interesting aspect of the study was the manner in which the target was derived. Specifically, a knowledge engineering approach was used in an interviewing process of agricultural experts to identify which corn production management practices and phenological growth stages were sensitive to moisture availability and to assess the degree of change in moisture availability necessary to measurably impact these. The results suggested two major periods of vulnerability@ April-May and July-August. The first corresponds with spring planting and emergence. Too much spring rainfall usually leads to planting delays, diminished fertility and discourages the vertical penetration of root systems. This places the crop at an increased risk if the rainfall drops below normal during the Summer. The second period is the combined corn reproduction, ear development and grainfill stages. Moisture and nutrient uptake is high during this period and insufficient amounts of either are detrimental (Huff and Neill, 1982). The target criteria were thus set as a wet late spring (May) followed by a dry mid to late summer (July, August) to facilitate testing our hypothesis of climate negatively impacting corn production. In order to operationalize PTA, this information was formed into coefficients for a simple target, B, of +1.0 for wet conditions (Mays) followed by -1.0 for dry conditions (Julys, Augusts) as shown in Fig. 2. Additionally, long sequences of these wet/dry combinations were sought after (15-year sequences) in the hope that some discernable effect or impact might emerge when yield data were examined. Years not included in each of the 15-year sequences of Fig. 2 were set to zero.

Results of the PTA were a new time series which best fit the target. In this case approximately 90 percent of the signs of AT were in agreement with B; however, the magnitudes were all ¡ 10.401 . This led us to cautiously proceed, further testing the results in a Monte Carlo framework (see Richman and Easterling, 1988, pp. 10,994-11,002 for further details). The key result desired were the PTA scores, which in a T-mode analysis, are the spatial patterns associated with wet Mays followed by dry Julys and Augusts. Two adjacent 15-year panels are shown in Fig. 3 for the years 1951-1965 and 1966-1980.

Those areas in Fig. 3 isoplethed by $+1\sigma$ (H's) are interpreted as a positive match to the target, whereas those isoplethed by -1σ (L's) are interpreted as an inverse match (dry Mays followed by wet Julys/Augusts) . The results indicate a dipole of these conditions in northern Illinois/Indiana versus southern Illinois/Indiana which reversed phase through time (see Richman and Easterling, 1988, their Fig. 7, for detail). These were found to have a measurable impact on corn production when yield data were subsequently examined.

The second example is a S-mode analysis taken from Richman and Lamb (1989). The scientific question posed was: how do short-term synoptic rainfall patterns (based on 3-day totals) build into longer term rainfall patterns (based on 1 30-day totals) . The 3-day patterns had been identified previously and rigorously tested for stability (Richman and Lamb, 1985, 1987, 1988).

These spatial patterns (Fig. 4a) served as the input data while the 30- day regionalizations (Fig. 4d) formed a precise target to 4 decimal places (in contrast to the previous example) . Results of the PTA (Fig. 5) show an excellent fit for 14 of the 15 patterns, thereby confirming that there is a strong link between the two temporal scales (3- and 30-day) , although their VARIMAX-based regionalizations of Fig. 4 differ somewhat. Calculation of the PTA scores (time series) enabled us to test exactly when the longer-term patterns were "shocked" by high-frequency rainfall events, as well as providing information on the nature of how synoptic events provide the building block of climate. Further information is contained in Richman and Lamb (1989) .

May 1949	+	1.0
July 1949	-	1.0
Aug 1949	-	1.0
May 1950	+	1.0
July 1950	-	1.0
Aug 1950	-	1.0
●		●
●		●
●		●
●		●
●		●
May 1963	+	1.0
July 1963	-	1.0
Aug 1963	-	1.0
May 1964		0.0
July 1964		0.0
Aug 1964		0.0
●		●
●		●
●		●
●		●
●		●
May 1980		0.0
July 1980		0.0
Aug 1980		0.0

Figure 2: Target matrix for 1949-1963 wet May (+1.0) and dry July and August (-1.0). Similar matrices were used in remaining analyses (i.e. 1950-1964, 1951-1965, etc., with the last being 1966-1980). From Richman and Easterling (1988).

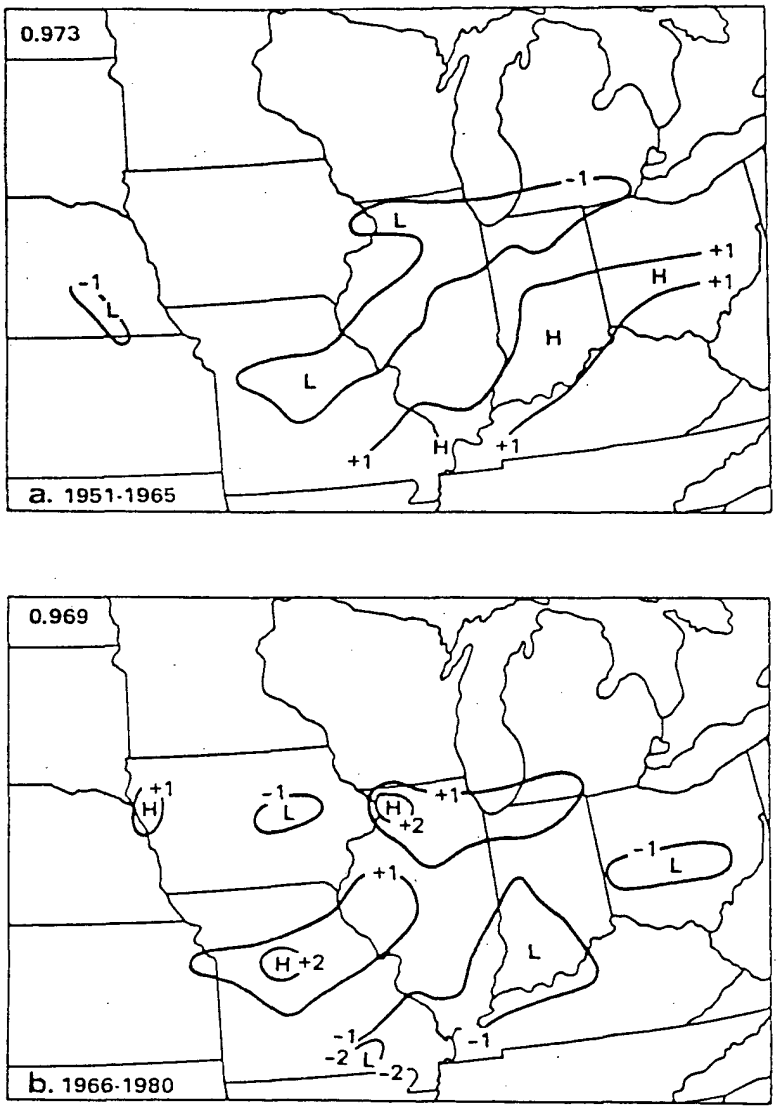

Figure 3: Spatial maps of the PTA scores (in Z-score units) (matrix F in Fig. 1b) for two analyses based on wet May/dry July and August for (a) 1951-1965 and (b) 1966-1980. The coefficient in the upper left-hand corner of each map represents the PTA scores correlation with actual rainfall deviations. From Richman and Easterling (1988).

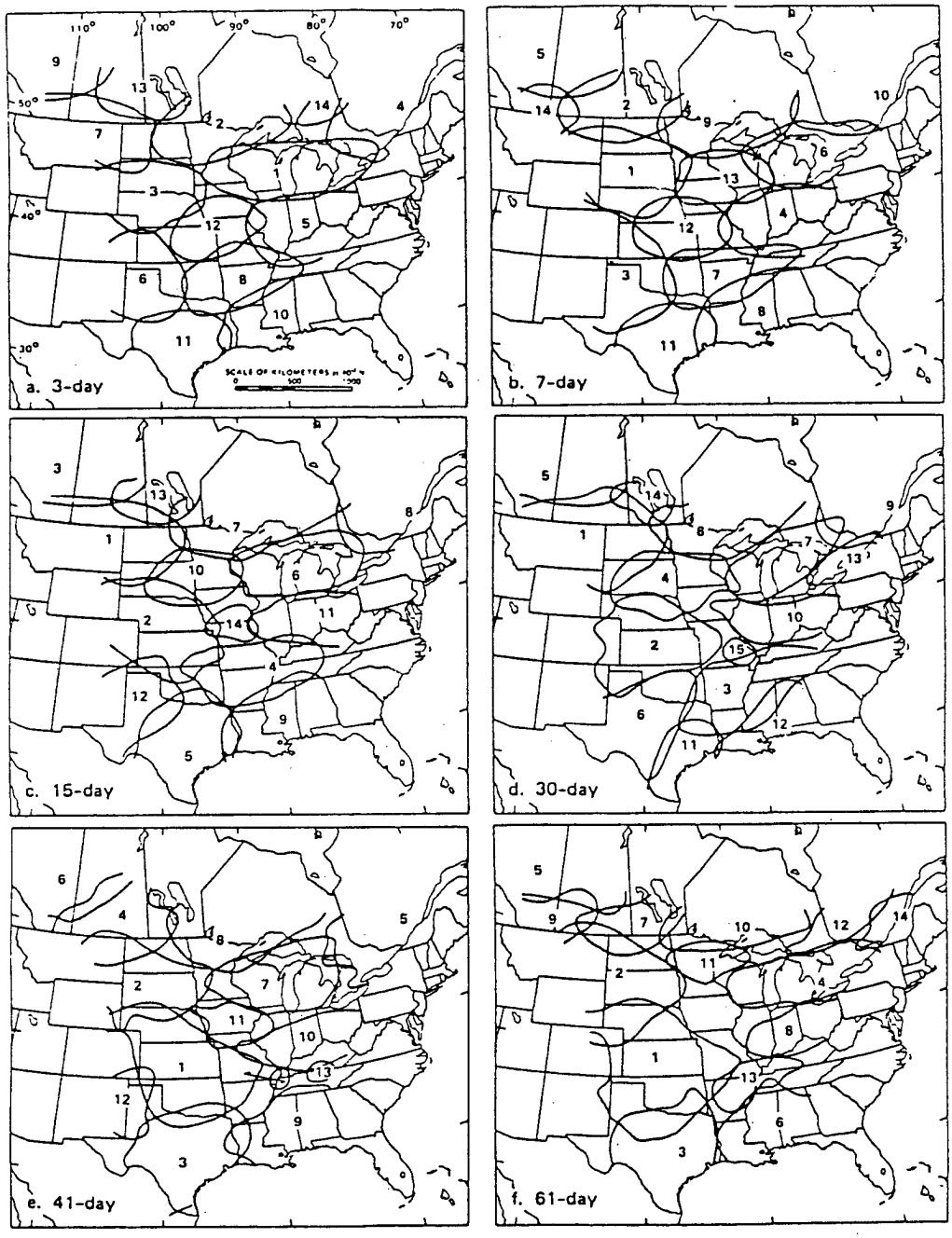

Figure 4: Regionalization of central North America based on the +0.4 loading isopleths of Varimax Rotated Principal Components patterns for (a) 3-day rainfall totals, (b) 7-day rainfall totals, (c) 15-day rainfall totals, (d) 30-day rainfall totals, (e) 41 day rainfall totals, and (f) 61-day rainfall totals. From Richman and Lamb (1988).

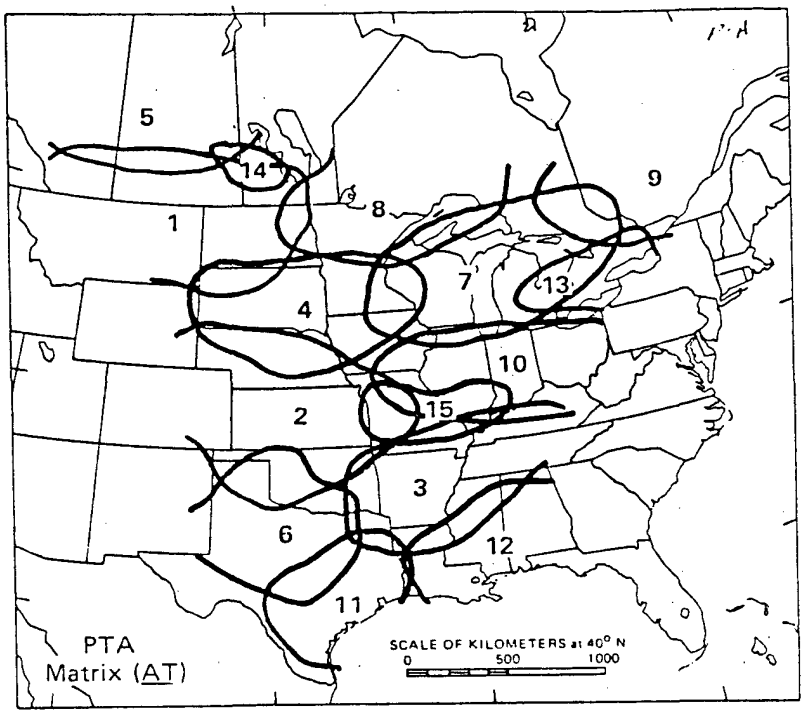

Figure 5: PTA least-squares fit matrix (AT) (see Fig. 1a) of three-day data to thirty-day target (Fig. 4d). The +0.4 PTA loadings are isoplethed to yield a regionalization of 3-day rainfall optimally matching the 30-day regionalization. From Richman and Lamb (1989).

Summary and concluding remarks

This paper mathematically describes PTA and its application to climate research. Since this technique has not been widely used in the geophysical literature, it is instructive to point out the basic differences between PTA and the traditional approach of extracting individual EOFs/PCs and relating these to a secondary variable or target.

The traditional unrotated approach would have yielded a series of standard predetermined patterns for our rectangular domains having little physical meaning themselves (Richman, 1986, 1987) . Application of a linear transformation might have helped to increase our chances of finding physically meaningful modes (e.g. , see Richman and Lamb, 1985, 1987) ; however, finding an optimal relationship between any individual EOF/PC and the target would likely be a chance occurrence. The PTA differs in that it does not examine each vector individually, rather it weights each vector retained in a new linear combination to maximally fit the target. The applications of PTA herein with prescribed targets in a PCA framework had positive results locating coherent spatial regions which contained the types of temporal fluctuations desired (wet Mays/dry Julys, Augusts and the inverse situation in the first example or those based on short-period rainfall in the second example) . However, there is no guarantee that the data can be transformed to fit the target since the correlation/covariance structure remains a fixed property. Consequently the target should be defined with care and deliberation.

Future applicatIons of PTA would benefit if some method of placing quantitative confidence limits on the degree of target fit could be resolved. This issue is perhaps the weakest link in PTA at present, since there has been little applied research published on the technique. So, while PTA offers new freedom to specify an interesting hypothesized spatial pattern or time series to a PCA, it also adds some new constraints?? target specification and assessment. Thus with PTA one can no longer use default criteria on statistical packages to arrive at a final analysis with no intermediary intervention (see Richman, 1988) , rather it demands the full utilization of the investigator's knowledge of the study domain. In cases where there is some a priori theoretical idea of a cause and effect (say, based on first principles, knowledge engineering, or some previous exploratory research) , the target can be constructed to reflect the forcing to look for a response. Such diverse meteorological applications as time series modeling of El Nino, emergence of geopotential patterns thought to be associated with drought, and grouping chemical elements with potential sources can benefit from a technique such as PTA. It is hoped other scientists will exploit this interesting multivariate tool.

Acknowledgements. This research was supported by NSF grant ATM 85-20877. The author extends his gratitude to Peter J. Lamb for his constructive comments on the applications work and to Linda Riggin, Rebecca Runge and Phyllis Stone for their technical assistance.

References

Barnston, A.G., and Livezey, R.E., 1987: Classification, seasonality and persistence of low-frequency atmospheric circulation patterns. *Mon. Wea. Rev.*, **115**, 1083-1126.

Browne, M.W. , 1967: On oblique procrustes rotation. *Psychometrika*, **32**, 125-132.

Huff, F. A. and J. C. Neill, 1982: Effects of natural climate fluctuations on the temporal and variation in crop yields. *J. Clim. Appl. Meteor.*, **21**, 540-550.

Kang, I-S . and N-C. Lau, 1986: Principal modes of atmospheric variability in model atmospheres with and without anomalous sea surface temperature forcing in the tropical Pacific. *J. Atmos. Sci.*, **43**, 2719-2735.

Lau, N-C. and K-M. Lau, 1986: Structure and propagation of intraseasonal oscillations appearing in a GFDL GCM. *J. Atmos. Sci.*, **43**, 2023-2047.

Lorenc, A. C. , 1984: The evolutIon of planetary scale 300 mb divergence flow during the FGGE year. *Quart. J. Roval Meteor. Soc.*, **110**, 427-441.

Pitcher, E. J. and J. E. Geisler, 1987: The 40- to 50-day oscillation in perpetual January simulation with a general circulation model. *J. Geophys. Res. (Atmospheres)*, **92**, 11,971-11,978.

Richman, M. B. , 1986: Rotation of principal components. *J. Climatology*, **6**,293-335.

Richman, M. B. , 1987: Rotation of principal components: A reply. *J. Climatology*, **7**, 511-520.

Richman, M. B. , 1988: A cautionary note concerning a commonly applied eigenanalysis procedure. *Tellus*, **40B**, 50-58.

Richman, M. B. and W. E. Easterling, 1988: Procrustes Target Analysis A multivariate tool for identification of climate fluctuations. *J. Geophys. Res. (Atmospheres)*, **93**, 10,989-11,003.

Richman, M. B. and P. 1 . Lamb , 1985 : Climatic pattern analysis of three- and seven-day summer rainfall in the central United States: Some methodological considerations and a regionalization. *J. Clim. Appl. Meteor.*, **24**, 1325-1343.

Richman, M. B. and P . J . Lamb , 1987 : Pattern analysis of growing season precipitation in southern Canada. *Atmos.-Ocean*, **25**, 137-158.

A

Richman, M. B. and P. J . Lamb , 1988 : On the modes of growing-season precipitation over central North America. *Proc. Twelfth Annual Climate Diagnostics Workshop.* U. S. Dept. of Commerce, Washington, DC, 284-291.

Richman, M. B. and P. J . Lamb, 1989 : On the interannual variability of growing season precipitation in central North America. *Proc. Thirteenth Annual Climate Diagnostics Workshop*, U. S. Dept. of Commerce, Washington, DC, in press.

Volmer, J. P. , M. Deque and D. Rousselet, 1984: EOF analysis of 500 mb geopotential: a comparison between simulation and reality. *Tellus*, **36A**, 336-347.

Walsh, J. E. and M. B. Richman, 1981: Seasonality in the associations between temperature over the United States and North Pacific Ocean. *Mon. Wea. Rev.*, **109**, 767-783.

White, D. A. , 1988: Climate regionalization: A comparison of principal component analysis rotation schemes. Unpublished Ph.D. thesis. The Pennsylvania State University.

Statistical models for cloud-free viewing climatologies

D.D. Grantham
Geophysical Laboratory, Hanscom Air Force Base, Mass., USA

Abstract Many space satellite technologies require a cloud-free path or viewing area of the earth's surface. Any sensor or system operating in the visible, infrared or submillimeter regions of the electromagnetic spectrum will be affected by clouds along the transmission path. Currently available cloud climatologies are not adequate to evaluate cloud impacts on emerging new space-borne systems. Therefore, statistical models must be developed to extend current cloud climatologies to describe the probability of cloud- free lines-of-sight and cloud-free fields-of-view from space to earth and vice versa. A major problem with cloud climatologies is the viewing angle bias introduced by the manner in which cloud scenes are observed (Grantham and Boehm, 1986). As a satallite passes over a scene, the amount of cloud cover will be less at its zenith angle than at its limb scan angle. A ground observer will estimate the sky cover relative to an imaginary sky dome. Neither system gives an accurate estimate of earth cover. Thus, new methods must be developed to normalize such climatologies before they can be used as imput for descriptive cloud models.

A brief update on modeling PCFLOS climatology will be given. Then new procedures will be described to statistically evaluate a cloud simulation model using a new data base from a six station network of whole-sky imagery systems. This network will used to develop joint occurrence CFLOS statistics with high temporal resolution (one-minute CFLOS and cloud-free area data). A major emphasis in the simulation model evaluation will be how to incorporate spatial and temporal correlations of CFLOS and cloud-free areas to span distances from less than a kilometer to hundreds of kilometers and to span times from minutes to days.

References

Grantham, D.D., and Boehm, A.R., 1986: The effect of viewing aspect on climatological cloud distributions. *Proc. 3ICSC*, Vienna.

A Gaussian curve fitting algorithm for a satellite-derived cloud climatology

A.J. Gorman and J. McGregor
Institute of Geophysics, Victoria University, Wellington, NZ

Abstract

We develop a new approach for the fast and efficient derivation of a regional cloud climatology from satellite data. By the adaptation and utilization of a gaussian curve fitting algorithm which was first developed in the study of fish distributions (MacDonald and Pitcher, 1979) we derive climatologically relevant information. The data base used was provided by the New Zealand Meteorological Service. It consists of over 50 000 images from the AVHRRs (Advanced Very High Resolution Radiometers) flown on the NOAA polar-orbitting satellites. The images cover an area of 128 x 192 km in the southern part of the North Island, New Zealand over a period from October 1981 to the present.

Existing algorithms developed primarily for operational purposes derive cloud parameters from single images. These algorithms which are often very complex generally perform well for operational applications, however in the case of climatological studies, the detailed spatial pattern analysis inherent in these methods is largely unnecessary. Climatological studies require the analysis of the many thousands of images and complex spatial analysis employed by these methods would necessitate a huge amount of computer resources. An additional consideration is that existing algorithms are much less successful at identifying cloud parameters when the underlying surface terrain is rapidly varying (as in the case of New Zealand). Consequently they would require futher development and presumably made even more complicated for application in such regions.

In this paper we develop an algorithm which is independent of the initial spatial analysis of imagery and yet is able to produce a regional cloud climatology. The method employed is based on the finding that frequency distributions of the AVHRR's radiance counts, for a given pixel or group of pixels for a given period of time, display some relatively well defined characteristics (Gorman and McGregor, 1988) similar to those found by MacDonald and Pitcher (1979). The sum of four independent Gaussian distributions adequately describe these frequency distributions and these can be considered to represent the earth's surface and the different levels of cloud in the earth's atmosphere. The gaussian fitting routine evaluates the parameters of each distribution, and thus directly provides mean sensed temperature and variance at each of these levels from which the frequency of occurence of different cloud type can be found.

References

MacDonald, P.D.M., and Pitcher, T.J., 1979: Age groups from size- frequency data: a versatile and efficient method of analyzing distribution mixtures. *J. Fish. Res. Board Canada*, **36**, 987-1001.

Gorman, A.J., and McGregor, J., 1988: The use of AVHRR satellite data for climatological studies. *Weather and Climate*, (to appear).

An orographic wave cloud climatology using AVHRR satellite data

J. McGregor and S.K. Riches
Institute of Geophysics, Victoria University, Wellington, NZ

Abstract

Orographic wave clouds formed off mountain ranges provide an important indicator of prevailing meteorological conditions and in particular warning of possible hazards to aviation (Knudsen, 1988). Satellite imagery reveals New Zealand's various mountain ranges as important sources of such wave clouds.

In this study we use seven years of Advanced Very High Resolution Radiometer (AVHRR) data from the NOAA series of polar orbitting satellites to investigate wave clouds formed off the Tararua mountain range in the southern North Island of New Zealand. The data consists of more than 10 000 images for each channel of the AVHRR instrument. This provides an excellent base for a climatological study, though clearly with a data base of this magnitude computer processing techniques are the only feasible means of analysis.

We have developed and implemented a pattern recognition algorithm which analyses the satellite images and recognises the presence of wave cloud activity east of the Tararua Ranges. The algorithm provides wavelength and cloud top temperature and when applied to the entire data set allows the examination of the frequency of occurence, seasonal dependence, as well as the frequency distributions of wavelengths and cloud top temperatures.

References

Knudsen, P., 1988: Mountain lee wave forecasting for aviation. Report for Dip. Appl. Sc.(Met), VUW.

Sampling errors in satellite-derived tropical rainfall climatology using a space-time stochastic model

Thomas L. Bell
Laboratory for Atmospheres, Goddard Space Flight Center, Greenbelt, MD, USA

Introduction

The roles of tropical rainfall both in the energy budget of the planet and in affecting planetary waves that control weather patterns over the globe are important ones, and yet rainfall rates in the tropics are very poorly monitored at present. NASA has recently undertaken a study of the feasibility of orbiting a satellite specifically designed to provide quantitative measurements of rainfall in the tropics. the Tropical Rainfall Measuring Mission (TRMM). The motivation for the mission and its scope are discussed by Simpson *et al.* (1988).

A primary goal of TRMM will be to provide accurate monthly averages of tropical rainfall within areas of the order of 500 km × 500 km. There will be two sources of error in these averages, broadly speaking: inaccuracies in the measurements of rain rate , and "sampling" problems associated with the satellite's only being able to observe a given area intermittently. The impact of the first kind of error. "retrieval" error, may in principle be considerably reduced by taking averages over enough observations (by using monthly averages of the data over large enough areas) provided retrieval algorithms can be developed that generate unbiased estimates of rainfall.

The size of the second kind of error, arising from intermittent observation by the satellite, depends on how well sampled the area is during a month, and is determined by the orbit of the satellite and the size of the swath scanned by the satellite as it passes over, and by the statistical characteristics of the observed rainfall. It is the dominant contribution to the error in monthly averages if systematic error in the retrieval algorithms is small. We shall describe here a baseline calculation of this sampling error assuming that information is available only from the TRMM satellite itself. Although we shall focus on the particular observational configuration offered by TRMM, our approach is obviously applicable to studies of sampling errors for other satellite systems monitoring other geophysical quantities.

As a measure of error we shall use the root mean square (r.m.s.) difference between the actual rain rate averaged over a month and the mean of the satellite observations during that month. The true monthly averaged rain rate is

$$R = \frac{1}{T}\int_0^T \mathrm{d}t \, \frac{1}{A}\int_A \mathrm{d}^2\mathbf{x}\, r(\mathbf{x},t), \tag{1}$$

where $r(\mathbf{x},t)$ is the rain rate at location $\mathbf{x}$, t is the time since the beginning of the month, and T and A are the period (1 month) and area averaged over. The satellite observes some part A_i of the area at times t_i during the month. The area average of the observed rainfall is given by

$$r_i = \frac{1}{A_i}\int_{A_i} \mathrm{d}^2\mathbf{x}\, r(\mathbf{x},t_i) \tag{2}$$

A satellite-based estimate of the true rainfall R can then be written as

$$\hat{R} = \sum_{i=1}^{M} A_i r_i \Big/ \sum_{i=1}^{M} A_i, \tag{3}$$

where M is the number of overflights of the area during the period T. More sophisticated weighted averages of the observations are possible, making better use of the spatial and temporal correlations of the rainfall. Equation (3) simply gives each observation at each point in the area equal weight.

The r.m.s. error E can now be written in terms of these definitions as

$$E^2 \equiv \langle (\hat{R} - R)^2 \rangle, \tag{4}$$

where the brackets $\langle \cdot \rangle$ indicate an average over an ensemble of possible histories of rainfall during the month. The error E represents the typical size of errors in satellite estimates of monthly averaged rain over many months of observations or over many climatologically similar areas. Implicit in using r.m.s. error is the idea that the errors $\hat{R} - R$ might be approximately normally distributed with standard deviation E. We find that this is the case in our simulations, even though the instantaneous area-averaged rainfall is far from being normally distributed.

The r.m.s error E in (4) is in principle completely determined by the covariance statistics of point rainfall. It is a difficult and subtle task, however, to extrapolate the statistics obtained from rain gauges to the area and time averages needed in (4), because the spatial and temporal variability of rainfall are so extreme. The areal coverage provided by radar is more nearly comparable to the averaging areas to be used for TRMM, but well calibrated data from the tropical oceanic regions are not easy to find. In the study presented here we have in fact limited ourselves to radar data collected in the GATE (Global- Atmospheric-Research-Program Atlantic Tropical Experiment) during the summer of 1974.

An early attempt at obtaining E was made by Laughlin (1981), who estimated it for a satellite that visits the area at equal intervals Δt and views the entire area each time. He was able to write E^2 in terms of the variance of the area-averaged rain rate σ_A^2, and of the correlation time τ_A of the area- averaged rain rate, as

$$E^2 = \sigma_A^2 f(\Delta t, \tau_A, T). \tag{5}$$

His derivation is reviewed by Shin and North (1988), who have improved on his method by taking into account the actual visit times of the satellite and fractional coverage of the visits, albeit with some approximations.

Our approach here will be to simulate the rainfall over an area with a statistical model, and to "fly" a satellite in a TRMM-like orbit over the simulated rainfall, computing the r.m.s. error (4) from multiple trials each a month long. The rainfall model is adjusted to have spatial and temporal variability with covariance statistics matching as well as possible those observed in GATE. Some choices must be made in extrapolating the GATE results to spatial and temporal scales larger than those of GATE. These choices affect the size of E we compute.

The advantages of the Monte Carlo approach are that it offers a convenient vehicle for including in the calculation of E the effects of the dependence of rainfall statistics on the fraction of the area observed by the satellite during a given pass; and it gives some insight into the probability distribution of errors. The disadvantages are that it gives results whose accuracy depends on the number of months in the simulation. As always, the results depend on the ability of the model to capture the relevant statistics of real rain.

The methods and results presented here are described in greater detail by Bell *et al.* (1989).

Method

The Monte Carlo calculation requires a model for the time varying rain field and a description of the sampling characteristics of the satellite. The orbit of the satellite is determined using the approximations described by Brooks (1977). The viewing characteristics of the satellite instruments are assumed to be similar to those of the Electrically Scanning Microwave Radiometer (ESMR) flown on the NIMBUS V satellite. This implies that in our calculations, when the field of view of the instruments is included, the effective size of the swath seen by the satellite extends to about 54° to either side of nadir.

The model for the rain field will be briefly described here. See Bell (1987) for more details. It is based on the possibility of generating a spatially correlated field of variables that are multivariate Gaussian, by the standard technique of expressing the field as a sum of uncorrelated Fourier components,

$$g(\mathbf{x},t) = \sum_{\mathbf{k}} a(\mathbf{k},t)\exp(i\mathbf{k}^{\mathsf{T}}\mathbf{x}), \tag{6}$$

where $\mathbf{x}$ labels grid points on a 1024 km $\times$ 1024 km grid with a grid spacing 4 km. The transformation (6) can be carried out very rapidly numerically using "fast-Fourier transform" (FFT) methods. Once the Gaussian field g is computed, it is converted at each grid point to a rain rate with a transformation $r = \mathcal{R}(g)$, arranged so that r is set equal to zero when g falls below a threshold, and non-zero r are lognormally distributed with parameters that match rain rate data. In our simulations r is nonzero 8.3% of the time, and the mean and variance of $\ln r$ is fixed at $\mu = 1.13$ and $\sigma^2 = 1.1$, following the estimates for GATE rainfall developed by Kedem *et al.* (1989).

The behavior of the Fourier amplitudes $a(\mathbf{k},t)$ in (6) must be specified. These are assumed to be independent first-order Markov processes with zero mean and variances adjusted to generate the desired spatial correlations in the rain field. The correlation time of each amplitude depends on the wavenumber $\mathbf{k}$. These correlation times are adjusted so that the correlation times of area-averaged rain rate, as a function of the size of the area, agrees with what is observed in the GATE data. Details of these procedures, and of the GATE statistics that are used to prescribe the statistics of the model, are given in Bell *et al.* (1989). As a result of the fitting process, the spatial correlation of the model rain rate field as a function of spatial separation s, for rain rates with 4 km spatial resolution, is described by the empirical fit

$$r(s) = (1.2s - 2.2)^{-0.29}\exp(-s/78), s \geq 4\text{km}.$$

The variance of rain rate averaged over a 512 km square, [which would be σ_A^2 in Eq. (5)], is $0.18\,\text{mm}^2/\text{h}^2$. The correlation times of area averaged rain rate [τ_A in Eq. (5)] range from 0.8 hours for a 4 km $\times$ 4 km area to 10.6 hours for a 512 km $\times$ 512 km area.

Once the statistical properties of the model are determined, a Monte Carlo estimate of the r.m.s. error (4) is in principle obtained by simulating many months of rainfall, and computing the r.m.s. difference between the satellite estimate (3) and the true mean (1). If we let $\hat{R}^{(\alpha)}$ and $R^{(\alpha)}$ be respectively the estimated and true mean rain rate during month α, and define

$$\Delta R^{(\alpha)} = \hat{R}^{(\alpha)} - R^{(\alpha)} \tag{7}$$

to be the error for that month, a Monte Carlo estimate of E based on N simulated months would be

$$\hat{E}^2 = \frac{1}{N}\sum_{\alpha=1}^{N} (\Delta R^{(\alpha)})^2 \tag{8}$$

and the standard error of this estimate would be

$$\sigma(\hat{E}^2) = \frac{1}{\sqrt{N}}\{\text{var}[(\Delta R^{(\alpha)})^2]\}^{1/2} \tag{9}$$

The Monte Carlo accuracy is proportional to $N^{-1/2}$. In order to increase the accuracy of the Monte Carlo calculation, we have estimated the r.m.s. error E for 6-day averages instead of for 30-day averages. It can be shown that, to an accuracy of a few percent, for averaging times $T \geq 6$ days the error E^2 scales with $1/T$, and so the error E^2 for $T = 30$ days is just 1/5 the error found for $T = 6$ days. With this device the Monte Carlo accuracy (9) for the same length computer run can be improved by a factor of $5^{1/2}$.

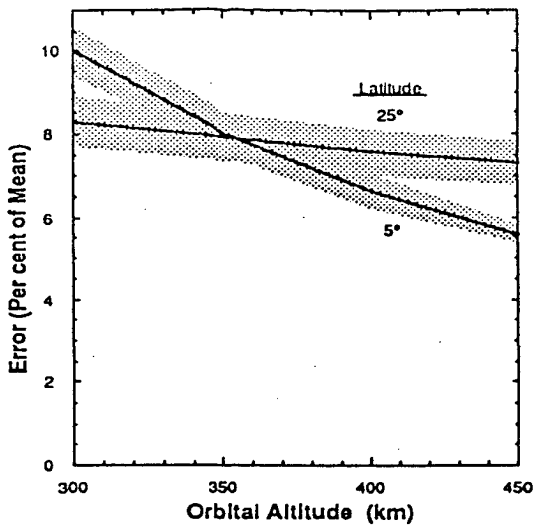

Figure 1: Sampling error for monthly averaged rainfall over a 512 km square area for a satellite in a 35° inclination orbit. The shaded areas denote s confidence limits.

Monte Carlo Results

The sampling error associated with TRMM-like satellite observational patterns was first obtained for 30° inclination satellite orbits at two altitudes, 300 km and 450 km. The error E was evaluated for monthly averages over 512 km square boxes centered at two latitudes, 5°N and 25°N, assuming GATE-like statistics as described in the previous section. The observational patterns of the satellite were obtained for a 30-day orbit, broken up into 6-day periods with the break points well away from the times when satellite observations occur. For the 25° latitude box, the sampling patterns (both altitudes) in each period were similar enough that the error E^2 was computed from a 300-day Monte Carlo run sampled according to a single representative 6-day period. For the 5° latitude case, the error E^2 was computed from the average of the errors found for each of the five periods in the month, using 60-day Monte Carlo simulations for each. The average error E^2 for a 6-day period was then scaled down by a factor of 5 to obtain an estimate of the 30-day sampling error, as explained in the previous section.

Results are plotted in Fig. 1 as a function of altitude, with a power-law interpolation between the estimates at the two altitudes. The shaded area indicates $\pm\sigma$ limits from Eq. (9), converting the uncertainty in $\hat{E}^2$ to the uncertainty in $\hat{E}$ using the relation

$$\sigma(\hat{E}) = \sigma(\hat{E}^2)/2\hat{E} \tag{10}$$

valid for small normally distributed deviations about the true mean [i.e., $\sigma(\hat{E}) \ll E$]. The error $\hat{E}$ is expressed as a percentage of the mean $\langle r \rangle = 0.445$ mm/h.

A similar Monte Carlo calculation was carried out for a 35° inclination orbit at 350 km altitude, which may be nearer the best orbit for TRMM (Simpson *et al.*, 1988), for boxes at the same two latitudes. For this orbit the sampling error found was

$$E(5°\text{N})/\langle r \rangle = (8.3 \pm 0.7)\% \tag{11}$$

$$E(25°\text{N})/\langle r \rangle = (7.2 \pm 0.5)\% \tag{12}$$

(Uncertainty is $\pm\sigma$.) The error at 5°N is not appreciably changed by the increase in the orbital inclination. The error at 25°N is slightly reduced, presumably because the satellite samples are spread out over a greater portion of the day.

The usefulness of the r.m.s. error estimate E depends somewhat on the probability distribution of the errors. If the errors are normally distributed, one expects the error for a given month's estimated rain rate to be smaller than $2E$ 95% of the time. Rainfall is notorious for its highly skewed distributions, however, and normality of the error distribution cannot be taken for granted. We find that, even though the instantaneous rain rates averaged over a 512 km area are highly skewed in the model (the larger rain rates appearing nearly lognormal, in fact), the errors (7) are consistent with a normal distribution, and a Gaussian fit to their distribution easily passes a chi-squared test for goodness of fit.

Conclusions

The size of the sampling error we estimate for a TRMM-like satellite is encouragingly small—less than 10% . The results depend, of course, on many assumptions about the nature of rainfall statistics in the tropics and on the assumption that nearly unbiased retrieval of rain rates can be achieved.

Acknowledgements

The work described above was done in collaboration with A. Abdullah, R.L. Martin, and G.R. North.

References

Bell, T.L., 1987: A space-time stochastic model of rainfall for satellite remote-sensing studies. *J. Geophys. Res. (Atmos.), 92, 9631-9643.*

Bell, T.L., A. Abdullah, R.L. Martin, and G.R. North, 1989: Sampling errors for satellite- derived tropical rainfall: Monte Carlo study using a space-time stochastic model. *Submitted to J. Geophys. Res. (Atmos.).*

Brooks, D.R., 1977: An introduction to orbit dynamics and its application to satellite-based Earth monitoring missions, *NASA Ref. Pub. 1009, National Technical Information Service, Springfield, Virginia 22161, 84 pp.*

Kedem, B., L.S. Chiu, and G.R. North, 1989: Estimation of mean rain rate: Application to satellite observations, *submitted to J. Geophys. Res. (Atmos.).*

Laughlin, C.R., 1981: On the effect of temporal sampling on the observation of mean rainfall, Precipitation Measurements from Space, Workshop Report, *ed. by D. Atlas and O.W. Thiele. NASA publ., available from Goddard Space Flight Center, Greenbelt, MD 20771.*

Shin, K.-S., and G.R. North, 1988: Sampling error study for rainfall estimate by satellite using a stochastic model, *J. Climate Appl. Meteorol., in press.*

Simpson, J., R. F. Adler, and G.R. North, 1988: A proposed Tropical Rainfall Measuring Mission (TRMM) satellite, *Bull. Amer. Meteor. Soc., 69, 278-295.*

Characterisation of cumulus cloud fields for calculating the distribution of solar radiation

P.K. Love
Institute of Geophysics, Victoria University, Wellington, NZ

Abstract

A knowledge of the spatial distribution and temporal variation of solar radiation is required for many purposes. Existing networks of solar radiation stations have low spatial densities and relatively short histories. Thus there is a need to supplement data from these stations with data from other sources. Such additional data can be obtained from surface and satellite observations of cloud and from global circulation models.

In order to identify simple parameters from which the amount of solar radiation reflected and transmitted by a field of Cumulus clouds might be determined, reported distributions of cloud size and a model which gives the radiative characteristics of an individual cloud as a function of cloud size and shape, droplet size distribution and the direction and wavelength of incident radiation, have been employed to calculate the bulk radiative characteristics (reflectance, transmittance and absorptance) of the cloud field.

Assuming an exponential distribution of cloud size (Houzumi *et al.*, 1982) the bulk radiative characteristics can be determined accurately from the distribution decay constant. As the decay constant can be related to cloud cover (Houzumi *et al.*, 1982) or maximum cloud diameter (Kalthoff and Schaller, 1986) it is possible to estimate the radiative characteristics from parameters that can be observed from the surface or by satellite. Alternatively, if fractional cloud cover and liquid water content are known the radiative characteristics can be determined without requiring the decay rate. This method is well suited for use with data from global circulation models. Estimates of the bulk radiative characteristics based upon other variables, such as mean cloud size, give inferior results.

References

Houzumi, K., Harimaya, T., and Magono, C., 1982: The size distribution of cumulus clouds as a function of cloud amount. *J. Meteor. Soc. Japan*, **60**, 691-699.

Kalthoff, N., and Schaller, E., 1986: Modification of solar radiation by dispersive cumulus cloud fields. *Beitr. Phys. Atmos.*, **59**, 409-426.

A critical review of two decades of teleconnection studies in the United States and Europe

Robert E Livezey
Climate Analysis Center, NMC/NWS/NOAA, Washington D.C. USA

Abstract

Teleconnections were referred to by O'Connor twenty years ago as "favoured modes for coupling large-scale abnormalities of the atmospheric circulation as determined statistically or empirically", and more recently by Livezey (1988) as "coherent variability between distantly separated centres of action". The principal focus of teleconnection research in the United States has been on extratropical low-frequency, quasi-stationary atmospheric structures, but has expanded rapidly over the last decade to include first the oceans and tropics and very recently non-stationary, intermediate time-scales (10-60 days) fluctuations.

In particular, classification of modal quasi-stationary circulation patterns has received considerable attention since Wallace and Gutzler's (1981) paper and has evolved to the pint where serious attempts are being made to study the persistence and transition properties of classified patterns. Strong tropical signals embodied in the ENSO and 30-60 day oscillation phenomena and a growing awareness of their role in north American climate have provided the impetus for both tropical-extratropical teleconnection studies and the application of sophisticated techniques to describe the time-space structures of these non-stationary tropical circulation systems. The search for tropical-extratropical links has since expanded to include the Atlantic sector while the analysis of non-stationary modes has now been extended to the difficult problem of intra-seasonal (10-60 days) variability in the extratropics.

The availability of large computers has permitted the application of powerful algorithms to the various problems listed above. Nevertheless, the outcome of these experiments can often be artificial, if sufficient care is not taken in the choices of filters, data windows, side conditions and constraints, or as a result of basic properties of the analysis techniques themselves. Frequently, the experimental results will accommodate multiple interpretation as well.

The various problems that have been addressed in modern teleconnection studies, the approaches used to study them and their associated strengths and weaknesses and some major findings will be reviewed for work spanning the last 20 years, with special emphasis on the last decade. Examples will be presented to illustrate some of the inherent difficulties in these studies and possible ways around some of the problems will be suggested.

Use of statistical methods in the search for teleconnections

Barbara G. Brown Richard W. Katz
Environmental and Societal Impacts Group, NCAR, Boulder, USA

Introduction

Many of the results of recent studies devoted to the search for atmospheric/oceanic teleconnections are based on empirical analyses of climate data that rely extensively on statistical techniques. However, in some cases inappropriate statistical methods have been applied or assumptions have been ignored. Consequently, the strength of some alleged linkages may have been exaggerated.

Brown and Katz (1987) considered the use of statistical methods in teleconnections research from a historical perspective. In the present study, statistical approaches that are currently being taken by teleconnections researchers are evaluated, keeping in mind the lessons drawn from the historical review. In particular, the problem of multiplicity is considered. This problem arises, for example, when many correlation coefficients are computed but only the largest are selected. With only a few exceptions (e.g., Preisendorfer and Barnett, 1983; Livezey and Chen, 1983), the implications of multiplicity have not been fully appreciated within the meteorological community. Another issue, initially considered by Katz (1988), concerns how temporal correlation may affect the identification of leading, lagging, or feedback relationships. In addition, the implications of autocorrelation for the problem of multiplicity are not well understood. To demonstrate the magnitude of the problem of multiplicity in the search for teleconnections, and to investigate the effects of interactions between autocorrelation and multiplicity, the results of a simulation study are described.

Multiplicity and autocorrelation

Multiplicity

Multiplicity is a well-known statistical problem that arises when a large number of statistical hypotheses are tested (e.g., when the results of an experiment are stratified in many ways). The effect of multiplicity is such that the probability of rejecting at least one null hypothesis in error (i.e., the probability of Type I error) increases geometrically as more hypotheses are tested (Tukey, 1977). For example, the probability that at least one of ten independent tests of hypotheses will be judged in error to be significant, given that each is tested at the 0.05 level, is 0.401—much greater than 0.05.

Multiplicity should be an important issue in teleconnections studies in which a large number of correlation coefficients are computed. However, the tendency has been to report those correlations that are significant according to the criteria used to evaluate the significance of individual correlation coefficients. Often only the maximum correlation (in absolute value) in a set is reported.

Some attempts have been made to counteract the effect of multiplicity. For example, some researchers have used a level of 0.01 instead of the more commonly used level of 0.05, to reduce the number of correlations selected as being significant (e.g., Nicholls, 1985). In other approaches to compensating for the problem of multiplicity, the important distinction is made between the level of the individual tests, α say, and the overall level of the combination of tests. In particular, it would be desirable to select values of α for the individual tests that will produce an acceptable α_o (e.g., $\alpha_o = 0.05$) for the set of tests. The Bonferroni inequality leads to one method of this type in which the possibility of dependence among the tests is taken into consideration (Neter et al., 1983). With this approach,

$$\alpha = \frac{\alpha_o}{k} \tag{1}$$

where k is the number of correlations tested, would be used to test the significance of the individual correlations. This procedure is conservative, guaranteeing that the overall level is less than α_o.

Walker (1914) also suggested and applied a method for taking into account the problem of multiplicity. Walker's method consisted of determining a critical value r_c such that

$$\Pr\{\max_{1 \le i \le k} |r_i| > r_c\} = \alpha_o \tag{2}$$

where the value of α_o used by Walker was 0.50. Applying the known distribution of the maximum value of a set of independent random variates (e.g., Mood et al., 1974, pp. 182-184), r_c is the value of the correlation coefficient such that

$$\Pr\{|r_i| > r_c\} = 1 - (1 - \alpha_o)^{1/k} \tag{3}$$

for $1 \le i \le k$. In a modernized version of this approach, a value of α_o such as 0.05 would probably be used. Consequently, Walker's approach can be viewed as differing from the more modern Bonferroni procedure only insofar as it does not allow for dependence among tests.

Autocorrelation

In a simulation study, Katz (1988) demonstrated that the existence of autocorrelation in meteorological and oceanographic time series can have substantial effects on cross-correlation functions estimated in teleconnection studies. For example, the value of the contemporaneous cross-correlation is 'smeared out' across other time lags to make leading and lagging relationships apparent when none is really present.

One method of counteracting the problem of autocorrelation is to remove this dependence from the time series by pre-whitening (e.g., Katz, 1988). Alternatively, autocorrelation can be taken into account by applying a 'variance-inflation' factor based on the values of the autocorrelation coefficients (Bartlett, 1955, p. 289; Katz, 1988; Trenberth, 1976). This technique is analogous to the adjustment for time averages termed the 'effective number of independent samples' (e.g., Madden, 1979). The practical effect of this procedure is to reduce the number of degrees of freedom used in the t-test of significance of the sample cross-correlation coefficients.

Simulation study design

The simulations were based on time series models described in Katz (1988). These models consist of first-order autoregressive processes in which pairs of time series may have non-zero contemporaneous cross-correlations, but no leading, lagging, or feedback relationships.

Sets of s = 2, 5, 10, 20, and 50 time series were considered in individual simulations. The simulation experiment was repeated 500 times for each combination of selected autocorrelation and cross-correlation parameters, for each value of s. The simulated time series each had a length of 50, a value that is similar to the number of years typically included in modern teleconnection studies. A standard multiple congruential uniform random number generator with shuffling was utilized to create the simulated time series.

Values of both 0 and 0.5 were assigned to the first-order autocorrelation coefficient (ϕ) and the contemporaneous cross-correlation coefficient (γ). In a given simulation, all time series were assumed to have the same autocorrelation. The cross-correlation between time series 1 and 2 was set equal to either 0 or 0.5, whereas the cross-correlations of time series 1 with time series 3 through s were always set equal to 0.

The sample contemporaneous cross-correlations between series 1 and all the other series were computed for each simulation (that is, correlations of all possible pairs were not considered). This approach mimics that taken in many teleconnection studies in which a particular time series (e.g.,

Southern Oscillation Index) is correlated with a large number of other time series. Thus, the number of correlations computed in each simulation, k, is equal to $s - 1$.

The value of the maximum (absolute value) of the sample cross-correlations was recorded for each simulation of a set of s time series. In addition, the significance of each computed correlation was evaluated according to seven different approaches: (i) $\alpha = 0.05$; (ii) $\alpha = 0.01$; (iii) Bonferroni ($\alpha_o = 0.05$); (iv) Walker ($\alpha_o = 0.50$); (v) modernized Walker ($\alpha_o = 0.05$); (vi) variance inflation ($\alpha = 0.05$); and (vii) variance inflation plus modernized Walker ($\alpha_o = 0.05$). Note that approaches (i), (ii), and (vi) make no attempt to compensate for multiplicity and that only (vi) and (vii) take autocorrelation into account.

Table 1 contains the critical r-values (r_c) and α-values associated with these approaches for the values of s employed in the study.

Table 1: Critical r-values (r_c) and values of α associated with the seven testing approaches investigated, for various numbers of time series. For the cases involving variance inflation, $\phi = 0.5$

		Number of time series (s)				
Approach		**2**	**5**	**10**	**20**	**50**
$\alpha = 0.05$	α	0.050	0.050	0.050	0.050	0.050
	r_c	0.279	0.279	0.279	0.279	0.279
$\alpha = 0.01$	α	0.010	0.010	0.010	0.010	0.010
	r_c	0.361	0.361	0.361	0.361	0.361
Bonferroni	α	0.050	0.012	0.006	0.003	0.001
($\alpha_o = 0.05$)	r_c	0.279	0.351	0.387	0.416	0.451
Walker	α	0.500	0.159	0.074	0.036	0.014
($\alpha_o = 0.50$)	r_c	0.098	0.202	0.255	0.298	0.345
Walker	α	0.050	0.013	0.006	0.003	0.001
($\alpha_o = 0.05$)	r_c	0.279	0.350	0.386	0.416	0.450
Variance	α	0.050	0.050	0.050	0.050	0.050
Inflation (VI)	r_c	0.361	0.361	0.361	0.361	0.361
Walker	α	0.050	0.013	0.006	0.003	0.001
($\alpha_o = 0.05$) & VI	r_c	0.361	0.449	0.493	0.528	0.569

Similarities exist among some of these approaches. The r_c-values for the variance inflation and $\alpha = 0.01$ approaches are identical by accident, due only to the choice of $\phi = 0.5$. However, the closeness of the r_c-values associated with the Bonferroni and modernized Walker approaches is somewhat contrary to expectations, as these procedures are based on different assumptions. Nevertheless, it can be shown that both techniques produce approximately the same values of α when α_o is relatively small.

Results

$\gamma = 0$

Distributions of the maximum sample contemporaneous cross-correlations (in absolute value) obtained in each simulation, for the case of no actual contemporaneous cross-correlation (i.e., $\gamma = 0$), are displayed in the form of box plots in Figure 1.

These plots indicate the strong effect of multiplicity in leading to spuriously large maximum values as the number of time series increases. For example, the median value of the maximum sample cross-

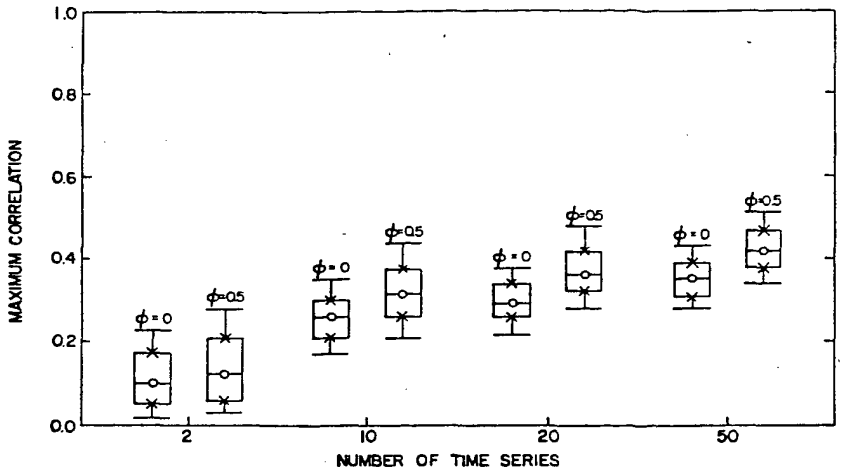

Figure 1: Box plots depicting distributions of values of maximum sample cross-correlations (in absolute value) for simulations with $\gamma = 0$. The plots show the 0.90th, 0.75th, 0.50th, 0.25th, and 0.10th quantiles of the distributions

correlation with 50 time series is 0.35. The impact of autocorrelation is to increase the magnitude of this multiplicity effect to a large degree.

A Type I error occurs if at least one of the computed correlations in a simulation is deemed significant, or equivalently, if the maximum correlation is significant. Probabilities of a Type I error for the $\gamma = 0$ case are displayed in Figures 2 and 3.

It is evident from these diagrams that many of the approaches to testing significance do not adequately handle multiplicity. For example, the method of applying the $\alpha = 0.05$ significance level in individual tests rapidly leads to a very large overall significance level as the number of series is increased (e.g., for $s = 10$, the probability is 0.35). Moreover, the effect of multiplicity is considerably worsened when the time series are autocorrelated (e.g., the probability associated with $\alpha = 0.05$ is 0.66). With regard to counteracting the problem of multiplicity, the Bonferroni approach (approximately equivalent to the modernized Walker approach) appears to lead to adequate results (i.e., an overall significance level somewhat less than 0.05) in the case of no autocorrelation. However, when the series are autocorrelated, the overall significance values are increased to unacceptable levels. This discrepancy between the observed and desired values of α_o arises because the nominal levels for the individual tests are no longer correct in the presence of autocorrelation. In that case, the combination of the variance-inflation approach with the Bonferroni (or modernized Walker) method leads to results that are insensitive to the number of time series.

$\gamma = 0.5$

For the case of an actual contemporaneous cross-correlation of 0.5, the distributions of sample maximum cross-correlations (not shown) are relatively insensitive to the effects of multiplicity. However, the probability that the sample cross-correlation that is maximum in absolute value will have the wrong sign (i.e., will be negative) increases as the number of time series increases, up to 0.15 for $s = 50$ and $\phi = 0.5$. Similarly, the probability that the maximum sample cross-correlation will not be the correlation between time series 1 and 2 is as high as 0.32 for $s = 50$ and $\phi = 0.5$. Both of these probabilities are larger for autocorrelated time series than for series without autocorrelation.

Another probability of interest in the case of $\gamma = 0.5$ is the probability of attaining a 'right

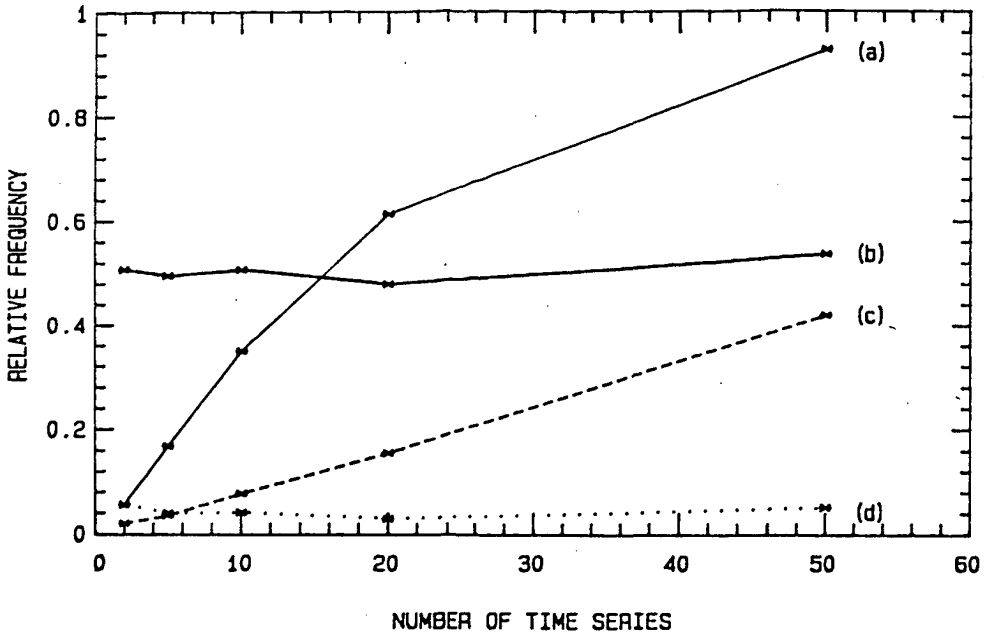

Figure 2: Probability that the maximum sample cross-correlation in a single simulation with $\gamma = 0, \phi = 0$ is significant, according to various criteria: (a) $\alpha = 0.05$; (b) Walker ($\alpha_o = 0.50$); (c) $\alpha = 0.01$; (d) Bonferroni or modernized Walker ($\alpha_o = 0.05$)

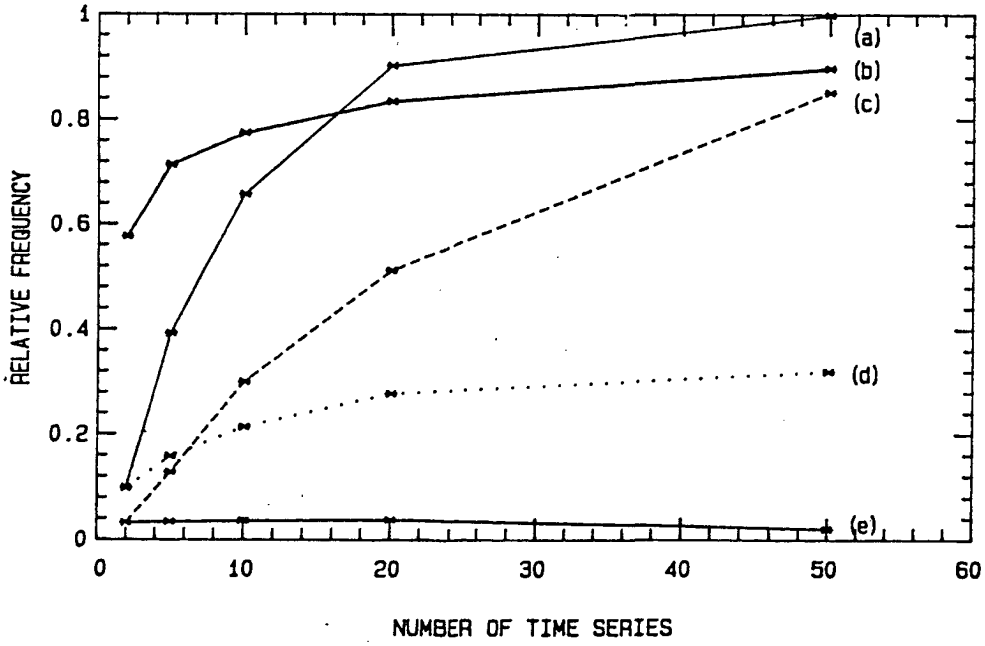

Figure 3: As in Figure 2, with $\gamma = 0$, $\phi = 0.5$. (a) $\alpha = 0.05$; (b) Walker ($\alpha_o = 0.50$); (c) $\alpha = 0.01$ or variance inflation ($\alpha = 0.05$); (d) Bonferroni or modernized Walker ($\alpha_o = 0.05$); (e) Bonferroni or modernized Walker ($\alpha_o = 0.05$) plus variance inflation.

answer'—the probability that the sample cross-correlation between time series 1 and 2 will be significant and the other sample correlations will be nonsignificant. The values of these probabilities for the $\gamma = 0.5$ simulations are illustrated in Figures 4 and 5.

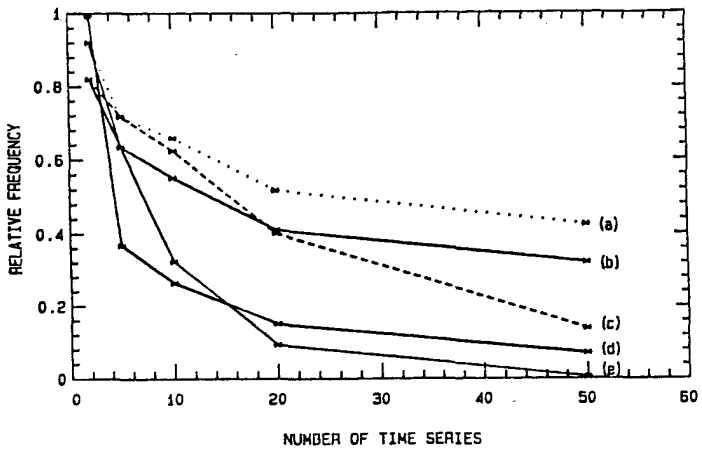

Figure 4: Probability of obtaining the 'right answer' (i.e., correlation between series 1 and 2 is significant; correlation between series 1 and all other series is non-significant), with $\gamma = 0.5, \phi = 0$, utilizing various approaches: (a) Bonferroni or modernized Walker ($\alpha_o = 0.05$); (b) $\alpha = 0.01$; (c) Walker ($\alpha_o = 0.50$); (d) $\alpha = 0.05$

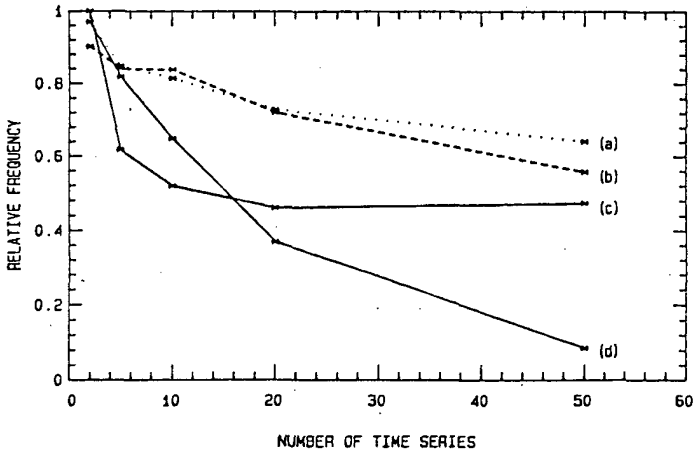

Figure 5: As in Figure 4, with $\gamma = 0.5$, $\phi = 0.5$. (a) Bonferroni or modernized Walker ($\alpha_o = 0.05$); (b) Bonferroni or modernized Walker ($\alpha_o = 0.05$) plus variance inflation; (c) $\alpha = 0.01$ or variance inflation; (d) Walker ($\alpha_o = 0.50$); (e) $\alpha = 0.05$

These probabilities are clearly affected by the number of time series as well as by autocorrelation. However, it appears that the Bonferroni (or modernized Walker) approach performs reasonably well for this purpose, even for large numbers of time series. In contrast, the $\alpha = 0.05$ method performs

quite poorly at discriminating among the correlations, particularly for relatively large numbers of time series.

Conclusions

The results of the simulation study indicate that the impacts of multiplicity in teleconnection studies can be extensive. In particular, autocorrelation can greatly increase the magnitude of these impacts. Among other things, the multiplicity effect can lead relatively frequently to observed maximum correlations that are spuriously large when no cross-correlation actually exists. This result has important implications for the results of studies in which only the maximum among a set of correlations is reported. The results also suggest that use of a small α (e.g., $\alpha = 0.01$) may not always provide adequate compensation for the effects of multiplicity. A positive result of the study is the evidence suggesting that multiplicity may be successfully counteracted by both using methods of taking into account autocorrelation (e.g., through the variance-inflation technique) and by applying appropriate strategies for obtaining an acceptable overall significance level (e.g., the Bonferroni or modernized Walker approaches).

References

Bartlett, M.S., 1955: *Stochastic Processes*, Cambridge University Press, Cambridge.

Brown, B.G., and R.W. Katz, 1987: A historical perspective on the role of statistics in teleconnections research. *Preprints, Tenth Conference on Probability and Statistics in Atmospheric Sciences*, 6–8 October 1987, American Meteorological Society, Edmonton, Alberta, Canada, 101–106.

Katz, R.W., 1988: Use of cross correlations in the search for teleconnections. *J. of Clim.*, 241–253.

Livezey, R.E., and W.Y. Chen, 1983: Statistical field significance and its determination by Monte Carlo techniques. *Mon. Wea. Rev.*, **111**, 46–59.

Madden, R.A., 1979: A simple approximation for the variance of meteorological time averages. *J. of App. Met.*, **18**, 703–706.

Mood, A.M., F.A. Graybill, and D.C. Boes, 1974: *Introduction to the Theory of Statistics*. McGraw-Hill Book Company, 564 pp.

Neter, J., W. Wasserman, and M.H. Kutner, 1983: *Applied Linear Regression Models*, Richard D. Irwin, Inc., 547 pp.

Nicholls, N., 1985: Impact of the Southern Oscillation on Australian crops. *J. of Clim.*, **5**, 553–560.

Preisendorfer, R.W., and T.P. Barnett, 1983: Numerical model-reality intercomparison tests using small-sample statistics. *J. of the Atmos. Sci.*, **40**, 1884–1896.

Trenberth, K.E., 1976: Spatial and temporal variations of the Southern Oscillation. *Quart. J. R. Met. Soc.*, **102**, 639–653.

Tukey, J.W., 1977: Some thoughts on clinical trials, especially problems of multiplicity. *Sci.*, **198**, 679–684.

Walker, G.T., 1914: Correlation in seasonal variations of weather, III. On the criterion for the reality of relationships or periodicities. *Memoirs of the Indian Meteorological Department*, **21**, part IX, 12–15.

The teleconnection pattern between the Arctic ice area and the 500 hPa geopotential height field during the northern hemisphere summer

Zhi-fang Fang
Institute of Meteorology, Chengdu, China

Introduction

Hoskins and Karoly (1981) used the basic numerical model, as a result, the Rossby wavetrains produced in the upper troposphere. The long wave lengths propagate strongly poleward as well as eastward resulting in a wavetrain path, similar to a great circle. Horel and Wallace (1981) have shown that the warm episodes in equatorial sea-surface temperature in the Pacific tend to be accompanied by below-normal 700 hPa height in the North Pacific, above normal heights over western Canada, and below normal heights over the southeastern United states. This is PNA teleconnection pattern. It is very reminiscent of the Rossby wave-'trains' in the model results.

Up to now, the research of the teleconnection pattern between the polar cold source and the upper troposphere was seldomly analysed. Although the effect of sea ice on atmospheric circulation is weaker than the effect of low latitude sea surface source, but according to the observed data, the sea ice existence obviously influences on the climate and weather in the world.

This study is primarily based on the monthly mean 500 hPa geopotential height field (1951-1982) and the Arctic ice area (1953 -1977) during July and August in the Northern Wemisphere. In this paper, the teleconnection pattern between the Arctic ice area and the 500 hPa geopotential heights during the Northern Hemispheric summer is investigated.

The remote response of the atmosphere to the arctic sea ice cold source

The correlation field between the Arctic ice area and the 500 hPa geopotential height field during July and August are analyzed.

Fig. 1 shows a correlation field in August. There exists a maximum correlation coefficient -0.554, it appeared at (70°N, 170°W) near the North Pole. The fact indicates that when the Arctic sea ice area is stronger than normal in Summer, owing to the reflective index in the Arctic ice area was increased, then the receipts of the solar energy in the underlying earth's surface was decreased, therefore the geopotential height near the polar area is lower than normal height, that is, the low pressure over the pole is stronger, and vice versa.

The Arctic sea ice cold source not only effects the low pressure over the Pole, but it effects the far area from the source region, that is located at middle and low latitudes. In Fig. 1 , there exist other correlation centers, for example: they are located at (55°N, 105°W) and (35°N, 75°W) with correlation coefficients 0.336 and -0.426, respectively.

The correlation field between the Arctic sea ice and 500 hPa gph during July is very similar to the correlation field in August (Fig. was omitted).

The teleconnection pattern between the Arctic sea ice and 500 hPa gph during summer

I used the method similar to that used by Wallace and Gutzler (1981).

Figure 1: The correlation field between the Arctic sea ice area and 500 hPa gph during August

First, I take the point at (7O°N, 17O°W) as base grid point, and make a one-point correlation map at 500 hPa in August (Fig. 2 (a)). In Fig. 2(a), there exist three alternating positive and negative correlation centers. They are located at (70 °N, 17O °W), (55 °N, 1O5 °W) and (35 °N, 75°W), with the correlation coefficient values 1, -0.589 and 0.542 respectively. These coefficients are maximum values in Fig. 2(a). Then I take points at (55 °N, 105 °W) and (35°N, 75°W) as base grid point and make two one-point correlation maps at 500 hPa in August (Fig. 2(b) and 2(c)).

Figure 2: The one-point correlation map in August. (a)(7O °N, 17O °W) as base grid point;(b) (55 °N, 1O5 °W) as base grid point;(c) (35 °N, 75 °W) as base grid point.

In the three one-point?? maps, the correlation coefficients on three correlation centers reach significant levels at $\alpha = 0.01$. The correlation centers are called action centers, it forms a teleconnection pattern. The horizontal scale and orientation of the pattern resemble a wavetrain on the spheric atmosphere (Hoskins and Karoly, 1981), but forced by the Arctic ice as a cold source.

By use of same method for July, the teleconnection pattern is very similar to August.

(Fig. was omitted).

Comparing Fig. 2 with Fig. 1, it is obvious that the three action centers in Fig. 2 coincide with the some correlation centers in Fig. 1 very well. This fact indicates that the Arctic sea ice cold source tends to be accompanied by the teleconnection pattern at 500 hPa.

Analyses of the character of the teleconnection pattern

Fig. 3 shows a schematic diagram of wavetrain and jet stream. Heavy arrows indicate axes of climatological mean jet streams in July, shaded areas indicate centers of action of the teleconnection pattern in July. In Fig. 3, the centers of action can cross the westerly jet and into the subtropical area, but they only exist in the westerly belt (The subtropical high ridge is located near 25 °N in July).

Figure 3: The schematic of wavetrain and jet stream.

Figure 4: The 1000-500 hPa thickness difference field between four stronger Arctic ice years and four weaker Arctic ice years.

Fig. 4. is the 1000-500 hpa thickness difference field between four stronger Arctic ice years (1964, 1965, 1967 and 1969) and four weaker Arctic ice years (1960, 1968, 1971 and 1977) in August.

Comparing Fig. 4 with Fig. 2, it is clear that the three action centers in Fig. 2 just coincide with the three centers in Fig. 4. This fact demonstrates an equivalent barotropic structure of the teleconnection pattern.

The map of standard deviations in July and August are analyzed. The values of standard deviation near three action centers are obviously larger than values in the same latitude area, in order to demonstrate that there exists a teleconnection pattern. (Fig. was omitted)

Summary

According to the foregoing statistical discussion, it may be noted:

1. There exists a teleconnection pattern. It resembles a wavetrain on the spheric atmosphere, and the long wave lengths propagate strongly eastward and southward in a wavetrain path, away from the forcing region.

2. The result shows an equivalent barotropic structure with larger amplitude at 500 hPa, but the source is forced by the Arctic sea ice, only obvious in summer.

3. When the Arctic ice area during summer is stronger, then the polar low pressure may be stronger, the Canadian high pressure region higher and the Northern American trough stronger also, and vice versa.

References

Hoskins, B.J. and D.J. Karoly, 1981: The steady linear response of a spherical atmosphere to thermal and orographic forcing. *J. Atmos. Sci.*, **38**, 1179-1196.

Horel, J.D. and J.M. Wallace, 1981: Planetary-scale atmospheric phenomena associated with the Southern Oscillation. *Mon. Wea. Rev.*, **109**, 813-829.

Wallace, J.M. and D.S. Gutzler, 1981: Teleconnection in the geopotential height field during the Northern Hemisphere winter. *Mon. Wea. Rev.*, **109**, 784-812.

Blackmon, M.L. and Y.H. Lee, 1984: Horizontal structure of 500 mb height fluctuations with long, intermediate and short time scales. J. Atmos., **41**, 961-979.

Some applications of statistics to solar-atmospheric relationships

Dennis J. Shea
NCAR, Boulder, Colorado, USA

Introduction

For many years researchers have tried to find a relationship between solar and atmospheric variability. Pittock (1978, 1983) examined a subset of the vast amount of literature dealing with these associations. In general, he found that they did not pass rigorous statistical testing or additional observations. Pittock (1978) lists a set of conditions which he thinks should be satisfied in these relationships. They are: (i) large amplitude correlations, (ii) constant phase relationship, (iii) at least five or six cycles, and (iv) a hypothesized solar-atmospheric relationship which can be supported by a plausible and testable physical hypothesis. Pittock (1983) further states that because climatological data sets are often inadequte for rigorous statistical testing, the above conditions can be modified. He states that "within the limits of moderation and good judgement it is therefore acceptable and even useful to publish inconclusive but suggestive results, *provided that they are identified as such*".

Recently Labitzke (1987) noted an apparent relationship among stratospheric temperatures at the North Pole, equatorial stratospheric winds, and the 11-year solar cycle. This relationship is examined using Monte Carlo simulations. It is demonstrated that Pittock's conditions (i) and (ii) are satisfied and, although there is *no* substitute for real data, the necessity of five or six cycles may be relaxed. After establishing the statistical significance between the 11-year solar cycle and the North Pole stratospheric temperatures, some solar-atmospheric associations are described that *suggest* that this signal is present in *both* the stratosphere and troposphere. The focus of this paper is the statistical methodology used to investigate the significance of the above relationship. Therefore, the statistical results will be for the northern hemisphere winter only, where winter is defined as the mean of January and February values.

Before proceeding further, several terms used throughout the rest of the text are described.

1. Winds in the equatorial stratosphere change direction every 24 to 30 months. The mean period is about 27 months. Thus, westerly (easterly) winds in a particular January, for example, tend to be followed by easterly (westerly) winds in the succeeding January. Occasionally two successive years will have winds in the same direction. This phenomenon is called the Quasi-Biennial Oscillation (QBO).

2. The "bootstrap" procedure (Efron, 1982) is a statistical technique which can be used to determine the variability of *any* statistic ($\hat{X}$) using the original data sample. Briefly, the original data are randomly sampled (with resampling allowed) a large number of times (N). Each time the statistic is recalculated (X_1, X_2, ..., X_N). These estimates are an approximation to the sampling distribution of $\hat{X}$. The mean of the N estimates should approximate the original $\hat{X}$ and the true value. The variance of the estimates should approximate the sampling distribution of $\hat{X}$. This allows the establishment of confidence limits on the original statistic. In addition, an estimate of the bias may be obtained.

3. In general, atmospheric data are highly correlated in both space and time. For example, a correlation pattern between, say, the solar cycle and atmospheric temperatures at a particular pressure level will result in large areas of apparently significant correlations even after adjusting for the time dependence. A procedure for testing a collection of spatially correlated values for statistical significance (i.e., field significance) is described by Livezey and Chen (1983). Essentially, the original series is simulated via a Monte Carlo technique and the correlations

are recalculated N times. The resulting distribution of percent area covered by significant correlations allows the assessment of whether the original area covered by significant correlations could have arisen by chance.

Solar cycle and stratospheric temperatures at the poles

Labitzke (1987), using 30 mb winter ([January+February]/2) temperature data spanning the 31 year period 1956-1986, noted when the 50-mb equatorial winds were westerly (17 years) that the sunspot number and north pole 30-mb temperatures were low, and conversely for high sunspot numbers. Figure 1, from Labitzke (1987), updated through 1988 to include 18 westerly wind years, shows that the linear correlation between these two variables is +0.77. This result is significant at the 1% level using 16 degrees of freedom (dof). Even if only 10 dof are used (to allow for autocorrelation) it exceeds the 5% significance level of 0.62. Using the bootstrap procedure it can said with 95% confidence that the true correlation is between 0.54 and 0.91. Although they had no explanation for this relationship, this suggestive result led Labitzke and van Loon (1988; hereafter LvL) and van Loon and Labitzke (1988; hereafter vLL) to *explore* further this apparent association.

The first step was to establish, in a more rigorous fashion, the statistical significance of the relationship which results from partitioning the observed data by the phase of the QBO. Two Monte Carlo tests were used. A characteristic of each test is that the randomization must retain some similarity to the original series being modeled. For example, the first test uses a first order Markov process to simulate the oscillating pattern exhibited by the north pole temperatures.

The correlation between the 30-mb January-February average temperature at the North Pole and the solar flux during the three solar cycles spanning the 33 year period 1956-88 (Fig. 2) is 0.15. However, if one correlates the 18 winters in the west phase of the QBO with the solar flux in the same winters the correlation is 0.77. Thus, these winters are in phase with the solar cycle (Fig. 3). The correlation for the 15 winters when the QBO was in its east phase is -0.43 (Fig. 4). Clearly, the correlation between the solar cycle and the 30 mb temperatures is masked by the QBO. Partitioning the data by QBO phase indicates that the QBO modulates the effect of the solar–atmospheric association, at least in winter.

Since the series in Figs. 2–4 are the foundation upon which the solar-atmospheric studies discussed here originally were based we establish the statistical significance of the *pair* of series shown in Figs. 3 and 4. As a first step, the null hypothesis (no correlation) is made and tested for significance at the 5% level using $r_5 = 1.96/\sqrt{n_e - 2}$ where n_e is the number of independent samples. The latter was determined through an approach discussed by Livezey and Chen (1983), which takes into account the autocorrelations in both the temperature and solar flux series. Applying this method to the 33 winters shown in Fig. 2, the number of independent samples is reduced to 23. Thus r_5 =0.43 and we cannot reject the null hypothesis. Even if $n_e = 33$ the null hypothesis could not be rejected at the 5% level. The same approach cannot be used for Figs. 3 and 4 because the sampling interval varies due to the irregular east-west phase variations. We ask instead the question: How likely is it that a series such as the 30-mb temperatures in Fig. 2 by being split into two series according to the state of the QBO will follow the solar cycle in the manner of Figs. 3 and 4? To answer this question we employ the following Monte Carlo technique (hereafter, Test 1): First, the lag-one-year autocorrelation of the temperature series in Fig. 2 was determined to be -0.42. Second, one thousand first-order autoregressive temperature series (Markov process) of length 100 were generated by

$$T_m = -0.42T_{m-1} + \epsilon_m$$

where T_m and e_m are a normalized temperature and a random number, respectively, at time m. Third, the middle 33 values of each Markov series were partitioned by the phase of the QBO. Finally, correlations between the solar flux and simulated temperature series were calculated. The resulting

distribution of the "west" and "east" phase correlations (r_w and r_e, respectively) are shown in Fig. 5. The circle has a radius of length $\sqrt{(0.77)^2 + (-0.43)^2}$. The coordinate (+0.77,–0.43) is indicated by an asterisk. Points lying outside this circle are pair correlations which exceed the observed correlations. In the simulation of 1000 series shown in Fig. 5 only 6 were outside the circle. In four additional similar tests at most 7 of the 1000 pair correlations fell outside the circle. This is convincing evidence that the correlations probably did not occur by chance.

Test 1, using a Markov model to simulate the 30 mb stratospheric temperature data represented the initial attempt to determine the significance of the series shown in Figures 3 and 4. Subsequently, Glenn Brier (personal communication, 1988) suggested an alternate Monte Carlo test (Test 2) to minimize the effects of autocorrelation. In Test 2 the phase of the QBO was randomized and the observed solar flux and stratospheric temperature data were used to calculate the correlations. To be consistent with the observations, this randomization was subject to two constraints: (i) no more than two successive phases could be the same and (ii) in a series of 33 phases 18 must be "west" phases and 15 "east" phases. The resulting scattergram derived from 1000 simulations is displayed in Fig. 6. Only 1 out of 1000 simulations exceeded the observed pair correlations. The narrow clustering of the simulated east-west correlations may be attributed to the constraints imposed on each simulated series. Brier (1988, personal communication) has independently performed this randomization test with similar results.

Solar-geopotential height correlation patterns

Correlations between the solar cycle and the 30 mb geopotential heights over the northern hemisphere during winter are low with only a small area (<5%) having correlations which are locally significant at the 5% level. After partitioning the data according to the phase of the QBO, however, large areas are covered by locally significant correlations (See Figs. 5a and 7a in LvL). Large positive correlations during the west phase are generally replaced by large negative correlations during the east phase. During the east (west) phase 30+% (10+%) of the area is covered by values locally significant at the 5% level. These patterns have field significant levels of better than 5% and 10%, respectively. Figure 7 shows a scattergram of percent area covered by correlations which are locally significant at the 5% level that resulted from randomizing the QBO phases as in Test 2. Two hundred simulations were run. Not one Monte Carlo pair exceeded the observed levels of field significance. The uniqueness and significance of the investigated solar–stratospheric association is clear.

Correlations between the solar cycle and 700 mb geopotential heights after partitioning by the east and west QBO phases were field significant at the 5 and 2.5% levels, respectively. Barnston and Livezey (1988) have also tested the field significance of these patterns using a more robust test. Their results indicate even higher significance levels. This has led the long-range forcasters at Climate Analysis Center in Washington, D.C. to incorporate the solar-atmospheric association into their forcasting methodology.

Solar-surface temperature association

The correlation pattern for winter between the solar flux and surface air temperature on the Northern Hemisphere during the west phase of the QBO shows a large area of negative correlations over the U.S. (Fig. 8). Charleston, South Carolina which is near the center of this pattern has a correlation of –0.69 and a 95% bootstrap interval of –0.46 to –0.83. Barnston and Livezey (1988) have tested the solar-temperature associations over the U.S. and found them significant at the 5% level during the west phase.

Summary

An association between the 11-year solar cycle and the atmosphere is masked by the QBO. Partitiong the data according to the phase of the QBO yields highly significant correlations. Monte Carlo simulations indicate that these correlations are not likely to have occurred by chance. It has also been shown that the solar–atmospheric association is present from the stratosphere to the surface.

References

Barnston, A.G. and R.E. Livezey (1988): An Evaluation of an Association Between the 11-Year Solar Cycle, The QBO, and the Atmosphere. *Proceedings Climate Diagnostic Workshop. 31 October-4 November. 1988. Cambridge, Mass.*

Efron, B., (1982): The Jacknife, the Bootstrap and Other Resampling Plans. *Soc. Industr. Appl. Math.. Philadelphia, J.W. Arrowsmith, Bristol, England 92 pp.*

Labitzke, K. (1987): Sunspots, the QBO, and the Stratospheric Temperature in the North Polar Region. *Geophys. Res. Lett., 535-537.*

Labitzke, K. and H. van Loon (1988): Associations Between the 11-Year Solar Cycle, the QBO and the Atmosphere. Part I: the Troposphere and Stratosphere in the Northern Hemisphere in Winter. *J. Atmos. and Ter. Physics 50, 3: 197-206.*

Livezey, R.A. and W.Y. Chen (1983): Statistical Significance and its Determination by Monte Carlo Techniques. *Mon. Wea. Rev. 111, 46-58.*

van Loon, H. and K. Labitzke (1988): Associations Between the 11-Year Solar Cycle, the QBO and the Atmosphere. Part II: Surface and 700 mb in the Northern Hemisphere in Winter. *J. Climate 1: 905-920.*

El Niño-Southern Oscillation and rainfall variability

Neville Nicholls
BMRC, Melbourne, Australia

Introduction

Conrad (1941) examined the dependence of interannual rainfall variability on the long-term mean annual rainfall, using data from 384 stations spread across the globe. He defined the relative variability of annual rainfall as the mean of the absolute deviations of annual rainfalls from the long-term mean, expressed as a percentage of the long-term mean. Conrad found that a function relating relative variability to mean precipitation fitted his data very well. The relative variability decreased, in general, as the mean precipitation increased. Over some large areas, however, the relative variability deviated in a consistent way from the global relationship with mean rainfall.

Some of these deviations were due to the influence of the El Niño-Southern Oscillation (ENSO) phenomenon on rainfall. Nicholls (1988), using Conrad's data, compared the relationship between relative variability and mean rainfall in areas affected by ENSO with the relationship elsewhere. The relative variability was typically one third to one half higher for ENSO-affected stations compared with stations with the same mean rainfall in areas not affected by ENSO. McMahon et al. (1987) have shown that rainfall (and streamflow) variability is higher in Australia and southern Africa (both areas affected by ENSO) than elsewhere.

This study (Nicholls and Wong, 1989) extends and confirms the studies of Conrad and Nicholls. More stations have been used. Only post-1950 data have been used (Conrad and Nicholls used pre-1941 data). A more conventional definition of relative variability, the coefficient of variation, was used in preference to Conrad's definition. The functional dependence of the variability on ENSO's influence is examined in more detail rather than simply dividing stations into a group affected by ENSO and a group not affected (as was done in Nicholls, 1988). The effect of latitude on variability is also considered. Mean annual rainfall and the effect of ENSO on rainfall tends to be larger in low latitudes so the results of Conrad and Nicholls might just reflect an effect of latitude on variability. This possibility has been allowed for by explicitly considering the effect of latitude, as well as mean rainfall and ENSO, on the relative variability.

Data and method

The data used here were obtained from the NCAR surface climatology data set. All stations with at least 25 years of annual rainfall totals post-1950 were used. This provided a total of 974 stations. For each station the long-term mean annual rainfall (P) and its standard deviation (s) were calculated. The coefficient of variation (V), the ratio of the standard deviation to the long-term mean (s/P), was calculated to provide a measure of the relative variability of annual rainfall.

A quantitative measure of the strength of the relationship between ENSO and the rainfall at each station was needed to examine the dependence of V on ENSO. The absolute value of the correlation between annual rainfall and annual values of the Southern Oscillation Index (SOI) was used as this measure. The SOI used here was the difference in pressure between Tahiti (17S, 150W) and Darwin (12S, 131E), standardised to a mean of zero and a standard deviation of 10. Monthly values of the SOI were provided by the National Climate Centre of the Australian Bureau of Meteorology. Annual values were calculated by averaging the twelve monthly values. The annual SOIs were then correlated with the annual rainfalls at the 974 stations and the absolute values of these correlations (R) were noted.

Preliminary work indicated that a relationship between latitude and rainfall variability existed. This relationship was strongest with the absolute value of the latitude (i.e. ignoring whether a station was north or south of the equator). So the absolute value of the latitude of each station (L) was noted. The elevation of the station was also noted since this might affect variability.

The correlations between variability, mean rainfall, latitude (unsigned), elevation, and the correlation of annual rainfall with the SOI (also unsigned) are listed in Table 1. Of the 974 stations with at least 25 years data since 1950, 19 did not have their elevation listed. This left 955 stations to use to calculate the correlations listed in the table. Elevation was not significantly correlated with variability and was not considered further. The other variables were all significantly correlated with each other, although most correlations were small in magnitude. Mean rainfall had the strongest relationship with variability, followed by latitude and the correlation with the SOI. As noted above, mean precipitation and the correlation of annual rainfall with the SOI are significantly correlated with latitude. Explicit inclusion of latitude as an independent variable in the following analysis is necessary therefore to confirm that the results of Conrad (1941) and Nicholls (1988) do not simply reflect the influence of latitude on variability.

Table 1: Correlations between the coefficient of variation of annual rainfall (V), mean annual rainfall (P), latitude (unsigned) of the station (L), correlation of annual rainfall with the SOI (unsigned, R), and the elevation of the station (E). Correlations with magnitudes exceeding 0.11 are significant at the 1 percent level.

	V	P	L	R
P	-0.40			
L	-0.22	-0.42		
R	0.18	-0.15	-0.15	
E	0.05	-0.19	-0.02	-0.02

The values of V, P, R, and L from the 974 stations were fitted, initially, to the following functional relationship:

$$V = (a/(b + P + g(R, L)) + c + h(R, L))(1 + k(R, L)) \quad (1)$$

where a, b, and c are parameters to be determined. The functions $g(R, L)$, $h(R, L)$, and $k(R, L)$ are each of a similar form i.e. $tR + uL + wRL$, with t, u, and w all parameters to be determined. Different values of t, u, and w could be expected for the three functions g, h, and k. In the absence of the functions g, h, and k, equation (1) would be of the form used by Conrad (1941) and Nicholls (1988) i.e. with relative variability increasing nonlinearly with decreasing mean rainfall. Conrad (1941) explains why such a dependence is expected.

Equation 1 is of a very general form, allowing latitude and the correlation with the SOI to affect the relationship between variability and mean rainfall in several ways. The functions g, h, and k respectively allow the latitude and correlation to affect the slope of the relationship between V and P, allow the possibility of an additive effect of R or L on V, or of a multiplicative effect. Initial fitting of equation (1) to the data revealed that six of the nine parameters in the functions g, h, and k were not significantly different from zero. These parameters were therefore dropped, leaving the following simplified version of equation (1):

$$V = (a/(b + P + dR + eRL)) + c)(l + fL) \quad (2)$$

Here a, b, c, d, e, and f are the parameters to be determined by fitting the equation to the data from the 974 stations. Only the latitude (through the term fL) has a multiplicative effect on V and there

is no evidence of any additive effect. The term $dR + eRL$ affects the slope, or more correctly, the rate of change of the slope with P, The eRL term is an interaction effect showing that the effects of latitude and correlation with the SOI are **not** independent of each other, i.e. the effect of R on V will vary with L.

The above equation was fitted to the data for the 974 stations using the method of false position (Ralston and Jennrich, 1979), as was done in Nicholls (1988). The method is available in the SAS statistical analysis system and is described in SAS (1985).

Results

The result of fitting the data to equation (2) is the following equation, which accounts for 94 percent of the variance in V:

$$V = (150/(244 + P - 1010R + 23.47RL) + 0.15)(1 - .0068L) \quad (3)$$

Here the mean rainfall, P, is in millimetres, the latitude, L, is in degrees, and V and R are dimensionless. All of the six fitted parameters in equation (3) are significantly different from zero. In the absence of effects from the SOI and latitude this equation indicates that variability decreases as mean precipitation increases, with an asymptote of 0.15. Conrad (1941) and Nicholls (1988) found that a similar relationship between relative variability (as defined by Conrad) and mean precipitation accounted for much of the variance in the relative variability. Thus equation (3) confirms, on recent data, with more stations, and with a more conventional definition of variability, the results of Conrad (1941).

The final term in equation (3) indicates that latitude has a multiplicative effect on variability. Increasing latitude **reduces** variability over all values of the mean precipitation. The effect of this term is substantial. At a latitude of 30 degrees, in the absence of effects from the SOI, the multiplicative latitude term indicates that variability would be 80 percent of the corresponding variability at the equator. Variability at 60 degrees latitude is typically 60 percent of that at the equator, for the same mean precipitation (again ignoring effects due to the SOI).

The SOI does have a substantial effect on variability. The -1010R term in equation (3) indicates that a station with a strong relationship with the SOI will have a steeper relationship between variability and mean precipitation, i.e. the SOI will have little effect on the variability at stations with very large mean annual rainfall but typically enhances the variability substantially at stations with lower annual rainfall. The increased variability associated with the SOI confirms the results of Nicholls (1988).

The interaction term (23.47RL) indicates that increasing latitude weakens the effect of the SOI on variability. The effect of the SOI is strongest at the equator but actually reverses at latitude 43 degrees. Polewards of this latitude an increase in the correlation with SOI, according to equation (3), causes variability to decrease. This decrease is in fact very small and few stations polewards of latitude 43 degrees exhibit strong correlations with the SOI anyway but this term does indicate that the strongest effects of the SOI on variability are at low latitudes.

Concluding remarks

This study has confirmed the conclusion of Conrad (1941) that relative variability of annual rainfall decreases with higher mean rainfall. The conclusion of Nicholls (1988) that variability is typically higher, for a specific mean rainfall, in areas affected by ENSO has also been confirmed, at least for locations equatorwards of 43 degrees, a region that includes most of the stations strongly affected by ENSO. The Southern Oscillation amplifies climate variability in those areas it affects, even when the effects of latitude and mean rainfall are removed. These conclusions have been confirmed using about

three times as many stations as were used by Conrad and Nicholls, on recent data independent of the set used by Conrad and Nicholls, and using a more conventional definition of relative variability.

The study has revealed a clear dependence of variability on latitude with variability decreasing substantially as we move away from the equator, after removal of the effects of long-term mean rainfall and ENSO on variability. The cause of the dependence of variability on latitude requires explanation. It might arise from the tendency for convection to provide a larger proportion of annual rainfall in the tropics, or from the ability of occasional tropical synoptic systems (e.g. tropical cyclones) to produce very large amounts of rainfall.

The study has also revealed an interaction effect between latitude and correlation with the SOI. In the tropics stations strongly correlated with the SOI do tend to be more variable but this tendency weakens as we move polewards. Eventually, at 43 degrees latitude the relationship reverses and polewards of this latitude increasing correlation with the SOI implies slightly lower variability. This reversal of the relationship at higher latitudes is, to some extent, an artefact of the fitting process since there are few stations strongly correlated with the SOI at these latitudes.

In summary, variability of annual rainfall tends to be higher

- where mean annual rainfall is low,
- at lower latitudes, and
- where the Southern Oscillation has a strong influence (at least in tropical and subtropical latitudes).

The regions with the most variable annual rainfall are tropical deserts strongly affected by the Southern Oscillation.

The implications of the dependence of variability on latitude and the Southern Oscillation are wide-ranging. Nicholls (1988) suggested that the biota in areas where ENSO amplified variability should be better adapted to frequent climate variations than the biota elsewhere. Human patterns of usage of rainfall should also be adapted to the differences in variability in regions of different mean rainfall, latitude, and degree of influence from ENSO, if best use is to be made of this rainfall. The differences in variability in rainfall will lead to differences in frequencies of major droughts and floods, i.e. runoff variability (McMahon et al., 1987). Extrapolating European and North American models and methods for coping with droughts and floods to tropical countries affected by ENSO (and thus with higher relative variabilities, for the same mean rainfall) may not be appropriate.

References

Conrad,V., 1941: The variability of precipitation. *Mon. Wea. Rev., 69, 5-11.*

McMahon,T.A,, B.L.Finlayson, A.Haines, and R.Srikanthan, 1987: Runoff variability: a global perspective. *In The Influence of Climate Change and Climatic Variability on the Hydrologic Regime and Water Resources, IAHS Publication no. 168.*

Nicholls,N., 1988: El Niño - Southern Oscillation and rainfall variability. *J. Climate, 1, 418-421.*

Nicholls,N., and K.K.Wong, 1989: Dependence of rainfall variability on mean rainfall, latitude, and the Southern Oscillation. *Submitted to J. Climate.*

Ralston,M.L., and R.I.Jennrich, 1979: A derivative-free algorithm for nonlinear least squares. *Technometrics, 1, 7-14.*

SAS, 1985: SAS User's Guide: Statistics. SAS Institute Inc., 956 pp. [Available from SAS Institute, Inc., Box 8000, Cary, NC 27522-8000.]

Prediction of extremes of the Southern Oscillation with POP analysis

Jin-Song Xu
Max Planck Institüt fuer Meteorologie, Hamburg, FRG

Abstract The space-time characteristics of an ENSO lifecycle in the Southern Hemisphere sea level pressure (SLP) data are identified with the "Principal Oscillation Pattern" (POP) analysis which is designed to identify standing and migrating patterns in a geophysical multicomponent time series. Besides characteristic patterns, the POP technique provides a time evolution equation, which allows a prediction of the temporal development of the patterns' coefficients.

The data considered are monthly mean SLP anomalies of the area 15°S to 50°S and for periods 1951–58, and 1972–83. All variability on time scales shorter than 15 months are filtered out. The data are normalized by the standard deviation at each grid point.

One relevant migrating pattern is found with an oscillation period of about 34 months. It shows a temporal evolution similar to the SLP anomaly Southern Oscillation composites found by van Loon and Shea. The cross spectral analysis for the time series of POP coefficients and the El Nino SST-index indicates that the extratropical SLP anomalies evolve parallelly to the El Nino SST-index on a time scale of 20 to 40 months.

In a number of hindcast experiments, it was attempted to predict the extremes of the Southern Oscillation in the 70's and 80's: The phase turned out to be well predictable with a lead time of a about one year in advance. The scheme is less sucessful in predicting the duration of an ENSO event.

Spectrum of univariate time series models with application to the Southern Oscillation

Pao-Shin Chu
Dept Meteorology, Univ Hawaii

Richard W. Katz
ESIG/NCAR, Boulder, Colorado

Introduction

The state of the Southern Oscillation (SO) is generally described by an index (SOI), which is the normalized sea-level pressure difference between Tahiti and Darwin. Based on the Fourier transform of the autocovariance or autocorrelation function (frequency-domain approach), many studies have found a broad range of large variance in the spectrum of the SOI, with a peak around 3–5 years (e.g., Trenberth, 1976; Chen, 1982).

Recently, Chu and Katz (1985) showed that temporal fluctuations in the SO, sampled between 1935 and 1983, can be adequately represented by parametric time series models. For instance, a third-order autoregressive [AR(3)] model is representative of the seasonal SO fluctuations and an autoregressive-moving average [ARMA(1,7;1)] model fits the monthly SO fluctuations well. Since these models were selected on the basis of a time-domain criterion, it is interesting to see what sort of spectral characteristics such time series models can produce. The purpose of the current study is to assess whether the well-known quasi-periodicity of the SO also can be reproduced from a time-domain approach (see also Chu and Katz, 1989). We will also examine the spectrum of the SO when a much longer time series (1856–1986) is used.

Modeling the SOI

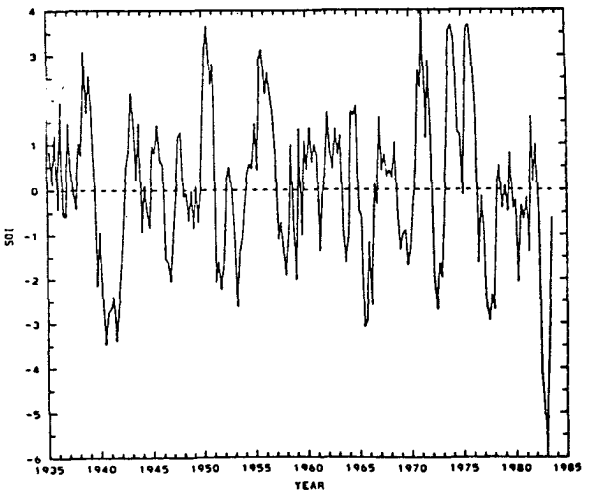

Figure 1: Time series plot of the seasonal SOI from Spring 1935 to Summer 1983 (Source: Chu and Katz, 1985, p. 1882).

Figure 1 shows the time series of the seasonal SOI from Spring 1935 to Summer 1983; the large negative anomalies between Summer 1982 and Spring 1983 in association with the strong El Niño event are most conspicuous. The Bayesian Information Criterion (BIC), introduced by Schwarz (1978), was used

to objectively determine the appropriate order of an ARMA process. It is expressed mathematically as

$$\mathrm{BIC}(p;q) = N\ln\hat{\sigma}_a^2(p;q) + S\ln N \tag{1}$$

where $\hat{\sigma}_a^2(p;q)$ denotes an estimator of the variance σ_a^2 of the error terms based on fitting an ARMA$(p;q)$ process to the data, and p and q are the orders associated with the autoregressive and moving-average parameters, respectively. In (1), N is the total number of observations, S the total number of parameters estimated [i.e., $S = p + q + n$, where n is the total number of additional parameters (e.g., means and standard deviations used to compute SOI)]. A model with the minimum BIC value is generally preferred.

Table 1: Estimated error variance $\hat{\sigma}_a^2$ and BIC value of ARMA$(p;q)$ models for the seasonal SOI time series. Source: Chu and Katz (1985, p. 1883).

p	q	$\hat{\sigma}_a^2(p;q)$	BIC$(p;q)$
0	0*	3.279	272.5
1	0	1.689	149.1
2	0	1.696	155.2
1	1	1.710	156.6
3	0	1.505	137.3
2	1	1.662	156.6
1	2	1.537	141.3
4	0	1.484	139.8
5	0	1.468	143.0

* Uncorrelated process.

Table 1 lists the error variance and BIC value for eight seasonal models, as well as for an uncorrelated process. An AR(3) process appears to be the model with the smallest sum of orders ($p + q = 3$) that has relatively low error variance; in particular, exhibiting the lowest BIC value. This model is of the form

$$X_t = \phi_1 X_{t-1} + \phi_2 X_{t-2} + \phi_3 X_{t-3} + a_t \tag{2}$$

where the parameter estimates are $\hat{\phi}_1 = 0.6885$, $\hat{\phi}_2 = 0.2460$, $\hat{\phi}_3 = -0.3497$, and $\hat{\sigma}_a^2 = 1.505$.

Figure 2a displays the sample autocorrelation function of the seasonal SOI and the theoretical autocorrelation function for the AR(3) process. The theoretical autocorrelation function drops below zero at lag four, like the sample autocorrelation function. It then continues a damped oscillation about zero at higher lags. Figure 2b is a plot of the sample partial autocorrelations, which are small after the first three lags. This pattern also suggests that the seasonal time series might be described by purely AR processes.

The BIC method was also employed to help identify an optimal model for the monthly SOI. The first part of Table 2 lists the error variance $\hat{\sigma}_a^2$ and BIC value for several models. Among these candidate models, an ARMA(1;1) process has the smallest BIC value. In keeping with the goal of parsimony and the general features of ARMA processes, a single higher-order AR term (i.e., lag 2, 3, ..., or 12) is added to the ARMA(1;1) process. The error variance and BIC value for these additional models are included in the second part of Table 2. Results indicate that either the ARMA(1,7;1) or ARMA(1,9;1) model has the smallest error variance and BIC value.

For simplicity, an ARMA(1,7;1) model was selected and its theoretical autocorrelation function is shown in Figure 3a, along with the sample autocorrelation function of the monthly SOI. There is a

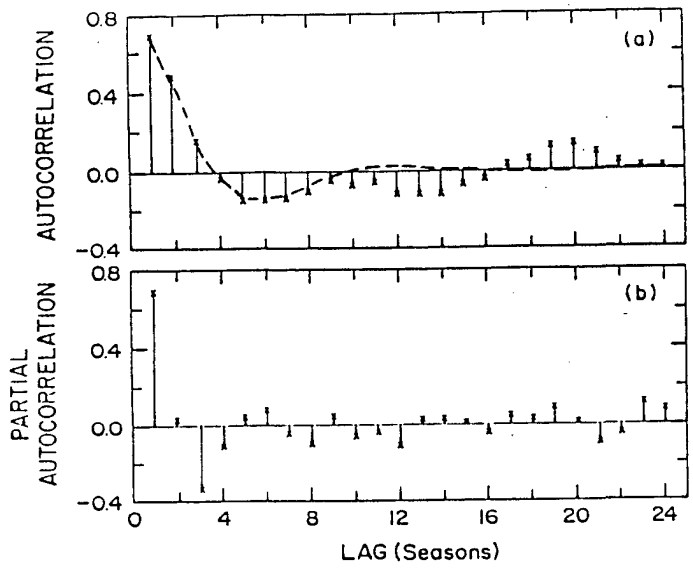

Figure 2: 2(a) Sample autocorrelation function of the seasonal SOI and the theoretical autocorrelation function (broken line) for AR(3) process. 2(b) Sample partial autocorrelation function of the seasonal SOI: Spring 1935 through Summer 1983 (Source: Chu and Katz, 1985, p. 1883).

Table 2: Estimated error variance $\hat{\sigma}_a^2$ and BIC value of ARMA models for monthly SOI time series. Source: Chu and Katz (1985, p. 1880).

ARMA($p;q$) models				ARMA(1,$p;q$)			
p	q	$\hat{\sigma}_a^2(p;q)$	BIC($p;q$)	p^{**}	q	$\hat{\sigma}_a^2(1,p;q)$	BIC(1,$p;q$)
0	0*	2.789	751.9	3	1	1.532	421.1
1	0	1.683	463.4	4	1	1.535	422.2
2	0	1.591	436.8	5	1	1.535	422.2
1	1	1.546	420.0	6	1	1.521	416.9
1	2	1.548	427.2	7	1	1.481	401.3
3	0	1.539	423.8	8	1	1.484	402.5
2	1	1.550	427.9	9	1	1.480	401.0
4	0	1.533	434.2	10	1	1.488	404.1
				11	1	1.501	409.2
				12	1	1.501	409.2

* Uncorrelated process.
** Single higher-order lag of AR process.

good agreement between the two curves. In Figure 3b, the sample partial autocorrelations exhibit a damped sine wave and are relatively small after the first lag. This selected ARMA(1,7;1) process is given by

$$X_t = \phi_1 X_{t-1} + \phi_7 X_{t-7} + a_t - \theta_1 a_{t-1} \tag{3}$$

where the parameter estimates are $\hat{\phi}_1 = 1.011$, $\hat{\phi}_7 = -0.115$, $\hat{\theta}_1 = 0.680$, and $\hat{\sigma}_a^2 = 1.481$.

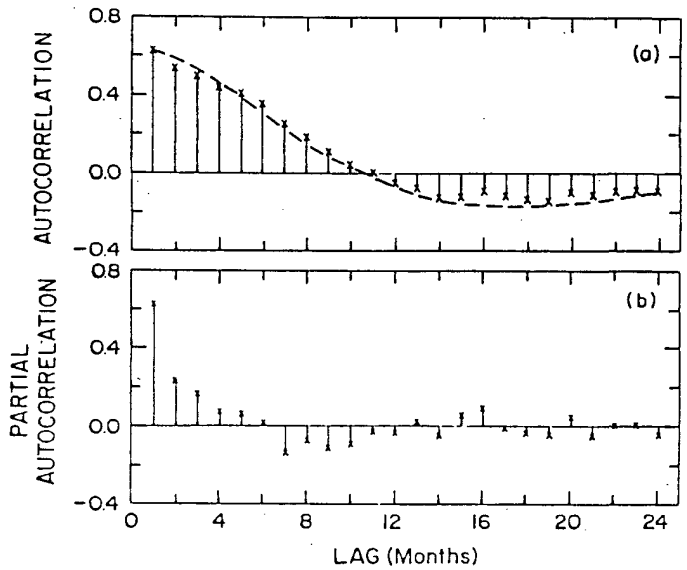

Figure 3: 3(a) Sample autocorrelation function of the monthly SOI and theoretical autocorrelation (broken line) for ARMA(1,7;1) process. (b) Sample partial autocorrelation function of the monthly SOI: January 1935 through August 1983 (Source: Chu and Katz, 1985, p. 1881).

Spectrum of SOI

Frequency-domain approach

A smoothed estimate of the sample spectral density function from a frequency-domain approach is obtained using the following formula:

$$\hat{s}(f) = 2\left[1 + 2\sum_{k=1}^{m-1} r(k)W(k)\cos(2\pi f k \Delta t)\right]\Delta t \tag{4}$$

where $m, r(k), W(k)$, and Δt are the maximum lag (i.e., truncation point), sample autocorrelation function, lag window, and time interval between observations (i.e., one month or one season), respectively. We use the Parzen lag window, i.e.,

$$W(k) = \begin{cases} 1 - 6\left(\frac{k}{m}\right)^2 + 6\left(\frac{|k|}{m}\right)^3 & |k| \le \frac{m}{2} \ , \\ 2\left(1 - \frac{|k|}{m}\right)^3 & \frac{m}{2} < |k| \le m \ , \\ 0 & |k| > m \ . \end{cases} \tag{5}$$

As shown in Figure 4, the preferred period of the seasonal SOI based on the frequency-domain approach is at time scales of more than 8 seasons, and a large peak is present near 20 seasons (5 years). The sample spectral density function of the monthly SOI using (4) is shown in Figure 5. Again, a large portion of energy is concentrated near 50 months (slightly more than 4 years).

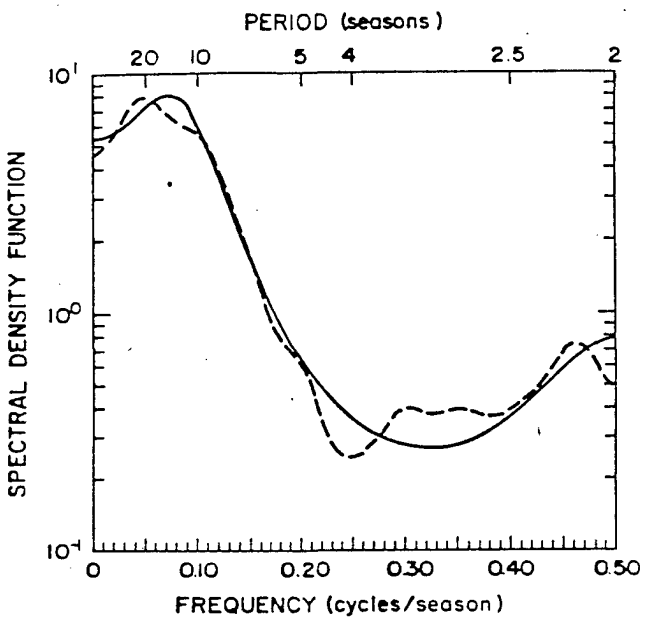

Figure 4: Spectral density function of the seasonal SOI from the frequency-domain approach (broken curve) and time-domain approach (solid curve). Analysis period is from Spring 1935 to Summer 1983. Parzen lag window is used with maximum lag of 30 seasons (broken curve). Note that the scale on the ordinate is logarithmic, whereas the scale on the abscissa is linear (Source: Chu and Katz, 1989, p. 88).

Time-domain approach

The generalized form of the theoretical spectrum of an AR(p) process can be expressed as (Box and Jenkins, 1976)

$$p(f) = \frac{2\sigma_a^2}{|1 - \phi_1 e^{-i2\pi f} - \phi_2 e^{-i4\pi f} - \cdots - \phi_p e^{-i2\pi p f}|^2} \tag{6}$$

For an AR(3) model, (6) reduces to$p(f) =$

$$\frac{2\sigma_a^2}{1 + \phi_1^2 + \phi_2^2 + \phi_3^2 - 2(\phi_1 - \phi_1\phi_2 - \phi_2\phi_3)\cos 2\pi f - 2(\phi_2 - \phi_1\phi_3)\cos 4\pi f - 2\phi_3 \cos 6\pi f} \tag{7}$$

The spectral density function is defined as

$$s(f) = \frac{p(f)}{\sigma^2} \tag{8}$$

where σ^2 is the variance of the X_t process.

For the mixed ARMA$(p;q)$ model, the generalized form of the theoretical spectrum is

$$p(f) = 2\sigma_a^2 \frac{|1 - \theta_1 e^{-i2\pi f} - \cdots - \theta_q e^{-i2\pi qf}|^2}{|1 - \phi_1 e^{-i2\pi f} - \cdots - \phi_p e^{-i2\pi pf}|^2} \tag{9}$$

In the case of an ARMA(1,7;1) process, the theoretical spectrum becomes

$$p(f) = 2\sigma_a^2 \frac{1 + \theta_1^2 - 2\theta_1 \cos 2\pi f}{1 + \phi_1^2 + \phi_7^2 - 2\phi_1 \cos 2\pi f - 2\phi_7 \cos 14\pi f + 2\phi_1\phi_7 \cos 12\pi f} \tag{10}$$

Given the three parameters estimates and the white noise variance for an AR(3) model from (2), the theoretical spectral density function using (7) and (8) is displayed in Figure 4. A large portion of power is found in the lower frequency end, with a peak somewhere near 14.3 seasons (~4 years). The theoretical spectral density function of an AR(3) model also displays an increase in energy in the high-frequency tail, just like the sample spectral density function. For the monthly SO fluctuations, the spectral estimates from the time-domain [using (10)] and frequency-domain approaches are also reasonably consistent (Figure 5).

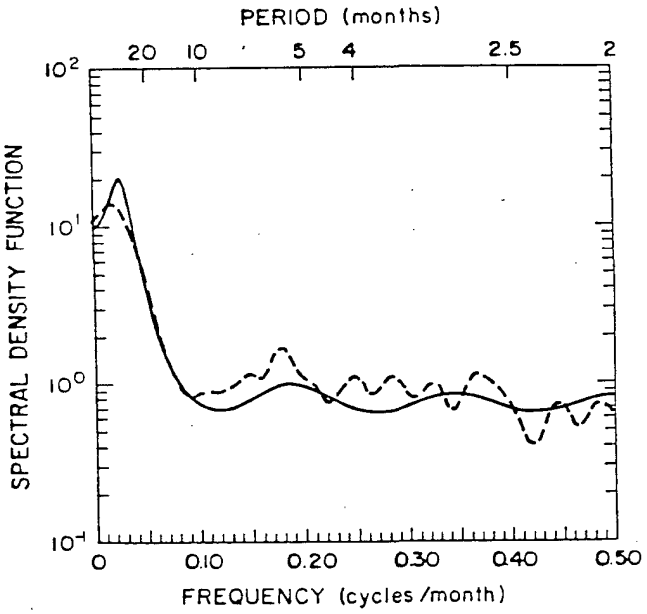

Figure 5: Spectral density function of the monthly SOI from the frequency-domain approach (broken curve) and time-domain approach (solid curve). Analysis period is from January 1935 to August 1983. Parzen lag window is used with a maximum lag of 60 months (broken curve) (Source: Chu and Katz, 1989, p. 89).

The difference between these two approaches, as revealed in either Figures 4 or 5, is partially due to the fact that the selected time series models only attempt to mimic the general behavior of the SO fluctuations and are not necessarily representative of its details. This selection is made in order to achieve parsimony and maximize predictability (Chu and Katz, 1987). Another reason for the difference between the two approaches is simply the uncertainty in point estimates of the sample spectrum.

Spectrum of SOI from a historical data set

All of the aforementioned work has been based on a relatively short record length, namely, from 1935 to 1983. Recently, a historical data set of the monthly SOI dated back to 1856 was provided to us by P.D. Jones (Climatic Research Unit, University of East Anglia). This larger data base presents an unusual opportunity to examine secular changes in the Southern Oscillation, since the SOI signal may possibly be different from time to time (Elliot and Angell, 1988).

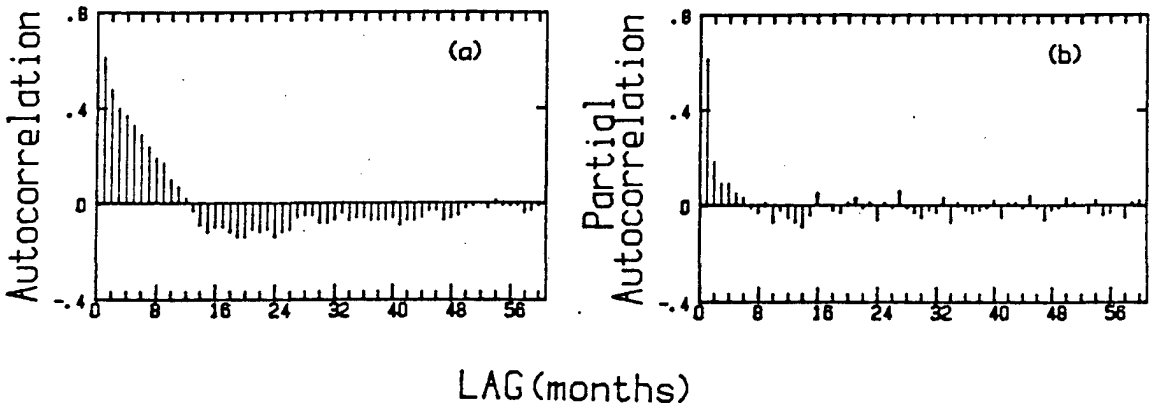

Figure 6: 6(a) Sample autocorrelation function of the monthly SOI. (b) Sample partial autocorrelation function of the monthly SOI: January 1856 through December 1986.

Figure 6 displays the autocorrelation and partial autocorrelation functions of the monthly SOI (1856 to 1986) for lags up to 60 (months). In general, the patterns revealed in Figure 6 resemble those in Figure 3. Following the procedure described in Section 2, a mixed ARMA(1,14;1) process has been identified as the optimal model to represent the monthly fluctuations of this historical data set. Figure 7 shows the sample and theoretical spectra for this data set.

Again, the estimates based on the frequency-domain and time-domain approaches are reasonably consistent. We also derived the theoretical spectra for ARMA(1;1) and ARMA(1,7;1) processes; neither of the processes shows any intermediate peak in the spectrum.

References

Box, G.E.P., and G.M. Jenkins, 1976: *Time Series Analysis: Forecasting and Control* (rev.), Holden-Day, 575 pp.

Chen, W.Y., 1982: Assessment of Southern Oscillation sea-level pressure indices. *Mon. Wea. Rev.*, **110**, 800–807.

Chu, P.-S., and R.W. Katz, 1985: Modeling and forecasting the Southern Oscillation: A time-domain approach. *Mon. Wea. Rev.*, **113**, 1876–1888.

Chu, P.-S., and R.W. Katz, 1987: Measures of predictability with applications to the Southern Oscillation. *Mon. Wea. Rev.*, **115**, 1542–1549.

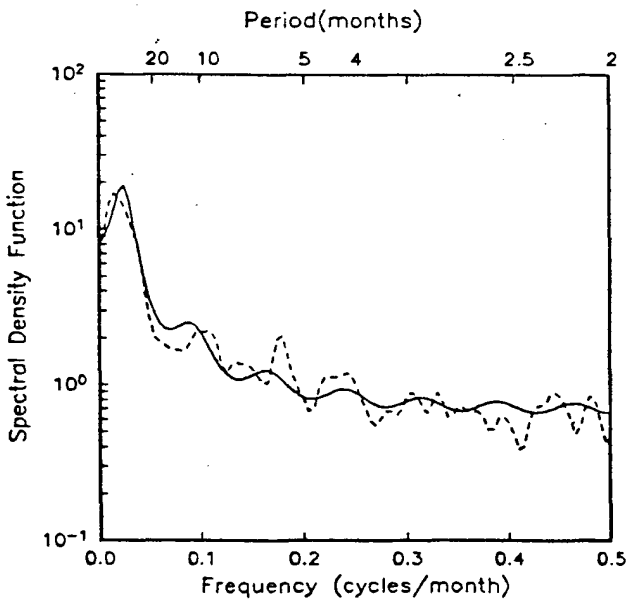

Figure 7: Spectral density function of the monthly SOI from the frequency-domain approach (broken curve) and the time-domain approach (solid curve). Analysis period is from January 1856 to December 1986. Parzen lag window is used with a maximum lag of 100 months (broken curve).

Chu, P.-S., and R.W. Katz, 1989: Spectral estimation from time series models with relevance to the Southern Oscillation. *J. Climate*, **2**, 86–90.

Elliot, W.P., and J.K. Angell, 1988: Evidence for changes in Southern Oscillation relationships during the last 100 years. *J. Climate*, **1**, 729–737.

Schwarz, G., 1978: Estimating the dimension of a model. *Ann. Statist.*, **6**, 461–464.

Trenberth, K.E., 1976: Spectral and temporal variations of the Southern Oscillation. *Quart. J. Roy. Meteor. Soc.*, **102**, 639–653.

Multivariate assessments of the anthropogenic greenhouse effect based on observational climatic data from both hemispheres

Christian-D. Schönwiese
J.W. Goethe University, Institute for Meteorology and Geophysics, Frankfurt, FRG

Introduction

As a consequence of human activity a substantial increase of the atmospheric concentration of a number of trace gases is observed. So, the atmospheric carbon dioxide (CO_2) concentration has increased over the past 200 years from preindustrial estimates of approximately 280 ppm (10) to a value of 347 ppm in 1986 at Mauna Loa Observatory, Hawaii (8), see Fig. 1.

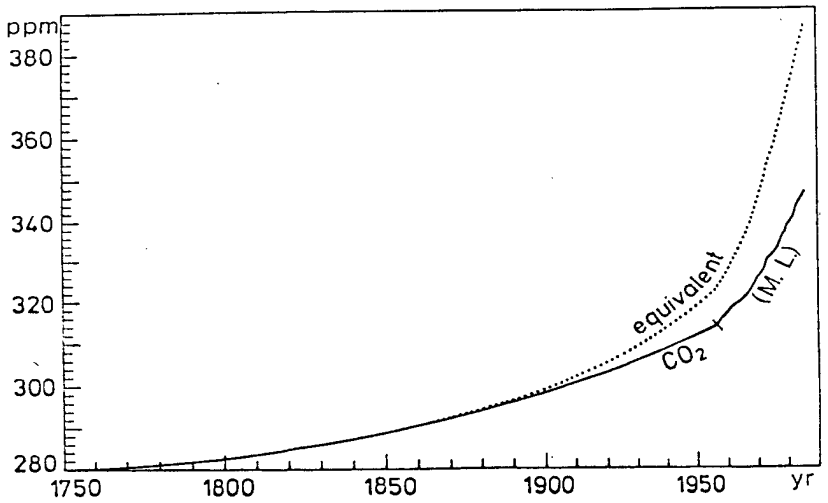

Figure 1: Measured (Mauna Loa (8)) and reconstructed (10) annual mean atmospheric CO_2 concentration (using a double-logarithmic regression in case of the reconstructed data (12c)), in addition 'equivalent' CO_2 concentration (19).

The corresponding radiative effect of some additional trace gases such as the chloroflourocarbons (CFCs), methane (CH_4), nitrous oxide (N_2O), tropospheric ozone (O_3) etc. can be expressed in terms of CO_2 'equivalents' (19), see again Fig. 1, contributing also to the greenhouse warming.

The climate response to an atmospheric CO_2 doubling was simulated by climate models of different complexity. It is only the (three-dimensional) general circulation models (GCMs) that can properly simulate not only the response of the most important climate elements (temperature, precipitation etc.) but also their regional patterns. Neglecting the '81' experiment in Fig. 2, the result of the recent GCM CO_2 doubling experiments is a globally averaged temperature increase near the ground of 1.3-5.2 K.

It is very important to verify the anthropogenic greenhouse effect projected by climate models, as early as possible, by means of observational statistics. The major problems concern the use of appropriate climatic data sets, the implication of natural forcing parameters (multivariate analysis),

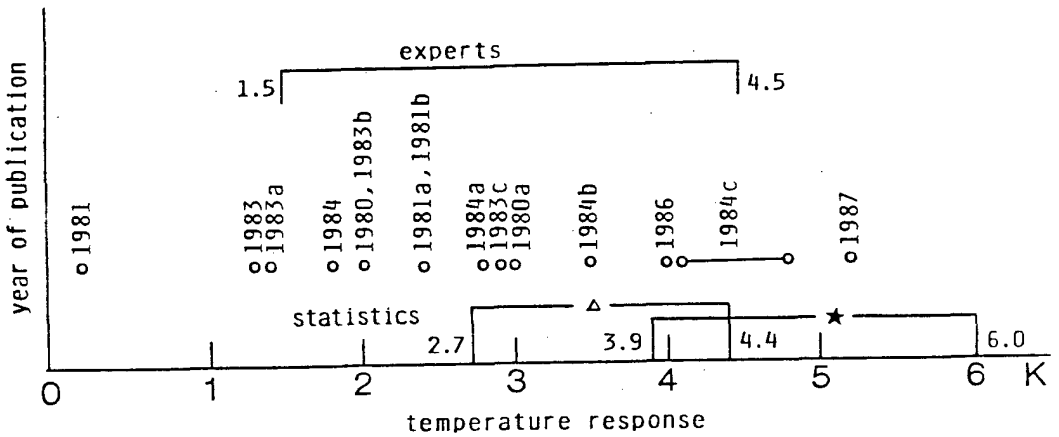

Figure 2: Annual and global mean temperature increase (near surface) in case of an atmospheric CO_2 doubling according to GCM experiments published since 1980 (the numbers indicate the year of publication, authors see (17,19) and corresponding statistical assessments with (*) and without ($\triangle$) phase shift of the temperature response in respect to the CO_2 concentrations.

proper signal and signal-to-noise assessments and, last not least, assessments of the time lag of the climate response in respect to the greenhouse gases forcing. In a series of statistical verification studies (12,13,16) of the climate model results it was tried to obtain some assessments of both the present and the projected climate response to increasing greenhouse gases. Recently (17) we modified some of the natural forcing parameters, included ENSO (El Niño/southern oscillation) parameters, used not only CO_2 but also the 'equivalent' CO_2 time series and introduced time lags.

Data base

In particular, the following anthropogenic and natural forcing parameter time series are used (annual data).

1. Atmospheric CO_2 concentration, alternatively 'equivalent' CO_2 concentration, both as shown in Fig. 1. The CO_2 data before 1958 are calculated by means of a double-logarithmic regression based on the ice core data from Neftel et al. (10), later on the Mauna Loa observations (8) were used. In order to get a best fit the ice core regression data were corrected by +1 ppm. The added 'equivalent' data are from Tricot and Berger (19).

2. Volcanic activity parameters, four alternative time series: stratospheric 'dust veil index DVI from Lamb (9); acidity index AI from Hammer et al. (5) based on Greenland ice core reconstructions (only northern hemisphere; same index implying regional corrections not used here); 'Smithsonian volcanic index' SVI based on the Smithsonian volcanoe chronology edited by Simkin et al. (18) modified by Schönwiese (14); same index but again modified by Schönwiese and Cress (15) implying an empirical stratospheric residence time of the volcanogenic particles based on AI/SVI intercomparisons (SVI*).

3. Solar forcing, six alternative parameters, later reduced to four alternative parameters, mainly based on solar activity (relative sunspot numbers SRN and derived hypotheses discussed elsewhere (12)) and the solar diameter oscillation hypothesis as supposed by Gilliland (3) in terms of hypothetical temperature oscillations TSD.

4. El Niño/southern oscillation (ENSO) forcing represented by the tropical Pacific sea surface temperature (SST) anomalies as reconstructed by Wright (20) or Schneider and Schönwiese (11), respectively.

These forcing parameter time series are correlated with time series of the following observational climatic time series.

1. Air temperature near the ground, focussed on land areas, northern hemisphere TNH-J since 1851, southern hemisphere TSH-J (62.5° S) since 1858 and global TGL-J (since 1858) mean estimates from Jones et al. (7), alternatively hemispheric and global mean estimates since 1881 from Hansen and Lebedeff (6) TNH-H, etc.

2. Sea surface temperatures, hemispheric and global means, data alternatively since 1856 from Folland et al. (2) SNH-F etc., or since 1854 from Jones et al. (7) SNH-J etc.

3. (c) Global mean sea level data since 1881, alternatively from Barnett (1) LGL-B or Gornitz et al. (4) LGL-G.

In addition to these hemispheric or global and annual averages we used in case of the northern hemisphere air temperature near the ground (land areas) also gridded monthly data (5° degree latitude and 10° longitude grid; results presented in (17)). A corresponding global analysis using the 'box data' from Hansen and Lebedeff (6) is in preparation (for an analysis of stratospheric data see elsewhere (13)).

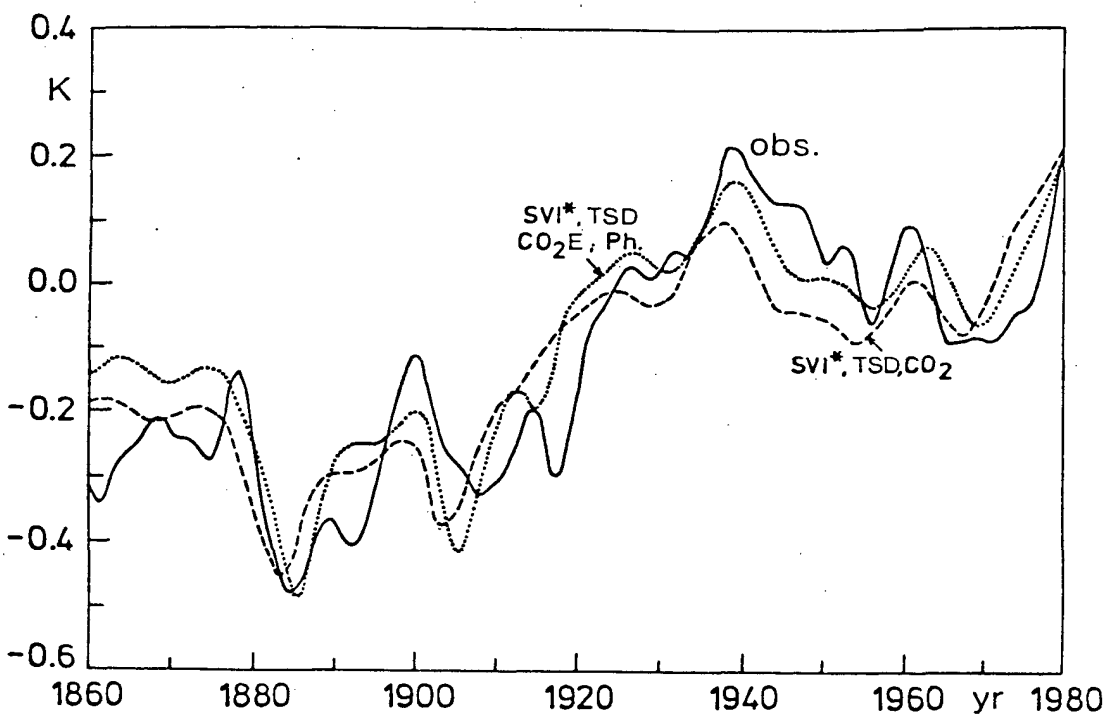

Figure 3: Observed 10 yr low-pass filtered mean northern hemisphere temperature fluctuations, solid line (7), and statistical reproductions using the volcanic SVI*, the solar TSD parameter and the observed CO_2 increase, dashed line, or the 'equivalent' CO_2 increase implying a 20 yr phase shift, dotted

Statistical method

Based on an univariate correlation analysis using annual as well as 3 yr and 10 yr Gaussian low-pass filtered data, in the first approach a simple linear multivariate regression model was evaluated

$$A = a + bV + cR + dE + eC \tag{1}$$

where A is any climatic element, V any volcanic parameter, R any solar parameter, E any ENSO parameter and C the CO_2 or 'equivalent' CO_2 forcing. All of these parameters V, R, E and C are alternatively used (only one volcanic, solar etc. parameter in each regression). One gets a matrix of regression coefficients explaining the observed climatic time series variance to a certain extent. The reliability of the results is checked by means of usual statistical tests of the univariate and multivariate correlation coefficients taking account for autocorrelation (reduced degrees of freedom) and non-Gaussian distributed quantities. Moreover, a coherence analysis was applied to assess the spectral features of the correlations.

In the second approach time lags (of the climatic elements in respect to the forcing parameters, the latter leading) are introduced. Fig. 3 presents two examples of alternative reproductions of the observed northern hemisphere air temperature (land areas) fluctuations, 10 yr low-pass filtered data, as reproduced by the different multiple regression models. It is found that the observed temperature decrease approximately 1940-1970 can be hypothetically explained by the volcanic SVI or, alternatively, by the solar TSD parameter (detailed discussion see elsewhere (12)). Fig. 4 shows similar reproductions for the northern hemisphere.

As soon as the regression coefficients are known any climate signals, observed or projected, can be computed. These signals describe the climate response to any forcing. For instance, a CO_2 doubling signal S, related to the air temperature near the ground, is obtained from

$$S = A_{max} - A_{min} = f(\overline{V}, \overline{R}, \overline{E}, C_{max} = 600 \text{ ppm}) - f(\overline{V}, \overline{R}, \overline{E}, C_{min} = 300 \text{ ppm}) \tag{2}$$

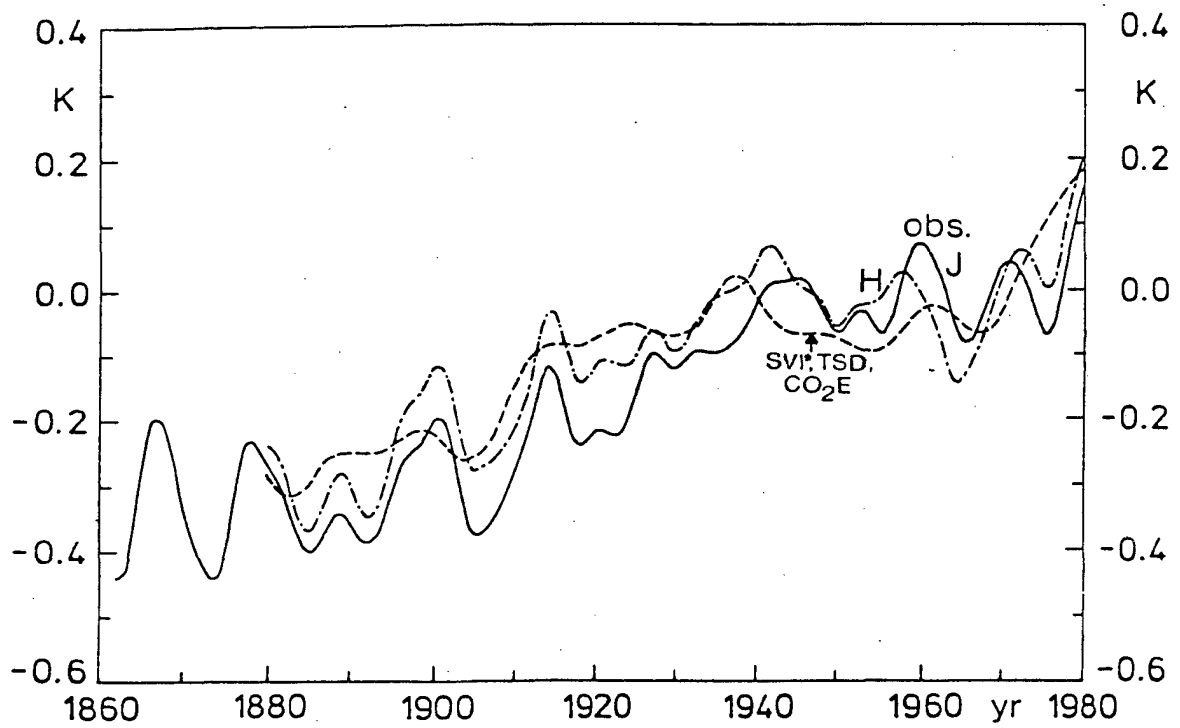

Figure 4: Similar to Fig. 3, but southern hemisphere, observed data from Jones et al. (7), solid line, or Hansen and Lebedeff (6), dashed-dotted line, statistical reproduction using the 'equivalent' CO_2 increase without phase shift, dashed line.

where $\overline{V}$, $\overline{R}$ and $\overline{E}$ are the long-term averages of the natural forcing parameters and C the CO_2 concentrations. Note that these signals describe the response of any climate element only in respect to one selected forcing parameter but that, nevertheless, this signal assessment is based on a multivariate statistical analysis (using the multiple regression coefficients). In the case that the observed standard deviation s of the (in general annual) climatic data is defined to represent the climatic 'noise' N (=s), S/N are assessments of the related signal-to-noise ratios specifying the signal confidence levels.

Some results

Only a few results can be presented here neglecting the regional and seasonal pattern of the climatic response to increasing greenhouse gases. Table 1 summarizes some of these signal assessments concerning the mean hemispheric and global data where the signals are evaluated from the multivariate analysis of 10 yr or 3 yr low-pass filtered data. The Tables specify the following.

1. 'Industrial' signals using the observed preindustrial (C_{min}) and recent (C_{max}) atmospheric trace gas concentrations, in case of CO_2 C_{min} = 280 ppm and C_{max} = 347 ppm, in case of 'equivalent' CO_2 C_{min} = 280 ppm and C_{max} = 386 ppm (see Fig. 1).

2. 'Projected' signals, i.e. extrapolations based on the observational statistics, in case of CO_2 C_{min} = 300 ppm and C_{max} = 600 ppm, in the 'equivalent' case C_{min} = 300 ppm and C_{max} = 900 ppm.

Note that in the 'industrial equivalent' case the same observed temperature (or sea level) change is attributed to the increasing trace gas concentrations than in case that 'only CO_2' is considered. The introduction of the 'equivalent' approach, therefore, means less sensitivity of the climate response to

Table 1: Extremely abbreviated results concerning the multivariate statistical assessments of the climate signals forced hypothetically by the anthropogenic increase of the greenhouse gases; 10 yr or if '*' indicated 3 yr low-pass filtered data. (Explanations and abbreviations see text; ± specifies the standard deviations arising from the different regression models.)

record	period	mean mult. correlation	'industrial' signals in K or (LGL) cm only CO_2	'equivalent' (S/N)	reduced to CO_2	projected signals in K or (LGL) cm CO_2 doubling	'equivalent'
TNH-J	1881-1980	0.76	0.7±0.2	0.6±0.2 (2.4)	0.4±0.1	3.2±0.8	3.5±1.2
TNH-J	1851-1980	0.78	0.7±0.2	0.7±0.2 (3.0)	0.5±0.1	3.3±0.8	4.1±1.3
*TNH-J	1881-1980	0.70	0.8±0.2	0.7±0.2 (2.6)	0.4±0.1	3.5±0.9	3.8±1.0
*TNH-H	1881-1980	0.75	1.0±0.2	0.8±0.3 (3.2)	0.5±0.2	4.4±1.0	4.6±1.5
TSH-J	1881-1980	0.86	0.8±0.1	0.7±0.1 (4.1)	0.5±0.1	3.5±0.6	4.1±0.9
TSH-J	1858-1980	0.85	0.8±0.1	0.8±0.1 (4.3)	0.5±0.1	3.5±0.4	4.3±0.4
*TSH-J	1881-1980	0.81	0.8±0.2	0.8±0.2 (4.3)	0.5±0.1	3.8±0.8	4.4±1.0
*TSH-H	1881-1980	0.72	0.6±0.1	0.6±0.1 (3.6)	0.4±0.1	2.7±0.2	3.3±0.4
TGL-J	1881-1980	0.81	0.8±0.2	0.7±0.2 (3.2)	0.4±0.1	3.4±0.7	3.8±0.8
TGL-J	1858-1980	0.83	0.7±0.1	0.7±0.1 (3.6)	0.4±0.1	3.3±0.5	4.0±0.6
*TGL-J	1881-1980	0.78	0.8±0.2	0.7±0.2 (3.4)	0.5±0.1	3.6±0.8	4.1±0.9
TGL-H	1881-1980	0.77	0.8±0.2	0.7±0.2 (3.3)	0.5±0.1	3.6±0.8	4.1±1.1
SNH-F	1881-1980	0.63	0.5±0.2	0.5±0.2 (2.9)	0.3±0.2	2.3±0.9	2.8±1.3
SSH-F	1881-1980	0.64	0.5±0.1	0.5±0.1 (3.9)	0.3±0.1	2.2±0.3	2.7±0.4
SGL-F	1881-1980	0.66	0.5±0.1	0.5±0.1 (3.3)	0.3±0.1	2.3±0.5	2.8±0.7
*SGL-F	1881-1980	0.60	0.5±0.1	0.5±0.1 (3.5)	0.3±0.1	2.4±0.4	3.0±0.5
SNH-J	1881-1980	0.75	0.7±0.2	0.6±0.2 (3.6)	0.4±0.2	3.1±1.0	3.6±1.4
SSH-J	1881-1980	0.74	0.6±0.1	0.6±0.1 (3.5)	0.4±0.1	2.7±0.3	3.2±0.4
SGL-J	1881-1980	0.78	0.6±0.1	0.6±0.1 (3.5)	0.4±0.1	2.9±0.6	3.4±0.9
*SGL-J	1881-1980	0.74	0.6±0.2	0.6±0.1 (3.4)	0.4±0.1	2.8±0.8	3.3±1.1
LGL-B	1881-1980	0.95	28±3	27±4 (5.9)	17±2	127±13	154±22
LGL-G	1881-1980	0.87	16±1	15±2 (5.2)	10±1	70±6	85±10

Table 2: Similar to Table 1, but implying a phase shift of 20 yr (gas concentrations leading) and only land based air temperatures.

record	period	mean mult. correlation	'industrial' signals in K only CO_2	'equivalent' (S/N)	reduced to CO_2	projected signals in K CO_2 doubling	'equivalent'
TNH-J	1881-1984	0.84	0.8±0.1	0.9±0.1 (3.5)	0.6±0.1	3.8±0.5	5.1±0.7
*TNH-J	1881-1983	0.74	1.2±0.2	1.3±0.2 (5.1)	0.8±0.1	5.3±0.8	7.5±1.1
TSH-J	1881-1984	0.91	1.0±0.1	1.2±0.1 (6.6)	0.7±0.1	4.7±0.4	6.7±0.7
*TSH-J	1881-1983	0.84	1.2±0.2	1.3±0.2 (7.4)	0.8±0.1	5.2±0.6	7.6±0.9
TGL-J	1881-1984	0.88	0.9±0.1	1.0±0.1 (5.0)	0.7±0.1	4.3±0.4	5.9±0.6
*TGL-J	1858-1983	0.82	1.2±0.2	1.3±0.2 (6.4)	0.8±0.1	5.3±0.7	7.6±1.0

the greenhouse gases forcing. In consequence, using only the CO_2 time series, the climate response is overestimated. The 'equivalent' approach, however, can be used to assess a 'reduced' and therefore more correct CO_2 contribution to the climatic greenhouse effect. This is done in the way that the 'equivalent' CO_2 time series is used for the computation of the regression coefficients but the assessment of the 'reduced' CO_2 signals is based only on the CO_2 contribution.

In Table 1 every signal assessment is based on 12 combinations (using only three volcanic parameters: DVI, AI and SVI*) and additional 24 combinations introducing the ENSO parameters. The uncertainties ± are the signal standard deviations due to the use of different natural forcing parameters. Taking into account these incertainities, it is concluded that - on a global average and concerning the air temperature of the land areas near the ground - a temperature rise of 0.5-1.0 K (since preindustrial time) may be hypothetically attributed to the 'combined' greenhouse effect ('equivalent' approach, until 1986) and a contribution in the order of 0.3-0.6 K may be due to the CO_2 increase. In the case of the SST assessments, in particular using the data from Jones et al. (7), these statistical assessments are quite similar but in case of the sea level these assessments strongly depend on the underlying climatic data: 13-17 cm using the data from Gornitz et al. (4) but 25-30 cm using the data from Barnett (1; same magnitude as the observed overall sea level increase or even more).

The statistical extrapolation to a CO_2 doubling or corresponding 'equivalent' situation leads to a temperature increase of 2.7-4.4 K (CO_2) or 3.0-5.2 K ('equivalent', 'combined'). The CO_2 assessments are in fair agreement with the climate model (GCM) projections, see Fig. 2. The corresponding sea level assessments (70-170 cm), however, may lead to overestimations when compared with the recent expert statements.

One of the major problems arising in this context is that in Fig. 2 equilibrium climate model projections are compared with observational statistics which describe the non-equilibrium reality. It is, however, difficult, to assess a realistic phase shift of the climate in respect to the greenhouse gases forcing. Based on a statistical cross correlation analysis and statistical best fit strategies (see Fig. 3 and 4) a magnitude of roughly 20 yr may be supposed. Following this hypothesis the statistically assessed temperature rise in case of a CO_2 doubling (air temperature near the ground, global average) would amplify from 2.7-4.4 K (as stated above) to 3.9-6.0 K, see Table 2. Another problem is the non-linearity of the climate response. Assuming a logarithmic relationship as discussed elsewhere this temperature response would be damped by a factor of approximately 0.7 compensating, more or less, the phase shift effect.

References

(1) Barnett, T.P., 1987: Priv. comm.

(2) Folland, C.K., Parker, D.E., Kates, F.E., 1984: *Nature, 310, 670-673*

(3) Gilliland, R.L., 1983: *Climate Change 4, 111-131*

(4) Gornitz, V., Lebedeff, S., Hansen, J., 1982: *Science, 215, 1611-1614*

(5) Hammer, C.U., Clausen, H.B., Dansgaard, W., 1980: *Nature, 288, 230-235*

(6) Hansen, J., Lebedeff, S., 1987: *J. Geophys. Res., 92, 13345-13372*

(7) Jones, P.D., Wigley, T.M.L., Kelly, P.M.: *Monthly Weath. Rev., 110, 59-70 (1982); updatings Climate Monitor; US Carbon Dioxide Information and Analysis Center, data on magnetic tapes; priv. comm. (1987, 1988).*

(8) Keeling, C.D., 1985, 1987: Priv. comm.

(9) Lamb, H.H., 1983: *Climat. Monitor, 12, 79-80 (1983); priv. comm. (1985)*

(10) Neftel, A., Moor, E., Oeschger, H., Stauffer, B.,1985: *Nature, 315, 45-47.*

(11) Schneider, U., Schönwiese, C.D., 1989 : In preparation.

(12) Schönwiese, C.D.: *Arch. Met. Geoph. Biocl., Ser. B., 32, 337-360 (1983); 35, 155-178 (1984): Theoret. Appl. Clim., 37, 1-14 (1986).*

(13) Schönwiese, C.D.,1987: *Contr. Atmos. Physics, 60, 48-64.*

(14) Schönwiese, C.D.,1988: *Atmosfera, 1, 141-156*

(15) Schönwiese, C.D., Cress, A., 1988: *Meteorol. Rdsch., 41, 89-92*

(16) Schönwiese, C.D., Malcher, J., 1987: *J. Climatol., 7, 215-229*

(17) Schönwiese, C.D., Runge, K., 1988: *Report No. 76, Inst. Meteorol. Geophys., Univ. Frankfurt (FRG), in German*

(18) Simkin, T., Siebert, L., McClelland, L., Bridge, D., Newhall, C., Latter, J.H., 1981: Volcanoes of the World. *Stroudsburg; Supplements (1985).*

(19) Tricot, C., Berger, A.,1987: *Climat. Dyn., 2, 39-61.*

(20) Wright, P., 1984: *Monthly Weath. Rev., 112, 1913-1919*

Multiple recurrence analysis

F.W. Zwiers[1] and Hans von Storch[2]
[1]Canadian Climate Centre, Downsview, Ontario, Canada, [2] Max Plank Institute für Meteorologie, Hamburg,F.R. Germany

Abstract In this paper we extend the concept of recurrence analysis (Storch and Zwiers, 1988) to the spatial domain and to multivariable problems, and draw a connection between recurrence analysis and multiple discriminant analysis (MDA). We discuss the application of the tools of MDA to the analysis of climate sensitivity experiments. Diagnostic techniques for assessing the degree of recurrence displayed in climate sensitivity experiments are described as are several tests for apriori specified degrees of recurrence. Several techniques are illustrated by applying them to an El Niño sensitivity experiment conducted with the Canadian Climate Centre General Circulation Model. It is shown that it is possible to classify observed Northern Hemisphere 500 mb height anomalies into warm and non-warm (cold and non-cold) events with a considerable degree of success using classification rules based on data from control and El Niño climate simulations.

Reference

Storch, H. v. and Zwiers, F.W., 1988: Recurrence Analysis of Climate Sensitivity Experiments, *Journal of Climate, 1, 157-171.*

Current climate lead to global change

F. Kogan
NOAA/NESDIS/AISC, Washington D.C., USA

Abstract

This paper presents an evidence that technological progress in the period of the green revolution is accompanied by a strengthening in climate impact on Earth. Because of this impact, some global changes have been detected. An index has been developed for early detection of these changes. Analysis of this index showed that, even within the range of the existing climatic fluctuations, some sizeable global change has been initiated recently. This occurred due to "confrontation" between climate and technology. The problem is that technology increases some of the economic indicators so significantly that they reach a level of climatic constraints. This study was based on the analysis of a 40 year time-series of wheat yields in 103 regions around the world. Yield is a convenient indicator to use in environmental studies because it correlates with climate and weather. In addition, yield reflects technological changes and also changes resulting from an interaction between climate and technology. The latter component as shown in the study, contributes considerably to global change. The results of the climate impact are observed currently on the area which produces nearly 40 percent of global wheat. This area has a significant negative balance between precipitation and potential evapotranspiration. Climate impact leading to global change is increasing in intensity and expanding to new areas. Calculations indicate that in 15 to 25 years climate related stagnation in wheat production will probably affect an area producing 55 to 60 percent of the world wheat output.

References

Kogan, F., 1986: Climate constraints and trend in global grain production. *Intl. J. Agric. For. Meteor.*, 37, 89-107.

Kogan, F., 1986: The impact of climate and technology on Soviet grain production. Delphic Associates, 178.

Detecting shifts, trends and periodicities

C.F. Ansley
Dept. Accounting and Finance, University of Auckland, New Zealand

Abstract

A number of new techniques for analyzing seasonal time series in the time domain have been developed recently in the statistics literature. First, there is a class of "structural" models, in which seasonal, trend and irregular (stationary or white noise) components are combined in an additive model. See, for example, Kitagawa and Gersch (1984) and Harvey (1985). Second, there are methods (Franzini and Harvey, 1984; Shively et al., 1988) for testing whether the innovation variances in these components are zero, in effect testing the stability of polynomial trends and seasonal cycles. Finally, there are new methods for model diagnostics and for detecting outliers and level shifts in time series (Tsay, 1986; Kohn and Ansley, 1988; Kohn and Ansley, 1989; Bruce and Martin, 1989.)

This paper reviews structural models and the hypothesis testing and diagnostic methods for detecting irregularities or changes in the model structure. The methods are illustrated by application to monthly rainfall, mean temperature and sunshine data. Time domain structural models are fit to each series, isolating the trend, seasonal and irregular components, and these components are used to characterize long-term time variablility. Measures of influence on the results of particular points and groups of points are given to eliminate spurious findings caused by outliers in the data.

References

Bruce, A.G., and Martin, R.D., 1989: Keave-*k*-out diagnostics for time series. *J.R. Statist. Soc.*(to appear).

Franzini, L., and Harvey, A.C., 1984: Testing for deterministic trend and seasonal components in time series models. *Biometrika***70**, 673-682.

Harvey, A.C., 1985: Trends and cycles in macro-economic time series. *J. Bus. Econ. Statist.* **3**, 216-227.

Kitagawa, G., and Gersch, W., 1984: A smoothness priors-state space approach to time series with trends and periodicities. *J. Amer. Statist. Assoc.* **79**, 378-389.

Kohn, R., and Ansley, C.F., 1988: A fast algorithm for signal extraction influence and cross validation in state space models. *Biometrika*(to appear).

Kohn, R., and Ansley, C.F., 1989: A fast method for estimating outliers and level shifts in state space models. (submitted J.?).

Shively, T.S., Ansley, C.F., and Kohn, R., 1988: Fast evaluation of the distribution of the Durbin-Watson and other invariant test statistics in regression. (submitted J.?).

Tsay, R.S., 1986: Time series model specification in the presence of outliers. *J. Amer. Statist. Assoc.* **81**, 132-141.

Locating periods with linear trends in climatic data series

Vladimir T. Radiuhin and Boris L. Shilenko
All-Union Research Inst of Hydromet Information, World Data Centre, Obninsk, USSR

Introduction

One of the major characteristics of the climatic signal is the period of its occurrence in the time series of the climate system parameters. The problem of locating such change points in statistical characteristics can be treated as that of failure detection in the time series (Nikiforov, 1983).

Statistical properties of certain randomness tests frequently employed in climate change research were studied (Radiuhin and Mikhlin, 1986) and it was concluded as a result that for detecting monotonic changes in the time series mean value, the test based on the number of inversions of the series values is a most efficient one of all those considered. If the signal is not present in the whole series in question but only in a portion of it, then it is clear that the signal is more easily detected by statistical means if the tests used are computed only from that portion with a trend (at least, the detection will be the more reliable as the relative portion of the series without a trend becomes smaller).

An algorithm is given below based on computing the inversion test from the running segments of the series in question to locate portions with monotonic trends in the mean value and estimate the signal-to-noise (s/n) ratio in the portions. As in (Radiuhin and Mikhlin, 1987) by the signal-to-noise we mean the determined change in the mean value of the time series on the segment where the signal is present to the standard deviations from the trend concealing the signal,

Algorithm for locating portions with linear trends

Note that the inversion test statistic t is computed by the formula $t = 1 - 4Q/n(n-1)$, where n is the length of the part of the time series for which the statistic is computed and Q is the number of inversions (reversals??) in this part of the time series. When analysing a time series of length N computing the inversion test statistic t from the moving parts of length n with the moving step K generates a series of the statistic values of length $L = [(N-n)/K] + 1$ (where [.] denotes integer part). The values of t for the part of the series under consideration without a trend fluctuate about the zero mean level with a distribution according to the null hyiothesis of a trend absence (Kendall and Stuart, 1973 ; Radiuhin and Mikhlin, 1986). When a moving part covers the part with a trend the statistics distribution shifts from the centre of the segment, [-1,1] - the range of values of the statistic t to its ends (to the right in case of a positive trend and to the left in case of a negative trend). The extent of shift in the statistical series mean depends on the level of the s/n ratio in the initial time series (Radiuhin and Shilenko, 1989). If the monotonic signal disappears from the series analysed, the original distribution of the series of values of the inversion test statistic is recovered. Thus, there occur some changes in the mean value of the statistic series in certain moments (to be more exact, during some intervals) and one can try to detect these changes.

To implement the algorithm for locating parts of the time series with a monotonic trend the quantiles of the statistic extreme ($max\{t\}$) and $min\{t\}$) distributions for various lengths n of the moving parts and values of s/n were first estimated using the statistical simulation method (Radiuhin and Shilenko, 1988).

The algorithm for detecting the start and end points of a monotonic trend in the time series mean comprises the following major steps:-

1. Using the initial data series of the climate system characteristic analysed, a series of the inversion test statistic values is computed from the moving parts of length n;

2. Maximum and minimum values are determined among the ones of the series t;

3. Using the above values as well as the $max\{t\}$ and $min\{t\}$ distribution quantiles for a zero signal-to-noise ratio and a corresponding n, the hypothesis H_0 of the absence of a monotonic signal at any significance level is tested;

4. If H_0 is not rejected, no further analysis is performed. If H_0 is rejected, the alternative hypothesis H_1^i of the presence of a monotonic signal with the s/n_i ratio is defined using the $max\{t\}$ (or $min\{t\}$) value. As an alternative to the null hypothesis H_1^i is assumed with a corresponding signal-to-noise ratio, if $t_\alpha^{i-1} < max\{t\} \leq t_\alpha^i$ ($-t_\alpha^i \leq min\{t\} < -t_\alpha^{i-1}$), where t_α^i is the $\alpha\%$ quantile of the $max\{t\}$ or $min\{t\}$ distribution when there is a signal in the series with the s/n_i ratio.

5. The change points in the mean of the series of the statistic t are detected by the cumulative sum algorithm (Nikiforov, 1983), i.e. a series of the cumulative sum (CS) values is computed:

$$\rho_k = \sum_{i=1}^{k} [\ln \omega(t_i/\theta_0, \sigma_0) - \ln \omega(t_i/\theta_1, \sigma_1)], \; k = 1 \ldots L$$

where $\omega(t/\theta, \sigma)$ is assumed to be the density of normal distribution, θ_1, σ_1 correspond to the alternative hypothesis assumed at the previous step. Within the series part where the hypothesis of the signal absence is more probable the CS increases, while within the part where the alternative hypothesis is more probable the CS decreases. Thus, the part with a trend is the one where the CS decreases.

The algorithm has been tested using simulated time series and accuracy characteristics for defining the signal-to-noise ratio and trend start and end moments have been obtained (Radiuhin and Shilenko , 1988). The conclusion was drawn from this that using the algorithm described one can locate parts with a linear trend in the mean even at modest signal levels with a varying degree of uncertainty.

Estimating the effect of intraseries statistical persistence

The parameters necessary for the above algorithm's implementation, the results of testing the algorithm on simulated series have been obtained on the assumption of mutual independence of deviations from the trend. The results must be dependent on the presence of intra-series persistence, in particular, the time series autocorrelation can be taken for a determined signal even if there is none. Estimates have been obtained of the inversion test statistic distribution to see to what extent the results are affected on a sample of 1000 simulated realisations of the stationary Gaussian Markov sequence (correlation function $r(\tau) = \exp(-\beta|\tau|)$ for various values of the attenuation parameter β characterizing the intra-series persistence. With persistence increases the probability of rejecting the null hypothesis whose critical region boundary is set on the assumption of independence of the successive terms of the series appeared to grow due to the increase of the statistic variance. The values of the null hypothesis rejection probability estimates are given in Table 1 for various segment lengths.

Table 1. Values of probability of rejecting K on persistent series

β	0.95	0.90	0.80	0.70	0.60	0.50	0.40	0.30	0.20	0.10
e^{β}	0.39	0.41	0.45	0.50	0.55	0.61	0.67	0.74	0.82	0.90
n=20	0.173	0.175	0.177	0.187	0.197	0.209	0.227	0.243	0.266	0.310
n=25	0.168	0.169	0.178	0.189	0.193	0.209	0.224	0.233	0.246	0.290
n=30	0.179	0.186	0.186	0.202	0.207	0.212	0.231	0.244	0.264	0.298
n=35	0.172	0.178	0.192	0.199	0.204	0.216	0.226	0.242	0.268	0.298
n=40	0.173	0.180	0.186	0.201	0.211	0.214	0.223	0.234	0.268	0.289
n=45	0.172	0.178	0.189	0.196	0.206	0.223	0.230	0.247	0.269	0.314
n=50	0.175	0.179	0.184	0.187	0.199	0.211	0.216	0.227	0.251	0.301

From Table 1 one can see the probability of H_0 rejection increasingly exceeds the probability of first kind error α (in Table 1 results are given for α=0.1) with persistence increases (with decreasing β) expected on the assumption that H_0 is true, which under real conditions can be taken as evidence of the presence of the signal. However, comparing Figure 1a from (Radiuhin and Mikhlin, 1986): the dependence of the inversion test power on the signal-to-noise ratio is shown in it for testing the hypothesis of the stationarity of the time series and absence of persistence against the linear trend hypothesis) with the results shown in Table 1 for n=50 one can see that the distorting effect of intra-series persistence is not large. For example, with which corresponds to a twofold decrease of autocorrelation during one time step, the probability of rejecting H_0 for $\alpha = 0.1$ is 0.187 which accordin[illegible] Figure 1a from (Radiuhin and Mikhlin, 1986) is equivalent to the presence of a signal with the signal-to-noise ratio of approximately 0.3 while with $\beta = 0.1$ when autocorrelation during one step becomes but 0.1 smaller the probability of rejection H_0 increases amounting to 0.301 which is equivalent to the presence of a signal with the signal-to-noise ratio of approximately 0.55. The presence of strong intra-series persistence is thus equivalent to the presence of a very slight determined signal in the series (equivalence here implies that the presence of autocorrelation is the stationary series causes H_0 to be rejected as frequently as in the case of the linear signal presence).

Location of warming and cooling periods in surface air temperature data series

The algorithm was used for analysing five data sets of hemispherically averaged mean annual and mean monthly surface air temperatures: a data set compiled by K. Ya. Vinnikov and others (Vinnikov *et al*, 1980; Vinnikov, 1985) (**S1**), a data set by P.D. Jones and others (Jones *et al*, 1982) (**S2**), ascertained series by P. D. Jones (Jones *et al*, 1986a) (**S3**), data by K. Ya. Vinnikov (Vinnikov *et al*, 1987) (**S4**) and Southern Hemisphere data (Jones *et al*, 1986b) (**S5**) as well as mean monthly (for January and July) mean annual Northern Hemisphere temperatures averaged over latitude circles. Estimates of the warming and cooling periods as well as the signal-to-noise ratio values for the portions of the time series for two lengths of moving segments (n = 25 and n = 50) and 90% significance level are given in Table 2.

The zero values of the signal-to-noise ratio given in the Table (and the corresponding time segments) denote that the null hypothesis is not rejected at the third step of the algorithm used; however, there are periods in the statistical series when it constantly has non-zero values. Dashes in some squares of the Table denote that for the respective series there are not even insignificant (in the above sense) arguments in favour of rejecting the hypothesis of no trend. When analysing Table 2 rather a good agreement could be noted of the results obtained from the Northern Hemisphere mean annual temperatures which could have been expected due to the high correlation of the series (e.g. the correlation coefficient between **S1** and **S2** is 0.955. between **S1** and **S3** - 0.933, between **S1** and **S4** - 0.940. between **S2** and **S3** - 0.973, between **S3** and **S4** - 0.940 (Jones *et al*, 1986; Vinnikov, 1985). Portions with insignificant or weakly significant cooling in the second half of the last century are found in series

Table 1: Periods with linear trends detected in the series of hemispherically averaged annual mean surface air temperature.

Series	n	Warming period	s/n	Cooling period	s/n
S1	25	1909 - 1936	2.0	1941 - 1969	-0.0
	50	1905 - 1936	3.0	1943 - 1958	-1.0
S2	25	1910 - 1936	2.0	1947 - 1969	-0.0
	50	1905 - 1937	3.0		
		1886 - 1904	0.5	1870 - 1886	-0.0
S3	25	1886 - 1904	0.5	1870 - 1886	-0.0
	50	1898 - 1939	1.5	1943 - 1959	-0.0
		1854 - 1871	0.0	1871 - 1885	-0.5
S4	25	1886 - 1906	0.0		
		1912 - 1933	2.5	1937 - 1967	-0.0
	50	1900 - 1938		1865 - 1880	-0.0
				1944 - 1960	-1.0
S5	25	1889 - 1943	1.0		
	50	1901 - 1948	2.5		

S3 and **S4** which agrees with the conclusions of (Jones *et al*, 1986). In the Southern Hemisphere series, warming since the begining of this century covers a longer time period. The cooling period which is insignificant or weakly significant in the Northern Hemisphere series is not found in **S5** with the help of this algorithm. In Fig 1 illustrating the application of the algorithm described to some mean annual and mean monthly temperature series the series proper are shown as well as the inversion test statistic series obtained for the moving segment length $n = 25$ and cumulative sum value series portions with significant warming and cooling periods.

Conclusion

The results from the algorithm for detecting in a time series parts with linear trends applied both to the simulated series with given characteristics and the real climatic time series which are well-known and well-studied, tell in favour of the suggested method which enables estimating with a varying degree of uncertainty start and end points of the linear signal obscured by noise. There is evidence (Radiuhin and Mikhlin, 1986) to believe that this is also true of a monotonic signal which is not greatly different from the linear one. The algorithm enables objectivizing the process of searching for new empirical facts of the climatic signals on the basis of many time series, which is next to impossible by the subjective visual approach.

References

Jones, P.D., Wigley, T.M.L., and Kelly, P.M., 1982 : Variations in surface air temperatures: Part 1. Northern Hemisphere. 1881-1980. *Mon. Wea. Rev.*, **110**, 59-72.

Jones, P.D., Raper, S.C.B., Bradley, R.S., Diaz, H.F., Kelly, P.M., and Wigley, T.M.L.,1986a: Northern Hemisphere surface air temperature variations: 1851-1984. *J. Clim. Appl. Meteor.*, **25**, 161-179.

Jones, P.D., Raper, S.C.B., and Wigley, T.M.L., 1986b: Southern Hemisphere surface temperature variations: 1851-1984. *J. Clim. Appl. Meteor.*, **25**, 1213-1230.

Kendall, M., and Stuart, A., 1973: *Statistical inferences and relationships*, Nauka (Moscow), 900pp. (in Russian).

Nikiforov, I.V., 1983: *Consecutive detection of changes in time series properties*, Nauka (Moscow), 199 pp. (in Russian).

Radiuhin, V.T., and Mikhlin, Ya. E., 1986: Comparing the effciences of some nonparametric tests used in climate change analysis. *Proc. VNIIGMI-WDC*, **129**, 17-26 (in Russian).

Radiuhin, V.T., and Mikhlin, Ya. E., 1987: Using non-parametric randomness tests for climate change analysis. *Proc. 3ICSC*, Vienna (Austria), 256-264.

Radiuhin, V.T., and Shilenko, B.L., 1988: Algorithm for locating periods with linear trends in the mean value of time series. *Proc. VNIIGMI-WDC*, **143**, 3-9 (in Russian).

Radiuhin, V.T., and Shilenko, B.L., 1989: Location periods with linear trends in climatic data series. *Preprints 13th Annual Climate Diagnostics Workshop*, Cambridge, Massachusetts. Oct. 31-Nov. 4, 1988.

Vinnikov, K. Ya., 1985: Contemporary variations of the global climate. A review. *Seria Meteorologia*, Obninsk. *Proc VNIIGMI-WDC*, **8**, 52pp. (in Russian).

Vinnikov, K. Ya., Groysman, P. Ya., Lugina, K.M., and Golubev, A.A., 1987: Change in mean air temperature of the Northern Hemisphere for the period 1841-1985. *Meteor. Gidrol.*, **1**, 45-55 (in Russian).

Vinlikov, K. Ya., Gruza, G.V., Zakharov, V.E., Kirillov, N.P., Kovyneva, N.V., and Rankova, E.Ya.,1980: Contemporary variations of the Northern Hemisphere climate. *Meteor. Gidrol.*, **6**, 5-17 (in Russian).

Temperature trends at the South Pole

Kevin E. Trenberth
NCAR, Boulder, Colorado USA

Abstract A detailed analysis of the annual cycle and trends in atmospheric temperatures at the South Pole is presented. Missing data are common, especially in the stratosphere, and the usual practice of computing monthly means as an average of all available observations produces unreliable results because the annual cycle is aliased onto the interannual variations and longer term trends. A methodology to rectify this involves computation of the smoothed mean annual cycle for each day of the year and then analyzing the anomalies.

Introduction

Attention has been focused on the Antarctic temperature trends and atmospheric circulation in recent years since the discovery of the 'ozone hole'. The latter refers to the large decreases in ozone over Antarctica during the southern spring months. Total ozone decreases at the South Pole for 1964-1985 have been documented by Komhyr *et al.* (1986). Largest decreases are found in the months of October and November although small decreases also occur in autumn and winter months.

Changes in ozone imply changes in solar heating rates in the stratosphere and thus changes in temperature. Such effects only occur after the sun has returned to Antarctica but the changes in ozone are directly responsible for changes in temperature, and the response time should be short (Kiehl *et al.*, 1988). Also, in the lower stratosphere in winter ozone has a long lifetime and local changes in both ozone and temperature are dominated by advective processes. In this case, both ozone and temperature changes should go hand-in-hand. Newman and Randel (1988) found 70 mb temperatures and total ozone amounts to be highly correlated both spatially and temporally from 1979 to 1986 in the southern hemisphere. Both Newell and Selkirk (1988), and Newman and Randel note that part of the ozone decrease in recent years is not paralleled by temperatures. For these reasons in particular, and because of the larger issue of climate change, perhaps arising from changes in greenhouse gases, there is considerable interest in observed changes in temperatures over Antarctica.

A major difficulty, usually ignored, in analyzing meteorological parameters, especially in the stratosphere, is that of properly taking into account the effects of missing data. Almost always, monthly mean temperatures are computed solely from the available observations, whether it be 62 (twice daily) or one observation. But especially in the high latitude stratosphere, there is a pronounced annual cycle so that differences in mean temperatures between the first and last days of, say, October at the South Pole at 30 mb is 27°C. Accordingly, a monthly mean based on a single observation on the first or last day of the month would be expected to exhibit an anomaly of -13.5°C or $+13.5$°C, respectively. What can and does happen is that the large amplitude mean annual cycle is aliased onto the interannual variations and long–term trends.

Data

The Antarctic program of scientific observations is divided into summer, when access is available to the continent by icebreakers and conditions are more favorable for flying, and winter, when wintering-over parties become isolated to a large extent. Radiosonde observations have often been made twice daily in the "summer", from about October through February, but once daily is more common in the winter half year. There are also marked differences from year to year (Fig. 1) and a high failure rate after 1975 below 100 mb.

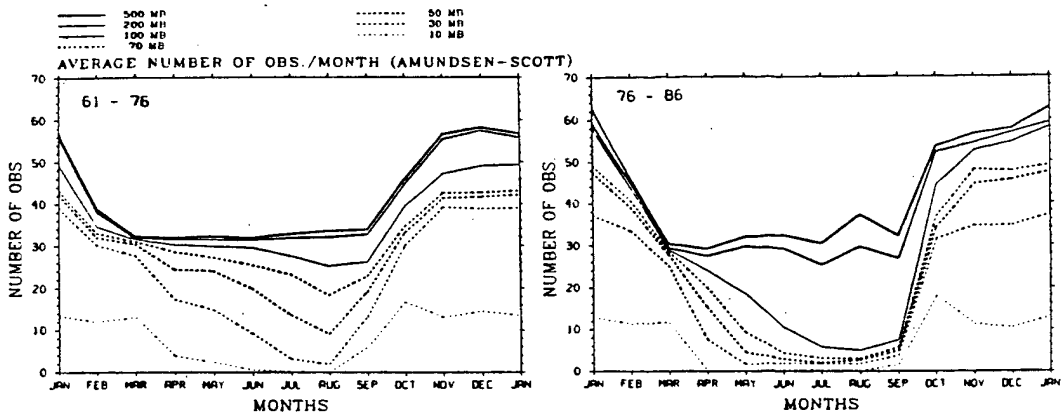

Figure 1: Average number of observations as a function of time of year and level at the South Pole for 1961-1976 (left) and 1976-1986 (right).

The result has been only a handful of observations May to September above 100 mb in the last decade or so. The pattern is better in Summer. In 1986 and 1987 additional data are available as a result of scientific expeditions to Antarctica to document the ozone hole phenomenon. In particular, NOAA recorded many ozonesondes at the South Pole, most of which go to pressures less than 10 mb, and they have been added to the data set.

In addition to analyzing data from Amundsen-Scott station (the South Pole) a similar analysis has been done for McMurdo Sound (78°S 167°W).

Mean annual cycle

We have computed the mean daily temperatures at each level at both stations (e.g. see Fig. 2).

It was not possible to obtain a daily value for each day of the year at 30 and 10 mb. Because many of the daily means are based on few values, there are large standard errors in these daily means. However, nearly all of the true annual cycle variance can be captured by fitting the first four harmonics to the daily data, and such results are then based upon many more observations and are much more stable. A least squares fit to the daily means has been used to define the overall mean and first four harmonics. Where there are no missing days, this gives results identical to standard harmonic analysis. But this method gives superior results when values are missing.

The mean annual cycle (Fig. 3) reveals lowest mean annual temperatures at 50 mb but the amplitude of the annual cycle increases with height and the annual range is about 60°C at 10 mb. Lowest overall temperatures, below −90°C, are found at 30 mb in August.

One now well known feature near the surface that can be seen at the South Pole at 500 mb (Fig. 2) is the long winter with the absence of a distinct temperature minimum, referred to as the coreless winter. Lowest temperatures occur in August or September in the troposphere, in early July at 10 mb and progressively later at lower levels. The spring warming occurs more rapidly than the autumn cooling and begins at the highest levels available and progresses downwards. Highest temperatures occur in December at 10 mb and January at 100 mb. Direct solar heating in the stratosphere following the return of the sun is important in the springtime warming. The annual cycle asymmetry can be attributed in large part to the rapid rates of solar heating versus the relatively slow rates of longwave cooling which occur on time scales of 2–3 weeks. However, the dynamics of the spring warming is probably also a factor.

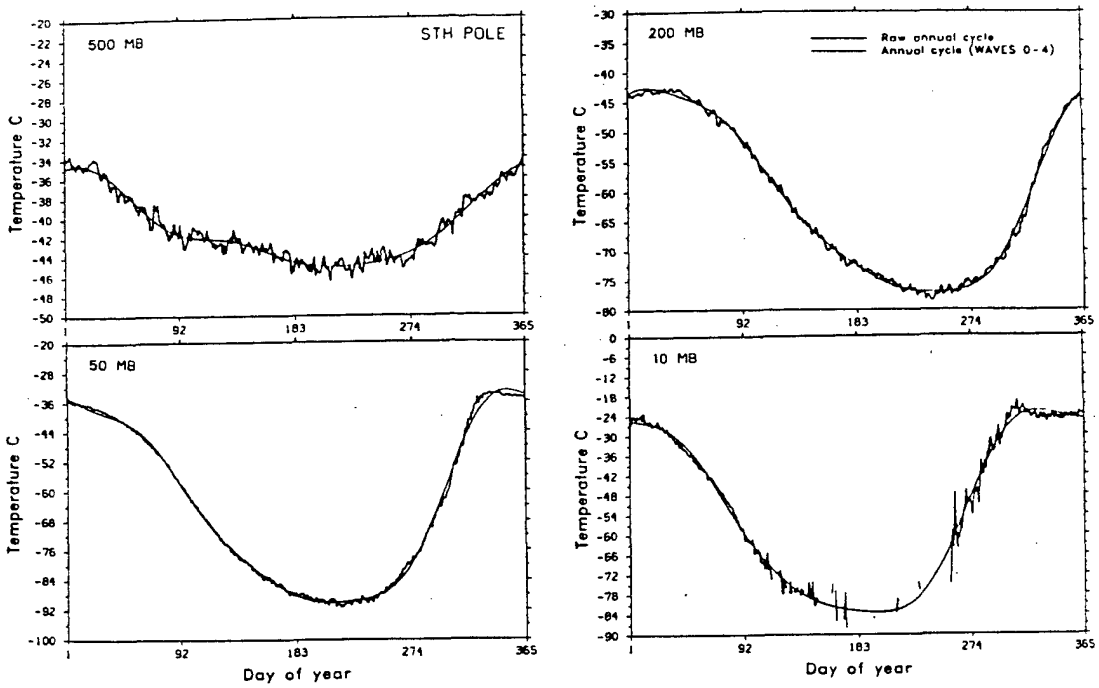

Figure 2: Mean annual cycle of temperature (°C) at the South Pole at 500, 200, 50 and 10 mb. Shown are the daily mean values over all observations and the fit of the first four harmonics.

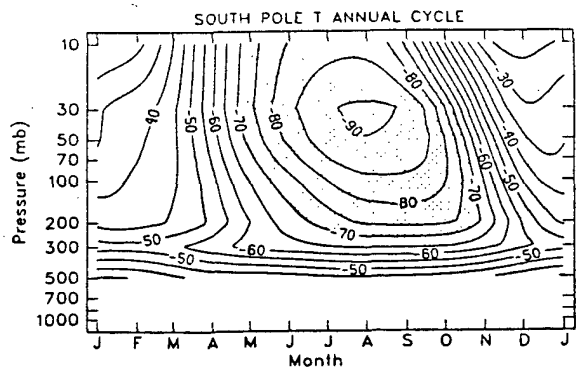

Figure 3: Temperature (°C) mean annual cycle at South Pole.

Temperature trends

To remove any possible effects of the annual cycle being aliased onto interannual variability and long term trends because of missing data, we first subtract the appropriate mean value from each observation and then analyze the resulting anomalies. Time series of temperature anomalies at five standard pressure levels for 3-month seasons (Fig. 4) show largest variability in the spring at the time of the stratospheric warmings.

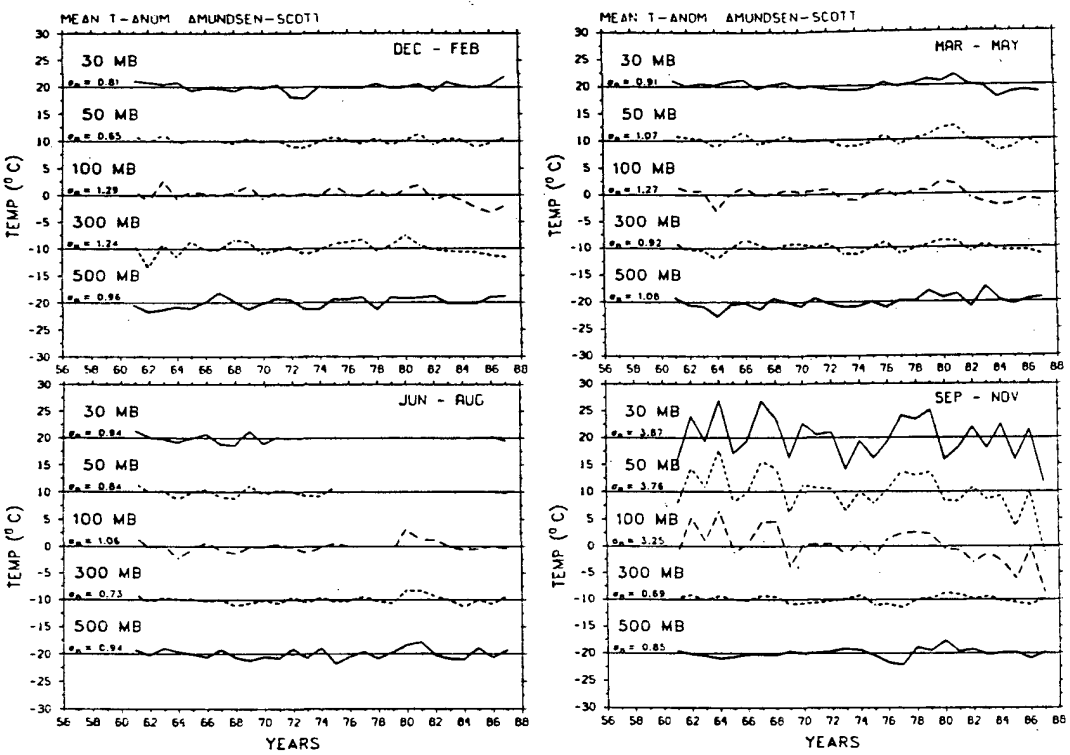

Figure 4: Time series of temperature anomalies (°C) at the South Pole for the four conventional seasons December–February, March–May, June–August and September–November at five levels. The mean for each level is offset by 10°C. The standard deviation of each series is given at left

In December–February, March–May and June–August the standard deviation of all series is ~1°C. The downward trend at 100 mb (but not other levels) in December–February arises from December and January, not February, and is only really noticeable for 1985–87. There is little to distinguish the March–May or June–August season records.

In spring, September–November, the year-to-year variability above 200 mb is much greater, with standard deviations of 3 to 4°C. The variability is greatest at the highest levels in October and at 50–100 mb in November (Fig. 5).

In September there is little of note. In October, a downward trend in temperatures is most evident at 50 and 100 mb, but it is only 1985–87 when the values have gone outside the range of previous variability. There is no evidence of any trend, however, at and below 200 mb. Note also the sawtooth character of the temperature variations indicating the influence of quasibiennial fluctuations that are also present in other months.

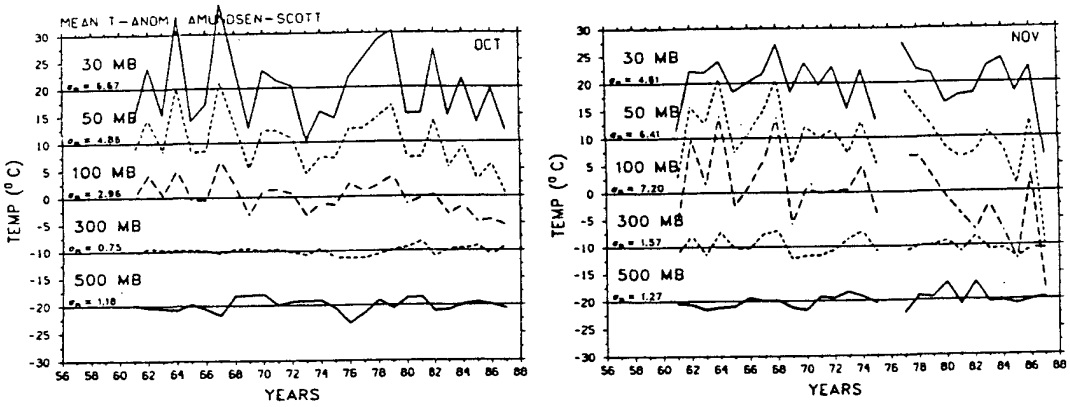

Figure 5: Time series of temperature anomalies (°C) at the South Pole for October and November. The mean for each level is offset by 10°C and the standard deviation for each series is given at left

.

The most extreme variations are found in November with standard deviations of 7.2°C at 100 mb. Temperatures in 1985 were very low at 100 and 50 mb but these proved to be modest compared with 1987 when the lowest values on record occurred at all levels from 200 to at least 30 mb. The departures from normal exceeded −20°C at 50 mb and −18°C at 100 mb. At 200 mb the departure was −7.5°C. Randel (1988) noted these extreme anomalies, which arise from a delay in the spring final warming of approximately 20 days, were apparently due to the record low ozone levels observed during 1987. Based on the NMC analyses, Randel found anomalies relative to 1980–86 of up to −16°C. Our anomalies of −21°C relative to 1961–86 means are more representative of the true extent of these extreme departures. The much colder air in November 1987 is directly attributed to the decreased solar heating arising from the record low ozone amounts.

A comparison of results in Figs. 5 with results generated by simply computing monthly means from all available data and subtracting the long term mean, reveals differences in individual monthly values as large as 12°C for some Octobers at McMurdo Sound. For recent years, our method gives mean October temperatures that are up to 8°C lower (mean bias 1980–85 is −4°C) than those by the straight averaging method, a consequence of a bias in the time of observations toward the latter part of the month. Thus the recent downward trend is more clearly evident when the distribution of data is properly taken into account.

The 1979–1986 period has been widely used for comparisons for ozone hole related studies because of the availability of satellite data. In Fig. 5, for October at the South Pole, 1979 was the third warmest year in the 27-year record above 70 mb and linear trends over the past nine years are not representative. Only from 1985 to 1987 and from 100 to 50 mb do the recent temperatures drop below the range of previous variations.

Concluding remarks

The decreases in ozone over Antarctica in the southern spring have led to temperature decreases at the South Pole from 1985 to 1987 that clearly go beyond the bounds of previous variability . The temperature decreases arise from a delay in solar heating and thus in the spring warming, and are strongest between 50 and 100 mb in October and November but there is a residual effect evident at 100 mb even in December, and January of the following year. The anomalies were most extreme

in November 1987 from 200 to 30 mb; as much as 21°C below normal. But there is no evidence of significant trends below 200 mb at anytime, or anywhere from February to September.

Improper treatment of missing data can seriously distort the apparent temperature record. Unfortunately missing data is the rule not the exception. An appropriate way to handle the problem and thus avoid the aliasing of the annual cycle into interannual variations and long-term trends is to define a stable (smoothed) temperature annual cycle for each day of the year in order to properly identify anomalies.

References

Kiehl, J.T., B. A. Boville and B. P. Briegleb, 1988: Response of a general circulation model to a prescribed Antarctic ozone hole. *Nature*, **332**, 501-504.

Komhyr, W. D., R. D. Grass and R. K. Leonard, 1986: Total ozone decrease at South Pole, Antarctica, 1964-1985. *Geophys. Res. Lttrs.*, **13**, 1248-1251.

Newell, R. E., and H. B. Selkirk, 1988: Recent large fluctuations in total ozone. *Quart. J. Roy. Meteor. Soc.*, **114**, 595-617.

Newman P. A. and W. J. Randel, 1988: Coherent ozone-dynamical changes during the southern hemisphere spring, 1979-1986. *J. Geophys. Res.*, **93**, 12585-12606.

Randel, W. J., 1988: The anomalous circulation in the southern hemisphere stratosphere during spring 1987. *Geophys. Res. Lttrs.*, **15**, 911-914.

Dectecting periodicities in data obscured by noise

Francis M. Fujioka[2] and Tai-Houn Tsou[1]
[1]Dept. of Statistics, University of California, Riverside, California, USA
[2]Forest Service, U.S. Department of Agriculture, Riverside, California, USA

Introduction

Cyclic behavior is often apparent in meteorological observations, most notably due to harmonic forcing attributable to the earth-sun relationship. Periodic behavior is not always so obvious, however; weather cycles–if they exist at all–sometimes must be detected statistically. A large body of theory of the statistical analysis of time series is devoted to second-order statistics (e.g., Priestley, 1981; Box and Jenkins, 1976), which is particularly appropriate (but not exclusively) for Gaussian noise, since the higher-order moments vanish identically, in that case. In the case of non-Gaussian noise, however, the higher-order moments can provide further information about the underlying processes. In this paper, we describe a statistical method that uses third- and fourth-order *cumulants*—which can be expressed in statistical moments (Kendall and Stuart, vol. 1, 1969)—to detect harmonics in data. A brief introduction to statistical methods for detecting periodicity in noisy data is presented in the next section. Two new tests based on higher-order spectra are then described. Finally, the performance of these tests is evaluated on Monte Carlo data that simulate mixed spectra processes.

Mixed Spectra

Consider the zero mean discrete parameter stochastic process of the form

$$X_t = \sum_{i=1}^{k} R_i cos(\omega_i t + \phi_i) + \sum_{j=0}^{\infty} \alpha_j \varepsilon_{t-j}$$

where $\{R_i\}$, $\{\omega_i\}$ and $\{\alpha_j\}$ are constants, $\{\phi_i\}$ are independently identically distributed uniform $(-\pi, \pi)$ random variables, and $\{\varepsilon_j\}$ are independently identically distributed random variables, uncorrelated with the harmonic part. The first series specifies the underlying periodic behavior, and the second series represents noise; for notational convenience, we denote these by Y_t and Z_t, respectively. We follow Priestley's development of the theory of analysis of this mixed spectrum process (Priestley, 1981; 613-653). It is assumed that the noise process has zero mean, unit variance, and a finite fourth moment. Other conditions require the summability of sequences involving the alphas.

X_t is called a mixed spectrum process because its integrated spectrum, H(ω), can be represented by the decomposition

$$H(\omega) = H_1(\omega) + H_2(\omega)$$

where the right-hand side terms correspond to the integrated spectra for the harmonic process and the noise process, respectively. H_1 is a step function, with jumps at $\{\omega_i\}$, and H_2 is an absolutely continuous function given by the integrated noise spectral density. Let h_1 and h_2 denote the corresponding spectral mass function and spectral density function, respectively.

In practice, the component spectra and associated parameters are estimated from the data $\{X_t\}$, $t = 1, \cdots, N$. The procedure outlined by Priestley first requires a test for the existence of H_1—the signal; if one or more statistically significant spectral component is detected, the parameters corresponding to the amplitude and frequency of the harmonic(s) are estimated, and this information is used to recover H_2. In what follows, we describe three tests of the null hypothesis, $H_0 : R_i = 0, \forall i$, that use the second-order moments (Priestley, 1981), and one by Tsou (1987), based on higher-order cumulants, for obtaining the mixed spectrum.

Whittle's Test

Whittle (1952, 1954) noted that, under the null hypothesis $H_0 : R_i = 0, \forall i$, the periodogram of the X_t process was asymptotically related to the periodogram of ϵ:

$$I_{N,X} \sim 2\pi h_2(\omega) I_{N,\epsilon}(\omega)$$

If $h_2(\omega)$ is known, H_0 can be tested with the statistic

$$g^{(W)} = \frac{\max_{1 \le p \le [N/2]} [I_p / 2\pi h_2(\omega_p)]}{\sum_{p=1}^{[N/2]} [I_p / 2\pi h_2(\omega_p)]}$$

where $I_p = I_{N,X}(\omega_p)$. The statistic follows Fisher's g-distribution, asymptotically, with [N/2] degrees of freedom (Fisher, 1929). Usually, h_2 is not known, and must be estimated; other difficulties arise, in this case, including a loss of power in the presence of nonzero amplitudes, and difficulty in distinguishing h_1 from h_2, particularly when the noise process has narrow bandwidth (sample size can be crucial, in this case).

Grouped Periodogram Test

Priestley describes another test of $H_0 : R_i = 0, \forall i$, attributed to Bartlett—the grouped periodogram test. The name arises from the grouping of the periodogram ordinates into [N/2k] sets, where k is some integer less than the bandwidth of the noise process. From this grouping, the statistic γ_k is calculated

$$\gamma_k = \frac{I_{p'} / [2\pi h_2(\omega_{p'})]}{\sum_{p=(l-1)k+1}^{lk} I_p / 2\pi h_2(\omega_p)}$$

where

$$I_{p'} / [2\pi h_2(\omega_{p'})] = \max_{(l-1)k+1 \le p \le lk} [I_p / 2\pi h_2(\omega_p)]$$

Under H_0, γ_k asymptotically follows the Fisher g-distribution, with k degrees of freedom. Moreover, $h_2(\omega)$ is approximately constant within each group, for k small enough compared to the noise bandwidth, so the statistic

$$g_k^{(B)} = I_{p'} / \sum_p I_p$$

may be used approximate to γ_k. As in the previous case, $g_k^{(B)}$ asymptotically follows Fisher's g-distribution with k degrees of freedom, under H_0.

P(λ) Test

Priestley derived a test of H_0, which focused on the tail behavior of the autocovariance function of X(t). He noted that, for large lags, the autocovariance of the noise part vanishes asymptotically, whereas the autocovariance of the harmonic part is oscillatory, if H_0 is not true. Accordingly, he constructed a function P(λ), of the form

$$P(\lambda) = \frac{1}{2\pi} \sum_{m < |s| \le n} \hat{C}_X(s) \cos(\lambda s), \qquad 0 \le \lambda \le \pi$$

where $\hat{C}_X(s)$ is the sample autocovariance of X, and m is a truncation parameter, beyond which the sample autocovariance of the noise process essentially vanishes. $P(\lambda)$ is used to test for the presence of harmonics, by systematically examining the peaks it induces on the sample autocovariance function. A more general form of P is used, incorporating two covariance lag windows $w_n^{(1)}$ and $w_m^{(2)}$ (n and m are parameters)

$$P(\lambda) = \frac{1}{2\pi} \sum_{s=-(N-1)}^{N-1} [w_n^{(1)}(s) - w_m^{(2)}(s)]\hat{C}_X(s) \exp(-i\lambda s)$$

Priestley drew an analogy between a statistic, J_q, that uses cumulative sums of P, and the theory of random walks. He showed that, asymptotically for large N, the density analog of J_q satisfies the diffusion equation, and that

$$\lim_{N\to\infty} p\left[\frac{\max_{0<q<[m'/2]} J_q}{[(1/2\pi)G(\pi)]^{1/2}} \leq a\right] = 2\Phi(a) - 1$$

where m' is chosen to achieve some suitable partitioning of λ over the interval $(0, \pi)$, Φ is the standard normal distribution function, and $G(\pi) = \int_0^\pi h_2^2(\omega)d\omega$. The $P(\lambda)$ test procedure allows iterative testing for the presence of several harmonics.

High-Order Spectra Statistics

The tests above have some distinct disadvantages. Whittle's test requires the spectral density function, which is usually not available, and therefore must be estimated. Moreover, when H_0 is false, the power of the test is greatly reduced, because the harmonic components inflate the spectral density function at their respective frequencies. Both the grouped periodogram test and the $P(\lambda)$ test require cautious partitioning of the sample autocovariance function; in the former, k must be chosen to strike a balance between the ratio of the upper and lower bounds of $h_2(\omega)$, and the degrees of freedom for the test. We offer a procedure by Tsou (1987) as an alternative, for the case of non-Gaussian noise. It uses higher-order cumulants of X_t.

Two new statistics are proposed, $G^{(b)}$ and $G^{(t)}$; $G^{(b)}$ uses a submanifold of the so-called bispectrum, $h_X(\lambda, 0)$

$$G^{(b)} = \frac{\max_{1\leq p\leq n} I_p/|h_X(\lambda_p, 0)|}{\sum_{p=1}^{n} I_p/|h_X(\lambda_p, 0)|}$$

and $G^{(t)}$ uses a submanifold of the trispectrum, $h_X(\lambda, 0, 0)$

$$G^{(t)} = \frac{\max_{1\leq p\leq n} I_p/|h_X(\lambda_p, 0, 0)|}{\sum_{p=1}^{n} I_p/|h_X(\lambda_p, 0, 0)|}$$

Under $H_0 : R_i = 0, \forall i$, the G statistics follow Fisher's g-distribution, asymptotically. For a sample sequence of size N and significance level α, the test rejects H_0 for $G > z_\alpha$, where $z_\alpha \approx (-1/n)\ln(1 - (1 - \alpha)^{1/n})$, and $n = [N/2]$. This is similar to Whittle's test, except that the $G^{(b)}$ and $G^{(t)}$ statistics use information about the mixture process available in the third- and fourth-order moments, respectively. When H_0 is not true, the odd moments–hence, odd polyspectra–of Y_t, the harmonic process, are exactly zero: the fourth-order moment is some specified form, such that $|h_Y(\lambda_p, 0, 0)|$ is small, compared to the noise trispectrum, $|h_Z(\lambda_p, 0, 0)|$. Moreover, if the $\{\varepsilon_j\}$ in Z_t arise from a (non-Gaussian) symmetric probability density (Z_t is then called a symmetric noise process), $h_Z(\lambda, 0)$ vanishes, and $G^{(t)}$ will be used, in that case.

Table 1: Characteristics of simulated series used in the comparison of statistical tests. SNR is the signal-to-noise ratio.

Series	ω_1	R_1	ω_2	R_2	SNR
1	1.5708	0.5000	—	—	0.5000
2	2.6507	1.0000	—	—	0.5292
3	1.5708	0.5000	1.4726	0.8000	0.8000
4	2.6507	1.0000	2.7489	1.5000	0.7937
5	0.2577	1.2000	—	—	0.4333

The singular disadvantage of higher-order spectra is the increased complexity in estimation. In addition to the need to compute higher-order moments, or their equivalent cumulants, one is again faced with decisions regarding spectral windows and truncation parameters. Tsou (1987) discusses some salient points for this procedure, and provides FORTRAN-77 code for the purpose. The bispectrum calculation takes the form

$$\hat{h}(\lambda, 0) = (2\pi)^{-2} \sum_{u,v=-N+1}^{N-1} K_M(u, v)\hat{C}_3(u, v) \exp(-i\lambda u)$$

where $K_M(u, v)$ is a smoothing window of lag M, and $\hat{C}_3(u, v)$ is the estimated third-order cumulant of X(t). Similarly,

$$\hat{h}(\lambda, 0, 0) = (2\pi)^{-3} \sum_{u,v,s=-N+1}^{N-1} K_{M'}(u, v, s)\hat{C}_4(u, v, s) \exp(-i\lambda u)$$

where $\hat{C}_4(u, v, s)$ is the estimated fourth-order cumulant of X(t), and $K_{M'}(u, v, s)$ is a smoothing window of corresponding order, and lag M'.

Comparison of Methods

Five simulation datasets were constructed to serve as test models for the statistical procedures described above. Each contained a harmonic process and a noise process. In the first four series, N=256 and the noise process was second-order autoregressive with exponential shocks

$$Z_t = -1.2Z_{t-1} - 0.6Z_{t-2} + \varepsilon_t$$

In the fifth series, N=512 and noise took the form of a fourth-order moving average process with double exponential shocks, i.e., a symmetric non-Gaussian noise process

$$Z_t = \varepsilon_t + 2.4\varepsilon_{t-1} + 0.4\varepsilon_{t-2} - 0.84\varepsilon_{t-3} + 0.21\varepsilon_{t-4}$$

The first two series have a single harmonic, and the next two series have two harmonics (Table 1). The series are specified so that the harmonic part of the spectrum is distinct from the noise part in the first and third cases, but overlap of the respective spectral peaks occurs in the second and fourth cases (Fig. 1).

None of the tests that use second-order statistics was able to detect all of the harmonics in the simulations. The statistics of the high-order spectra, on the other hand, left little doubt in rejecting the null hypothesis of no harmonics in the data (Table 2).

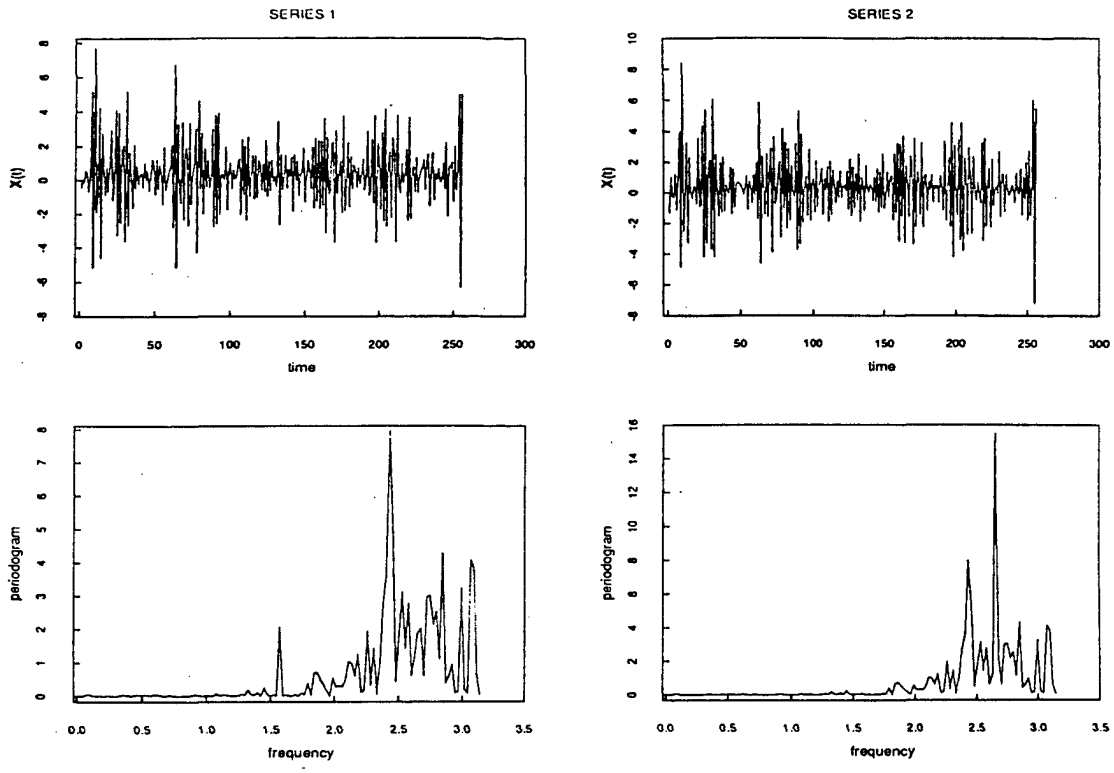

Figure 1: Simulated time series 1 and 2 (top), and their corresponding periodograms(bottom).

Table 2: Significance probabilities of the statistics obtained from the 5 simulated series.

Series	$g^{(W)}(\omega_1)$	$g^{(W)}(\omega_2)$	$\gamma_{12}(\omega_1)$	$\gamma_{12}(\omega_2)$	J_q	$G^{(b)}(\omega_1)$	$G^{(b)}(\omega_2)$	$G^{(t)}(\omega_1)$	$G^{(t)}(\omega_2)$
1	0.007	—	<0.001	—	0.817	<0.001	—	<0.001	—
2	0.332	—	>0.999	—	0.044	<0.001	—	<0.001	—
3	0.977	0.0013	<0.001	<0.001	0.192	<0.001	<0.001	<0.001	<0.001
4	0.459	0.759	>0.999	0.723	0.055	<0.001	<0.001	<0.001	<0.001
5	0.072	—	>0.999	—	0.144	—	—	0.005	—

In these examples, the tests based on $G^{(b)}$ and $G^{(t)}$ are clearly superior. Of the 7 harmonic components in the 5 series, the high-order spectrum statistics were significant at the 0.1% level in all but one case; in series 5, the $G^{(t)}$ statistic had a significance probability of 0.00513—still a highly significant result. The grouped periodogram test statistic with 12 groupings was the next most effective; it detected the harmonics in series 1 and series 3. This statistic was sensitive to the number of groupings, and did not perform as well with group sizes of 4 and 8 (not shown). The Priestley test did not do well in these examples, but it was the only procedure, other than the high-order spectra tests, that sensed a harmonic, when the harmonic spectra overlapped the noise spectra; the Priestley test barely rejected the null hypothesis at the 5% level in series 2, and barely missed rejecting at the same level in series 4. None of the other second-order tests detected the harmonics in series 4, which had a narrow separation between ω_1 and ω_2.

We conclude that the G statistics based on the high-order spectra are more powerful than the Whittle, grouped periodogram, and Priestley tests, particularly when the harmonic and noise spectra overlap. Further work is needed, however, to set guidelines for choosing smoothing windows and truncation parameters that the G tests require. A tool for detecting periodicities in a mixed spectrum process should find good use in meteorology, particularly for non-Gaussian noise (e.g., Stewart and Essenwanger, 1978). We intend to apply this technique on fire weather data described approximately by a Gumbel distribution (Fujioka and Tsou, 1985).

References

Box, George E. P., and Gwilym M. Jenkins, 1976: Time Series Analysis: Forecasting and Control. *Holden-Day, Inc., San Francisco, California. 575 p.*

Fisher, R. A., 1929: Tests of significance in harmonic analysis. *Proc. Roy. Soc. Ser. A. 125, 54-59.*

Fujioka, Francis M., and Tai-houn Tsou, 1985: Probability modeling of a fire weather index. *Proc. Eighth Conference on Fire and Forest Meteorology, April 29 - May 2, 1985, Detroit, Michigan. 239-243.*

Priestley, M. B., 1981: Spectral Analysis and Time Series. *Academic Press Inc., New York. 890 p.*

Stewart, D. A., and O. M. Essenwanger, 1978: Frequency distribution of wind speed near the surface. *J. Appl. Meteor., 17, 1633-1642.*

Tsou, Tai-Houn, 1987: Detecting the hidden periodicities by higher order spectrum. Ph. D. dissertation. Dept. of Statistics, University of California, Riverside, California. 154 p.

Whittle, P., 1952: The simultaneous estimation of a time series harmonic components and covariance structure. *Trabajos. Estadist., 3, 43-57.*

Whittle, P., 1954: The statistical analysis of a Seiche record. *J. Marine Research, 13, 76-100.*

Early instrumental data for the Southern Hemisphere - its usefulness for the reconstruction of climate

P.D. Jones
Climate Research Unit, University of East Anglia, Norwich, UK

Introduction

In order to identify and understand past climatic change we require long series of instrumental climate data. The lengths of the available time series determine to a large extent what studies can be undertaken. Longer records help attempts to identify causative factors in climate variations and they enable ideas and theories which may be statistically based to be tested with independent data. Researchers often bemoan the lack of long instrumental records in well-known climatological data bases, when, in many cases, the necessary data are hidden away in some long forgotten meteorological archive.

The purpose of this article is threefold. First, potential sources of early data are illustrated with particular reference to the Southern Hemisphere. Second, techniques are developed which can be used to assess the homogeneity of long data series. Finally, the potential usefulness of the early data is shown with two examples - the development of time series of hemispheric scale temperature for climatic change studies, and the reconstruction of pressure patterns over the Southern Hemisphere.

Early climatological sources

The basic sources of station climatological data on a global basis are World Weather Records (WWR), Monthly Climatic Data for the World (MCDW) and Reseau Mondial. The first two sources have been combined at the National Center for Atmospheric Research (NCAR) in Boulder, Colorado and are available digitally (Spangler and Jenne, 1986) as the World Monthly Surface Station Climatology (WMSSC). Much data has been added to this source by numerous individuals around the world. Reseau Mondial was a forerunner of MCDW for 1910-34 and, whilst much of this source has been included in WMSSC, considerable quantities of station data have been omitted.

Additional information to the above can be obtained in two basic ways. First, national meteorological archives can almost always provide a greater station density and in some countries these data may be digitised. Second, one should examine meteorological archives in other countries, principally countries such as the United Kingdom, France, The Netherlands, Germany, Spain, Portugal and the United States. The early European colonists often took meteorological measurements and these were taken back to Europe for storage and sometimes publication. In the case of New Zealand, Australia and parts of southern Africa, there is considerable potential for early data in the United Kingdom. Meteorological observations made at the Foreign and Colonial Stations of the Royal Engineers and the Army Medical Department for 1852-1886 were published in 1890 by HMSO, London. Early observations taken in Auckland, New Zealand for the 1850s are not available in New Zealand (Salinger, pers. comm.).

Another example concerns mean-sea-level pressure (MSLP) records from Tahiti. The difference between monthly-mean MSLP data at Tahiti and Darwin forms the most commonly used index of the Southern Oscillation (Chen, 1982). The data series back to 1935 is well-known and has long been published. However, because of a fire at Papeete in Tahiti, sometime during the late 1920s, all the early records were lost. However, because Tahiti is a French dependency, copies of many early records were returned to France. Using these data, it has been possible to extend the Tahiti pressure series back to 1876, although there are a few periods of no data, probably because these records were lost in transit, (see Ropelewski and Jones, 1987 for details).

These are just two examples. Other potentially useful publications include Annales du Bureau Central Meteorologique de France (1879-1914), Journal of the Scottish Meteorological Society, Meteorologische Zeitschrift (1886-1940) and Osterreichschen Gesellschaft für Meteorologie (1860-1885). Details of these and many other sources are given in Bradley et al. (1985). Included in Bradley et al. is perhaps the most important and least known source of early instrumental temperature data - that produced by H.W. Döve during the 1830s-1870s and published by the Prussian Academy of Sciences. In this source, Döve published, with original source details, monthly-mean temperature records from as many as 1500 stations all with data before 1860. Whilst most of these sites are in the Northern Hemisphere, there are a few in the Southern Hemisphere (see Jones et al. 1986a). The only copies of Döve's publications known to the author are in the Meteorological Office Library in Bracknell, U.K.

Whilst early climate data extend back for some Southern Hemisphere locations to the late eighteenth and early nineteenth centuries, data for the Antarctic region is generally restricted to the twentieth century. Routine recording only began during or just before the International Geophysical Year in 1957/8 although records back to the late 1940s are available for the Peninsula region. Numerous expeditions were made to the region between 1890 and 1950, however, and many of these took meteorological measurements - sometimes for as long as three years. The most comprehensive list of information on these expeditions and sources of data has been compiled by Venter (1957).

Even today there are problems in obtaining climatological data from the Antarctic region. Data are often missing in sources such as MCDW and WWR. In order to improve the basic data base, Jones and Limbert (1987), through personal contacts and nationally published sources, managed to locate much of the missing data. A data bank of 29 stations for the continent has been assembled. Antarctic data have also been published by Jacka et al. (1984). This source contains much useful information but perpetuated many of the data inaccuracies in MCDW and from the Global Telecommunication System (GTS).

Assessment of homogeneity

A climatological time series is said to be homogeneous if the variations are caused only by variations of weather and climate (Conrad and Pollak, 1962). Although observers may take readings with meticulous care, non-climatic influences can easily affect the readings. Mitchell (1953) and others (e.g., Bradley and Jones, 1985) have identified the four most common causes of inhomogeneities:-

- changes in instrumentation, exposure and measurement technique
- changes in station location
- changes in observation time and the method used to calculate monthly means
- changes in the environment around the station; for temperature with regard to the increase in city growth around the site, while for precipitation the growth of vegetation around the gauge.

The most important factors as far as individual stations are concerned are changes in station locations and changes in observation time and method (e.g., the change from using maximum and minimum temperature to that using measurements based on fixed hours to calculate monthly mean temperature). Depending on the type of change, jumps in monthly mean temperatures and pressures can be of the order of 2°C and 3hPa respectively. To ensure the homogeneity of long time series it is necessary to determine correction factors, which in most cases will vary seasonally. This is best done with a period of simultaneous observations at both sites or with the two observation practices. Since suitable overlapping records, however, are rarely available, it is almost always necessary to resort to comparisons with other, more distant stations to derive the required corrections.

Data homogenization

The homogeneization of a time series of station data can be achieved in a two-stage process. Firstly, transcription and genuine mistakes affecting individual values must be corrected before the second and more important aspect of ensuring the station time series is homogeneous. The time series may contain data errors from genuine mistakes, or from key punching or (handwritten) transcription errors. Some such errors can be found by flagging outliers; for example values at least three standard deviations from monthly means. These outliers can then be checked against the original documents and/or against neighbouring station data if these are available. The ability of this technique to pick up errors clearly depends on the size of the error relative to natural variability in the data. With temperature, for example, errors of less than 1°C will often go unflagged, and may only be identifiable by independent comparison with an adjacent neighbouring station. Errors of exactly 1°C are, in fact, probably quite common, considering the number of errors noticed where mean temperatures are exactly 10°C too warm or cold. Another common error is the omission of the minus sign for temperature. The outlier flagging method can identify such errors, provided the true temperature value is not near 0°C. Although outlier flagging may fail to identify some errors, it is likely to pick up all large errors.

The second stage of homogeneity testing compares records from neighbouring sites (Conrad and Pollak, 1962; Bradley and Jones, 1985). The methods assume that non-climatic factors influencing one record will become apparent when the record is compared with neighbouring site records. Generally, tests of homogeneity involve the null hypothesis that a time series of differences between adjacent station data sets will exhibit the characteristics of a random series (Mitchell, 1961). Non-randomness may be apparent either as a trend, a jump, or an isolated anomaly in the difference series. The ability to detect non-randomness in the difference time series obviously depends on the variability of the series, which in turn depends on the distance between the neighbouring stations and the region of the world. For temperature, a denser network of stations is required in polar regions compared to the tropics where temperature variations are less both spatially and from year to year.

To be specific, I will consider the case of a step change or discontinuity in the difference series. Once a discontinuity has been found it is necessary to check station history information to see what caused the abrupt change. In some cases there may be no confirmation in either station's history. For this reason it is always necessary to look for discontinuities first rather than assume all the necessary information concerning station moves, etc. has been documented. For many stations, station histories are incomplete and information concerning earlier locations has been lost.

Once errors have been detected (and this may involve multiple station intercomparisons in order to identify the errant record), corrections must be made. With abrupt errors, correction of monthly-mean temperatures through the use of neighbouring records can be easily made (Jones et al. 1986b). The correction value may vary from month to month. This type of correction procedure has been applied to over 3200 temperature records from the Northern and Southern Hemispheres in producing the Climatic Research Unit/U.S. Department of Energy (CRU/DOE) temperature data set. Details of the stations compared are given in two technical reports (Jones et al. 1985, 1986a). In our analyses we have used subjective judgement to decide whether to accept a record, or to correct it or delete it from the data bank. Judgements have been based on a careful study of many time-series difference plots. A related technique, involving a more objective judgement, has been applied to the Historical Climate Network (HCN) of 1219 stations in the United States by Karl and Williams (1987). These workers extended the analysis to include precipitation time series homogeneity (using ratios rather than differences) and attempted to assess the reliability of any corrections made.

Urbanization effects

In many examples, the difference time series plots may reveal gradual changes in one or more station time series. For temperature, the gradual increase at one site may be related to growth of the city

around the site. With these types of error it is much more difficult to estimate a correction factor with any reliability since confidence limits on the trend in the difference series are invariably wide, and since it is difficult to decide just when such a trend began (or ended). Furthermore, trends may be obscured by other errors. In our analyses, we have omitted stations that exhibit trends when their records are compared with neighbours.

It has been suggested, from studies of a few stations over the United States, that the urbanization effect might explain a significant portion of the 0.5°C rise in hemispheric mean temperatures over the last 100 years (Kukla et al., 1986; Wood, 1988). The effect of urbanization will, of course, be considerably reduced by spatial averaging because not every station is affected. The key question is not how much single sites are affected, but how much regional and hemispheric estimates are affected.

Using the HCN network, Karl et al. (1988) have assessed the importance of urbanization effects and corrected for the problem in regional average time series. They have corrected individual time series based on population changes, after first deriving a relationship between population and urban warming bias. With data for the United States, when the corrected data are compared with estimates produced by Jones et al. (1986b) for the same region, the latter show a residual urban bias of, at most, 0.1°C (Wigley and Jones, 1988; Karl and Jones, 1989; Jones et al., 1989). It is unlikely that the hemispheric estimates are more seriously affected than the United States. The urban warming problem, is however, potentially more serious in analyses which have not involved detailed, station-by-station assessments of time series homogeneity (e.g., Hansen and Lebedeff, 1987). In comparisons with homogenized U.S. data, Hansen and Lebedeff's data show a large residual warming (0.4°C), presumably due to urbanization effects (for details, see Karl and Jones, 1989).

Southern hemisphere mean temperature

Until recently, most studies of global temperature assumed that temperature variations over the Northern Hemisphere could be used to indicate Southern Hemisphere variations as well. The development of a Southern Hemisphere time series based on land station data by Jones et al. (1986a,c), Figure 1, shows that this assumption is not valid. Figure 1 shows gradual warming in the Southern Hemisphere over most of the record, with little indication of the cooling trend between 1940 and 1970 that is so apparent in the Northern Hemisphere record (Jones et al., 1986b).

How reliable is this curve of Southern Hemisphere temperature trends? At best, coverage can only be claimed for about 25% of the total surface area including oceans. The availability of station data over the land areas also varies with time. Prior to the 1950s, the area covered is less than 25%, particularly in the nineteenth century. Nevertheless, the general reliability of the land-based data is verified by comparison with marine data. On decadal time scales after about 1900, the land and marine data (the latter from Folland et al., 1984) agree well, even for the uncorrected marine data. Agreement is even better using the corrected data - note that Folland et al.'s corrections have been made entirely independent of any land data. Of course, the marine data are themselves only really representative of parts of the Southern Oceans. There are few marine data south of 40°S, and very little in the southeastern Pacific Ocean except near the South American coast.

To further assess the reliability of the land-based record back in time, it is necessary to estimate how well reduced networks can approximate the period of best coverage between 1941 to 1980. This has been achieved with a technique which has been termed 'frozen grids'. The grid available for successive decades, 1861-70, 1871-80, etc. is used to estimate "hemispheric temperatures" for the 1941-80 period. Comparisons between the frozen grid estimates and those achieved by using all available grid points quantifies the additional uncertainty caused by the lack of coverage. Table 1 shows the results for all possible grids up to 1931-40. Although the earlier grids, particularly during the last century, imply a greater uncertainty in hemispheric averages, they indicate that, even in the nineteenth century, the prevailing level of temperature on a decadal time scale is well estimated by the early sparse networks.

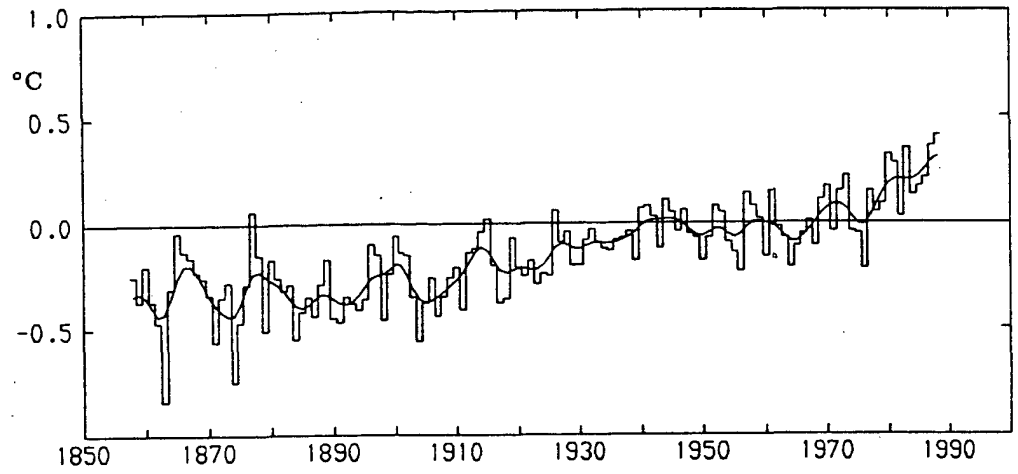

Figure 1: Southern Hemisphere surface air temperature averages, 1858-1988 based on land values. Values are expressed as anomalies from the 1951-70 reference period.

Table 1: Comparisons of means and standard deviations for the time-varying and frozen grids.

Grid type	Mean (°C) (1941-80)	Standard deviation (°C) (1941-80)	Max. no. of grid points
Time varying	0.00	0.13	123
Frozen:			
1851–60	-0.01	0.22	7
1861–70	-0.03	0.16	11
1871–80	-0.02	0.16	19
1881–90	-0.01	0.15	25
1891–1900	0.00	0.15	33
1901–10	-0.02	0.13	46
1911–20	-0.03	0.14	57
1921–30	-0.03	0.13	61
1931–40	-0.02	0.13	76

The most important factor in Southern Hemisphere temperature trends has not yet been covered - what influence would Antarctica have had to the series prior to 1957? For 1957-87, the mean temperature for the Southern Hemisphere is the same whether Antarctica is included or not. This is because the differences between Antarctica and the rest of the available data, given the relatively small area of Antarctica, are too small to have any marked effect. Whether or not this is the case prior to 1957 is impossible to say, although, given the 1957-87 result, it is probably the best assumption to make.

Earlier records are available from Antarctica, from the expedition period around the turn of the century and during the 1940s/1950s. However, these come either from the Peninsula or the Ross Sea region, and Raper et al. (1984) has shown that these regions are not representative of the continent as a whole. In order to get reliable continental estimates, much wider coverage is essential. One possible way of achieving this is through isotopic information from shallow ice cores which are capable of giving year-to-year time scale resolution. Fieldwork to extract such cores is just beginning and, as yet, results are only available from the Peninsula region (Robin, 1983).

Reconstruction of circulation patterns over the Southern Hemisphere

Gridded sea level pressure data (MSLP) for the Southern Hemisphere are available from analyses routinely undertaken at the World Meteorological Centre (WMC) in Melbourne, Australia. The monthly-mean charts are derived from daily observations and are available from June 1972. The analysis procedure used to derive the daily charts is described by Guymer (1978); but see also Karoly et al. (1986). The relatively short length of this data set is in marked contrast to the Northern Hemisphere situation where analyses extend back to the nineteenth century. The Australian analyses are, however, not the only chart series available for the Southern Hemisphere. Between 1951 and 1962 the South African Weather Bureau produced monthly-mean pressure charts, again derived from daily charts. All the data have been published in map and numerical form in the journal NOTOS.

These chart series can be extended back to the early twentieth century (except over the data-sparse regions of the Southern Oceans and over Antarctica before 1957) using station sea-level time series data which are available from a number of sites. The reconstructions have a number of potential uses. First, reconstructions of gridded data based on the station data allow the reliability of both the NOTOS and Australian analyses to be made by direct comparison. Second, the magnitude and character of circulation changes over the present century can be examined. Third, comparisons with regional gridded series produced by New Zealand and by Argentina and the Falkland Islands can also be made.

The mathematical details of the technique have been detailed elsewhere (Jones et al., 1983, 1987; Jones, 1987). In particular, Jones and Wigley (1988) describe a similar analysis for the Antarctic region. The technique uses principal components regression developing a series of equations relating grid-point MSLP values over the Southern Hemisphere to the available station network of MSLP data as predictors. After first ensuring the homogeneity of all the individual station time series, the grid-point network and the station MSLP data are reduced to principal components (PCs). High-order components which are assumed to be unwanted noise are ignored. Only those PCs that explain most (e.g., 90 or 95%) of the variance of each data set are retained. The amplitude time series of each grid-point PC is then regressed against the amplitude time series of the station network PCs. Station network PCs are retained as predictors only if their t-values are greater than 1. (The choice of $t=1$ as a screening criterion is based on extensive experience with this technique in other applications. The precise value of the t cutoff doesn't noticeably affect the results.) The PC regression equations are then transformed back to the original variable space, leading to a set of predictor equations, one for each grid point.

Grid point values can now be reconstructed to the latest first year of the station network data. The homogeneity of the station data ensures that the reconstructions are also homogeneous and so contain the effect of long time scale circulation changes, insofar as these are an integral part of the raw station data.

The data set used in this analysis comprised 78 station records. The principal source of information is WWR, but this has been augmented in a few cases (Mauritius, Tahiti and the Antarctic Peninsula). As noted above, before any analysis can be undertaken it is essential to assess the long-term homogeneity of the assembled station set of MSLP data. Station pressure and MSLP data in WWR are frequently in error. The two data sets are often interposed and much early pressure data has not had the correction for gravity applied. Additionally, some station time series contain pressure data which have been corrected to the 24-hour mean. In recent decades, 24-hour means have not be used, leading to inhomogeneities in the time series. Obviously, it is more difficult to assess the homogeneity of stations in data sparse regions such as the island stations in the Southern Oceans between 40 and 60°S. Here, the best that can be done is to verify extremes in other sources and to monitor trends or jumps in time series plots.

The reconstruction technique was applied by dividing the Southern Hemisphere into three equal sectors at 20°W, 140°W and 100°E. This separation was made partly on computational grounds. However, it is also important because of the scale of existing teleconnections. The Southern Oscillation phenomenon involves a strong out-of-phase relationship between pressure variations in the Indonesia/Australian region and those in the central and eastern parts of the subtropical Pacific Ocean. Correlation coefficients between stations in each region are of the order -0.6 to -0.8 (Berlage, 1966; Trenberth, 1976). These regions have therefore been considered separately, since any analysis of the phenomenon based on the reconstructed data demands that the teleconnections not be built in to the data as a result of the reconstruction method.

The regression equations were calibrated using the Australian gridded data for June 1972 - April 1985. Ideally, the regression equations should be derived separately for each month of the year (see for example, Jones, 1987), but with only 13 cases this is not to be recommended. Instead, following Jones and Wigley (1988), the three months of the standard seasons were used as separate cases. This means the calibration exercise is undertaken with either 38 or 39 months of data. The results in terms of average explained variance at the 65 grid points in each region are given in Table 2.

The reconstructed data were then compared with the NOTOS data for the years 1951-62. This comparison can be considered as a verification procedure for the regression relationships, but it also acts as a test for the NOTOS data. (In the same way, the calibration results give some insight into the reliability of the Australian gridded data - for further details, see below and also Jones and Wigley, 1988). The best verification results are generally obtained for the spring (SON) season and the worst for the summer (DJF). This is in contrast with results for the mid to high Northern latitudes (Jones, 1987; Jones et al., 1987), which show a strong seasonal cycle with best results in winter (DJF).

In many parts of the Southern Hemisphere, the results are much better than these average results would imply. (Equally, there are many areas where the results are worse.) Spatial maps of the explained variance from the winter (JJA) season, for both the Australian and NOTOS chart series, are shown in Figures 2 and 3. Similar results are achieved with the other seasons. Calibration performance (Figure 2) is poorest near Antarctica and over the main oceanic areas, and is certainly related to the lack of suitable ocean island data. Verification period performance (Figure 3) is similar to calibration period performance in areas where this exceeds 50% of the variance. In calibration-poor regions, verification performance is exceedingly poor.

The reconstructions can be used to compare the Australian and NOTOS chart series. Figure 4 shows the difference between the NOTOS charts and the reconstructions for the 1951-62 period. The differences range from +8mb to -2mb, with the NOTOS data being 8mb higher over the southeastern Pacific in the vicinity of 60°S, 120°W. A similar finding has been made when the technique was applied to the Antarctic region (Jones and Wigley, 1988). As this area is the largest in the world without

Table 2: Regression equation calibration: reconstructions back to 1951

Australasian	Season	N_G	N_S	C	V
	DJF	13	12	0.745	0.490
	MAM	12	12	0.739	0.512
	JJA	11	11	0.805	0.498
	SON	10	10	0.798	0.547
South American	Season	N_G	N_S	C	V
	DJF	13	13	0.665	0.299
	MAM	12	11	0.693	0.419
	JJA	13	10	0.659	0.426
	SON	12	10	0.693	0.454
Southern African	Season	N_G	N_S	C	V
	DJF	13	10	0.673	0.366
	MAM	13	10	0.605	0.377
	JJA	13	10	0.650	0.394
	SON	12	9	0.728	0.516

N_G Number of PCs of the grid-point pressure network retained (such that $N_G < 95\% < N_{G+1}$)
N_S Number of PCs of the station pressure sites retained (such that $N_S < 95\% < N_{S+1}$)
C Mean variance explained at each grid point over the calibration period (Jun 1972 - Apr 1985)
V Mean variance explained at each grid point over the verification period (Jan 1951 - Dec 1962)

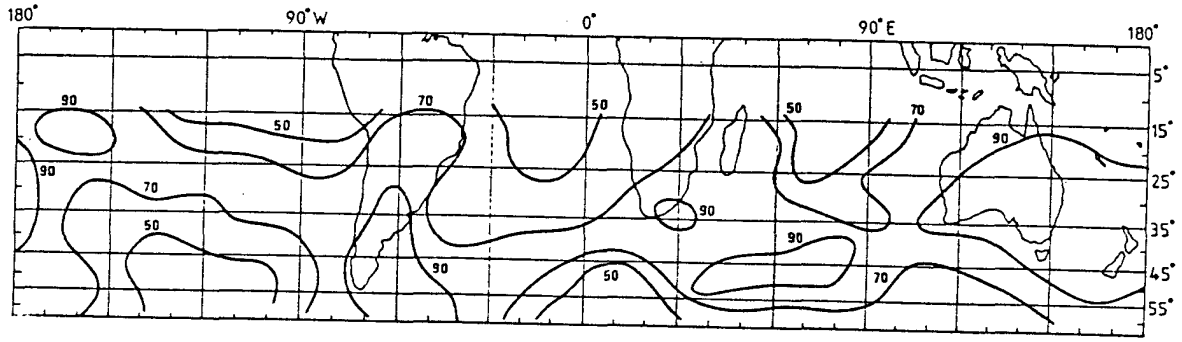

Figure 2: Variance (%) explained by the reconstructions over the calibration period (June 1972-April 1985 using the Australian analyses) for the JJA season.

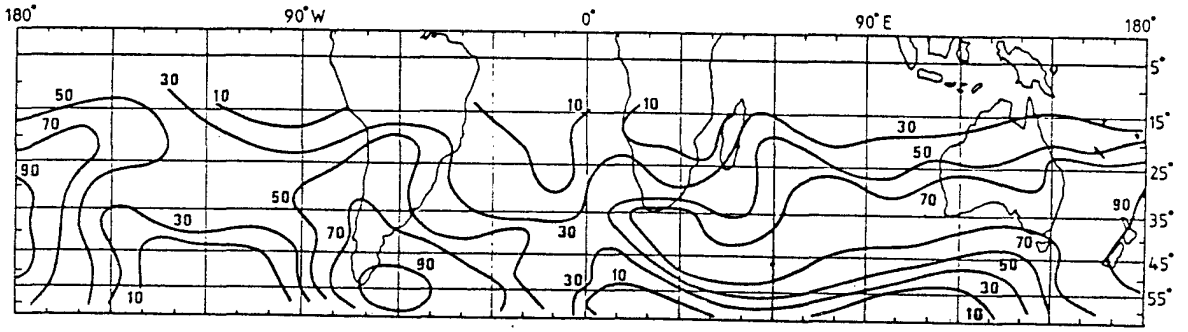

Figure 3: Variance (%) explained by reconstructions over the verification period (1951-1962 using the NOTOS analyses) for the JJA season.

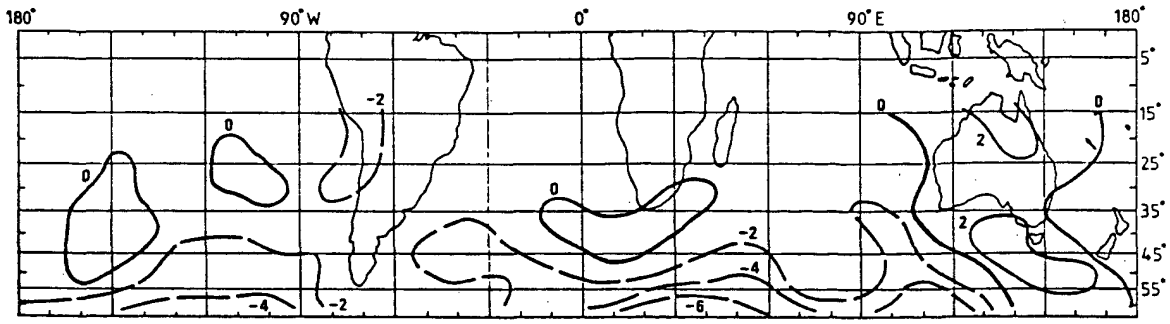

Figure 4: Difference in pressure (millibars) between the reconstructions and the NOTOS charts over the 1951-62 period for the JJA season. Negative values indicate reconstruction charts lower than NOTOS.

any basic station data it is difficult to say which analysis is correct. Elsewhere the NOTOS charts are about 2-4mb too high along the western coast of South America, about 2mb too high off the western coast of Southern Africa, about 2-4mb too high over the Indian ocean south of Australia, and about 2mb too low over parts of Australia.

The reconstruction technique by its very nature assumes the Australian charts are correct. Data collected during the period of the First Global GARP experiment (FGGE) in 1979 from drifting buoys would suggest the Australian data are nearer than the NOTOS data to the true pressure values in the 50-60°S zone. Many studies have intimated, however, that pressure was anomalously low in the circum-Antarctic westerlies during 1979 (Karoly et al. 1984). Only a further drifting buoy study can help to answer what the long term normal MSLP values in the extreme south of the Pacific Ocean should be. Over the Australasian sector, the New Zealand (NZ) gridded sea level pressure data set provides another means of directly comparing the Australian (A) and NOTOS (N) data. The difference map (not shown) is similar in many respects to Figure 4. This suggests that the NZ charts are similar to NOTOS and in some disagreement with the Australian. This result is confirmed if the NZ and A charts are directly compared over the 1972-85 period.

Conclusion

Although most early records of instrumental climate data have been located, there is still the possibility that important material is hidden away in some archive. However, even if additional data for a site can be found, it is likely that the new records will not be homogeneous with more recent data. Most long-term climate records contain periods when the records are non-homogeneous. Reasons for these inhomogeneities can generally be related to station moves and changes in the methods used to calculate monthly mean temperature and pressures.

Early instrumental data are particularly useful for improving the spatial coverage of data in regional and hemispheric time series. The available data base of gridded monthly-mean Southern Hemisphere MSLP data, from Australian analyses, is only available on a continuous basis back to 1972, in marked contrast to the much longer Northern Hemisphere data base. Considerable amounts of station data are, however, available, some of which goes back to the turn of the century and earlier. These data have been used in a principal components regression technique to reconstruct gridded MSLP data for the Southern Hemisphere back to 1951 and, with more limited coverage, to 1910.

The reconstructions allow the Australian analyses to be compared with the earlier NOTOS chart series for 1951-62 and with other regional chart series for areas of the Southern Hemisphere. Because the reconstructions contain the effects of climatic change implicit in the station data, the various

gridded data sets can be directly compared. The comparisons point to serious discrepancies between the data sets. However, because of the data sparseness in many areas of the Southern Hemisphere it is not always possible to resolve the differences.

References

Blackman, R.B., and J.W. Tukey 1959: The measurement of power spectra *Dover*

Berlage, H.P., 1966: The Southern Oscillation and world weather. *K. Ned. Meteorol. Inst. Meded. Verh. 88, 152pp.*

Bradley, R.S. and Jones, P.D., 1985: Data base for isolating the effects of increasing carbon dioxide concentrations. pp.29-53. *In: Detecting the Climatic Effects of Increasing Carbon Dioxide, DOE/ER-0235 (M.C. MacCracken and F.M. Luther, Eds.). U.S. Dept. of Energy, Carbon Dioxide Research Division.*

Bradley, R.S., Kelly, P.M., Jones, P.D., Goodess, C.M. and Diaz, H.F., 1985: A Climatic Data Bank for Northern Hemisphere Land Areas, 1851- 1980. *U.S. Dept. of Energy, Carbon Dioxide Research Division, Technical Report TR017, 335pp.*

Chen, W.Y., 1982: Assessment of Southern Oscillation sea level pressure indices. *Monthly Weather Review 110, 800-807.*

Conrad, V. and Pollak, L.D., 1962. Methods in Climatology, *Harvard University Press, Cambridge, Massachusetts, 459pp.*

Folland, C.K., Parker, D.E. and Kates, F.E., 1984: Worldwide marine temperature fluctuations 1856-1981. *Nature 310, 670-673.*

Guymer, L.B., 1978: Operational application of satellite imagery to synoptic analyses in the Southern Hemisphere. *Technical Report No.29, Bureau of Meteorology, Australia. 87pp.*

Hansen, J. and Lebedeff, S., 1987: Global trends measured surface air temperature. *Journal of Geophysical Research 92, 13345-13372.*

Jacka, T.H., Christou, L. and Cook, B.J., 1984: A data bank of mean monthly and annual surface temperatures for Antarctica, the Southern Ocean and South Pacific Ocean. *ANARE Research Notes 22, Antarctic Division, Dept. of Science and Technology, Kingston, Tasmania. 98pp.*

Jones, P.D., 1987: The early twentieth century Arctic High - fact or fiction? *Climate Dynamics 1, 63-75.*

Jones, P.D. and Limbert, D.W.S., 1987: A data bank of Antarctic surface temperature and pressure data. *U.S. Dept. of Energy, Carbon Dioxide Research Division, Technical Report TR038, 52pp.*

Jones, P.D. and Wigley, T.M.L., 1988: Antarctic gridded sea level pressure data: An analysis and reconstruction back to 1957. *Journal of Climate 1, 1199-1220.*

Jones, P.D., Wigley, T.M.L. and Briffa, K.R., 1983: Reconstructing surface pressure patterns using principal components regression on temperature and precipitation data. *II International Meeting on Statistical Climatology, Lisbon, 26-30 September 1983, 4.2.1-4.2.8.*

Jones, P.D., Raper, S.C.B., Santer, B.D., Cherry, B.S.G., Goodess, C.M., Kelly, P.M., Wigley, T.M.L., Bradley, R.S. and Diaz, H.F., 1985: A Grid Point Surface Air Temperature Data Set for the Northern Hemisphere. *U.S. Dept. of Energy, Carbon Dioxide Research Division, Technical Report TR022, 251pp.*

Jones, P.D., Raper, S.C.B., Cherry, B.S.G., Goodess, C.M. and Wigley, T.M.L., 1986a: A Grid Point Surface Air Temperature Data Set for the Southern Hemisphere, 1851-1984. *U.S. Dept. of Energy, Carbon Dioxide Research Division, Technical Report TR027, 73pp.*

Jones, P.D., Raper, S.C.B., Bradley, R.S., Diaz, H.F., Kelly, P.M. and Wigley, T.M.L., 1986b: Northern Hemisphere surface air temperature variations: 1851-1984. *Journal of Climate and Applied Meteorology 25, 161-179.*

Jones, P.D., Raper, S.C.B. and Wigley, T.M.L., 1986c: Southern Hemisphere surface air temperature variations: 1851-1984. *Journal of Climate and Applied Meteorology 25, 1213-1230.*

Jones, P.D., Wigley, T.M.L. and Briffa, K.R., 1987: Monthly mean pressure reconstructions for Europe (Back to 1780) and North America (to 1858). *U.S. Dept. of Energy, Carbon Dioxide Research Division. Technical Report TR037, 99pp.*

Jones, P.D., Kelly, P.M., Goodess, C.M. and Karl, T.R., 1989: The effect of urban warming on the Northern Hemisphere temperature average. *Journal of Climate (in press).*

Karl, T.R. and Williams, C.N.Jr., 1987: An approach to adjusting climatological time series for discontinuities inhomogeneities. *Journal of Climate and Applied Meteorology 26, 1744-1763.*

Karl, T.R., Diaz, H.F. and Kukla, G., 1988: Urbanization: Its detection in the United States climate record. *Journal of Climate 1 (in press).*

Karl, T.R. and Jones, P.D., 1989: On the urban biases in global temperature trends. *Bulletin of the American Meteorological Society (in press).*

Karoly, D.J., 1984: Typicalness of the FGGE year in the Southern Hemisphere. *In: GARP Special Report No.42, WMO/TD-No.22. pp.129-143.*

Karoly, D.J., Kelly, G.A.M., Le Marshall, J.F. and Pike, D.J., 1986: An atmospheric climatology of the Southern Hemisphere based on ten years of daily numerical analyses (1972-1982). *Long-Range Forecasting Research Report Series No.7, World Meteorological Organization, WMO/TD-No.92, 73pp.*

Mitchell, J.M.Jr., 1953: On the causes of instrumentally observed secular temperature trends. *Journal of Meteorology 10, 244-261.*

Mitchell, J.M.Jr., 1961: The measurement of secular temperature changes in the eastern United States. *Research Paper No.43, Weather Bureau, U.S. Dept. of Commerce, Washington, D.C.*

Raper, S.C.B., Wigley, T.M.L., Mayes, P.R., Jones, P.D. and Salinger, M.J., 1984: Variations in surface air temperature. Part 3: The Antarctic, 1957-82. *Monthly Weather Review 112, 1341-1353.*

Robin, G. de Q. (Editor), 1983: The Climatic Record in Polar Ice Sheets. *Cambridge University Press, 212pp.*

Ropelewski, C.F. and Jones, P.D., 1987: An extension of the Tahiti-Darwin Southern Oscillation Index. *Monthly Weather Review 115, 2161-2165.*

Spangler, W.L. and Jenne, R.L., 1986: World Monthly Surface Station Climatology, NCAR, 21pp (updated yearly), unpublished.

Trenberth, K.E., 1976: Spatial and temporal variations of the Southern Oscillation. *Monthly Weather Review 109, 1150-1168.*

Venter, R.J., 1957: Sources of meteorological data for the Antarctic. pp.17-38 *In: (M.P. van Rooy, Ed.) Meteorology of the Antarctic, Pretoria, Weather Bureau, South Africa.*

Wigley, T.M.L. and Jones, P.D., 1988: Do large-area-average temperature series have an urban-warming bias? *Climatic Change 12, 313-319.*

Wood, F.B., 1988: Comment: On the need for validation of the Jones et al. temperature trends with respect to urban warming. *Climatic Change 12, 297-312.*

Wind rose similarity after 140 years

Arnold Court
Emeritus Professor of Climatology
California State University, Northridge CA 91330

Introduction

Wind rose comparison procedures have not been discussed hitherto in the literature of climatology, nor, for that matter, has even the proper construction of such representation of the frequencies and/or strengths of winds from various directions. This paper summarizes the development of wind roses during the middle 19th century, in complete disregard (with one exception) of statistics and graphical theory. Polygonal and cursive roses, introduced in 1840 and 1842, were gradually supplanted, in the following century, by spoke roses, at first plain, then barred, feathered, and segmented, eventually telescoping; finally sector roses appeared. To indicate where Winds, would ferry ships or pollution, while preserving their names by direction of origin, roses were drawn downwind, Some with inverted labels and cursive roses were extended inward from outside base circles.

None of these, except some recent sector roses, correctly represented the magnitude (of frequency, strength, etc.) from each direction by the area enclosed: spokes may be proportional to magnitude, but do not cover the sector to which they apply. Two spoke roses for identical numbers of sectors can be compared visually or statistically, but when each is for a different number of sectors, or the same number differently arranged (as for magnetic vs. true direction), direct comparison is misleading. This problem is discussed later, in comparing a 16-sector rose of wind passage from hourly observations in 1848 on a Mississippi barrier island with a 12-sector rose for a nearby buoy, 1981-1984.

First roses

Originally, wind roses were simple circular diagrams of the names of winds from the various directions – 4, 8, 12, 16, or 24. As such they showed only direction, without regard to length of radius vector, or spoke. The first published diagram to be called 'wind rose'; by Baron (Christian) Leopold von Buch (1774-1853), did not involve frequencies or strengths of winds from various directions, but instead the average barometric pressure, given numerically for each of eight sectors of a circle. To show these pressures graphically, von Buch (1819) didn't use spoke length, but reverted to Cartesian form, with pressure on ordinate and direction on abscissa (Fig. 1). This permitted interpolation for the wind direction associated with overall average pressure, so that the circle could then be divided into directions from which wind 'brought' low or high pressure.

H. W. Buek(1826) gave a similar diagram for wind vs. pressure at Hamburg, and among the diagrams consolidated by Heinrich Wilhelm Dove(1803-1879) from his assorted journal articles into his 'Meteorologische Untersuchungen' (1837) were several showing 'the influence of wind direction on the pressure, temperature, and moisture of the atmosphere' by numbers around a circle according to wind direction. Radii separated high from low, warm from cold, moist from dry. Four of these, 'barometric and thermal windroses' for the northern and southern hemispheres, appear as part of a plate in the physical atlas (1840) of Heinrich Berghaus (1797-1884). Wind effects on pressure were no longer graphed after the realization, around 1850, that 'the law of storms' governs wind flow around pressure centers.

The first true wind roses to be published illustrated the results of four years' operation of Alexander Follett Osler's (1808-1903) recording windvane and 'anemometer', installed in 1837 at the Philosophical Institution of Birmingham. It recorded continuously the wind direction from a vane and wind pressure (pounds per square foot) from a pressure plate, which could be calibrated while an anemometer (for

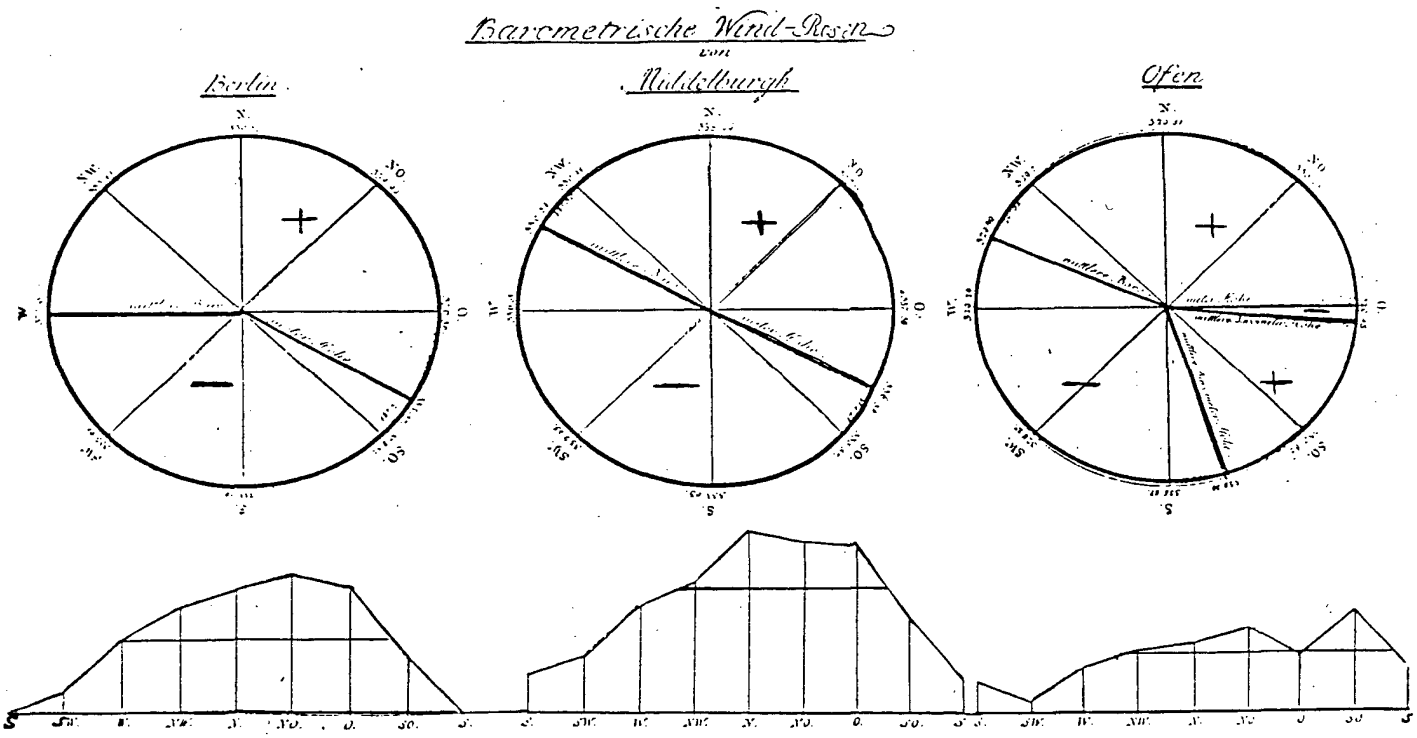

Figure 1: First known diagram to be called 'Wind Rose' shows average atmospheric **sea level pressure** in Paris 'Lignes' (1 ligne = 3mb) with winds from each of eight directions (given as vertical lines, not columns) on rectangular coordinates without any scale (lower) and by numbers around circumference of circle (upper) for Berlin, Middelburgh (Seeland, Netherlands) and Ofen (German name for Buda, old west part of Budapest). Mean pressure lines shown; colors and + and - added. **Ueber barometrische Wind-Rosen** read 18 May 1819 by Leopold **von Buch** to Koniglich Akademie der Wissenschaft in Berlin. **Abhandlungen** 1818-1819, pages 83-102.

wind speed) could not, at least until railway trains could attain sufficient speed along a straight track in calm air. Osler (1840), a glass manufacturer and amateur meteorologist, nowhere explains or comments on the construction of his diagrams, engraved by J. W. Lowry. Apparently Osler prepared the originals himself: he was an expert draftsman, illustrating his business correspondence (now in the archives of the Birmingham City Library) with sketches of the elaborate chandeliers he made and sold.

Osler's first diagram (Fig. 2) was simply a series of 16 cartesian diagrams, each showing wind frequency from a specific direction for each hour of the day during the four years, arranged around the sides of a hexadecagon in directional order. The second was a cartesian diagram of wind force (pressure) for all directions, by hours, for each season. The third was a series of cartesian diagrams of wind force by hours for each season and direction, arranged four deep around a hexadecagon. Finally, Osler's fourth Figure (Fig. 3) held five polygonal wind roses, with spoke length proportional to average wind force, from each of 16 directions for each season and for the entire year. The ends of the thin spokes were connected by a heavier line to create the polygonal rose, which became the most common representation of winds for the next century. Often the spokes themselves were suppressed, and sometimes the polygon was rounded, freehand, into a smooth curve.

Development

No comment on the novelty or ingenuity of Osler's representation was recorded in the account of the tenth meeting of the British Association for the Advancement of Science in Glasgow, at which the diagrams were shown. The general reaction was surprise that the diurnal course of wind force so closely parallelled that of temperature. Nor were Osler's roses copied very quickly.

Leon (Louis) Crétien Lalanne (1811-1892) apparently had not seen them when he compiled, for the French translation (1843) of the 'Complete Course of Meteorology' by Ludwig Friedrich Kamtz (1801-1867), an extensive appendix on 'The graphic representation of meteorological tables'. He offered three ways of representing hourly wind data : (1) by isopleths(a technique he developed and used extensively) on a cartesian grid of hour vs. month (a diagram later called 'chronoisopleth') (2) by eight lines, one for each direction, of wind frequency vs. months and (3) the 'monthly rose of wind duration' of 12 closed curves, one for each month, on a polar diagram of directions – a bowl of spaghetti almost impossible to decipher. He definitely preferred the first (isopleth) representation.

Two cursive roses on the same polar grid were used by (Lambert) Adolphe (Jacques) Quetelet (1796-1878) in his 575-page Climate of Belgium (1849) to show the annual frequencies from each of 32 directions of (1) surface winds (SW was most frequent on 42338 hourly readings from an Osler anemometer) and (2) cloud movements (most often from WSW on 15408 observations, 1833-1846, four times daily). Although he almost certainly had seen Osler's paper, Quetelet didn't mention it, and used cursive roses, not polygonal; dots marked the ends of the spokes, themselves not shown.

Wind roses of an entirely different type were used by Janes Henry Coffin (1806-1873) in his memoir on 'Winds of the Northern Hemisphere' (1854), prepared to answer a request of the Association of American Geologists and Naturalists in 1845 and read (1848) in preliminary form three years later as the first paper in the first physical science section of the initial meeting of the successor organization, the American Association for the Advancement of Science. On sets of three equally-spaced concentric circles, wind frequencies were shown by shading the areas between vectors pointing inward from the outer circles in summer, the inner circle in winter; each inter-circle band represented 30%. The shading extended from the base circle to the smooth envelope of the inward vectors.

Cursive roses without ribs or spokes, similar to those of Lalanne and Quetelet were adopted by Alexander Dallas Bache (1806-1867), Superintendent (1843-1867) of the U.S. Coast Survey, to illustrate the results of hourly wind estimates, day and night, by his staff at four coastal sites around the Gulf of Mexico and three on the Pacific coast, 1847-1855. Such roses may have been shown at the third meeting of the AAAS, of which Bache was incoming president, to illustrate his preliminary report

Figure 2: Report of the British Association for the Advancement of Science, 1840. Plate 2, Figure 1. Report on the Observations recorded during the Years 1837, 1838, 1839, and 1840 by the Self-registering Anemometer erected at the Philosophical Institution, Birmingham. – A. Follett Osler, Esq.

Tenth report of the Brit. Assoc. for the advancement of Science 1840.

Diagrams Showing the Comparative force and direction of the wind obtained from the Sum of the hourly means given in Table VI. Plate 4

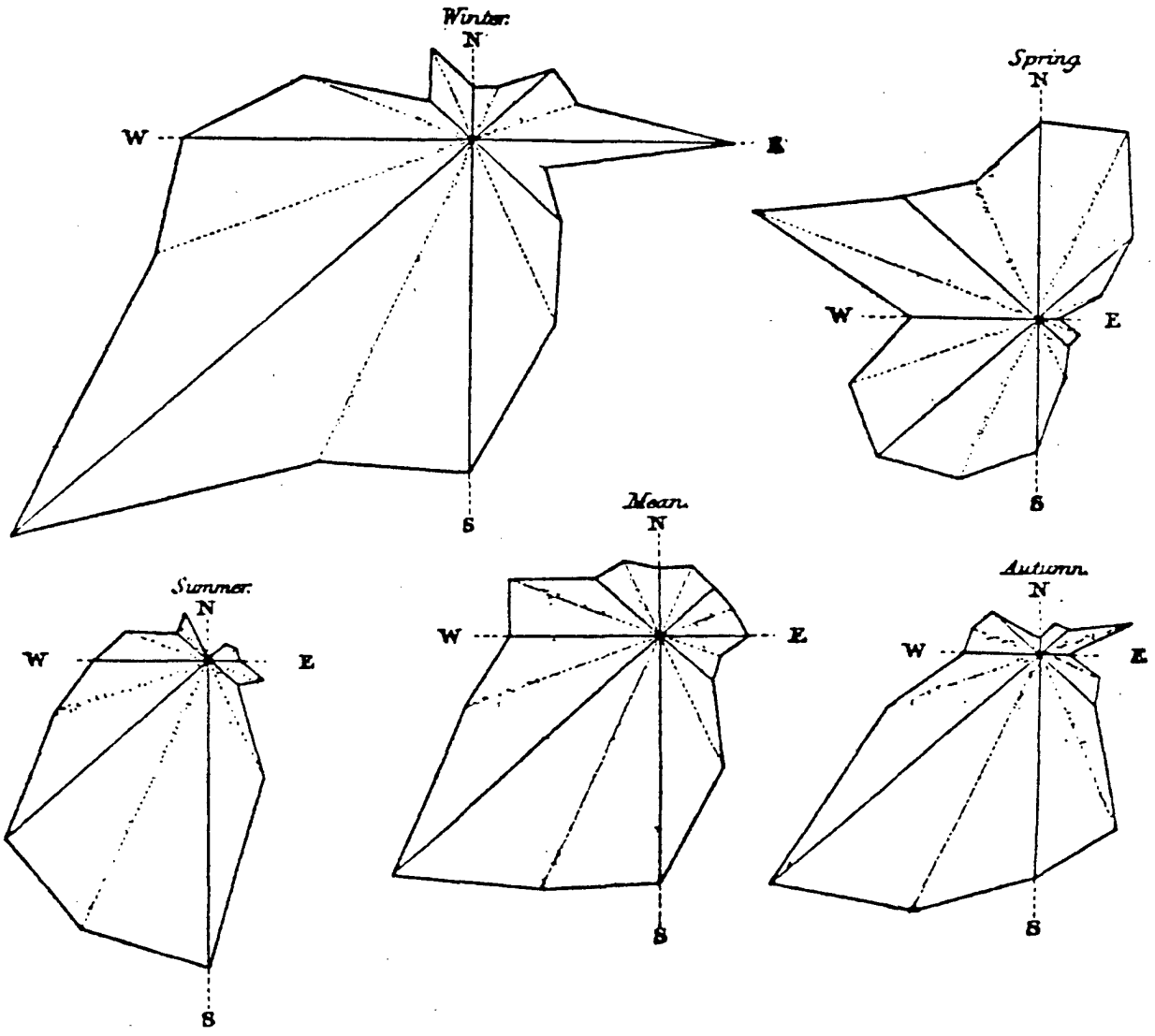

Figure 3: Abraham Follett Osler (1808-1903): Report on the Observations recorded during the Years 1837, 1838, 1839, and 1840, by the Self-registering Anemometer erected at the Philosophical Institution, Birmingham. **Report**, British Assn for the Advancement of Science (Glasgow, 1840) **10** : 321-346.

(1850) on winds at the first two sites: Fort Morgan, at the east entrance to Mobile Bay, and Cat Island, 12 km off the present Gulfport MS. Comparison of these 16-point roses to more recent data, for eight directions near Fort Morgan and for 12 directions near Cat Island, raises some interesting statistical questions.

Statistical

Statistical considerations first arose in connection with the first known use of Osler-type roses, although without credit to him. Robert FitzRoy (1805-1865), Captain (later Vice-Admiral) RN, early in 1855 started his new Meteorological Department in the Board of Trade to produce graphic representations of the extensive tabulations of marine wind data at the U.S. Naval Observatory under Matthew Fontaine Maury (1806-1873), Lt. USN. FitzRoy's instructions to his staff on the preparation of polygonal roses have been preserved *in extenso*, in the FitzRoy Papers in the British Public Record Office, Kew. Maury's circular numerical tables of wind frequencies were 'wind roses', so Fitzroy called his diagrams 'wind stars'; they were drawn downwind, 'to leeward'.

The first Wind Charts bearing 'wind stars', for the North and South Atlantic, by seasons, appeared in 1855, AUG and were circulated to various colleagues, mostly other fellows of the Royal Society. Archibald Smith (1813-1872), who became FRS in 1856 and three decades later was called 'a great mathematical genius' (in the obituary of his co-author, Sir Frederick J. 0. Evans, Captain RN (1814-1885), in the Monthly Notices of the Royal Astronomical Society 46: 184-186, 1886 FEB) replied, from 14 Ashley Place, London, on 1855 OCT 23:

> '... instead of making the radii of the stars proportional to the number of observations on that radius, they might be made proportional to the square root of this number. In that case the probability of the wind being between any two radii would be nearly proportional to the area of the star intercepted between them.' (Copy of letter in FitzRoy Papers, BJ 7/6.)

The Papers contain no response from FitzRoy, who did not alter his procedure for the nine additional maps published in the next half-year, and his reaction is not known.

Actually, Smith was only partly correct: for areas to be proportional to magnitudes, they should extend half-way to the next radius on either side, not to segments connecting spoke ends : each sector area should be a 'pie-slice', bounded by two intermediate radii and a circular arc. The conventional distortion leaves a sector's area at the mercy of its neighbors – and the total area of the polygon decreases as the variability from spoke to spoke increases. No further comment on this fundamental aspect of wind roses, or other circular diagrams, is noted for almost a century.

In two papers explaining and analyzing The Circular Normal Distribution, Emil J. Gumbel (1891-1964) plotted annual cycles on 'aequiareal' (1953, with Greenwood and Durand) and 'equivalent' (1954) polar coordinates, i.e. with square root scales on radii. They explained (Gumbel et al., 1953) that 'Leighly (1928) proposes to trace the square roots of the frequencies', but actually John Leighly (1895-1986) said only that 'Where the area of the figure is critical, the radii vectores ... must be adjusted' by 'the fundamental principles of equivalent mapping' (Leighly, 1928, p. 389). He did not use square roots on any diagram, there or elsewhere, instead mistakenly plotting temperature, an unbounded element, in polar coordinates, which are suitable only for lower bounded variables, adjusting the spokes to conserve curve slope, not area (Leighly, 1928, p. 390).

Comparisons

Two spoke wind roses, with spokes directly proportional to wind frequency or other attribute, can be compared satisfactorily by superposition only if they have the same number of sectors. To compare a 16-spoke rose to one of 8 spokes, the former can be converted to an 8-spoke rose by adding the frequencies

(but averaging the speeds) of the eight intermediate directions to those for the four cardinal and four semi-cardinal directions. The simplest method is to divide the intermediate spoke values equally, but more logical is division of each one in the same proportions as those of the two adjacent major spokes. Either method will preserve the total length of the spokes – but not the areas enclosing them, on a polygon rose or on an areally correct (square root) sector rose.

In a uniform (isotropic) wind field, each of four sectors has 25% of the occurrences so that each of four spokes represents 25%, and a sector rose has a radius of $\sqrt{25} = 5$ percentage units. But each of eight spokes is only half as long, and an 8-sector rose radius is only 2.526... units. The more sectors, the smaller the sector rose – unless the individual frequencies are divided by sector width to make them represent frequency per degree: 0.27778 percent per degree for the uniform field. These considerations apply to wind frequencies and other aspects which are summed, such as rain amounts from each direction, and to wind passage, the summed product of speed and duration. For speed or pressure, weighted averages must be used in reducing the number of spokes or sectors.

For pairwise statistical comparison of two roses, they may be sampled, randomly or systematically, around the outer arcs. Actually this can be done mathematically, without drawing the roses, but visualising them helps.

Such considerations arose in the study of the hourly wind data collected on the Gulf and Pacific coasts by the U. S. Coast Survey, 1847-1855. Results of this ambitious program were available only as wind passage, the product of total hours and average speed from each direction, by months and for the year. For Cat Island, tabular data are not available, only monthly, seasonal, and annual cursive 16-spoke roses with spokes suppressed (Fig. 4) (Dean, 1857). About 27 km to the southeast, a 12-meter discus hull meteorological buoy (No. 42007), with sensors 10 meters above water, has been transmitting data continuously since 1981.

In the extensive 3-year summary (NCDC, 1986), wind data are given, not for 8 or 16 sectors, but for 12, each 30°wide: 000°-030°,..., 330°-360°. For comparison with the 16-point Cat Island wind passage data, scaled from the cursive annual wind rose, annual wind passage from each of the 12 sectors at the buoy was obtained by multiplying average speed by relative frequency. To make the two roses nearly the same size, the buoy data were increased 25% before the square root was taken. Even so, estimated wind passage at the buoy was less than at the lighthouse, perhaps because the latter was obtained by converting the original force estimate (0 = calm,... 10 = tornado or hurricane) to speeds using a table usually credited to John Smeaton (1724-1792) but actually due to Samuel Rouse (1705-1775). Smeaton (1759), including Rouse's table in his treatise on waterwheels and windmills, questioned the accuracy of its speeds for wind forces greater than 6. Rouse's speeds for forces 4 and stronger are about 50% greater than those now assigned to the corresponding numbers of the 'Beaufort scale', which had been in use on land for more than half-a-century before being adapted to marine use around 1790 by Alexander Dalrymple (1737-1808) and in 1806 by Francis Beaufort (1774-1857), neither of whom ever used speeds for it.

Thus differences between the wind roses (Fig. 7) for Cat Island and Buoy 42007 arise primarily from the apparent overestimate of wind speeds in computing wind passage at Cat Island. The rose from the automatic buoy in unobstructed ocean is almost isotropic, while that for Cat Island, at the western point of the low triangular barrier island, bulges to NE, SE, S, and SW, indicating observer under-use of intermediate directions, and some wind deflection by the island.

Conclusions

Wind roses, introduced in 1840 and progressively refined and improved, offer excellent representations of the directional distribution of winds (and other phenomena), but require careful attention to statistical and meteorological principles. Sector roses, in which area, not length, corresponds to frequencies, speeds, or passage, are most useful, but comparison of roses differing in numbers of sectors demands statistical adjustments.

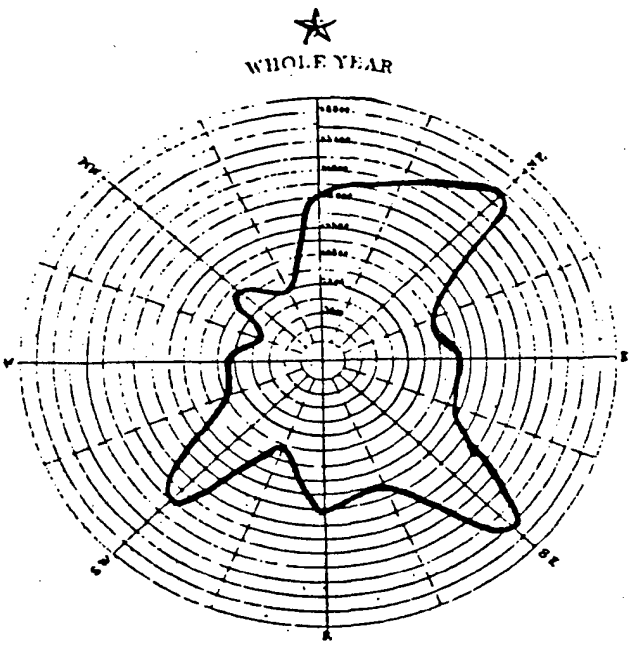

Figure 4: 'Diagrams representing the quantity of the winds... and their effect on the level of the sea at Cat Island, Mississippi Sound, from hourly observations by the U. S. Coast Survey in 1848... The circumference of the small circle nearest the centre of the diagram is the zero from which the distances are plotted... The space between any two... circles... represents 1800 miles' A. D. Bache: **'Report of the Superintendent of the United States Coast Survey '** for 1856, Appendix 45, Plate 39. Wind Passage compiled from conversion to miles per hour of wind force estimated on 0-10 'nautical scale' from 'streamer upon a flag staff'. (Bache, Proc. Amer. Assn Adv. Sci. 3: 50-53, 1850).

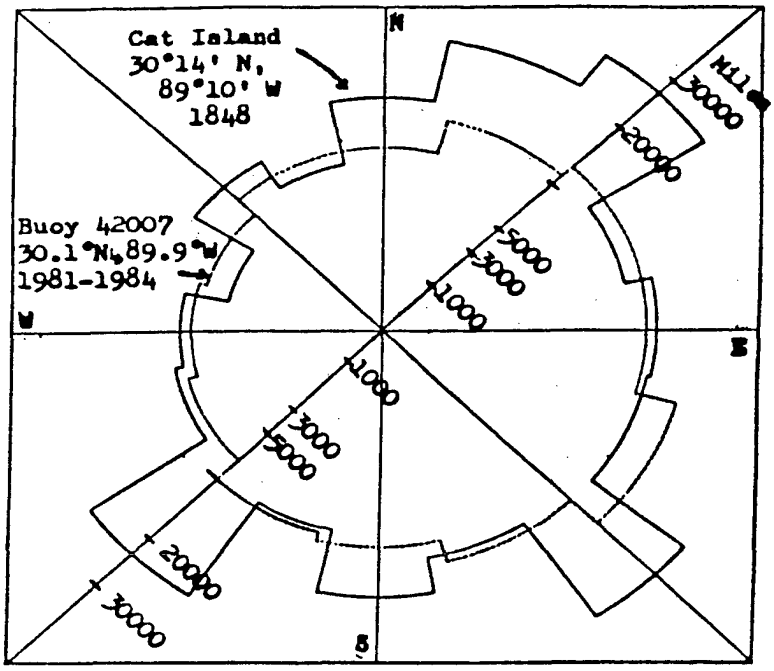

Figure 5: Annual wind passage (miles) at Cat Island MS, 1848, at Data Buoy 42007, 1981-1984; buoy passages from each of 12 sectors increased 25% to correspond to 16 sector-data from Cat Island.

References

Bache, A.D., 1850: Notes on the results of observations of the direction and force of the wind at the Coast Survey stations, at Mobile Point, and at Cat Island, Gulf of Mexico. *Proc. Amer. Assn. Adv. Sci.*, **3**: 50-53.

Berghaus, Heinrich, 1840: Windkarte der Erde. *Physikalischer Atlas*, 1st Abtheilung, No. 7., Gotha, Justus Perthes.

Buek, H.W., 1826: *Hamburgs Clima und Witterung*, Hamburg, August Campe, 152 pp.

Coffin, J.H., 1848: A report on the winds of the Northern Hemisphere. *Proc. Amer. Assn. Adv. Sci.* **1**: 34-35.

_____, 1854: Winds of the Northern Hemisphere. *Smithsonian Contrib. Knowledge* **6**, Art. V, 200 pp. 13 plates.

Dean, G.W., 1857: Notes on the effect of the wind upon the height of water in Cat Island Harbor, Mississippi. *Rpt. Supt. Coast Survey*, Appx. 45, pp. 276-278.

Dove, H.W., 1837: *Meteorologische Untersuchungen.* Berlin, Sander'schen Buchhandlung.

Gumbel, Emil J., A. Greenwood, and D. Durand, 1953: The circular normal distribution: theory and tables. *J. Amer. Statis. Assn.* **48**: 131-152.

_____, 1954: Applications of the circular normal distribution. *Ibid.* **49**: 267-297.

Lalanne, L., 1843: Appendice sur la représentation graphique des tableaux météorologiques, etc. In: L. Kaemtz, *Cours Complet de Météorologie*, trans. Ch. Martins. Paris, Delahays.

Leighly, J., 1928: Graphic Studies in Climatology, II. The polar form of diagram in the plotting of the annual climatic cycle. *Univ. Calif. Pubs. Geography* **2**(13): 387-407.

NCDC, 1986: Buoy Station 42007, Surface wind speed (knots), percent frequency of wind speed (kts) vs wind direction (tens of degrees). Climatic *Summaries of NDBC Data Buoys.* National Data Buoy Center (Nat. Wea. Svc., NOAA, USDC), NSTL MS, xvii + 339 pp. (pp. 73, 75-76).

Osler A.F., 1840: Report on the observations recorded during the years 1837, 1838, 1839, and 1840, etc. *Rpt. Brit. Assn. Adv. Sci.* **10**: 321-326.

Quetelet, A., 1849: *Sur le Climat de la Belgique.* Brussels, Hayez, 575 pp.(p. 4)

Smeaton, J., 1759: On the construction and effects or windmill sails. Part III of 'An experimental inquiry concerning the natural powers of water and wind to turn sails'. *Proc. Roy. Soc. London* **51** : 45-85. Reprinted in Tracts on Hydraulics, London, Spon, 1862.

von Buch, L., 1819: Ueber barometrische Wind-Rosen. *Abh. kk. Akad. Wiss.* Berlin, 1818-1819: 83-102.

Quality/value relationships for climate forecasts in prototype and real-world decision-making problems

A.H. Murphy, R. W. Katz, B.G. Brown
Department of Atmospheric Sciences, Oregon State University
Environmental & Societal Impacts Group, NCAR, Boulder USA

Abstract

In this paper we summarize the results of several studies related to the economic value of climate forecasts in prototype and real-world decision-making problems. Both single-stage problems consisting of individual isolated decisions and multiple-stage problems involving sequences of interrelated decisions are considered. Prototype problems include (several versions of) the familiar cost-loss ratio problem and a generic choice-of-crop problem, and real-world problems include the haying/pasturing problem, a particular choice-of-crop problem, and the fallowing/planting problem.

Specific attention is devoted to the relationship between forecast quality and forecast value in the context of these problems. Analytical and numerical results are presented to illustrate the general nature and shape of the quality/value "curves." The latter are shown to be inherently nonlinear and to be characterized by a quality threshold, below which climate forecasts are of no value. Some implications of these results - and other recent results related to comparative evaluation of forecasting systems (e.g., quality/value "envelopes" and the concept of sufficiency) - for the scientific and user communities are discussed.

References

Brown, B.G., Katz, R.W., and Murphy, A.H., 1986: On the economic value of seasonal precipitation forecasts: The fallowing/planting problem. *Bull. AMS*, **67**, 833-841.

Murphy, A.H., Katz, R.W., Winkler, R.L., and Hsu, W-R., 1985: Repetitive decision making and the value of forecasts in the cost-loss ratio situation: A dynamic model. *Monthly Wea. Rev.*, **113**, 801-813.

Wilks, D.S., and Murphy, A.H., 1986: A decision-analytic study of the joint value of seasonal precipitation and temperature forecasts in a choice-of- crop problem. *Atmos.-Ocean*, **24**, 353-368.

Valuing climate forecast information

S.T. Sonka, J.W. Mjelde, P.J. Lamb, S.E Hollinger, B.L. Dixon
?????

Abstract

This presentation will summarize the material reported in a paper of the same title that appeared in J. Clim. Appl. Meteor. in September 1987. It provides a framework for evaluating the economic benefits of the characteristics of climate forecasts in settings where sequential decisions are made. The dynamic programming decision model used is fully described in a forthcoming article in Amer. J. Agric. Econ. (Mjelde, Sonka, Dixon, and Lamb). In the present paper, illustrative results are provided for corn production in east-central Illinois. These results indicate that the production process examined has sufficient flexibility to utilize climate forecasts for specific production seasons but the value of those forecasts is sensitive to economic parameters as well as forecast characteristics. Forecast periods of greatest importance, as well as the relationships between forecast value, accuracy, and lead time, are evaluated.

Economic decisions on climatically variable areas

E.E. Zhukovsky
Agrophysical Research Institute , Leningrad, USSR

Introduction

Different factors in nature determining climate peculiarities at every geographic point are subject to great spatial variability . These factors define macro-, meso- and microclimatic variability of areas with different effects on (conditions to realise) many kinds of human weather-dependent activities. Therefore, the following three main problems are of particular interest: (1) the study of climatic variability, discovery of reasons for this variability, analysis of statistical structure, mapping, etc. ; (2) control of climatic variability to smooth or, vice versa, to create favourable climatic contrasts (e.g. micro-climate control in the field);(3) decision-making and planning on climatically variable areas (CVA) . The latter problem is least studied, though some aspects are are discussed in (Zhukov- sky 1987; Zhukovsky et al. 1986; Nasonova and Zakarian 1988). A general approach is discussed below; within the framework of this approach the decision-making on CVA is considered from the viewpoint of ideas and methodology widely applied in studies on the optimal use and evaluation of the economic efficiency of meteorological data (Zhukovsky 1981).

Methodology

Let the study area vary with climatic factor X which may be mean long-term air temperature, normal precipitation, probability of some meteorological event, etc. Let us specify a function $g(x)$ showing 'distribution' of various X values within the study area. If we assume that the area is divided into zones where X takes one of the values $x_1 \ldots x_l, \ldots x_m$ then the function $g(x)$ is discrete and the numbers $g_1 = g(x_1), \ldots, g_m = g(x_m)$ would indicate the portion of the total area of zones with appropriate x in the study area. E.g. $g_1 = 0.2$ means that the area where $X = x_1$ occupies 20% of the whole area. It is evident that $\sum_{i=1}^{m} g_i = 1$.

In other cases it would be more natural to assume X as a continuous value varying within a definite range $\langle x \rangle$. Here the function $g(x)$ is continuous too and it has all the features of the density distribution function. In particular, $\int_{\langle x \rangle} g(x)dx = 1$.

Then let us assume that some human acitivity d is planned in the study area. Depending on the way d is specified at particular points, three types of strategies S should be distinguished; they deal with the available (detail ?utility? rate of the) information on the area variability in different ways: - non-differentiated strategies (NDS), or class G; - detail-differentiated strategies (DDS), or class D; - partly-differentiated strategies (PDS), or class A.

For any NDS it is 'typical to make the single economic decision $d = \text{const}$; the simplest variant of this strategy is to plan according to the mean climatic conditions, i.e, $x = \bar{x}$ (here and later the bar means statistical averaging for all possible values of X). Realization of DDS means that a particular decision is made at every point according to the specified x value. PDS occupy a position between NDS and DDS and are made in the following way: the range of the X variation is divided into non-intersecting steps $H_1, H_2, \ldots, H_N$. These steps are used for area regionalisation, i.e. quasi-homogeneous areas are selected where $x \in H_i$ $(i = 1, 2, \ldots, N)$, and a decision $d_i = d(H_i)$ is made for every one of those areas.

In the general case a selection of d for any arbitrary point in space depends on the x value at that point and on the accepted planning strategy S. Thus, it is possible to put down that $d = d(x, S)$. Following the general principles of the theory of statistical decisions let us introduce the function $u(x, d)$ which shows the economic effect (gain or loss) per unit area at the d decision-making at the

specified x. In this case different planning variants may be compared on the basis of u value mean per unit area and determined as

$$U_S = \overline{u[x, d(x, S)]} \tag{1}$$

For example, for continuous X value it is possible to put down:

$$U_S = \int_{\langle X \rangle} u[x, d(x, S)] g(x) dx$$

For every x among a variety of admissible d solutions it is always possible to make a certain optimal economic decision d_π. Let us assume (for certainty) that u is benefit. Then d_π should meet the condition:

$$u[x, d_\pi(x)] = max_{\langle d \rangle} u(x, d) \tag{2}$$

We may assume that at the known (or supposed) $X = a$ the decision will be made in accordance with (2). Therefore, the terms below 'planning in accordance with X = a' or 'orientation for X = a' would mean the decision making of $d_\pi(a)$. To simplify the presentation, $d(a)$ will be used instead of $d_\pi(a)$ assuming that $d(a) = d_\pi(a)$.

Taking into account all mentioned for NDS oriented for mean climatic conditions , (1) may be presented as follows:

$$U_G = U_G(\bar{x}) = \overline{u[x, d(\bar{x})]} \tag{3}$$

Similarly, we shall have for DDS :

$$U_D = \overline{u[x, d(x)]}. \tag{4}$$

In case of PDS which is made on the basis of mean values of $X = \bar{x}_i$ within individual steps H_i we shall derive

$$U_A = U_A(\{\bar{x}_i\}) = \sum_{i=1}^{N} g_i \overline{u[x, d(\bar{x}_i)]} \tag{5}$$

In (5) the averaging for every i is made according to $x \in H_i$; g_i - is a part of area where $x \in H_i$.

It is evident that certain relations exist between (3) , (4) and (5), namely $U_G \leq U_A \leq U_D$, which show that greater details on the account of climate variability of the area lead to a higher economic effect mean for unit area, produced by the decision-making. In this case the difference

$$\Delta U_D = U_D - U_G \tag{6}$$

and dimensionless factor $\lambda = \frac{\Delta U_D}{U_G}$ will characterize (in absolute and relative units, respectively) the maximum possible benefit which may be got due to the use of data on CVA. By analogy to (6) , the difference

$$\Delta U_A = U_A - U_G \tag{7}$$

will show the benefit in absolute terms per unit area, provided by the substitution of non-differentiated planning into mean climatic conditions using differentiation of decision in accordance with mean X values within individual steps, while the relative value $\nu = \frac{\Delta U_A}{\Delta U_D}$ may be used as an efficiency factor of the study PDS. According to its physical sense ν means the portion of losses produced by the climatic variability of the area, compensated by differentiated planning. It should be noted that this scheme or the analysis would not change if the values u_{ij} mean losses, not benefits, in the problem. In this case $U_G \geq U_A \geq U_D$ and differences (6) and (7) should be replaced by the opposite ones. Respectively, (2) will have not *max* but *min*.

Decision-making for the area variable by the probability of a meteorological event

As a possible application of the above approach, let us consider a case when the climatic variability of the area is displayed through a variable probability of meteorological events. The situation when these events are observed will be denoted by F_1, while the alternative situation will be denoted by F_2; respectively. p_1 would mean the probability of the event F_1, and $p_2 = 1 - p_1$ would represent the probability of the event F_2. Thus $X = p_1$ in the problem considered.

Then let us assume that one of the two economic decisions should be made, i.e. d_1 or d_2 depending on the specified weather. It is supposed that the first decision is oriented for F_1 situation, while the second decision is oriented for the event F_2. Let us also assume that the square matrix $\|u_{ij} = u(F_i, d_j)\|$, $(i,j = 1,2)$ is known; the elements of this matrix characterise the economic consequences of appropriate man's activity under different weather conditions. It is easy to show, that if the decision-making is based on the Bayesian approach, i.e. according to a statistical criterion of the mean benefit maximum, then if p_1 and u_{ij}, $(i, j = 1,2)$ are specified the selection should be made according to the following rule

$$d_\pi = \begin{cases} d_1 & \text{if } p_1 \geq \pi \\ d_2 & \text{if } p_1 < \pi \end{cases} \tag{8}$$

where $\pi = \beta/(1 + \beta)$, $\beta = (u_{22} - u_{21})/(u_{11} - u_{12})$.

If we have information on particular p_1 values at various points of the study area, the above rule may be applied for a necessary differentiation of economic decisions.

As the first approximation, let us assume: the regionalisation resulted in a number of climatically homogeneous zones satisfying m values of the variable p_1 value. Let us denote these values as p_{11}, ...p_{1k}, ..., p_{1m} and let us compare two variants of planning i.e. NDS, when a single decision is made for the whole area in accordance with (8) depending on the ratio between π and $\bar{p}_1 = \sum_{k=1}^{m} g_k p_{1k}$, with g_k = part of area, where $p_1 = p_{1k}$, and DDS, when the same rule (8) is applied but the optimal decision is made for every climatically homogeneous area(zone). It is easy to show that the benefit ΔU_D got in this case may be computed from the following equation

$$\Delta U_D = \begin{cases} (r_1 + r_2) \sum_{p_{1k} \leq \pi} (\pi - p_{1k}) g_k & \text{if } \bar{p}_1 \geq \pi \\ (r_1 + r_2) \sum_{p_{1k} > \pi} (p_{1k} - \pi) g_k & \text{if } \bar{p}_1 < \pi \end{cases} \tag{9}$$

where $r_1 = u_{11} - u_{12}$ and $r_2 = u_{22} - u_{21}$. ΔU_D is a maximum if $\bar{p}_1 = \pi$. In this case it follows from (9) that

$$[\Delta U_D]_{max} = \frac{r_1 + r_2}{2} \Delta p_1$$

where $\Delta p_1 = \sum_1^m |p_{1k} - \bar{p}_1| g_k$ is the mean absolute deviation of p_1 from $\bar{p}_1$ at individual points. It is very interesting to note the analogy between (9) and the results obtained in Winkler(et al., 1983).

Equation (9) may be easily generalized for the case when space variability of the climatic probability p_1 is described by some continuous function $g(p_1)$. In this case the following ratio will be valid instead of (9):

$$\Delta U_D = \begin{cases} (r_1 + r_2) \int_{p_1 \leq \pi} (\pi - p_1) g(p_1) dp_1 & \text{if } \bar{p}_1 \geq \pi \\ (r_1 + r_2) \int_{p_1 > \pi} (p_1 - \pi) g(p_1) dp_1 & \text{if } \bar{p}_1 < \pi \end{cases} \tag{10}$$

To make it concrete , it should be taken into account that the range of p_1 variations is always physically limited from 0 to 1. Proceeding from this it is possible to use the beta-distribution for the analytical approximation of the function $g(p_1)$:

$$g(p_1) = p_1^{a-1}(1 - p_1)^{b-1}/B(a, b) \tag{11}$$

Here a and b are positive parameters, and $B(a,b)$ is the Euler integral of the first order, determined as

$$B(a,b) = \int_0^1 p_1^{a-1}(1-p_1)^{b-1}dp_1 = \Gamma(a)\Gamma(b)/\Gamma(a+b)$$

(Γ - gamma function). If we put (11) into the general formula (10), we obtain (Zhukovsky, 1987):

$$\Delta U_D = \begin{cases} (r_1+r_2)[\pi I_\pi(a,b) - \bar{p}_1 I_\pi(a+1,b)] & \text{if } \bar{p}_1 \geq \pi \\ (r_1+r_2)[\bar{p}_1 \hat{I}_\pi(a+1,b) - \pi \hat{I}_\pi(a,b)] & \text{if } \bar{p}_1 < \pi \end{cases} \quad (12)$$

Here $I_\pi(w,z)$ is the incomplete beta-function ratio determined as

$$I_\pi(w,z) = \int_0^\pi p_1^{w-1}(1-p_1)^{z-1}dp_1/B(w,z)$$

tabulated by Karl Pearson and $\hat{I}_\pi(w,z)$ is the integral of the function $I_\pi(w,z)$ up to 1. $\bar{p}_1 = a/(a+b)$ For the case when $\bar{p}_1 = \pi$, it follows from (12)

$$[\Delta U_D]_{max} = (r_1+r_2)\bar{p}_1[I_{\bar{p}_1}(a,b) - I_{\bar{p}_1}(a+1,b).$$

If we change a and b, parameters in (11) it is possible to get a great variety of symmetric and asymmetric distributions. In particular, a family of curves symmetric relative to the point $\bar{p}_1 = 0.5$ corresponds to the situation $a = b$; moreover when $a = b = 1$ this will be the simple uniform distribution $g(p_1) = 1$. For this case (10) gives

$$\Delta U_D = \begin{cases} (r_1+r_2)(\pi^2)/2 & \text{if } \pi \leq 0.5 \\ (r_1+r_2)(1-\pi)^2/2 & \text{if } \pi > 0.5 \end{cases}$$

If $a < b$ (11) determines one-peaked curves with a positive asymmetry, while in case of $a > b$ the asymmetry is negative. Fig. 1 gives curves showing that in case of various types of $g(p_1)$ distributions the character of relations between ΔU_D and π is subject to changes. The asymmetry of p_1 distribution causes the fall of $[\Delta U_D]_{max}$ value, moreover its maximum value is in accordance with the law of uniform distribution.

It is interesting to give a specific case here. Let F_1 and F_2 indicate a presence or lack of some dangerous meteorological event, and d_1 and d_2 indicate realisation or non-realisation of protective measures. Then the values of u_{ij} mean losses, moreover, a model is used in many studies where the matrix $||u_{ij}||$ is as follows:

	d_1	d_2
F_1	C	L
F_2	C	0

Here C indicates losses for protective measures and L means damage caused by the dangerous event if protective measures are lacking. (Thompson, 1976; Murphy, 1977; etc). Taking into account the general relations obtained above, it is possible to show that in this case the losses at NDS mean per unit area would be as follows:

$$U_G = \begin{cases} C & \text{if } \bar{p}_1 \geq C/L \\ L\bar{p}_1 & \text{if } \bar{p}_1 < C/L \end{cases}$$

while the relative factor λ characterising the gain due to differentiation of decisions is determined as follows:

$$\lambda = \begin{cases} I_{C/L}(a,b) - (L\bar{p}_1/C)I_{C/L}(a+1,b) & \text{if } \bar{p}_1 \geq C/L \\ \hat{I}_{C/L}(a+1,b) - (C/L\bar{p}_1)\hat{I}_{C/L}(a,b) & \text{if } \bar{p}_1 < C/L \end{cases}$$

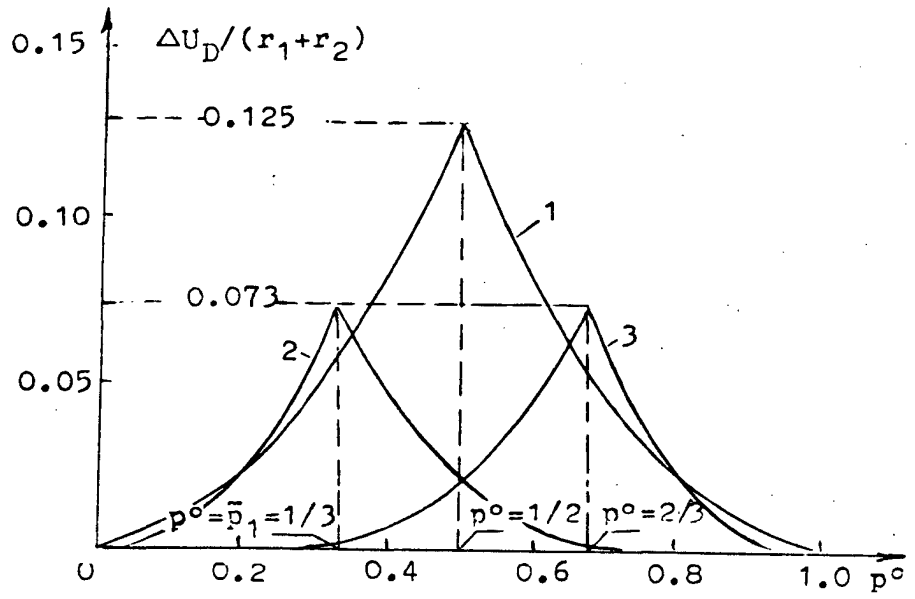

Figure 1: $\Delta \bar{U}_D$ value as π function in case of different variants of p_1 distribution. 1 - for uniform distribution $a = b = 1$; 2 - for positively asymmetric distribution $a = 2$, $b = 4$; 3 - for negatively asymmetric distribution $a = 4$; $b = 2$.

The maximum λ value is observed at $C/L = \hat{p}_1$ and, as it follows from the above formulae, at the arbitrary values of a and b

$$\lambda_{max} = I_{\hat{p}_1}(a, b) - I_{\hat{p}_1}(a + 1, b)$$

Let us take a definite situation when $a = b = 1$. In this case $\lambda_{max} = 0.25$. I.e. mean losses per unit area because of the climatic variability of the area tend to decrease by 25% in this case.

References

Murphy, A.H., 1977: The value of climatological , categorical and probabilistic forecasts in the cost-loss ratio situation. *Mon. Wea. Rev.* **105**, 7.

Nasonova, O.N., Zakarian Yu.A. 1988: On the efficiency of some problems on separation into steps during areal regionalisation - *Res. & Techn. Bull. Agronomic Physicas, No. 70.*

Thompson, J.C., 1976: Economic and social impact of weather forecasts. *Weather Forecasting and Weather Forecasts: Models, Systems and Users.* NCAR Boulder, Colorado, USA.

Winkler, R.L., Murphy, A.H, and R.W. Katz, 1983: The value of climatic information: a decision analytic approach. - *J. Climatology* **3**, 187-197.

Zhukovsky, E.E., 1981: Meteorological information and economic decisions. Leningrad, Gidrometeoizdat.

Zhukovsky, E.E., 1987a: Statistical models for optimisation of hydrometeorologic data use. In: *Use of statistical methods in meteorology.* Leningrad, Gidrometeoizdat.

Zhukovsky, E.E., 1987b: Statistical decisions and problem of the optimum use of meteorological information. Proc. 1st World Congress of Bernoulli Society, The Netherlands.

Zhukovsky, E.E., Zakarian, Yu.A., and M.G. Sanoian, 1986: On spatial differentiation of agrotechnical decisions. In: *Agroclimate and harvest programming.* AFI.

Estimates of dimension and entropy of weather and climate attractors

Klaus Fraedrich
Institut für Meteorologie, Freie Universität Berlin, Berlin, FRG

Introduction

Standard atmospheric circulation statistics provide **physical** information in terms of means, higher moments, space-time filtered or cross-spectral properties of the basic meteorological field variables: mean temperatures, eddy fluxes, energy conversions in appropriate space-time or wavenumber-frequency domains. Another type of data analysis is the **phenomenological** statistic. It is closely related to the real weather phenomena: storm tracks of tropical and extra-tropical cyclones changing with season or related to large scale flow anomalies, etc. This statistic accounts for individual weather pattern and leads to the phenomenological aspects of the dynamical system. In recent years another method of analysis has been used which complements the other two statistical approaches in the sense that **mathematical** properties are deduced; dynamical systems theory is applied to the weather and climate system.

In this sense nonlinear (or fractal) analysis techniques are developed to gain information on the route from linear systems towards an understanding of the nonlinearity of complex dynamics (Table 1) such as the weather or the global climate; several features on this route have been topics of meteorological and oceanographic research:

Table 1: From linear to nonlinear dynamics

Linear Dynamics	$\Longrightarrow$	Coherent Structures	$\Longrightarrow$	Chaotic Dynamics	$\Longrightarrow$	Nonlinear Dynamics
Balance:		Dispersion/ Dissipation		Nonlinearity/ Dissipation		

Basic concepts: Dimension and Entropy

Much of the present research interest on dynamical systems analysis methods applied to weather and climate processes can be traced back to Lorenz (1963). He revealed the dynamics of a low-order spectral model of convection and provided a mathematical model for turbulence or chaos: After discounting the initial transients, the flow of many of these nonlinear systems with three or more variables is firstly confined to a subset of the phase space of states spanned by the model components, and secondly characterized by a sensitive dependence on the initial conditions. That is, this subset or **strange attractor** is of smaller dimension than the phase space, and the flow, if applied to forecasts with initial errors, has limited predictability. Accordingly two properties are introduced to characterize the structure of a strange attractor and the flow on it, **dimension** and **entropy**.

Dimension

Dimension is roughly estimated by the number of independent variables (degrees of freedom or active modes) involved in the process and thus is a measure of its complexity. Dynamical systems theory defines a hierarchy of dimensions (some listed in Table 2), of which the correlation dimension is frequently used in meteorological applications, because its determination is relatively easy.

Table 2: Dimension

Generalised dimension	$D(q) = \lim_{l \to 0} \ln \sum(p(i)^q) / \ln l)/(q-1)$
Hausdorff dimension ($q \to 0$)	$D(0) = -\lim_{l \to 0} \ln M(l) / \ln l$
...A measure for the number cells increasing with $l \to 0$	
Information dimension ($q \to 1$)	$D(1) = -\lim_{l \to 0} \ln S(l) / \ln l$
...A measure for the information, $S(l)$, increasing with $l \to 0$	
Correlation dimension ($q = 2$)	$D(2) = \lim_{l \to 0} \ln \sum(p(i)^2) / \ln l$
$\ldots\sum(p(i)^2)$: probability for pair of points in the same box	
l:	size of a cell or a box i in the phase space
$\sum$:	sum over all cells $i = 1, \ldots, M(l)$ covering the attractor
$p(i) = \lim N(i)/N$:	probability of finding a point of the attractor in box i; N data points
$S(l) = -\sum(p(i) \ln p(i))$:	Shannon information of locating a trajectory in a specific cell i
	$D(0) \geq D(1) \geq D(2) \ldots$

Entropy

Entropy may be understood as a dimension in a space of time sequences (I in Table 3) or cylinder sets. In this sense entropy is a measure:-

1. for the rate of information about the state of a dynamical system changing with time;
2. for the rate of divergence of initially close pieces of trajectories on the attractor: an infinitesimal sphere expanding into an ellipsoid to which only the diverging axes contribute, that is the sum of positive Liapunov exponents $l(k) > 0$ (for fractals the $l(k)$ are weighted by the dimensions of the principle axes);
3. for a predictability time scale ($1/K$) or e-folding growth of initially small errors. Note that NWP-predictability refers to errors approaching the noise level, which is slowly?? due to nonlinearity.

Analysis techniques

Before computing dimension and entropy measures by suitable algorithms, the phase space of the system needs to be reconstructed from the data, because many observations provide only scalar signals.

Substitute phase space

To reconstruct the attractor, which is embedded in the phase space of the dynamical system, the classical method of delay-coordinates is used. This provides a state vector, $X(t_i) = [x(t_i), ..., x(t_i + (m-1)T)]$, in an m-dimensional (embedding) phase space spanned by samples of the time series, $x(t_i)$, delayed by a suitable time scale T. Delayed vector variables can also be used.

Algorithms

Two basic methods to calculate dimension (and entropy) may be mentioned (Table 4): The 'box-counting' algorithm is a direct application of the definitions. The 'pair-counting' algorithms provide another way to estimate dimension and entropy. Note that these algorithms give global estimates for the attractor properties; but, for example, the spectra $D(q)$, $K(q)$ provide some insight into the inhomogeneity. Some experiences are noteworthy:-

- About $n = 10^D$ data values?? are needed to resolve attractors of dimension D, although saturation has been achieved with smaller data sets;
- The first zero-crossing of the auto- correlation defines an approximate value for the delay-time T (linear independence);
- An attractor is sufficiently embedded when its dimension has reached saturation by satisfying the scaling law over a range of magnitudes. The embedding dimension m and the integer above the attractor dimension D are measures for the number of variables sufficient or necessary, respectively, to model the dynamics;
- Excessively high-dimensional embeddings lead to convergence of the correlation exponent ($D(2)$) for any dynamical system;
- A time series cannot be distinguished from random noise if, using for example the maximum norm, $C(q=2,m,r) = C(q=2,m=1,r)^m$;
- For error estimates see, for example, Holzfuss and Mayer-Kress (1985).

Instead of averaging the variable, number of pairs, to yield estimates of probabilities $p(m,r)$ for balls of fixed radius r, averages are taken over the variable radius, $r(m,p)$, of balls containing a fixed number of pairs (nearest neighbours) or probabilities p.

Applications

Results from dynamical systems analyses of weather and climate time series are presented in the following (Table 5).

Climate variables

In climate theory a hierarchy of models has been constructed which includes both the **deterministic** and the **stochastic** ansatz?? for model building. Many of the deterministic models are low-order systems exhibiting dynamical structures which range from zero-dimensional fixed points, through one-dimensional limit cycles to quasi-periodicity on tori of higher dimension. As the model-feedback construction has often been conceptual, there was a need for more quantitative information: the degrees of freedom involved or the number of active modes or variables needed in modelling. Nicolis and Nicolis (1984), Fraedrich (1987) and, recently, Maasch (1989) claimed an attractor dimension between 3 and 6, based on deep sea core records. Grassberger (1987), however, emphasized that

small data sets and smoothing procedures may lead to false conclusions.- Nonlinear systems analysis methods were also applied to ENSO signals on monthly and annual time scales (Hense 1987, 1988; Fraedrich 1988); a relatively low dimensionality (2-6) was detected in monthly data; no saturation was reached by the anually averaged SOI-signals so that the sampling time limited the predictability.

On the other hand, the stochastic hypothesis to explain climate fluctuations follows a concept which contrasts the deterministic one. It is hoped that these methods provide more insight into this problem.

Weather variables

The state of forecasting and modelling appears to be more advanced than for the more complex climate system. Therefore, practical aspects are related to predictability whereas the dimensionality and the number of modes involved is a more fundamental question. Associated with predictability is the spectrum of characteristic exponents which describes the rate of divergence of phase space trajectories in terms of a mode related instability or error growth rate (Table 5). Furthermore, besides the large scale flow, mesoscale and boundary layer processes also attracted attention. Studies of large scale variables by Fraedrich (1986, 1987), Essex et al. (1987), Henderson and Wells (1988), Kepenne and Nicolis (1988) suggest that the regional attractors associated with some meteorological time series of large scale variables (daily surface pressure, 500mb heights at various stations) are of relatively low dimension (6-8). But note also that other authors did not come to the same conclusions when using different large scale variables. A relatively large predictability (up to 20 days) was derived by Fraedrich (1987) and was substantiated by Kepenne and Nicolis (1989). Analyses of smaller scale processes of the atmospheric boundary layer (thunderstorm gusts, free convection) also suggest a low dimensionality of this (local) attractor (4 and 7-8, Henderson and Wells 1988; Tsonis and Elsner 1988).

Cyclone tracks

As most of these analyses are applied to a single variable time series, results from analyses of tropical and mid- latitude cyclone tracks (position vectors) are evaluated in the following (Fraedrich and Leslie, 1989):-

mid-latitude tracks Most interesting results were obtained for the eastern and western North Pacific storm tracks (12 hourly sampling, January/February 1972-86) after further subdivision into large scale flow anomalies (defined by the Pacific/North America pattern index; positive for stronger Aleutian low and Canadian ridge, and vice versa). Two subsystems with scales larger and smaller than about 700km can be distinguished in the eastern basin analysing all cyclone tracks; negative (positive) index months show a relative low dimensionality, $D(2) = 1.2 - 1.4$ (2-3), of the larger scale storm tracks and a predictability time scale of 3-5 days; the smaller scales have a noisy behaviour. This has implications for medium range predictability and its prediction.

tropical tracks Cyclone tracks in the Australian tropics (1959-80, 6 hourly sampling) reveal a dimensionality of 6-8 and a predictability time scale of 1-2 days. The tracks show some similarity with the Brownian motion process which should also be considered for the development of practical forecast tools.

Outlook

Future issues of meteorological and climatological applications of dynamical systems analysis are the question of a local or global representation of a possibly low-dimensional weather or climate

attractor; the spatial dependence of these measures, their local singularities, scenarios to chaos and the universality in the transition to turbulence; suitable measures for folding or curvature of the trajectories on the attractor and a mathematical concept for weather predictability and its prediction.

References

Eckmann, J.-P. and D. Ruelle: Ergodic theory of chaos and strange attractors. *Rev. Modern Phys.*, **57**, 617-656.

Grassberger, P. and I. Procaccia, 1984: Dimensions and entropies of strange attractors from a fluctuating dynamics approach. *Physica*, **13d**, 34-54.

Lorenz, E.N., 1963: Deterministic nonperiodic flow. *J. Atmos. Sci.*, **20**, 130-141.

Schuster, J.G., 1984: Deterministic Chaos. *Physik Verlag, Weinheim*, 220pp.

Termonia, Y. and Z. Alexandrowicz, 1983: Fractal dimension of strange attractors from radius versus size of arbitrary clusters. *Phys. Rev. Lett.*, **51**, 1265-1268.

Holzfuss, J. and G. Mayer-Kress, 1985: An approach to error- estimation in the application of dimension algorithms. *Synergetics Series*, **32**, 114-122.

Essex, C., T.Lookman and M.A.H. Nerenberg, 1987: The climate attractor over short time scales. *Nature*, **326**, 64-66.

Fraedrich, K., 1987: Estimating weather and climate predictability on attractors. *J. Atmos. Sci.*, **44**, 722-728.

Fraedrich, K. 1988: El Nino/Southern Oscillation predictability, *Mon. Wea. Rev.*, **116**, 1001-1012.

Fraedrich, K. and L. M. Leslie, 1989: Estimates of cyclone track predictability, Part I: Tropical cyclones. *Quart. J. Roy. Met. Soc.*, **??**, ??-??.

Grassberger, P., 1987: Do climate attractors exist? *Nature*, **323**, 609-612.

Henderson, H.W. and R. Wells, 1988: Obtaining attractor dimensions from meteorological time series. *Advances in Geophysics*, **30**, 205-237.

Hense, A., 1987: On the possible existence of a strange attractor for the Southern Oscillation. *Beitr. Phys. Atmos.*, **60**, 34-47.

Hense, A. 1988: Dimension analysis of experimental time series from nearest neighborhood information. *13th EGS General Assembly*, Bologna.

Kepenne, C.L. and C. Nicolis, 1988: Global properties and local structure of the weather attractor over western Europe. *13th EGS General Assembly*, Bologna.

Maasch, K.A., 1989: On the practicality of calculating attractor dimension from O-18 records.??

Mohan, T.R., J.S. Rao and R. Ramaswamy, 1989: Dimension analysis of climatic data. ??

Nicolis, C. and G. Nicolis, 1984: Is there a climatic attractor? *Nature*, **311**, 529-532.

Osborne, A.R., A.D. Kirwan, A.Provencale and L. Bergamasco, 1989: Fractal trajectories in the Kuroshio extension.

Radnoti, G., 1988: Characterizing the weather attractor. *13th EGS General Assembly*, Bologna.

Tsonis, A.A. and J.B. Elsner, 1988: The weather attractor over very short time scales. *Nature*, **333**, 545-547.

Table 3: Entropy

Generalised entropy	$K(q) = \lim_{n\to\infty} \lim_{l\to 0} \sum p(I)^q / n(q-1)$
Kolmogoroff entropy ($q \to 1$)	$K = K(1) = \lim_{n\to\infty} \lim_{l\to 0} \sum p(I) \ln p(I)/n$
Order-2 entropy ($q = 2$)	$K(2) = -\lim_{n\to\infty} \lim_{l\to 0} \sum p(I)^2/n \geq K$
I:	time sequence of n cells or boxes $i_0, i_1, \ldots i_n$ of size l. $\sum$: sum over I sequences of cells.
$p(I)$:	joint probability that a trajectory $X(t)$ is in box i_0 at t,..., box i_{m-1} at $t + (n-1)T$, with sampling time T.
	$K = \sum l(k)$ of all Liapunov or characteristic exponents $l(k) > 0$.

Table 4: Algorithms

box counting	application of definitions (Tables 1 and 2)
pair counting	(i) fixed radius (Grassberger and Procaccia 1983)
	$p(m,r) = 1/(N-1)$ [No. of pairs $X(t_i), X(t_j)$ with $\|X(t_i) - X(t_j)\| < r$]
	$C(q,m,r) = < p(m,r)^{q-1} >^{1/(q-1)}$ where $<>$ signifies average
	i.e. $1/N \sum$ over all points $j = 1, .., N$ in the embedding phase space
	scaling(:=) of dimension: $C(q,r) := r^{D(q)}$ for suitable m
	and entropy: $C(q,m) := \exp\{-(q-1)mK(q)\}$ for suitable range of r
	(ii) fixed mass (Termonia and Alexandrowicz 1983)

Table 5: Analyses of weather/climate time series

Authors	Dimension/Entropy	Time series
Nicolis & Nicolis 1984	3-4	0-18
Fraedrich 1986, 1987	6-7/20days; 4-5	sfc-p(day); 0-18
Grassberger 1987	no sat.	0 - 18
Hense 1987, 1988	2.5-6	ENSO: RR,SST(mon)
Essex, Lookman & Nerenberg 1987	6	9*500mb heights
Henderson & Wells 1988	5-6.5; 4-5.5	500mb index;gusts
Fraedrich 1988	no sat./1y	ENSO: SOI(year)
Kepenne & Nicolis 1988	7-8/ >20 days	9*500mb heights
Tsonis & Elsner 1988	6-7	w(in 11m,10s-mean)
Osborne, Kirwan, Provencale Bergamasco 1988	1-2	3*buoys(Kuroshio)
Radnoti 1988	no sat.	500mb (wave 5)
Fraedrich & Leslie 1989	6-7/1-2days	cyclone tracks
Maasch 1989	4-6	14*0-18 records
Mohan, Rao & Ramaswamy 1989	no sat.	0-18 record

Deterministic chaos model for the prediction of climatological weather cycles

A. Mary Selvam
Indian Institute of Tropical Meteorology, Pune, India

Introduction

The recently identified universal inverse power law form for the atmospheric eddy energy spectrum of the meteorological and climatological scales of temperature fluctuations indicates a close coupling between the short and long term periodicities in weather cycles (Lovejoy and Schertzer, 1986). Numerical weather prediction (NWP) models have had limited success because of the inherent nonlinearity of the governing equations which are sensitive to initial conditions and give chaotic solutions characteristic of deterministic chaos. In recent years there is growing conviction that NWP models based on conventional meteorological concepts and nonlinear partial differential equations are inherently unstable to computational approximations and round-off errors and are therefore incapable of improved performance with further increase in the resolution of the meteorological data network or computer precision and capacity (Lorenz, 1979; Weil, 1985; Mason, 1986; Lighthill, 1986; Reinhold, 1987; Shepherd, 1987; Tennekes, 1988). Accurate modelling of short and long term weather phenomena therefore require alternative conceptual models of atmospheric flows with robust computational techniques (Ottino et al., 1988). In this paper the newly emerging intensive research area of deterministic chaos is applied for atmospheric flows using the concept of 'cellular automata' computational technique. The energetics of atmospheric flows are modelled by structurally stable scale invariant governing equations which predict universal and unique spatiotemporal patterns for atmospheric flows.

Deterministic chaos in the ABL

Lorenz (1963) was the first to identify the existence of deterministic chaos in a mathematical model of atmospheric flows derived by severe truncation of the Navier-Stokes equations. Later extensive studies by other mathematical scientists revealed the existence of deterministic chaos in all mathematical models of physical systems (Fairbairn, 1986; Tavakol, 1988). The field of chaos is characterized by the strange attractor design with self-similar fractal geometrical structure. A selfsimilar object is characterized by its fractal dimension D which is equal to $dlnM/dlnR$ where M is the mass contained within a distance R in the object. The physics of deterministic chaos is not yet identified. Conclusive observational evidence for the existence of deterministic chaos in the planetary atmospheric boundary layer (ABL) was provided by Lovejoy and Schertzer (1986) who showed that the global cloud cover pattern exhibits fractal geometrical structure on scales ranging from the convective to the planetary scales. Further, the observed universal characteristic for shape and spectral slope of atmospheric eddy energy spectrum which follows an inverse power law of the form f^{-b} where f is the frequency and b the exponent ($\approx$1.8) is basically the 1/f noise spectrum generic to the field of chaos (Tang and Bak, 1988).

Conceptual model of deterministic chaos in the ABL

The turbulent shear flow in the ABL has an inherent mean upward momentum flux of frictional origin at the planetary surface. The turbulence scale upward momentum flux is progressively amplified in the vertical by buoyant energy supply from microscale fractional condensation by deliquescence even in an unsaturated environment and amplified further by the exponential decrease of atmospheric density

with height. Helical vortex roll (or large eddy) circulations form as a natural consequence of such turbulence scale buoyant energy flux in the ABL and are manifested as cloud streets and mesoscale cloud clusters (MCC) in the global cloud cover pattern (Mary Selvam, 1988a). Townsend (1956) has derived the following relation between the root mean square (r.m.s) circulation speed W of the large eddy of radius R which grows from the turbulence scale eddy of length r and r.m.s circulation speed w

$$W^2 = \frac{2r}{\pi R} w^2 \tag{1}$$

The rising large eddy carries the turbulent eddies as internal circulations which mix the environmental air into the large eddy volume. The steady state fractional volume dilution k of the large eddy by turbulent eddy fluctuations is given as

$$k = \frac{w_* r}{dW R} \tag{2}$$

where w_* is the turbulence scale buoyant acceleration and dW the corresponding acceleration of the large eddy. It may be computed and shown $k > 0.5$ for scale ratio $Z < 10$ where $Z = R/r$. Therefore identifiable large eddy growth occurs for scale ratios of 10 or more only since for smaller scale ratios the large eddy identity is erased by turbulent mixing. Large eddy growth therefore occurs in successive decadic scale range intervals giving rise to the observed coherent cloud structures which consist of a hierarchy of turbulent, convective, meso-, synoptic and planetary scale eddies, the larger eddies containing the inherent smaller eddies as internal circulations. Integrating equation 2 for large eddy growth starting from the turbulence scale length a at the planetary surface, the growth occurring at discrete length step intervals $dR = r$ we obtain

$$W = \frac{w_*}{k} ln Z \tag{3}$$

$k = 0.4$ for $Z = 10$. The model therefore predicts logarithmic spiral airflow in the ABL with the von Karman's constant k being equal to 0.4 as a natural consequence of the eddy growth mechanism by the universal period doubling route to chaos. The von Karman's constant is therefore more universal than the Feigenbaum's constants for organised chaos. The above concept of large eddy growth from microscopic domain eddy dynamical processes is analogous the computational techniques of 'cellular automata' and 'molecular dynamics' recently being applied for fluid flow simulations (Hayot, 1987; Rapaport, 1988). The strange attractor design traced by the atmospheric flow trajectories therefore consists of a nested continuum of logarithmic spiral curves, each spiral consisting of the upward and corresponding return downward flow. Further, it may be shown (Mary Selvam, 1988b) that the period doubling growth of eddies in atmospheric flows gives successive eddy lengths following the Fibonacci number sequence as a natural consequence, one complete vortex roll circulation being completed in five length step increments each on either side of the primary perturbation. The internal structure of one complete vortex roll circulation (Fig. 1) consists of balanced counter rotating circulations tracing out the quasi-periodic Penrose tiling pattern identified as the quasicrystalline structure in condensed matter physics (Janssen, 1988). The short range balance requirements of the eddy circulations with the Fibonacci winding number impose long range orientational order in the quasicrystalline structure for large eddies in atmospheric flows and is consistent with the observed long range spatiotemporal correlations of weather phenomena e.g., the El Niño Southern Oscillation (ENSO) cycle.

Dominant weather cycles (Limit cycles)

It was shown above that identifiable large eddy growth occurs for successive decadic scale range intervals. Therefore from equation 1 the following relations are derived for the length and time scales for the limit cycles in atmospheric flows.

$$\begin{aligned} a : R &= a : 10r : 10^2 r : 10^3 r : 10^4 r \\ t : T &= t : 40t : 40^2 t : 40^3 t : 40^4 t \end{aligned} \tag{4}$$

The 40-50 day oscillations in the general circulation and the ENSO phenomena may possibly arise from the diurnal surface heating since they correspond respectively to the first and second decadic scale range of eddy growth (4). Similarly the QBO (Quasi-biennial Oscillation) may arise as a result of the semi-diurnal pressure oscillation (QBO $\approx$ 0.5 day x 40^2. The 20-year periodicity in solar cycle and the associated weather patterns may be associated with the newly identified 5 minute oscillation of the sun's atmosphere (20yr $\approx$ 5 min. x 40^5. The growth of large eddies by energy pumping at smaller scales, namely, the diurnal surface heating and the semi-diurnal pressure oscillation as cited above is analogous to the generation of chaos in optical phenomena (Harrison and Biswas, 1986). Spectral analysis of long term high resolution surface pressure data will give the amplitude and phase of the limit cycles in the atmospheric flow pattern.

Climate prediction

The deterministic chaos model for atmospheric flows also predicts that vertical mass exchange occurs in the atmospheric eddy continuum fluctuations extending from the troposphere to the ionosphere and above resulting in the transport downwards of negative space charges from ionosphere and the simultaneous upward transport of positive space charges from lower troposphere. The charged aerosol current generated by the vertical mass exchange is shown to quantitatively generate the observed atmospheric electric field and the geomagnetic field and is consistent with the observation that atmospheric circulation patterns closely follow geomagnetic field lines and further, that climatic variations are preceded by corresponding geomagnetic field variations, Close monitoring of the global geomagnetic field variations may enable prediction of future climatic trends (Mary Selvam, 1987).

Stratospheric Ozone and Climate

The recently identified stratospheric ozone depletion (Heath, 1988) and a tropospheric ozone increase (Penkett, 1988) may be a manifestation of increased vertical mass exchange due to global warming related atmospheric eddy continuum energy enhancement.

Conclusion

The deterministic chaos model for atmospheric flows enables to predict the observed meteorological and climatological periodicities as simple multiples of solar insolation related fundamental periodicities in the ABL.

References

Fairbairn, W.,1986: *Phys.Bull.37, 300.*

Harrison, R.G. and D.J. Biswas, 1986: *Nature 321, 394.*

Heath, D.F., 1988: *Nature 332, 219.*

Hayot, F., 1987: *Physica 26D, 210.*

Janssen, T., 1988: *Phys. Rep. 168(2).*

Lighthill, J., 1986: *Proc. R. Soc. A407, 35.*

Lorenz, E.N., 1963: *J. Atmos. Sci.30, 130.*

Lorenz, E.N., 1979: *J. Atmos. Sci.36, 1367.*

Lovejoy, S., and D. Schertzer, 1986: *Bull. Amer. Meteorol. Soc. 67, 21.*

Mason, B.J., 1986: *Proc. R. Soc. A407, 51.*

Mary Selvam, A., 1987: *Proc. Int. Geosci. and Remote Sensing Symp. (IGARSS 1987).*

Mary Selvam, A., 1988a: *Proc. 8th NWP Conf. Amer. Meteorol. Soc. USA, Feb. 1988.*

Mary Selvam, A., 1988b: *Proc. III Inter-American Cong. Meteorol. and III Nat. Cong., Mexico City.*

Ottino, J.M., C.W. Leong, H. Rising, and P.D. Swanson, 1988: *Nature, 333, 419.*

Penkett, S.A., 1988: *Nature, 332, 204.*

Rapaport, D.C., 1988: *Phys. Rev. Lett. 60(24), 2480.*

Reinhold, B., 1987: *Science 235, 437.*

Shepherd, T.G., 1987: *J. Atmos. Sci. 44(8), 1166.*

Tang, C., and P. Bak, 1988: *Phys. Rev. Lett. 60(23), 2347.*

Tavakol, R.K., 1987: *Sci. Prog. Oxf. 71, 71.*

Tennekes, H., 1988: it Bull. Amer. Meteorol. Soc. 69(4), 368.

Townsend, A.A., 1956: *The structure of turbulent shear flow. Cambridge Univ. Press, Cambridge, 115.*

Weil, J.C., 1985: *J. Climat. Appl. Meteorol. 24(11), 1111.*

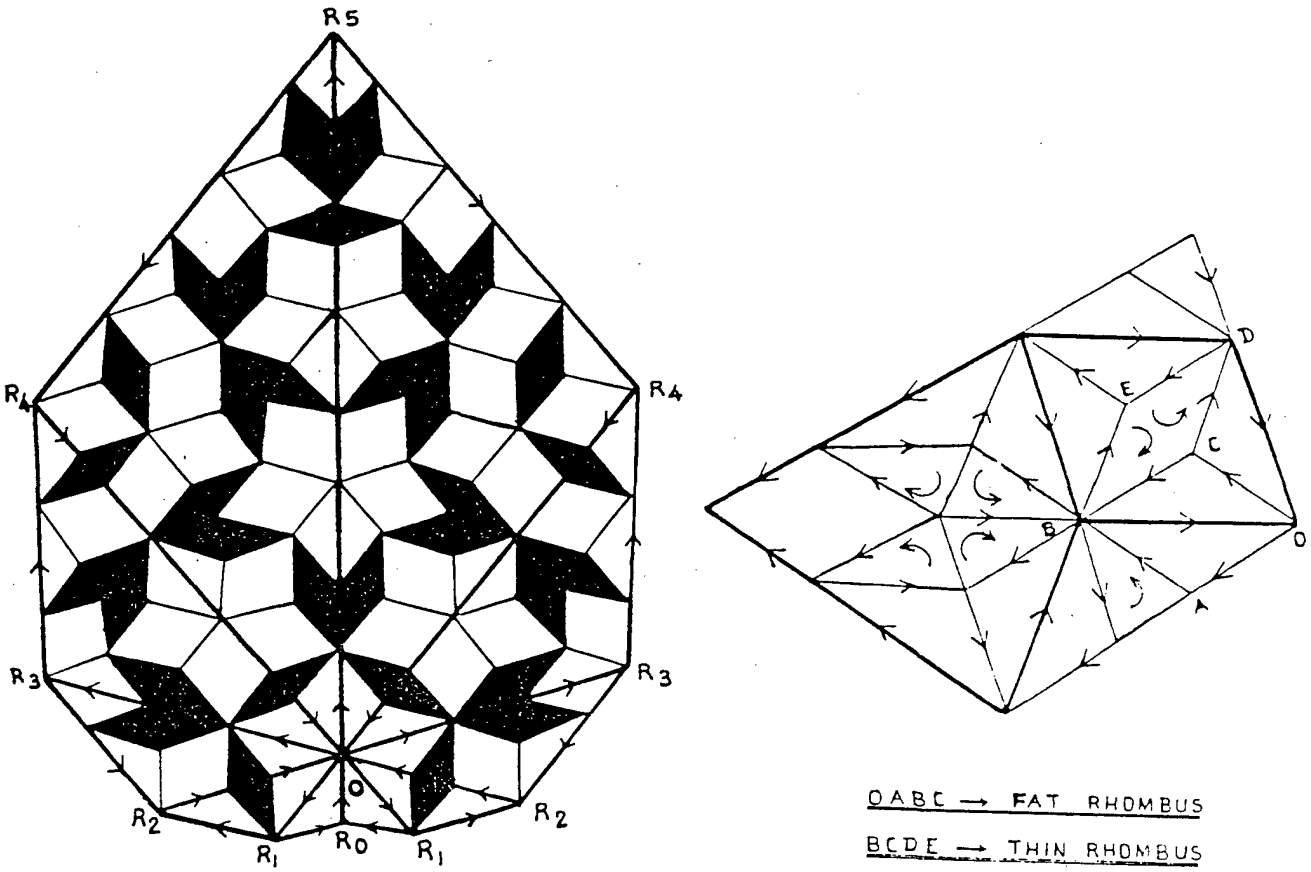

Figure 1: The internal structure of the large eddy circulation pattern in the ABL. A primary turbulence scale perturbation R_oO generates compensating return circulations on either side along isosceles triangles of successively increasing base lengths (large eddy radii) OR_1, OR_2, OR_3, OR_4, OR_5 such that the winding number $OR_2/OR_1 = OR_3/OR_2 = \ldots = \sqrt{5} + 1/2$ = golden mean. The internal structure of one complete vortex roll (large eddy) circulation with the Fibonacci (golden mean) winding number consists of the quasiperiodic Penrose tiling pattern formed by a mosaic of fat and thin rhombi as shown separately.

On a diffusion climate model

Stephen Goulter
New Zealand Meteorological Service

Introduction

Mixing length ideas were introduced into the theory of the general circulation of the earth by Defant(1926) who treated cyclones and anticyclones as turbulence elements. Then, it appeared to agree with calculations based on such a hypothesis, for estimates of the mixing length and the direction of transport were reasonable for heat content.

Turbulence ideas were invoked by Rossby(1941) in explaining the westerlies of middle latitudes, for an indirect Ferrel cell would otherwise give easterly winds at high elevations in middle latitudes (Figure 1), by momentum considerations.

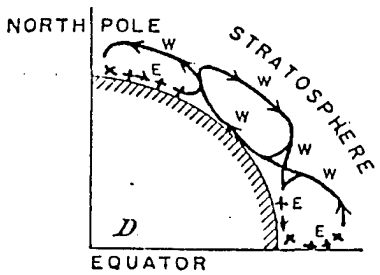

Figure 1: Schematic representation of the meridional circulation. After Rossby, 1941.

However difficulties soon appeared. The advent of extensive upper air soundings during the second world war enabled calculations of eddy fluxes and hence determinations of the budgets of heat, momentum, moisture etc for the earth's atmosphere. These showed that the direction of transport indicated by classical turbulence ideas was sometimes opposite to observed, with for example, energy transport towards lower latitudes, rather than higher, colder latitudes. The associated concept of negative viscosity has been extensively discussed in the interesting work by Starr(1968).

Rossby(1947) assumed a mixing hypothesis for a source of vorticity at the North Pole, and a sink at the South Pole, and by integrating the steady state vorticity equation, derived a westerly wind maximum in middle latitudes, (Figure 2) as well as explaining the distribution of zonal momenta on the sun.

Jet streams posed a problem also. The newly acquired knowledge of the upper winds showed that frequently a double jet occurred, one in sub-polar latitudes, and one in sub-tropical latitudes. This double jet structure caused Palmen(1951) to revise the Rossby model of the general circulation, Figure 3.

Rossby concluded that different laws may hold north and south of a jet stream and that something more complicated than classical turbulence theory was needed. However, it is clear that there may well be something in Rossby's approach since it is capable of predicting a westerly maximum in high middle latitudes.

Riehl(1973), summarising approaches based on classical turbulence theory, says: 'attempts to describe the main features of the average general circulation maintained through simple analytic solutions have not been entirely successful on the polar side of the statistical wind maximum. For the

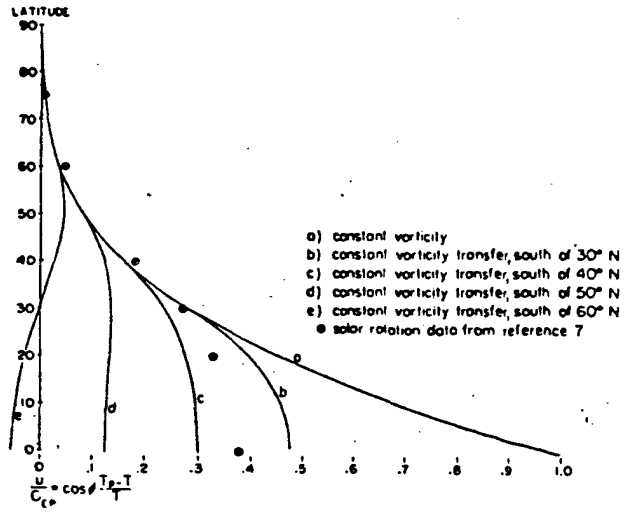

Figure 2: Zonal flow, as fraction of equatorial velocity, and function of vorticity parameter ϕ_c and latitude. Distribution of zonal motion in a thin atmospheric shell, measured relative to the underlying planetary surface, and expressed in fractions of the equatorial linear velocity of the planet. All profiles computed on the assumption that the polar angular velocity of the shell is equal to the angular velocity of the planet itself. After Rossby, 1947.

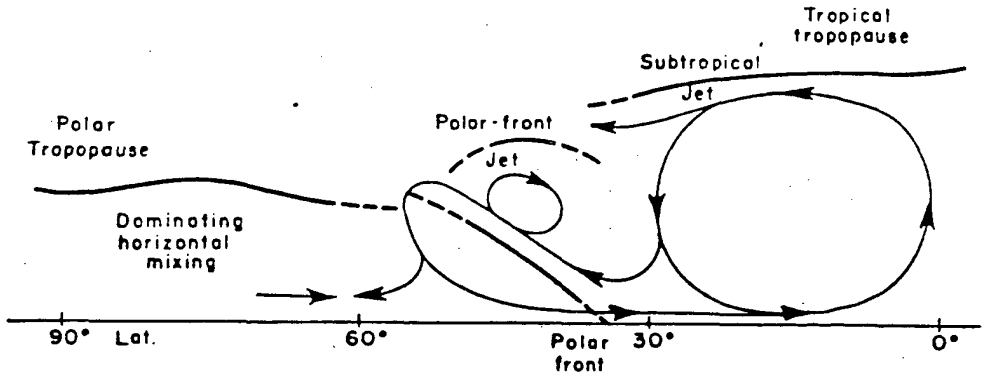

Figure 3: Schematic representation of the meridional circulation and associated jet stream cores in winter. After Palmen(1951). From Chapter 1, by H. Riehl, in World Survey of Climatology, editor H. Flohn

interaction between the hemispheres a more realistic first approximation may have been found. Very few efforts have been made to solve basic aspects of the general circulation with this type of approach; and these efforts have died out with the advent of high speed computers. Nevertheless the simple approach remains tempting and may be revived. Hypotheses alternate to Rossby may be advanced and tested.'

Here an alternate approach is outlined where one principle, that of momentum, is used to suggest a velocity profile, and then the consequences for vorticity transport, mixing and stability are examined. Some surprising and direct consequences are demonstrated. One is motivated here partly by the attractiveness of a simple approach, partly by Rossby's partial success, and partly by his, and Riehl's comment that different physical laws may hold predominant influences in differing regions of the earth. Exploration of the properties of simple analytical models is a valuable way of generating insight.

An objective is to find simple grounds for explaining large scale atmospheric structure, with a minimal set of assumptions. If some similarities are obtained, further simplification may be sought. If however no such similarities appear, fundamental revision is indicated. A possible criticism of the Rossby approach is the assumption of a critical latitude ϕ_c polewards of which vorticity mixing occurs. The jet structure only appears for suitable choice of ϕ_c and a question is: are other approaches possible, where such a parameter need not be assumed?

A Diffusion Hypothesis

Suppose

$$\frac{\partial u}{\partial t} = D\frac{\partial^2 u}{\partial y^2} \tag{1}$$

where $D > 0$. If D is constant we can therefore fit a simple diffusion model, using an estimated momentum fluctuation, and an expression for the spatial variation inferred for the zonal speed u.

For diffusion, one seeks some expression giving a momentum gradient. For emphasis placed on geometric factors which govern atmospheric flow on the large scale, we choose to work with the horizontal, zonal, frictionless equation of motion. Fixing the right hand side, we have

$$\frac{du}{dt} - fv = -\frac{1}{\rho}\frac{\partial p}{\partial x} = q$$

The right hand side is the pressure gradient force in the x-direction, which by integrating around the latitude circle can be supposed zero, since pressure is a continuous quantity. Since $v = \frac{dy}{dt}$, one gets integrating with respect to time,

$$u - fy = qt + c$$

Alternatively for a limited range of longitudes, by time averaging over sufficiently long time scales, one could reasonably suppose the right hand side constant, of small magnitude, summing the fluctuating pressure gradients of opposite sign. Each approach will give rise to different mean quantities u, etc which we shall continue to denote by u, etc.

Given $u = u_0 + fy$ then by choice of u_0, easterlies in low latitudes can be accommodated, and also a finite westerly momentum at the poles, in contra-distinction to the requirements of angular momentum conservation, which requires infinite velocities there. Since infinite velocities are not observed, the approximation $u = fy$ may not be unreasonable at some higher latitudes. u is the non-linear product of the form $y \sin \alpha y$. Near the equator the dependence is approximately quadratic, but close to the poles the variation is near linear. This may be regarded as a vorticity *potential* analogous to a stream function as a potential for velocity in classical 2D flow.

We use a β-plane approximation. $\frac{\partial u}{\partial y} = f + y\frac{\partial f}{\partial y} = f + \beta y$. The flow is inertially unstable, for $f - \frac{\partial u}{\partial y} = -\beta y < 0$. Also $\frac{\partial^2 u}{\partial y^2} = \frac{\partial f}{\partial y} + \beta + \frac{\partial \beta}{\partial y}y$, where $\beta = \partial f/\partial y = 2\Omega \cos\theta/R$, and $\partial\beta/\partial y =$

$-2\Omega \sin\theta/R^2 = -f/R^2$. Therefore

$$\frac{\partial^2 u}{\partial y^2} = 2\beta - \frac{fy}{R^2}$$

Since $\theta = \frac{y}{R}$ we therefore have $\frac{\partial^2 u}{\partial y^2} = 2\frac{2\Omega\cos\theta}{R} - \frac{2\Omega\sin\theta}{R^2}y = \frac{2\Omega}{R}(2\cos\theta - \theta\sin\theta)$.

The relative (anticyclonic) vorticity gradient ceases increasing, and begins to decrease, when $\frac{\partial^2 u}{\partial y^2} = 0$. Then

$$\Psi(\theta) = (2\cos\theta - \theta\sin\theta) = 0$$

Thus one derives the transcendental equation for the roots of Ψ

$$\theta\tan\theta = 2$$

which may be solved numerically, giving roots at $\theta_0 = \pm 61.8°$. For $|\theta| < \theta_0$, one has an increasing growth rate of $\frac{\partial u}{\partial y}$ with increasing southern/northern latitude, i.e. increasing anticyclonic vorticity with latitude in either hemisphere. At θ_0 there is a change in sign of rate of vorticity increase, and closer to the poles, the rate of growth of the anticyclonic vorticity becomes negative. The zonal speed $u = fy$ continues to increase with increasing latitude. Poleward of θ_0 there is a cyclonic tendency in the growth of vorticity, as the growth rate of anticyclonic vorticity becomes negative.

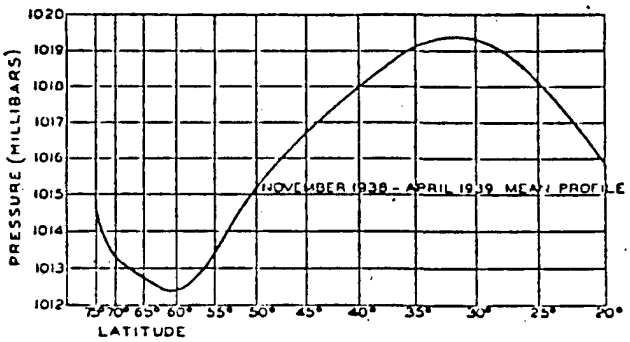

Figure 4: Latitudinal Pressure Profile for Northern Hemisphere. After Rossby , 1941.

Figure 4 shows the latitudinal profile for the northern hemisphere as published by Rossby (1941). A minimum in pressure appears just north of 60° N. The model predicts the position of the sub-polar trough, as found observationally. Inspection of Rossby's diagram on his three cell meridional model shows placement of the trough and sub-polar front near this position.

The vorticity across θ_0 is cyclonic with increasing latitude in both hemispheres by the model. Because of the sign change, the development of easterlies polewards is indicated, considering the changes in sign of $\frac{\partial u}{\partial t}$ from the diffusion equation. This is similar to the arguments of Kuo(1951) concerning strengthening easterlies/westerlies with damping barotropic eddies.

Figure 5 shows the pattern of winds and vorticity implied. The model predicts:

$$\frac{\partial u}{\partial t} > 0 \text{ for } |\theta| < \theta_0$$

$$\frac{\partial u}{\partial t} < 0 \text{ for } |\theta| > \theta_0$$

By Rayleigh's criterion(as modified by Kuo for motion on a rotating sphere), a change in sign of the gradient of absolute vorticity is associated with instability of small harmonic perturbations, and disturbances of more general form (Taylor, 1915). Thus one expects disturbances to amplify, and a preferred position for this is then θ_1, say.

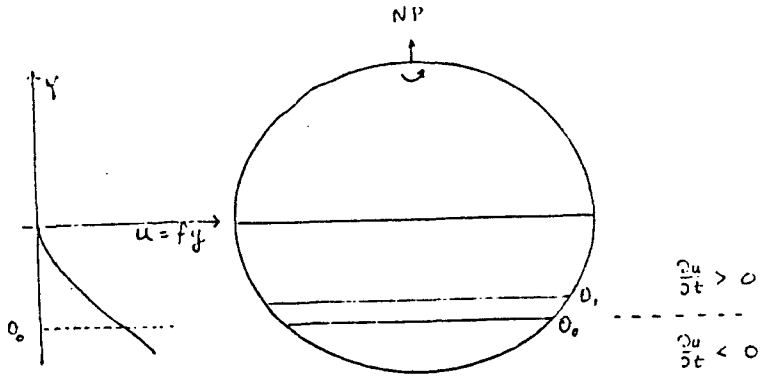

Figure 5: Profile due to Barotropic Diffusion Model.

The absolute vorticity is given by $f - \frac{\partial u}{\partial y} = -y\beta$ and the gradient of this is $\beta - \frac{\partial^2 u}{\partial y^2} = \beta - (2\beta - fy/R^2) = 0$. For the location of a sign change this requires solution of

$$\theta \tan\theta = 1$$

which gives roots at $\theta_1 = \pm 49.3°$ i.e. equatorward of the position of development of cyclonic tendency by some 12 latitude degrees. This is a latitude of barotropic instability(Kuo, 1949). A region enclosing this axis may be expected to have unstable i.e. amplifying disturbances.

Trenberth (1981) has analysed the eddy statistics of the southern hemisphere height fields in an examination of storm track locations and concludes that the main storm track is at 50° S (where a maxima in variance of the geopotential height field is, on short time scales.)

He presents a schematic meridional profile for the dominant dynamical processes operating at most longitudes. The separation and locations of the circumpolar trough and the main storm track closely matches the values θ_0, θ_1. See Figure 6.

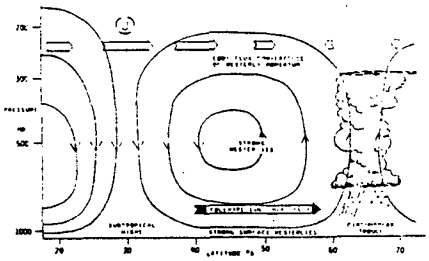

Figure 6: Schematic depiction of a meridional cross section of the dominant dynamical processes operating at most longitudes and for the zonal mean in the Southern Hemisphere. The subtropical jet (J) and the subtropical highs are located at 30°S. Transient baroclinic eddies in the storm track at 50°S produce a strong poleward eddy heat flux (solid arrow) in the lower troposphere, and a convergence of westerly momentum in the middle and upper troposphere (shown by the differences in the length of each open arrow which represent the momentum transport by the eddies) and drive a strong Ferrel cell, with maximum mean vertical motion in the circumpolar trough at 60–65°S. After Trenberth, 1981.

It is therefore suggested that the location of the storm track may be determined barotropically, with amplifying disturbances in the high troposphere weakening the zonal flow at 50 S.

Lin(1945) showed the transverse acceleration on a vortex filament is

$$\bar{a}_y = \frac{1}{\Gamma}\int\int v^2 \frac{dZ}{dy} dx dy = \frac{1}{\Gamma}\int\int v^2 \left(\beta - \frac{\partial^2 u}{\partial y^2}\right) dx dy$$

where $\Gamma = \int\int \epsilon dx dy$ is the circulation around the vortex element. Thus at the stationary value of the absolute vorticity, the transverse acceleration is zero, while because of the change of sign in dZ/dy the directions of accelerations reverse. For regions in which the vorticity gradient is of one sign, small perturbations north or south of vortices are stable, whereas because of the sign change in the gradient at θ_1 instability may arise due to no returning acceleration. Kuo (1949) finds that longer wavelength, slower moving disturbances are amplifying, while the shorter wavelength, faster moving disturbances damp.

If we equate the momentum transports to those due to vorticity transport, (Taylor, 1915):

$$\frac{\partial u}{\partial t} = -\frac{\partial}{\partial y}\left(ll'\left(\frac{\partial u}{\partial y}\right)^2\right) = -2ll'\frac{\partial u}{\partial y}\frac{\partial^2 u}{\partial y^2} = D\frac{\partial^2 u}{\partial y^2},$$

where $D = -2ll'\frac{\partial u}{\partial y} > 0$ for diffusion. The positivity of D, and the sign of $\frac{\partial u}{\partial y}$, implies that $ll' < 0$ in the northern hemisphere, and $ll' > 0$ in the southern hemisphere. This is a very interesting result, for

$$u'v' = ll'\left(\frac{\partial u}{\partial y}\right)^2 \begin{cases} < 0 \text{ in northern hemisphere} \\ > 0 \text{ in southern hemisphere} \end{cases}$$

i.e. equatorward momentum transport. The model predicts exactly the reverse structure to the observed poleward transport of momentum, which must occur to balance frictional dissipation in middle latitudes, and which occurs by quasi-geostrophic eddy flux (Holton, 1972).

The solution to the particular problem involves a function giving the velocity as initial state, and the equilibrium solution must have $\frac{\partial u}{\partial t} = 0$. Hence $\frac{\partial^2 u}{\partial y^2} = 0$ and the equilibrium profile is linear in y. Because of the sphericity of the earth, a non-beta plane treatment must take this into account.

For diffusion, the equation 1 may have substituted the wave solution form $e^{i(ky+\omega t)}$ which yields on substitution the relation $\omega = ik^2 D$. Hence

$$u = Re\{e^{i(ky+ik^2Dt)}\} = e^{-k^2Dt}\cos ky$$

is a solution, and the waves are dissipative and dispersive, for $\omega/k = ikD$. The summation over all frequencies k at a specified time gives the characteristic normal density function as the required solution with time dependent spread. For the FT of e^{-k^2Dt},

$$\int_{-\infty}^{\infty} u dk = \int_{-\infty}^{\infty} e^{-k^2Dt}e^{iky}dk = \sqrt{\frac{\pi}{Dt}}e^{-\frac{y^2}{4Dt}} \text{ and } \sigma^2 = 2Dt.$$

If the process is generalised, so that D can be negative, (negative viscosity) then u is unstable. Thus the up-gradient momentum transports (poleward) could be associated with unstable amplifying, and dispersive(concentrative) waves. Hassanein(1949) showed time dependent solutions of the Rossby wave equation have sloping ridge-trough lines, the tilt being positive(acute)/negative(obtuse) according as they are north/south of the zonal current, if they are amplifying. Damped waves give an increase of the zonal flow at the expense of eddies north and south, with reversed tilts to amplifying.

Therefore, *if barotropic type(Rossby) waves behave as diffusion processes in the N-S direction*, we may argue that poleward of the instability axis, the amplifying waves would give upgradient momentum transport. Equatorward of the jet stream axis, the amplifying waves would give downgradient transport of momentum at the expense of the mean flow. The process could correspond to a sharpening of velocity gradients, to the north and south of the instability, at the expense of the local mean flow. The exponential growth would soon render the formulation invalid, because other processes of eddy viscosity and flow deformation would take over.

One suspects therefore that these concentrative type amplifying barotropic waves may be related to the formation and location of the large scale jet streams, probably by interaction with the larger scale baroclinic processes. These ideas are consistent with those of Kuo(1951) concerning the role of amplifying/damping barotropic disturbances in respectively weakening/strengthening the zonal flow.

Earlier, Kuo had derived the condition for barotropic instability(1949) and in illustrating his theory, had considered velocity profiles, choosing the sine curve for the horizontal velocity profile. The

choice was arbitrary in that it was not deduced: the location of the axis of instability was determined by the choice of parameters.

This approach however derives a monotonic profile, also possessing the point inflectional character, related to the sine curve variation of Kuo, and based on a physical argument of horizontal and quasi-geostrophic flow. It uniquely locates a necessary axis for instability, which coincides closely with the location of the sub-polar trough as determined by Trenberth. Further, this suggests that the arguments given in Kuo's paper relating to a similar profile could apply here. Since these ideas related to momentum transport and the building up and weakening of zonal flow the relation to jet stream theory is obvious. Kuo used these arguments to outline a theory of the index cycle.

The e-folding time depends on $\frac{1}{k^2 D} = \frac{L^2}{4\pi^2 D}$. These vary as the square of the wavelength, so the longer the wavelength, the slower the rate. Also, if momentum and vorticity transports are equivalent, the e-folding rate is given by $\frac{1}{8\pi^2} \frac{L^2}{l^2 \partial u/\partial y}$, so the smaller $\partial u/\partial y$ or the smaller the mixing length l, again the slower the time development. A particularly interesting feature of this development in the model is that both particle and wave properties are embodied in the expression for D.

Shukla (1983) finds the deterministic limits of prediction of the long waves are of the order 4-6 weeks and for the shorter scale features in middle latitudes, of up to 2 weeks. The above model gives qualitative answers in this sense, comparing space scales with development times.

While the above approach is not capable of explaining jet stream structure in its present form, the diffusion formulation allows explanation of two major features of atmospheric structure: the sub-polar trough and a necessary latitude for instability. The presence of conditions for instability, allows both stable/unstable diffusive/concentrative waves, in a unified treatment. By contrast, Rossby's mixing approach only allows diffusion i.e. smoothing, requiring choice of a parameter to fit a jet stream structure. Similarly, the arbitrariness of choice of functional form and of location of an inflection point in Kuo's work on barotropic instability is removed.

If time dependent diffusion processes govern barotropic eddies, sloping structure can be expected, which gives freedom for the transport of quantities to satisfy the requirements of the balance of the general circulation.

Summarising, Lorenz(1967) says: 'It would therefore greatly facilitate the theoretical study of the general circulation if the statistical properties of the large scale eddies could in some manner be represented in terms of the zonally averaged motion upon which they are superposed.' 'The procedure which most naturally suggests itself consists of assuming that the horizontal eddy transports of angular momentum and sensible heat are proportional to the gradients of zonally averaged angular velocity and temperature, the factors of proportionality being suitable chosen Austausch coefficients.' However he notes 'the introduction of these large scale coefficients would give the wrong answer *in about half the atmosphere*' [1] and later gives an argument why such a procedure may not be expected to work, yet concludes that the adoption of similar approaches does lead to a number of correct conclusions.

It is suggested, by *symmetry* considerations, that the modification to classical turbulence theory required to 'give the right answer' in the other half of the atmosphere comes through allowance of the diffusion coefficient to be time dependent, of opposite sign according to whether the process(barotropic or baroclinic) is amplifying/damping(possibly involving also the relative velocity shear, by the vorticity equivalence argument). It is suggested that the diffusion equation setting allows a generalised description of the meridional transport properties of time dependent barotropic(or baroclinic) processes, as well as suggesting a definite axis of instability. These barotropic controls may determine the preferred location of the jetstreams, where large lateral gradients of velocity of opposite sign may be located.

The work of Kuo and Rossby has laid the basis for this approach, Rossby through the key physical insights concerning the possible role of diffusive processes, and Kuo through mathematical insight into the barotropic process. It is suggested combination of these ideas of diffusion and barotropy may be

[1] my emphasis

fruitful in developing insight into general circulation theory, even though the simple theory presented here is obviously quite preliminary in form.

The development and elaboration of further, alternate simple models is a subject of ongoing research.

References

Defant, A., 1921: Die zirkulation der atmosphare in den gemassigten breiten der erde. *Geograf. Ann.*, 3: 209–266.

Hassanein, S.A.M., 1949: A wave pattern changing with time as a solution of the vorticity equation for non-divergent motion. *Tellus*, **1**: 58-60.

Holton, J., 1972: *Introduction to Dynamic Meteorology.*Academic Press, New York and London, pp. 319.

Kuo, Hsiao-Lan, 1949: Dynamic instability of two dimensional non-divergent flow. *J. Meteor.*, **6**, 2: 105-122.

Kuo, Hsiao-Lan, 1951: Dynamical Aspects of the general circulation and the stability of zonal flow. *Tellus*. **3**. 268-284.

Lin, C.C., 1945: On the stability of two dimensional parallel flows. Parts I,II,III. *Quart. Appl. Math.*, **3**. 117-142; 218-234; 277-301.

Lorenz, E.N., 1967: The nature and theory of the general circulation of the atmosphere. WMO. pp 161.

Riehl, H., 1969: Mechanisms of the general circulation of the troposphere. Chapter 1, General Climatology. World Survey of Climatology, vol 2, ed. H. Flohn. Elsevier Publishing Company pp 266.

Rossby, C.G., 1941: The scientific basis of modern meteorology. *U.S. Department of Agriculture Yearbook*. 599–655.

Rossby, C.G., 1947: On the distribution of angular velocity in gaseous envelopes under the influence of large scale horizontal mixing processes. *Bulletin of the American Meteorological Society*. **28**: 53–68.

Starr, V.P., 1968: The Physics of Negative Viscosity Phenomena. McGraw Hill Inc. pp 236.

Shukla, J., 1983: On Physical Basis and Feasibility of Monthly and Seasonal Prediction with a large GCM. In *Proceedings of the WMO-CAS/JSC Expert Study Meeting on Long Range Forecasting*, Princeton, 1-4 December, 1982.

Taylor, G.I., 1915: Eddy motion in the atmosphere. *Phil. Trans. Roy. Soc.*, **A**, vol CCXV : 1-26.

Taylor, G.I., 1932: The transport of vorticity and heat through fluids in turbulent motion. *Proc. Roy. Soc. A*, **135**: 685–705.

Trenberth, K.E., 1981: Observed Southern Hemisphere eddy statistics at 500 mb: Frequency and spatial Dependence. *J. Atmos. Sci.*, **38**: 2585–2605.

Prediction of monthly mean temperature in Japan

T.Ueno, T.Aoki, K.Kurihara, N.Watanabe, K.Koizumi, Y.Miura
Long-range Forecast Division, Japan Meteorological Agency

Introduction

Some statistical models using multiple regression equations have been used for some kinds of weather forecasts beyond one month. New statistical models are being developed for experimental forecasts of monthly mean temperature in Japan.

Explanatory variables (predictors) used in the models are 500 hPa geopotential height values in the Northern Hemisphere (for the Z500 model) and global sea surface temperature (for the SST model) and both of them (for the mixed model).

AIC (Akaike Information Criterion) is used for selecting the useful predictors and determining the model for our prediction.

First, real monthly mean temperature data were used as objective variables (predictands). Second, we used the coefficients of principal component analysis (PCA) of the data as predictands.

Some verifications of the models were made changing the period in which lag correlations were calculated. Procedures of calculation in the models and the results are shown as follows.

Procedures

Each model is prepared under the following steps and AIC is used for selecting predictors or regression equations to be used at each step.

Calculation of lag correlations

Lag correlations are calculated between a predictand and all of predictors. Statistical significance is examined of each of the correlation coefficients. AIC is used for the check of significance. The correlation coefficients with no statistical significance are replaced by zero.

Selection of high correlation areas

A grid point with the maximum value of the correlation coefficients (the first Key-grid) is picked up. If two or more neighbouring grid points of Key-grid have non-zero values of the correlation coefficients, these points are defined as 'a high correlation area'. Second Key-grid is picked up out of the rest of grids. Same procedures are repeated. Thus, some high correlation areas are selected.

Check of independence of each grid point within a high correlation area

Correlations are calculated between a Key-grid and all other grids within a same high correlation area. The grids are excluded when the correlations are not significant. AIC is used again for the check of the statistical significance.

Average value in each of high correlation areas

A weighted average of grid values in each of high correlation areas is calculated by utilizing AIC as the weights. This AIC is the same one as used for the check of the significance in section 2.1.

Prediction by multiple regression equations

High correlation areas above-mentioned are candidates for predictors. Number of the candidates is limited to 15 in this case. Multiple regression equations are obtained in all possible combinations of the candidates.

Best five equations with small AIC's out of all equations are chosen. The AIC-weighted average of the results of predictions by selected equations is a final prediction.

Experiments

Two experiments of monthly mean temperature forecast for coming three months were made for the period 1981-1987. One of them is a experiment by a model in which the predictands are raw temperature data and the other is a PCA model experiment in which the coefficients of the principal component analysis are used as the predictands. The models in these experiments used the independent data set 1951-1980.

Performance of the models was investigated using the skill forecast=100, random forecast=0, false forecast=-100).

We used three models in the first experiment (non-PCA model experiment). These are Z500 model (monthly mean 10x10 grid point values of 500hPa geopotential height in the Northern Hemisphere are used as the predictors), SST model (monthly mean 4x4 grid point values of the global sea surface temperature as the predictors) and the Mixed model (both of 500hPa gph and SST are used as the predictors). The second experiment (PCA model experiment) was made only using 500hPa gph.

Each experiment was made for three different kinds of periods in which the lag correlations were calculated, i.e., 3-month, 6-month and 11-month periods.

Results

Table 1 shows the skill scores of the experiments. The leftside column (Z500, SST, Mix, PCA) indicates the kinds of the models. Z500, SST and Mixed models are non-PCA models. Numerals of 11, 6 and 3 in the second line mean the period in which the lag correlations were calculated, that is, the period of the predictors (predictor period). "11" means that data of predictors in last 11 months were used for the prediction. "Persist" means the persistency forecast. 1-month, 2-month and 3-month in the first line mean the coming first month, second month and third month, respectively (lead time).

The followings can be said from this table.

1. The persistency forecast has better skill score than the model forecast for the coming first month, but its skill score become less for the second and third month than the model forecast's one.

2. Z500 model forecast has better skill score than SST model and Mixed model. The skill score for the first month is the best when the predictor period is the last 3-month.

3. For the second and third month, Z500 model has better skill scores in the longer predictor periods.

4. PCA model has better skill scores than other models on the whole, especially in the case that the predictor period is 6-month.

Figs. 1-4 show the skill scores of PCA model in each forecast month. L=1, 2, 3 mean the coming first month, second month and third month, respectively. "M" means 'the predictor periods'. The following can be said from these figures.

1. Persistency forecast has the best skill scores in the cold season for L=1 and L=2, but its skill score becomes less for L=3.

2. The skill scores of PCA model for L=2 and L=3 are not less than that for L=1. The skill scores of PCA model for L=3 and M=6 are the best in the warm season (Fig.4).

Conclusion

The persistency forecast has better skill scores for the first month except for spring. A statistical model is important for the second and third month because it has better skills than persistency. PCA model has the best performance among statistical models on the whole.

A statistical model whose predictors are 500hPa and/or SST is not so satisfactory for the forecast of monthly mean temperatures. We may have the better skill scores in combination with the model forecasts and persistency forecast for each lead time and each season. In addition to that, it is more important to study the factors which affect the global climate in order to improve a statistical model.

References

Akaike, H., 1973: Information Theory and an Extension of the Maximum Likelihood Principle, *2nd International Symposium on Information Theory (Petrov,B.N. and Csaki,F. eds.) , Akademiai Kiado, Budapest,267-281*

Table 1: Skill Scores of each model. L: lead month, M: Lag calculation period (month), Per: Persistency forecast

L	1-mth				2-mth				3-mth			
M	11	6	3	Per	11	6	3	Per	11	6	3	Per
Z500	3.9	2.8	11.4		9.2	7.6	7.8		6.2	4.3	2.0	
SST	3.4	0.4	4.0	16.9	2.8	1.4	0.4	6.1	3.4	4.6	3.3	2.2
MIX	3.6	1.5	5.1		4.0	-1.0	9.1		3.2	6.0	5.3	
PCA	8.0	13.6	9.3		7.5	10.4	3.8		7.3	12.0	7.3	

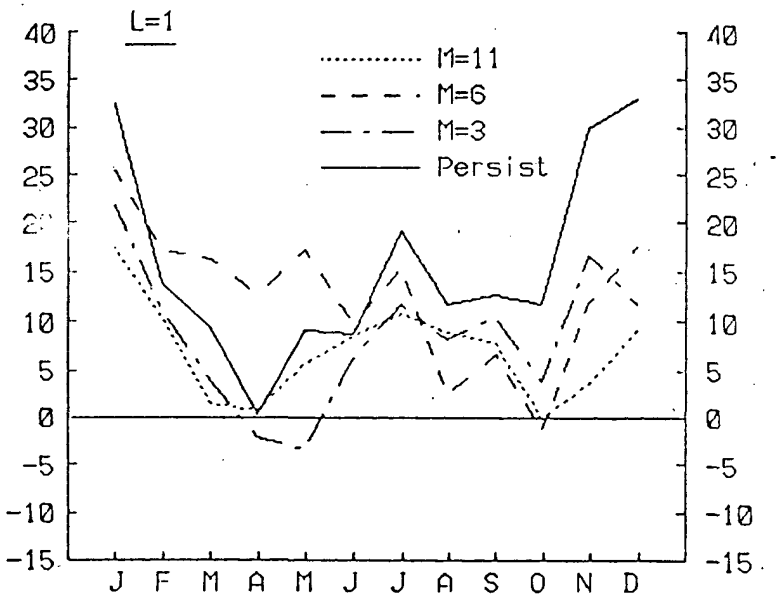

Figure 1: Seasonal change of skill scores of PCA model forecast and persistency forecast for lead month=1. M: Lag calculation period for PCA model.

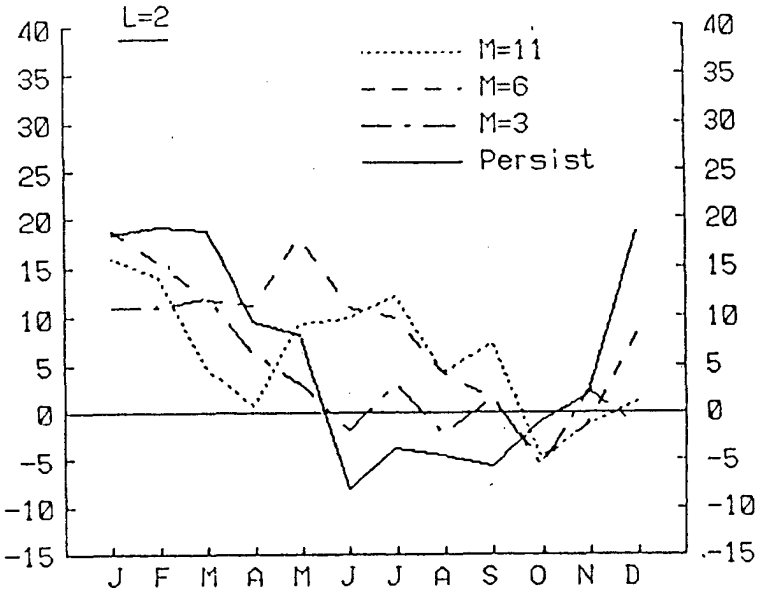

Figure 2: Same as Fig. 1 but for lead month=2.

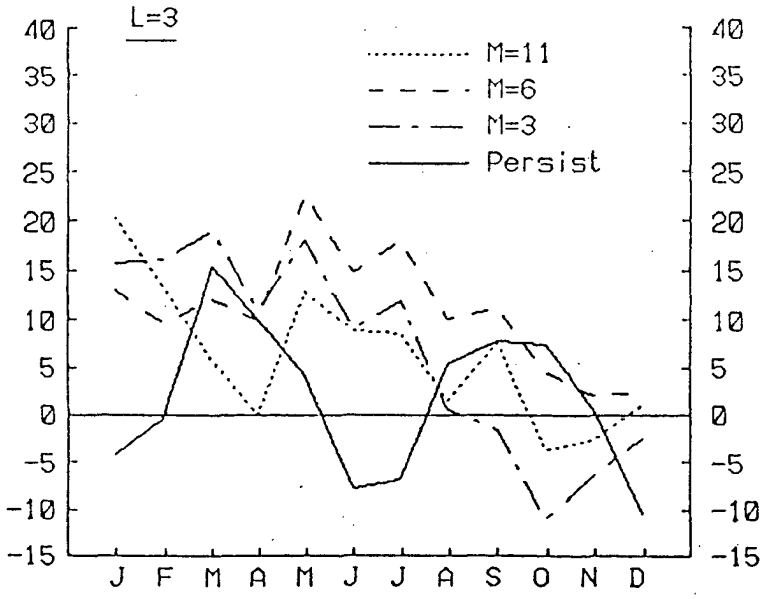

Figure 3: Same as Fig. 2 except for lead month=3.

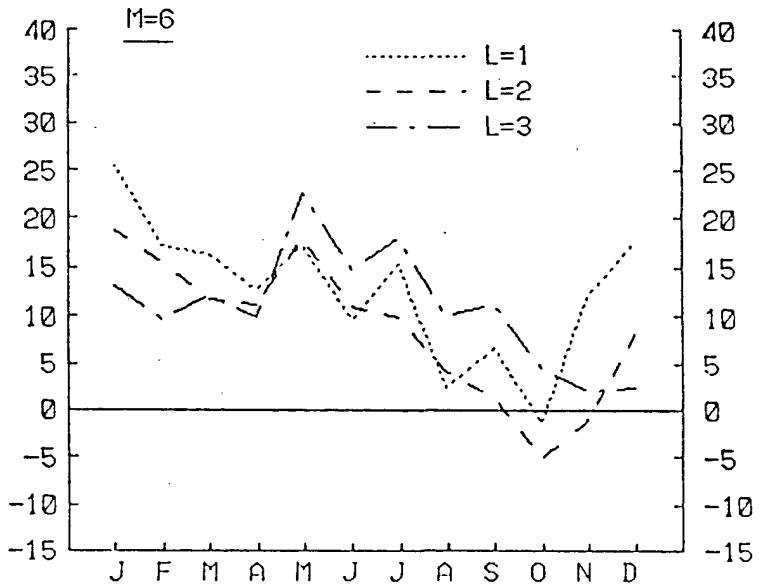

Figure 4: Seasonal change of skill scores of PCA model forecast for M=6.

Forecasting seasonal monsoon rainfall over India and adjoining countries

S.V. Singh, R.H. Kripapani, K.D. Prasad, S.D. Bansod
Institute of Tropical Meteorology, Pune, India

Abstract

The Indian summer monsoon rainfall shows considerable interannual variability. Attempts for its forecasting have been made now since well over 100 years through empirical techniques. A large number of regional and global parameters have been tried by various authors. Besides several authors have shown definite potential predictability in the Indian summer monsoon (Singh and Kripalani, 1986, Mon. Wea. Rev.).

The present authors had developed multiple regression equations for prediction of all India monsoon rainfall by using the subtropical ridge positions over India and West Pacific (Singh, S.V., et al. 1986, Adv. Atmos. Sci.). Subsequently we have explored the relationship of about 30 regional and global atmospheric/oceanic parameters (including ENSO parameters) for prediction of monsoon rainfall. We have selected 3 of these parameters, which represent different regional and global processes and show variance inflation factor of less than 2 in the multiple regression analysis, for further analysis. The multiple regression equations are developed by using these 3 parameters for prediction of monsoon rainfall on different spatial scale (from meteorological subdivisions to whole India) and temporal scale (monthly to seasonal) and cross validated by a jackknifed method. A sample of 37 years (1951-87) has been used. The Heidke skill scores for 3 nearly equiprobable category verifications have ranged from .3 to .5. Some positive skill scores ranging from .2 to .3 are obtained even for the subdivisions in the western and central India. Encouraged by these results we are now developing forecast techniques for prediction of seasonal rainfall for several tropical countries viz. Burma, Thailand, Phillippines, Indonesia, Sri Lanka, lying towards east of India.

Non-linear time series models of ENSO Indices

F.W. Zwiers[1] and Hans von Storch[2]
[1] Canadian Climate Centre, Downsview, Ontario, Canada
[2] Max Plank Institute für Meteorologie, Hamburg, F.R. Germany

Abstract The class of 'Threshold auto-regressive time series models' (TAR; Tong, 1983) is introduced. These non-linear models describe variations of the moments of nonstationary time-series by allowing parameter values to change with the state of an ancillary controlling time series and, possibly, an index series. The index series is used to indicate deterministic seasonal and regimal changes with time. Fitting and diagnostic procedures are described in the paper.

This class of models is applied to a 102 year seasonal mean tropical Pacific Sea Surface Temperature index time series. The models are controlled by a seasonal index series and one of two ancillary time series: seasonal mean Adelaide SLP and Indian Monsoon rainfall, which have previously been identified as possible precursors of extremes of the Southern Oscillation (SO).

Analysis of the fitted model gives clear evidence for the seasonal variation of the stochastic characteristics of the SO. It also shows that both the annual cycle and the autocorrelation structure of the SO index depend on the state of the SO. We found that the TAR model was able to make effective use of information in the time series of year-to-year change in Nov-Dec-Jan (NDJ) Adelaide SLP. The fitting procedure objectively chose an upper and lower threshold for this change in SLP resulting in 3 kinds of stochastic behaviour for each season. Tests of independence showed that the occurrence of a threshold crossing was related to the occurrence of an Warm or a Cold SO event.

Reference

Tong, H., 1983: Threshold Models in Non-Linear Time Series Analysis. *Springer-Verlag, Lecture Notes in Statistics, Vol. 21, 323pp.*

Effects of missing data on circulation statistics

Kevin E. Trenberth
NCAR, Boulder, Colorado

John W. Kidson
Meteorological Service, Wellington, NZ

Abstract The impact of missing data on general circulation statistics, including means, variances, and covariances, is assessed by systematically decreasing the number of twice-daily ECMWF analyses included in the monthly mean for several parameters. Because the standard error of a monthly mean depends on the standard deviation of the daily values and the effective number of independent observations during each month, results have been expressed as the ratio of the root mean square error (RMSE) in the monthly mean to the daily standard deviation, thus allowing fairly universal relationships to be developed for application to many parameters, and to different seasons, latitudes and longitudes. Results could be modeled sufficiently well with a first order autoregressive (Markov) process to allow simulated data to be used for further tests. If missing observations are randomly spaced, the RMSE increases by factors of 2–3 over equally spaced data and there is virtually no advantage due to autocorrelation in the data. If the missing data occur in one block, another factor of up to 2 increase in RMSE occurs.

Introduction

Various assumptions have been used to deal with missing data in analyzing station observations and analyses from operational forecast centers and it is worth while examining systematically the impact of missing data on climatological and general circulation statistics. The main interest is in compiling statistics for individual months so that questions about interannual variability can be addressed, and thus the number of observations available and their distribution throughout each month is important.

Discussion of the treatment of missing data in most papers is poor. Oort (1983), in his atlas of general circulation statistics, used a data cutoff of 10 observations per month for inclusion of a station in monthly statistics. Oort (1978) states that on average most rawinsonde stations report between 60 and 90% of the time and that ~5% of the stations report less than 50% of the time. A more complete review of problems with missing data is given in Kidson and Trenberth (1988) (henceforth KT). There appears to be a chronic problem with insufficient or missing data, although the problem is often ignored. We therefore need to know the impact of missing data on various statistics and what confidence can be placed on means, variances and covariances computed when some data are missing.

Sampling Experiments

Methods

Sampling experiments have been performed using global twice-daily grid point analyzed values from the European Centre for Medium Range Weather Forecasts (ECMWF). The data set is subsampled and the effects on statistics computed. The parameters examined were the zonal and meridional wind components, temperature, geopotential height, specific humidity and vertical motion (u,v, T, Z, q and ω, respectively) together with the variances $\overline{u'^2}$ and $\overline{v'^2}$, and covariances $\overline{u'v'}$ and $\overline{v'T'}$. Here the focus is on u.

For convenience in varying the sampling interval δt, statistics were derived for 32-day 'months' beginning at 0000 UTC on the last day of the previous month. In the first series of tests, estimates of the monthly mean statistics were computed using δt = 0.5, 1, 2, 4, 8, and 16 days, corresponding to N = 64, 32, 16, 8, 4, and 2 12–hourly observations in each sample. The resulting statistics are compared with those for N = 64 as the 'truth'.

The mean of the subsampled series will usually differ from the true mean. If the N values are independent, the mean will vary about the true mean with a standard deviation (the standard error) of $\sigma/\sqrt{N}$, where σ is the population standard deviation of the individual values. Results differ from this because the values are not independent and, as we are interested in statistics for individual months, the interannual variance is excluded.

In meteorology, time series typically have a red noise character; that is they are dominated by the low frequency part of the power spectrum. Often they can be reasonably statistically modeled using a first order autoregressive (Markov) process, AR(1), which is completely determined by the autocorrelation at lag 1. The extent of autocorrelation is linked to the equivalent sample size, and using the concept of effective time between independent observations, T_o, the effective number of independent observations in a sample $N_{eff} = N\delta t/T_o$ can be estimated. Methods for computing the appropriate T_o are given by KT. In general the relation between the standard deviation of the mean and the total standard deviation is

$$\sigma_m = \sigma/\sqrt{N_{eff}}. \tag{1}$$

Sample standard deviations s of a parameter x are computed relative to each monthly mean $\bar{x}_N$, rather than population standard deviations, where N refers to the number of observations. This standard deviation does *not* include interannual variations but has the advantage that it can be uniquely computed from each month of data. We also compute the standard deviation of mean values $\bar{x}_N$ relative to $\bar{x}_{64}$, $s_N(\bar{x})$. This is the root mean square error (RMSE) due to missing data as a function of N.

We anticipate from (1) that $s_N(\bar{x})$ will be related to $s(x)$ but with a correction needed to allow for the absence of the interannual variance. Accordingly, we express these as a ratio which lies in the range 0 to 1 and, if the autocorrelations are also computed from individual months, then the ratio becomes

$$\frac{s_N(\bar{x})}{s(x)} = \left[\frac{1}{N_{eff}(N)} - \frac{1}{N_{eff}(64)}\right]^{1/2} \tag{2}$$

(see KT). This is, to a good approximation, the expected ratio of the RMSE of the monthly mean to the daily standard deviation when all values are computed without the interannual variability included. We refer to it as the 'RMSE ratio'.

Thus, for an AR(1) process with $r_1 = 0.8$ at 12-hour lag, Table 1 gives the expected values of certain parameters of interest.

Table 1: Values of T_o in days, N_{eff}, σ_m/σ (from (1)) and s_N/s (from (2)) as a function of N and δt for an AR(1) process with $r_1 = 0.8$.

N	2	4	8	16	32	64
δt	16	8	4	2	1	1/2
T_o	-	-	5.36	4.48	4.24	4.19
N_{eff}	2	4	5.96	7.14	7.55	7.64
σ_m/σ	0.71	0.50	0.41	0.37	0.36	0.36
s_N/s	0.65	0.37	0.21	0.10	0.04	0.0

Note that it is only when $N > 4$ that $N_{eff} \neq= N$ in this case. The ratio of the population standard deviations σ_m/σ decreases exponentially to the interannual variability value while the RMSE ratio s_N/s decays to zero as N increases.

ECMWF data

As expected from (1) and (2), the standard deviation of the monthly means decreases with the sampling interval and generally retains the same geographic distribution as the standard deviation for the month for individual gridpoint values. The zonally averaged standard deviation of u has been averaged over all months of the year as a function of latitude (Fig. 1).

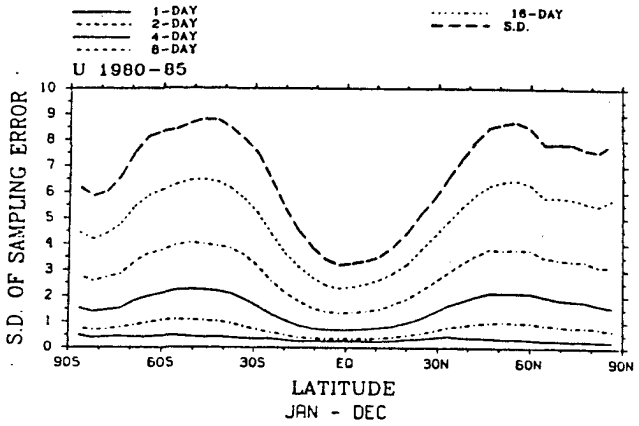

Figure 1: Zonally averaged standard deviation of the westerly wind component at 500 hPa and monthly means obtained using sampling intervals of 1, 2, 4, 8, and 16 days, in m s^{-1}

The standard deviation of the sample means $s_N(\overline{u})$ generally follows the same pattern as the standard deviation of the twice-daily values, $s(u)$, which shows the well-known minimum in the tropics and maxima at mid-latitudes.

The distribution of the ratio of $s_N(\overline{u})/s(u)$ for all gridpoints and months is given in Fig. 2.

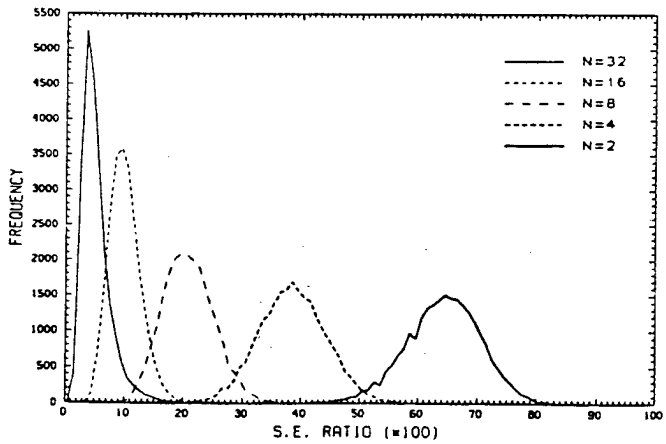

Figure 2: Histogram of RMSE of monthly means of the zonal wind component for sample intervals 1,2,4,8 and 16 days expressed as a fraction of the daily standard deviation for all gridpoints over with interannual variation excluded.

The overall mean values of the ratios for δt = 16, 8, 4, 2, and 1 day sampling intervals are 0.64, 0.38, 0.20, .09 and .04, respectively. In absolute terms these values correspond to the mean of the five lower curves in Fig. 1. To compare with (1) it is necessary to add the interannual variances and the new mean ratios are 0.67, 0.46, 0.33, 0.27 and 0.25 for the sampling intervals above.

When compared with results for an AR(1) series with the same autocorrelation (Table 1), $s_N(u)/s(u)$ is quite close to that expected from (2), but as N increases the ratio of σ_m/σ decreases exponentially to 0.25 rather than 0.36 in Table 1. This discrepancy arises because there is less interannual variability in the actual u series than for the corresponding AR(1) series. Thus there is an advantage in considering the RMSE as a fraction of the daily sample standard deviation, as in (2).

More generally, (2) was evaluated from the observed autocorrelations out to a lag of 64 half days for N = 2, 4, 8, 16, 32 and compared to the observed ratios for u, v, Z and ω at each grid point over the first 12 sample months. Generally the RMSE ratios show good agreement between those computed and those expected from (2).

Equal-spaced sampling of simulated data

An alternative approach to the estimation of RMSEs is to use the same sampling procedure with artificially generated data. For linear variables such as u, data were generated using $x_i = \rho x_{i-1} + \epsilon_i$ where ρ is the autocorrelation at a 12-hr lag and ϵ a normally distributed random number with standard deviation $\sigma(x)(1-\rho^2)^{1/2}$ and means are zero. The interannual variance due to the monthly means is removed and the results (Table 2) can be compared with those from ECMWF data for $\overline{u}$ and $\overline{\omega}$. The excellent agreement confirms the validity of the statistical approach for data with high and low autocorrelations.

Table 2: RMSE ratios $s_N(\overline{x})/s(x)$ obtained for 2 to 32 regularly-spaced simulated data with 12-hour lag correlations between 0.0 and 0.9. Also shown are the mean results for $\overline{u}$ and $\overline{\omega}$, along with their 12-hourly autocorrelation.

12-hr Corr.	Number of Observations 2	4	8	16	32
.9	.57	.31	.15	.07	.03
.8	.64	.38	.20	.10	.04
.6	.68	.45	.27	.14	.06
.4	.69	.47	.30	.17	.08
.2	.69	.48	.32	.19	.10
.0	.70	.49	.33	.21	.12
$\overline{u}$(.80)	.64	.38	.20	.09	.04
$\overline{\omega}$(.34)	.69	.47	.30	.18	.09

It may appear surprising that the results in Table 2 show little sensitivity to changes in the autocorrelation. Because the interannual variability is excluded, the RMSEs do not follow from (1) but rather follow from (2), and there is a big difference between σ and s. It is emphasized that Table 2 gives the ratio of the computed standard deviation of the monthly mean arising from less than perfect sampling to the within-month standard deviation. As a consequence of this lack of sensitivity to the autocorrelation, the results for $\overline{u}$ and $\overline{\omega}$ are less dependent on the method of averaging over many gridpoints and months.

Random sampling

Simulations were also undertaken to see how the variance ratios for the linear variable x would vary if the samples were taken at random throughout the month. The results (Table 3) show that the RMSE ratio depends mainly on the number of observations in the sample and corresponds to the results in Table 2 for $r_1 = 0$ unless the lag correlation exceeds 0.8.

Table 3: Random observations: As a function of the 12-hour autocorrelation ρ are given the standard deviation of the monthly means based on all 64 observations $V_m^{1/2}$, and the RMSE ratio. (61, 58 and 51 observations correspond to 5, 10 and 20% missing values respectively.)

ρ	$V_m^{1/2}$	Numbers of observations N				
		16	32	51	58	61
0.9	.511	.18	.08	.02	.00	.00
0.8	.367	.20	.11	.04	.03	.00
0.6	.250	.22	.12	.05	.03	.01
0.4	.192	.22	.12	.05	.03	.02
0.2	.154	.22	.12	.06	.03	.03
0.0	.126	.22	.12	.06	.04	.03

The conclusion from Table 3 is that randomly missing observations are much more serious than systematic sub-sampling, apparently because those missing parts of the series are under-represented. Persistence in the series does not help improve the statistics if computed only from the available data. Persistence, however, does help one replace missing data by interpolation or statistical modeling. Apparently for small data gaps ($< T_o$) and for linear statistics, interpolation of missing data is desirable. However, interpolation may have undesirable effects on second moment statistics.

Missing blocks of data

The worst (but not uncommon) case for missing data occurs when consecutive observations are lost. This was simulated by selecting a random starting time within the month to sample the required number of consecutive observations. The results (Table 4) show that the RMSE ratio increases substantially with the lag correlation.

For 20% missing data the RMSE ratios increase from 0.04–0.06 to 0.09–0.16 for the range of autocorrelations 0.3–0.8. As well as causing largest errors in computed statistics, missing blocks of data are also generally impossible to replace using interpolation or statistical modeling.

Applications

To apply these results and obtain magnitudes of the RMSE, values of s are needed. Fig. 3 shows a cross section of $s(u)$ for January 1979–1985 from ECMWF data.

The 12-hour annually averaged lag correlations for u are $\sim$0.8 which may be used with Tables 2-4 to determine the RMSE. At 300 hPa $s(u)$ exceeds $\sim$15 m s^{-1} in midlatitudes. Thus from Table 2, if data were available only every 2 days, the RMSE in $\overline{u}$ of $\sim$10%, or 1.5 m s^{-1} at 300 hPa would be expected. Or if only 11 equally spaced observations were available, the RMSE at 300 hPa would be $\sim 0.16 \times 15$ or 2.4 m s^{-1}. Alternatively, if 20% of the 64 possible 12-hourly observations were

Table 4: Contiguous missing data: As a function of the 12-hour autocorrelation ρ are given the standard deviation of the monthly means based on all 64 observations $V_m^{1/2}$, and the RMSE ratio. (61, 58 and 51 observations correspond to 5, 10 and 20% missing values respectively.)

ρ	$V_m^{1/2}$	Numbers of observations N				
		16 °	32	51	58	61
0.9	.511	.64	.40	.18	.08	.02
0.8	.367	.53	.32	.16	.09	.04
0.6	.250	.39	.24	.12	.07	.04
0.4	.192	.31	.19	.10	.06	.04
0.2	.154	.26	.15	.08	.05	.03
0.0	.126	.21	.13	.07	.04	.03

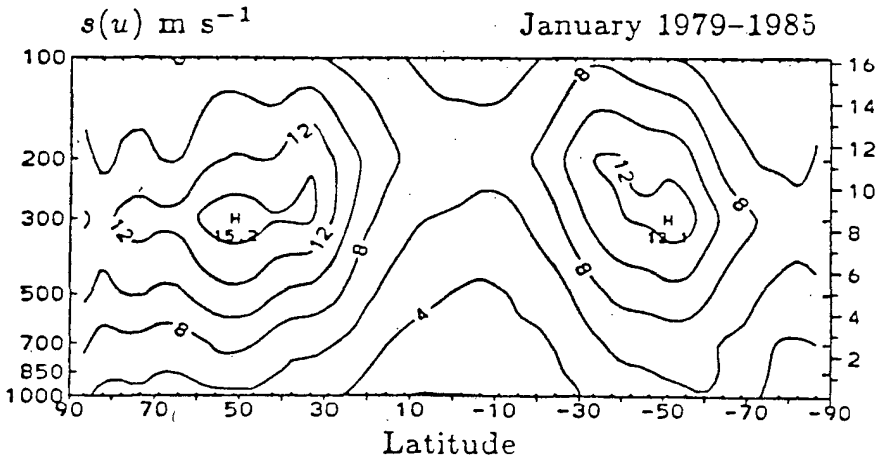

Figure 3: Cross sections of the standard deviation of the wind components u averaged around latitude circles for January from 1979 to 1985. Units m s^{-1}.

randomly missing, from Table 3, the RMSE in $\bar{u}$ would be $\sim$0.6 m s^{-1}. If the 20% of missing data were in one block, from Table 4, the RMSE would be $\sim$2.4 m s^{-1} at 300 hPa.

It is common for stations in Africa and South America to report with only 11 observations per month. Oort (1983) required a minimum of 10 observations/month for his statistics. For 11 observations/month randomly distributed the factor would be $\sim$ 0.27 so that the RMSEs in u at 300 hPa would be up to 4.1 m s^{-1}. KT provide other examples.

Our results give larger RMSEs due to temporal sampling than those of Oort (1978), mainly because Oort used once daily data which already contain RMSE errors in u of $\sim$0.5 m s^{-1} compared with twice-daily sampling. Another factor is that Oort averaged the RMSEs over the hemisphere whereas we suggest that it is more appropriate to average the ratio of the RMSE to the daily standard deviation.

Conclusions

The ratio of the RMSE of the monthly mean to the daily standard deviation depends on the autocorrelations and interval between samples. For the more persistent variables Z, u, T fewer observations at regular intervals are needed to define a monthly mean.

The observed RMSE ratios may be reasonably simulated using series generated by a first order Markov process. Random sampling increased the RMSE substantially compared with the same number of evenly spaced observations and had the effect that the percentage errors accumulated as if the series were white noise. When the missing observations were grouped together rather than being evenly spaced, the RMSE increased several fold.

The number of observations required to estimate a monthly mean depends on the variance of the daily data and the desired accuracy. Interpolation from the tables shows that the minimum requirement of 10 observations per month used by some investigators leads to a RMSE of 17-27% of the daily standard deviation. Clearly station data are not perfect and missing data can be an issue. We recommend that the amount of data missing and how it was handled should be reported in observational studies, especially where inferences concerning interannual variability and longer-term trends are being addressed.

References

Kidson, J. W. and K. E. Trenberth 1988: Effects of missing data on estimates of monthly mean general circulation statistics. *J. Climate*, **1**, 1261-1275.

Oort, A. H. 1978: Adequacy of the rawinsonde network for global circulation studies tested through numerical model output. *Mon. Wea. Rev.*, **106**, 174-195.

Oort, A. H. 1983: Global atmospheric circulation statistics, 1958-1973. NOAA Prof. Paper 14. U.S. Dept. Commerce. 180 pp plus fiche.

Cluster analysis of variables in climate research

K. Wolter
Climate Analysis Center, NMC/NWS/NOAA, Washington D.C. USA

Abstract

Anyone dealing with climate research will sooner or later face the dilemma to choose between climatic data fields that are relatively clean and short, or "noisy", riddled with gaps, and often longer. How can the latter kind be analyzed ? This paper is about one particular technique that exploits the inherent covariability of geophysical fields in order to retrieve the large-scale signal from noisy fields: *cluster analysis of variables*. It operates under the assumption that climate variability does not occur randomly in space - just like there are preferred and identifiable long-wave patterns in the midlatitudes, there are preferred regions of (co-)variability in the tropics, the most prominent example being the two surface pressure dipoles of the Southern Oscillation. Such 'centers of action' are defined, delineated, and separated from noisy regions by cluster analysis of variables. Note that this technique relates to the more popular cluster analysis of cases just as the "T mode analysis" of principal components is related to "S mode analysis". It has been applied to *tropical* ship data (Wolter, 1987), but appears extendable to *global* ship data (COADS), and various satellite-based data fields (e.g., high reflective cloudiness - HRC), to name but a few areas of interest.

Questions addressed include the choice of the clustering algorithm, cluster size selection (both *a priori* and *a posteriori*), statistical significance, and advantages and disadvantages compared to other techniques (e.g., rotated principal component analysis (RPCA)). What are these clusters good for ? Two examples: classification of regions in order to create time series that monitor climatic change, and use of such time series as *input* into RPCA studies (Wolter, 1988).

References

Wolter, K., 1987: The southern oscillation in surface circulation and climate over the tropical Atlantic, Eastern Pacific and Indian Oceans, as captured by cluster analysis. *J. Climate Appl. Meteor.*, **26**, 540-558.

Wolter, K., 1988: Modes of tropical circulation, Southern Oscillation, and Sahel rainfall anomalies. *J. Climate*, ?, ??-??.

Cluster analysis as an aid to the identification of persistent states

John W. Kidson
Meteorological Service, Wellington, New Zealand

Introduction

In recent years the question has arisen whether, by analogy with simple non-linear models, the atmospheric circulation exhibits multiple equilibria (e.g. Legras and Ghil, 1985; Hansen and Sutera, 1986), whether some of these preferred states show unusual persistence, and whether there are predictable paths for transitions between them. Mo and Ghil (1987) have claimed a number of similarities between quasi-stationary states of the southern hemisphere circulation defined by zonal wave numbers 0–4 and a relatively simple nonlinear dynamical model of large-scale atmospheric flow. Their results are not particularly encouraging as persistent states only occurred for 18% of the time during winter with an average of 2 events having a mean duration of 8 days per season. Only half the number of persistent states was observed during the summer (Mo, 1986) and overall the southern hemisphere was found to be less persistent than the northern hemisphere (Horel, 1985; Trenberth 1985), even with less restrictive measures of persistence.

Although Mo and Ghil's analysis used zonal filtering to retain only the long waves, it still includes some short period fluctuations associated with synoptic events and it is desirable to see whether more promising results might be obtained for the longer periods which are prominent in spectra for both southern (Kidson, 1988a) and northern (Shubert, 1986) hemispheres.

The results presented here relate to the low-pass filtered variations in the southern hemisphere circulation. Their characteristic modes have been determined by EOF analysis and cluster analysis has been applied to see whether multiple equilibria exist. As will be seen, the results are basically chaotic without evidence of preferred trajectories or clustering of states (except about the overall mean). It is difficult to group the analyses into a small number of preferred states without setting unreasonably loose criteria for merging and consequently the use of transition tables for prediction as advocated, for example, by Mo and Ghil (1987), has little value. Further details are given in Kidson (1988b)

Data

The data set used for this study is the archive of ECMWF analyses available online at NCAR for January 1980 to December 1986 on a R15 Gaussian grid at 0000 and 1200 UTC. Further details are provided by Trenberth and Olson (1988).

Analysis was concentrated on the 500 hPa level where, after removal of the mean annual cycle, a low-pass filter was applied to remove most of the variance for periods below 50 days.

EOF analysis

EOF analysis was undertaken for the complete 7-year sample and for 4 sub-samples grouped into 3-month seasons using a subset of 621 points from the R15 grid to give an approximately equal weighting by area.

The proportion of the variance associated with the first 10 EOFs for each case are given in Table 1. For the unnormalized data, the total variance contribution from the first 10 EOFs is 73.5% for the year and ranges from 82 to 85% for the individual seasons. The corresponding variance for the normalized data for the complete year is 67.0%. Overall there are approximately 100 independent data points for the year and 25 for each season so that the criteria of North et al. (1982) give the relative

error for each eigenvalue, $\delta\lambda_i/\lambda_i$, as $\pm 28\%$ for seasons and $\pm 14\%$ for the year. Consequently EOF patterns 2 and 3 are not well separated in the annual case, and some mixing can be expected between patterns 4–10. According to the test of Craddock and Flood (1969) only the first three eigenvectors are significant. They will be referred to later As Z_1 – Z_3. The projection of all states onto EOFs 2

Table 1: Percentage of variance contributed by first 10 EOFs for the complete year and for the seasons Spring (SON), Summer (DJF), Autumn (MAM) and Winter (JJA) using non-normalized low-pass filtered 500 hPa height anomalies, and for the complete year using normalized anomalies.

EOF	Year	Spring	Summer	Autumn	Winter	Year (norm.)
1	18.6	21.9	27.2	19.5	18.8	23.4
2	11.1	12.1	14.8	12.5	17.3	8.3
3	10.7	11.5	9.5	10.5	14.0	7.1
4	7.0	8.7	8.6	8.8	8.7	5.8
5	5.9	7.0	7.6	8.0	6.3	5.0
6	4.9	6.5	4.8	6.5	5.1	4.3
7	4.7	5.0	4.2	5.4	4.2	3.8
8	3.8	4.4	3.5	4.2	3.6	3.4
9	3.5	3.4	2.6	3.7	3.0	3.1
10	3.3	2.7	2.2	3.0	2.5	2.8
1–10	73.5	83.2	85.0	82.1	83.5	67.0

and 3 is shown in Fig. 1. As for the projections on the EOF 1,2 and 1,3 planes the pattern is chaotic with no evidence of any preferred paths or attractors.

Cluster analysis

Cluster analysis (Hartigan, 1975) provides an objective technique to group similar states in what is essentially a search for analogs. Initially there is one cluster per state, and the clusters are then repeatedly merged on the basis of the separation between them to form a tree structure. The separation between states can be computed in various ways and two important variations are simple linkage and complete linkage. In simple linkage the separation is taken to be the smallest distance between any members of the two clusters, so that it is possible to form long clusters in which the end states may differ appreciably from each other. For complete linkage, the separation is taken as the largest distance between any members of the two clusters so that the size of the cluster is kept as small as possible. While the process may be continued until the tree is complete and there is only one cluster comprising all the original states, it is normally stopped when a small number of clusters remains or the separation between the remaining clusters becomes too large in some sense. While objective tests may be constructed to decide the maximum separation below which merging is possible, this may be better decided subjectively on other than statistical grounds (Gabriel, 1985).

The cluster analyses below were made using complete linkage and both rms differences and pattern correlations between states were tried as measures of similarity. The pattern correlation is obtained by correlating the anomalies at matching grid points over the two states (e.g. Mo, 1986) and differences in amplitude are less important than differences in the phase of the patterns in determining their degree of similarity. Since the mean patterns associated with clusters determined on the basis of rms differences became increasingly bland as more states were added, and those obtained using pattern correlations tended to be more distinctive, only the latter are presented here.

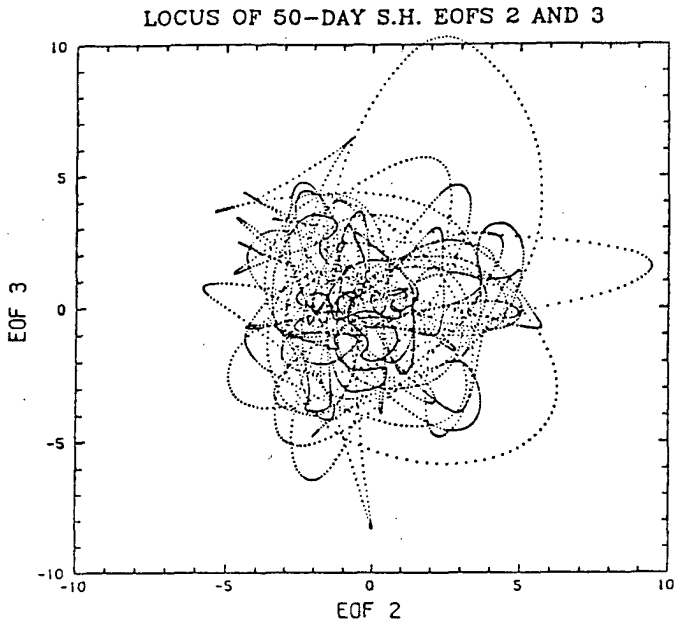

Figure 1: Locus of twice-daily states in phase space projected on to the planes defined by EOFs 2 and 3

All states

It was not feasible to calculate the separations between the anomaly patterns defined at 5-day intervals over all 621 grid points and instead the coefficients of the first 10 EOFs which account for 73.3% of the variance were used. Since the EOFs are orthogonal over the complete grid, the pattern correlation between pairs of states is identical to the pattern correlation between grid point values that are resolved in terms of the first 10 EOFs. Because of the 50-day low pass filtering of the original data, most of the initial merges were between consecutive states. The number of clusters remaining was still 108 when the pattern correlation dropped to 0.5 and when it was further dropped to 0.0 a total of 37 clusters remained from the original 499 states. A pattern correlation of 0.0 between the most distant points in the cluster implies that some of the states in the cluster have virtually no relation to each other, though all are positively correlated with the cluster mean.

The mean anomaly patterns for the states in the three clusters with the highest number of members are shown in Fig. 2. If multiple equilibria exist they are most likely to be associated with these patterns. Although the probability density of states is greatest near the origin the mean state is not identified with any of the most populous clusters. This may result from using pattern correlations rather than RMS differences to determine the separation between states, as small departures from the overall mean are easier to merge in the latter case.

Persistent states

Persistent or quasistationary states may be defined as intervals when the atmosphere is moving relatively slowly through phase space. These intervals may be detected by isolating a sequence of states which have relatively small differences between them compared to the differences between random pairs of states.

A persistent state or event was defined to be a sequence of 3 or more states separated by 5

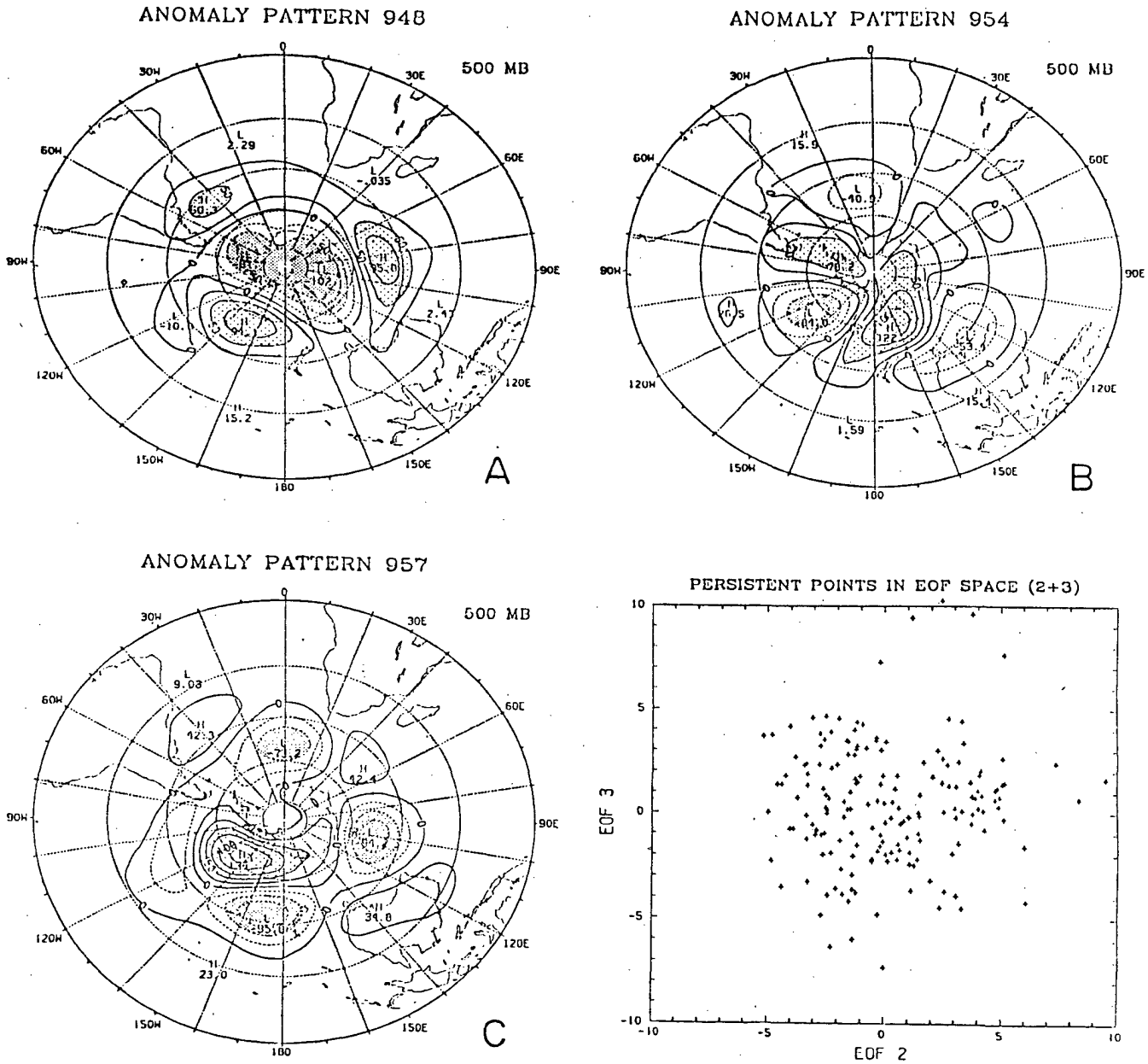

Figure 2: Mean anomaly patterns associated with the most populous clusters derived from 499 analyses separated by 5 day intervals: (a) Cluster 948, 31 members; (b) Cluster 954, 22 members; (c) Cluster 957, 21 members.

day intervals for which the pattern correlation between all pairs of states exceeded some minimum threshold. While the number of events found depended strongly on the minimum correlation, their average length showed little change. For a minimum correlation of 0.5, 123 events were found with a mean duration of 3.31 consecutive states at 5-day intervals. Increasing the threshold to 0.7 reduced the number of events to 58 but the mean duration dropped only to 3.07 states. Reducing the threshold to 0.0 increased the mean duration to 5.25 5-day periods but these can hardly be considered persistent states when they contain some patterns completely uncorrelated with each other.

To examine the distribution of these persistent events in phase space, plots were made of their coordinates projected onto the planes defined by EOFs 1-3 which account for ~40% of the overall variance.

Figure 3: Plot of Z_2 and Z_3 coordinates of all analyses included in persistent events determined by a minimum pattern correlation of 0.7

Fig. 3 shows the distribution in the Z_2–Z_3 plane of all states included in the 58 events obtained using the minimum pattern correlation of 0.7. A similar but denser pattern is obtained for the events obtained with a minimum correlation of 0.5. No obvious evidence of clustering can be seen and the same holds for the plots for the Z_1–Z_2 and Z_1–Z_3 planes (not shown). A comparison of Fig. 3 with Fig. 1 suggests that the density of *persistent* states does not increase towards the origin to the same extent as the density of *all* states and this is confirmed by a plot of the ratio of the two density distributions (not shown). States with large departures from the origin in any direction are more likely to be persistent than those close to the origin but they tend to occur when the movement slows as the anomaly reaches maximum amplitude in a similar manner to a simple harmonic oscillator such as a pendulum.

Although the distribution of the 58 persistent states obtained above in the EOF 1–3 planes appeared fairly homogeneous, cluster analysis was again carried out using the pattern correlation between the mean anomalies at each of the 621 grid points to form the similarity matrix. When the minimum pattern correlation for the multiple linkage clusters was set at 0.7, the same value as used to determine the persistent events, 50 clusters still remained. This number of clusters fell to 35 when the minimum

pattern correlation was reduced to 0.5, and to 11 when it was further reduced to 0.0. Since these clusters are likely to depend on the data sample used rather than any underlying physical cause they are not reproduced here. Five of the 11 clusters (including 20 persistent events) showed predominantly wave number 3 patterns, there were 2 partial and 2 complete wave number 4 patterns (including 27 events) and the remaining 2, which were merged from 11 events, depicted large anomalies in the south Pacific.

Summary and conclusions

From 7 years of 500 hPa analyses from the southern hemisphere three principal EOFs were found which accounted for 40% of the variance of the lowpass filtered fields.

Plots of the trajectories of the daily analyses in phase space projected on to the planes of the principal axes of variation, EOFs 1–3, showed apparently chaotic behavior and no sign of clustering about multiple equilibria. This was confirmed by cluster analysis using pattern correlations between the first 10 EOFs as a measure of similarity. The total of 499 states separated by 5-day intervals could be condensed only to 37 clusters by allowing some totally uncorrelated states to be included in the same cluster.

Persistent events were derived from this same set of 499 states with the requirement that the pattern correlation between all states included in the event exceeded some minimum value. The mean duration of these events did not exceed 3, or occasionally 4, consecutive states at 5-day intervals and was not very sensitive to the choice of minimum pattern correlation. A threshold of 0.5 produced 123 events, while increasing it to 0.7 reduced the number of events to 58 with little change in their mean duration. Cluster analysis again failed to provide a small number of groupings of similar events.

Since only 36% of states are included in persistent events when a reasonable criterion for matching patterns is used (pattern correlation of ≥ 0.7), these events are clearly separated by more than the fast excursions through large and infrequently visited parts of phase space observed in Mo and Ghil's (1987) model. The persistent states are widely distributed in phase space and a manageable number of clusters is obtained only through use of a criterion that allows some totally unrelated states to be grouped together. Even when persistent states are grouped by season and the number of clusters is small, most transitions occur between persistent and non-persistent states. The few transitions between persistent states that are observed are insufficient to establish a 'climatology'.

Acknowledgments. I would particularly like to thank Dr Kevin Trenberth for the opportunity to undertake this study in the Climate Analysis Section of the Climate and Global Dynamics Division of NCAR.

References

Craddock, J. M., and C. R. Flood, 1969: Eigenvectors for representing the 500 mb geopotential surface over the Northern Hemisphere, *Quart. J. Roy. Meteor. Soc.*, **95**, 576–593.

Gabriel, K. R., 1985: Exploratory multivariate analysis of a single batch of data. Chapter 4, *Probability, Statistics, and Decision Making in the atmospheric sciences*, A.H. Murphy and R.W. Katz eds. Westview Press, Boulder, CO. 545pp.

Hansen, A. R., and A. Sutera, 1986: On the probability density distribution of planetary-scale atmospheric wave amplitude. *J. Atmos. Sci.*, **43**, 3250–3265.

Hartigan, J.A., 1975: *Clustering algorithms.* John Wiley and Sons, New York. 351pp.

Horel, J. D., 1985: Persistence of the 500 mb height field during northern hemisphere winter. *Mon. Wea. Rev.*, **113**, 2030–2042.

Kidson, J. W., 1988a: Indices of the southern hemisphere zonal wind. *J. Climate*, **1**, 183–194.

——, 1988b: Interannual variations in the Southern Hemisphere circulation. *J. Climate*, **1**, (in press - December issue).

Legras, B., and M. Ghil, 1985: Persistent anomalies, blocking and variations in atmospheric predictability. *J. Atmos. Sci.*, **42**, 433–471.

Mo, K. C., 1986: Quasi-stationary states in the southern hemisphere. *Mon. Wea. Rev.*, **114**, 808–823.

—— and M. Ghil, 1987: Statistics and dynamics of persistent anomalies, *J. Atmos. Sci.*, **44**, 877–901.

—— and ——, 1988: Cluster analysis of multiple planetary flow regimes, *J. Geophys. Res.*, (in press).

North, G. R., T. L. Bell, R. F. Cahalan, and F. J. Moeng, 1982: Sampling errors in the estimation of empirical orthogonal functions, *Mon. Wea. Rev.*, **110**, 699–706.

Shubert, S. D., 1986: The structure, energetics and evolution of the dominant frequency-dependent three-dimensional atmospheric modes. *J. Atmos. Sci.*, **43**, 1210–1237.

Trenberth, K. E., 1985: Potential predictability of geopotential heights over the southern hemisphere. *Mon. Wea. Rev.*, **113**, 54–64.

——, 1987: The role of eddies in maintaining the westerlies in the southern hemisphere winter. *J. Atmos. Sci.*, **44**, 1498–1508.

——, and J. G. Olson, 1988: ECMWF global analyses 1979–1986: Circulation statistics and data evaluation. NCAR Tech. Note NCAR/TN-300+STR. 67 pp and Appendices.

Nearest neighbour analysis as applied to the geographic distribution of tornadoes

K.K. Leiker
Department of Geography, Westfield State College, Westfield Mass. USA

Abstract

Nearest-neighbor analysis, a spacing index, is used to examine the spatial distribution of tornadoes in New England. Tornado distribution maps are often used to assess tornado hazard potential. However, a major question about distribution maps concerns whether the distribution is random? Nearest-Neighbor analysis, developed by botanists in the 1950's, provides an index, R, which objectively describes any point distribution pattern.

The nearest-neighbor index , R, is equal to the actual mean spacing distance, D_{obs}, divided by the expected mean distance, D_{exp}, if that distribution were random. D_{obs} is the mean of the distances from each point (i.e, tornado) in the distribution to its nearest neighbor. D_{exp} is a Poisson function given as 1 over 2 times the square root of N/A, where N = number of points and A = the area of the distribution.

R ranges in a continuum from zero to 2.15: R = 0 indicates extreme clustering; 1.0 indicates a random pattern; and R > 1.0 represents dispersed patterns.

Nearest-neighbor analysis was applied to the distribution of tornadoes in the US New England region during the period 1950-1986. There were 334 tornadoes during this period, distributed in a very uneven pattern. The results show a nearest-neighbor index of R = 0.87, which indicates the distribution is not random and tends toward clustering.

Climatic stability at Bidar, Bijapur and Bellary

B.P. Ratnam and A.R.S. Bhat
University of Agricultural Sciences, Dharwad-580005, India

Introduction

The year-to-year fluctuations in the rainfall in India cause the shift of the climate of a station in the extreme years into the wetter or drier type from the normal. As much of the agriculture in India is rainfed the study of the frequency of climatic shifts into the wetter or drier side at a station over a long period is vital.

Material and methods

Three representative stations in North Karnataka viz., Bidar (17°51'N, 77°39'E, 664m), Bijapur (16°50'N, 75°47'E, 594m) and Bellary (15°09'N, 76°55'E, 449m) (see Fig.1) were selected. Monthly rainfall and temperature data for the period 1901-1974 were available.

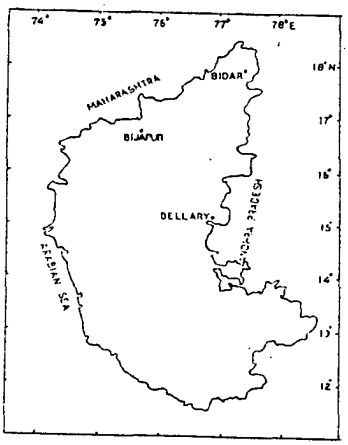

Figure 1: Location of the stations

The following three methods of climatic classification were used:-

1. The aridity index of de Martonne (1926),

$$I = \text{Annual precipitation (mm)}/[\text{Mean annual temperature}(^{\circ}C)+10]$$

The climatic classification based on this index is as follows:- greater than 30- forest; 20 to 30 - prairie; 10 to 20 - dry steppe and less than 10 - desert.

2. The moisture index of Thornthwaite and Mather (1955), .

$$I = 100 \times (P\text{-}PE)/PE$$

where P and PE are annual precipitation and potential evapotranspiration in mm.

Based on the moisture index the climate is classified as follows: above 100- A perhumid; 100 to 20-B humid of four sub-types; 0 to 20-C_2 moist subhumid; -33.3 to 0 - C_1 dry subhumid; -66.7 to -33.3 - D semiarid and -100 to -66.7 - E arid.

3. Troll (1965) used the duration of humid months ie., the months in which the

precipitation exceeds PE to classify the climate thus: 12 to 9.5 - tropical rainy; 9.5 to 7 - humid; 7 to 4.5 - wet-dry semiarid; 4.5 to 2 - dry semiarid and less than 2 - arid.

The climatic type of each individual year from 1901 to 1974 was determined for Bidar, Bijapur and Bellary according to the above three methods. The histograms showing the frequency of the different climatic types at each station were plotted in Figs.2a,2b, and 2c separately according to the three classification methods.

To study the degree of distortion from symmetry, skewness as computed by the Karl Pearson coefficient of skewness $\gamma = (\text{mean} - \text{mode})/(\text{standard deviation})$. In the present study it was difficult to find out the modal value. Hence the approximation$\text{mean} - \text{mode} \approx 3(\text{mean} - \text{median})$ was employed to give the actual formula used $g = 3(\text{mean} - \text{median})/(\text{standard deviation})$.

Results and discussion

Bidar is situated in the transitional belt in the northeastern corner of Karnataka, receiving a normal annual rainfall of 908mm. Both Bijapur and Bellary belong to the dry belt of North Karnataka, the normal annual rainfall being 521 and 528mm respectively (Fig.1). The normal annual PET at Bidar, Bijapur and Bellary are 1437, 1496 and 1600mm respectively. Because of the high PET Bellary is the driest station.

According to de Martonne(1926) prairie prevailed at Bidar in 55% of the years. Dry steppe was observed in 64% and 70% of the years at Bijapur and Bellary respectively (Fig.2a). The coefficient of skewness was 0.04 at Bidar, 0.37 at Bijapur and 0.04 at Bellary. The climatic tilt is from the most frequent type to the drier climatic type. At Bidar the tilt is from prairie to dry steppe, whereas at the other two stations it is from dry steppe to desert.

Semiarid is the most frequent type at Bidar(59%) and Bijapur(57 %) and arid(62%) at Bellary according to Thornthwaite and Mather(1955) (Fig.2b). The coefficient of skewness was -0.10 at Bidar, 0.23 at Bijapur and 0.20 at Bellary. Interestingly at Bidar the climatic tilt is towards the wetter side viz., from semiarid to dry subhumid whereas both at Bijapur and Bellary it is towards the drier side viz., from semiarid to arid.

At Bidar dry semiarid prevailed in 88% of the years, whereas arid was the most frequent type at Bijapur(57%) and Bellary(69%) according to Troll(1965, Fig.2c). The coefficient of skewness was 0.12 at Bidar, not estimable at Bijapur and -0.18?? at Bellary. The climatic tilt is towards the drier side at both Bidar and Bijapur viz., from dry semiarid to arid, whereas it is towards the wetter side viz., from arid to dry semiarid at Bellary.

Potential evapotranspiration (PET) occurring in the numerator in de Martonne's aridity index is an underestimation. Hence the most frequent climatic type is dry steppe at Bellary. Troll's classification puts a rigid condition that P must exceed PET for a month to be classified as wet. Therefore at Bijapur arid type has the highest frequency. Thornthwaite and Mather classification has been widely used and the results are realistic.

References

de Martonne, E. , 1926: Une nouvelle fonction climatologique: l'indice d'aridite. *La Meteorologie*, **68**, 449-458.

Thornthwaite, C.W., and Mather, J.R., 1955: The Water Balance. *Publications in Climatology*, **8(1)**, Drexel Institute of Technology, Laboratory of Climatology, Centerton, N.J., 104 pp.

Troll, C., 1965: Seasonal climates of the earth, in *World Maps of Climatology* (p28). ed. E. Rodenwalt and H. Jusatz. Springer-Verlag, Berlin.

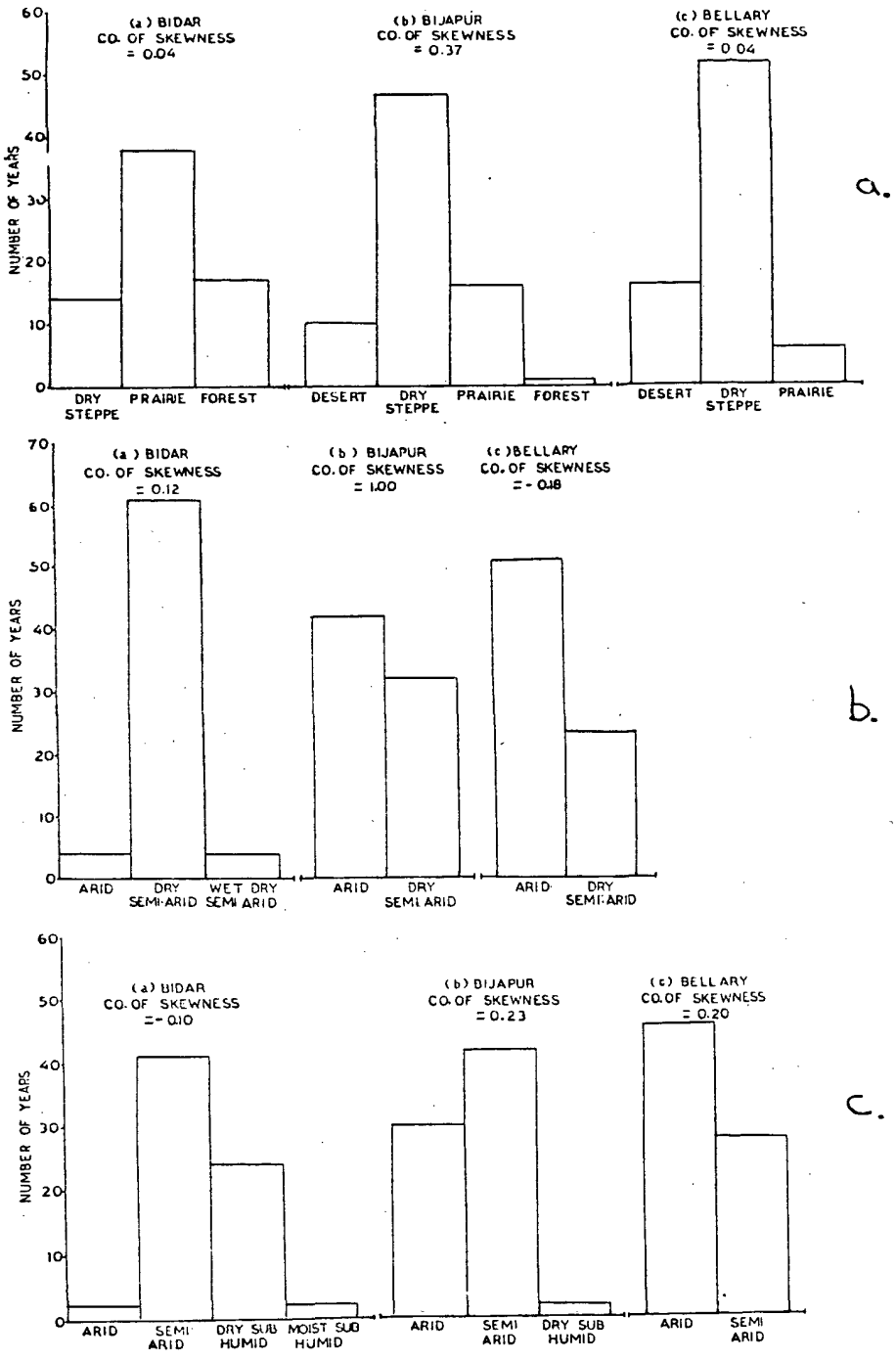

Figure 2: Histogram of the climatic types from 1901-1974 at Bidar, Bijapur and Bellary: classifications of a. de Martonne b. Troll and c. Mather.

Applications of the theory of extreme values in climatology

R. W. Katz
ESIG/NCAR, Boulder, Colorado

T. Farago
Central Meteor. Institute, Budapest, Hungary

Introduction and Summary

The importance of considering extreme climate events in assessing the impacts of climate on society is now widely recognized (e.g., Mearns et al., 1984; Wigley, 1985). Among other things, scenarios of future climate must adequately reflect any possible changes in the likelihood of extreme events. Little attention, however, has been devoted to developing methods that are appropriate for making assessments of the impact of extreme climate events.

Nevertheless, a well-developed statistical theory of extremes does exist (e.g., Leadbetter et al., 1983). Although there have been many attempts to apply it in climatology, this theory has not yet been successfully integrated with realistic applications. Most of the research has either: (i) dwelled on the theory of extremes with only a superficial application to climate (e.g., Tiago de Oliveira, 1986); or (ii) treated realistic climate problems without the proper application of theory (e.g., Tabony, 1983).

We review some of the specific issues that arise in attempting to apply the theory of extreme values to climate, issues for which clear-cut solutions have yet to be identified. First, the classical theory of extreme values is briefly outlined, both for the maximum of a sequence as well as for the number of exceedances of a threshold. Then the issue of the effect of serial correlation of climate time series on the theory of extreme values is considered. In particular, a blatant example of the misapplication of a theory based on means to extremes is identified in the climate literature. Next, the issue of how to take into account the seasonal cycles of climate time series is considered. The various approaches that have been proposed for dealing with this problem each possess certain advantages and disadvantages, making it unclear which one is preferable. Finally, one way in which the application of the theory of extreme values might aid in the resolution of certain questions related to climate impacts is suggested. Specifically, the question of how the likelihood of extreme climate events would change with changes in the average and variability of climate is addressed.

Classical Theory of Extreme Values

In this section, the so-called classical theory of extreme values is briefly reviewed. This theory is concerned with the extreme values of a sequence $X_1, X_2, \cdots X_n$ of independent and identically distributed (with common distribution function F, say) random variables. The distribution of the maximum

$$M_n = \max(X_1, X_2, \cdots, X_n) \tag{1}$$

as the sample size n tends toward infinity is of interest. In addition, the distribution of the number of exceedances of a threshold

$$N_n = \sum_{i=1}^{n} \chi_{\{X_i > c_n\}} \tag{2}$$

where χ is the indicator function, is considered as the threshold c_n and sample size n both become large.

At least from a probabilistic point of view, the classical theory of extreme values has been derived in nearly complete generality (e.g., Leadbetter et al., 1983). This theory is developed in a parallel, if not completely analogous, fashion to that for averages. In place of the Central Limit Theorem, it can be shown that the distribution of the maximum M_n tends toward one of three possible distributions

(termed Type I, Type II, and Type III extreme value distributions). Specifically, if

$$\lim_{n\to\infty} \Pr\{a_n(M_n - b_n) \le x\} = G(x) \tag{3}$$

where $a_n > 0$ and b_n are normalizing constants, then the distribution function G must be one of three possible forms. For instance, the Type I extreme value distribution, most commonly applied in climatology, is given by

$$G(x) = \exp(-e^{-x}) \tag{4}$$

where, $-\infty < x < \infty$.
except for a change in location and scale.

Necessary and sufficient conditions for the three possible forms of distribution function G in (3) to arise depend upon the shape of the right-hand tail of the distribution function F of the individual random variables [i.e., the behavior of $1 - F(x)$ for large x]. The Type I extreme value distribution appears in (3) when F has an infinite right-hand tail [i.e., $F(x) < 1$ for all x] with $1 - F(x)$ decreasing to zero at a sufficiently fast enough rate as x tends to infinity. In particular, nearly all of the distributions (e.g., exponential, gamma, lognormal, normal, Weibull) commonly fit to individual observations of climate variables give rise to the Type I extreme value distribution as the limiting distribution for the maximum.

It can also be shown that the limiting distribution of the number of exceedances N_n is Poisson, if the threshold c_n is increased at such a rate that, as the sample size n increases, the mean number of exceedances of the threshold remains roughly constant. Specifically,

$$\lim_{n\to\infty} \Pr\{N_n = k\} = \frac{e^{-\tau}\tau^k}{k!} \tag{5}$$

where

$$\tau = \lim_{n\to\infty} n[1 - F(c_n)] \tag{6}$$

This Poisson approximation has been applied, for instance, to the exceedance of thresholds by time series of wind speeds (Ross, 1987) and to the occurrence of below freezing temperatures (Wavlen, 1988). Moreover, Revfeim and Hessell (1984) represent the sequence of occurrences of extreme events (e.g., wind gusts) as a Poisson process.

Persistence of Climate

Although the classical theory of extremes makes the asssumption of independence, it is well known that climate time series typically possess positive autocorrelation. This question of the effects of serial correlation on extremes has created much confusion among climatologists. In particular, it is apparently commonly believed that the concept of the 'effective number of independent samples' is relevant in accounting for the effects of dependence on extremes (e.g., Tabony, 1983). This claim is a blatant example of the misapplication of a theory based on means to extremes.

In an attempt to clarify this issue, the nature of the extension of the classical theory of extreme values to the case of weak dependence is briefly reviewed. Recall that the Central Limit Theorem for averages still holds for stationary processes with weak dependence, but the normalizing constant representing the standard deviation of a time average must be adjusted. In particular, the persistence of climate time series inflates the variance of a time average relative to the independent case. This adjustment for variance inflation has led to the concept of the 'effective number of independent samples' (e.g., Madden, 1979).

The effects of dependence on extreme values are, however, quite different. For weak dependence, the normalizing constants a_n and b_n in (3) for the limiting distribution of the maximum are exactly the same as in the independent case. Even the rate of convergence to the limiting extreme value

distribution has been shown in some cases (e.g., stationary normal process) to be essentially unaffected by dependence. Similarly, the Poisson limit (5) for the number of exceedances of a threshold still holds under weak dependence. In this regard, it has been suggested (e.g., by Buishand, 1986) that the Poisson approximation works better in practice for climate time series if 'clusters' of individual exceedances are combined into a single exceedance event.

The type of stochastic processes usually employed to model climate time series (e.g., autoregressive-moving average process) do possess weak enough dependence that the classical theory of extreme values is still in force. Specifically, when dealing with a stationary normal process, the dependence is weak enough if the autocorrelations $\rho_n = \text{Corr}(X_i, X_{i+n})$ tend to zero at a fast enough rate that

$$\lim_{n\to\infty} \rho_n \log n = 0 \tag{7}$$

An issue that does have significant implications for applications of the theory of extremes concerns whether climate time series actually possess stong dependence (or 'long memory'). Under strong dependence [when, in particular, (7) does not hold in the case of a normal process], other forms of limiting distributions for the maximum than the Type I, II, and III extreme value distributions are possible (Leadbetter et al., 1983). In this regard, the so-called Hurst Phenomenon, which concerns the behavior of the 'rescaled adjusted range' (a rather complex form of extreme value statistic), is exhibited by many time series considered in water resources research (e.g., precipitation, stream flow). One of the possible explanations for this phenomenon is strong dependence (Mandelbrot and Wallis, 1968). Given this combination of theoretical developments and empirical observations, it is surprising that this issue has received so little attention in the climatological literature.

Seasonal Cycles

Although the classical theory of extremes makes the assumption of identical distributions, climate time series naturally contain seasonal cycles. Several approaches have been proposed for dealing with this problem. One technique involves simply standardizing each random variable to remove any seasonal cycles that might be present in the mean and variance; that is, constructing a new sequence of random variables

$$X_i' = \frac{X_i - E(X_i)}{[\text{Var } (X_i)]^{\frac{1}{2}}} \quad . \tag{8}$$

The classical theory of extremes can then be applied to the standardized sequence X_1', $X_2', \cdots, X_n'$ (as has been done, for example, in the case of extreme wind speeds by Zwiers, 1987). Although this procedure is theoretically sound, it may leave much to be desired from a practical point of view. The method measures extreme values at different times within the year relative to their respective mean and variance, rather than in absolute terms. Such a measure would not be very meaningful for many climate impact studies in which thresholds for extreme values are taken as fixed quantities.

A second approach consists of applying extreme value theory separately to individual time periods (e.g., months or seasons) and then combining these results to obtain a single distribution for the annual maximum (Carter and Challenor, 1984). If it is assumed that the maxima for the individual time periods are independent, then the combined distribution is simply the product of the individual extreme value distributions. A debate has raged in the climatological literature over whether this method is superior to simply fitting a single extreme value distribution directly to the annual maxima (Tabony, 1983).

The classical theory of extreme values has also been extended to this particular case of nonstationary time series. Expressions showing how the normalizing constants a_n and b_n in (3) become more complex for periodically varying means have been derived (Horowitz, 1980; Leadbetter et al., 1983).

However, it is not clear how realistic some of these theoretical developments are for climatological applications. Ballerini and McCormick (1988), for instance, show that the form of limiting distribution for the maximum in the case of a stationary process with weak dependence and periodically varying mean and variance is determined by the period of maximal standard deviation. They use an example of time series of daily temperature to motivate the problem. However, temperature is generally most variable in the winter, not the season during which the annual maximum temperature ordinarily occurs!

Climate Impacts

As mentioned in Section 1, the need to consider extreme events in climate impact studies is now recognized. Mearns et al. (1984) addressed the question of how the probability of occurrence of an extreme event would change as the overall climate changes (e.g., in terms of means and variances). Extreme high temperature events, such as the maximum temperature on a single day or on a run of consecutive days exceeding a threshold, were considered. A simulation approach was employed to obtain numerical results concerning the relationship between the likelihood of these extreme events and the mean, variance, and autocorrelation of time series of daily maximum temperature. More insight into the nature of these nonlinear relationships could be provided by direct reliance on extreme value theory. Specifically, this approach would enable analytical results to be derived. If progress is to be made on factoring consideration of extreme events into climate impact assessment, then the theory of extreme values needs to be exploited.

Acknowledgements

Research supported in part by U.S. National Science Foundation (U.S.-Eastern Europe Cooperative Science Program) and Hungarian Academy of Sciences.

References

Ballerini, R., and W.P. McCormick, 1988: Extreme value theory for processes with periodic variances (abstract). *Advances in Applied Probability*, **20**, 9.

Buishand, T.A., 1986: Extreme value analysis of climatological data. *Third International Conference on Statistical Climatology*. Austrian Society of Meteorology, Vienna, Austria, pp. 145–158.

Carter, D.J.T., and P.G. Challenor, 1984: Comments on 'Extreme value analysis in meteorology' by R.C. Tabony (with reply by R.C. Tabony). *Meteorological Magazine*, **113**, 43–52.

Horowitz, J., 1980: Extreme values from a nonstationary stochastic process: An application to air quality analysis. *Technometrics*, **22**, 469–478.

Leadbetter, M.R., G. Lindgren, and H. Rootzen, 1983: *Extremes and Related Properties of Random Sequences and Processes*. Springer-Verlag, New York.

Madden, R.A., 1979: A simple approximation for the variance of meteorological time averages. *Journal of Applied Meteorology*, **18**, 703–706.

Mandelbrot, B.B., and J. Wallis, 1968: Noah, Joseph, and operational hydrology. *Water Resources Research*, **4**, 909–918.

Mearns, L.O., R.W. Katz, and S.H. Schneider, 1984: Extreme high-temperature events: Changes in their probabilities with changes in mean temperature. *Journal of Climate and Applied Meteorology*, **23**, 1601–1613.

Revfeim, K.J.A., and J.W.D. Hessell, 1984: More realistic distributions for extreme wind gusts. *Quarterly Journal of the Royal Meteorological Society*, **110**, 505–514.

Ross, W.H., 1987: A peaks-over-threshold analysis of extreme wind speeds. *Canadian Journal of Statistics*, **15**, 328–335.

Tabony, R.C., 1983: Extreme value analysis in meteorology. *Meteorological Magazine*, **112**, 77–98.

Tiago de Oliveira, J., 1986: Extreme values and meteorology. *Theoretical and Applied Climatology*, **37**, 184–193.

Waylen, P.R., 1988: Statistical analysis of freezing temperatures in central and southern Florida. *Journal of Climatology*, **8**, 607–628.

Wigley, T.M.L., 1985: Impact of extreme events. *Nature*, **316**, 106–107.

Zwiers, F.W., 1987: An extreme-value analysis of wind speeds at five Canadian locations. *Canadian Journal of Statistics*, **15**, 317–327.

Bayesian error update of climatological distributions

A.R. Boehm
ST Systems Corporation, Lexington MA, USA

Abstract

The natural variability of weather causes noticeable error in specifying climatological distributions. Estimating this error is necessary to provide design engineers with the risk of exceeding a value. The binomial distribution gives the probability of a sample (iid) being above a given value. Thus, given a sample and a suitable prior distribution, Bayes law shows that the beta distribution gives the error in probability for a given value. One way to specify a beta distribution is with a mean and a sample size. Given that the beta mean can be specified for any value of the climatological distribution, the error in probability (fractile error) can then be calculated for any value. In addition, since the beta distributions continuously varying with value provide a joint density in fractile/value space, the error distribution for value at a specified fractile can also be calculated.

Weather samples are not independent. An equivalent independent sample size, $N_{\equiv}$, provides a method of taking dependence into account when specifying error. However, $N_{\equiv}$ for the variance of a sample can be quite different than $N_{\equiv}$ for distribution error. This difference is true in theory, e.g. a first order ARMA process, and with observed weather data. $N_{\equiv}$ has been investegated for several weather elements in particular sky cover and total sunshine.

The same theory can be used to specify error in spatial interpolation schemes. $N_{\equiv}$ is used both as a weight to account for the relative error among observation sites (due either to different observation instruments or periods of record) and is itself analysed in space taking into account the increase in error with increasing distance from observations.

References

Boehm, A., 1987: A parametric objective analysis of climatological cloud distributions. *Preprints 10CPS(AMS)*,Edmonton

Assessment of recent great Salt Lake climatic conditions using a Box-Jenkins model

R.C. Balling
Department of Geography, Arizona State University, Tempe AR, USA

Abstract

ABSTRACT. Between September, 1982 and June, 1983, the Great Salt Lake in western Utah rose an unprecedented 1.5 m resulting in serious economic and environmental damage in the area. Several researchers analyzed snowfall, temperature, and precipitation data from the watershed and concluded that the climatic events leading to the rise in the lake have a recurrence interval of about 100 years. Other information suggested a much longer recurrence interval for the unusual climatic events of the early 1980s. In this investigation, a Box-Jenkins model is applied to the long-term (1848-1987) water levels of the Great Salt Lake. The residuals from the model show that the recent disruption in lake levels is more than twice as large as any previous change in the 140-year record. Further statistical analysis of the Box-Jenkins residuals produces a recurrence interval of approximately 7000 years for the recent rise in the lake; the result is an order of magnitude higher than most previous estimates. The Box-Jenkins modeling approach used in this study appears to be useful in assessing a multi-dimensional departure from "normal" climatic conditions.

A framework for interpreting rainfall models

K.J.A. Revfeim
Meteorological Service, Wellington, NZ

Introduction

The appearance of phrases such as 'a new distribution' or 'a new method' in summaries or abstracts of papers on geophysical subjects is inclined to leave a reader somewhat skeptical about the substance of the claim. If it is a 'new' variant then the question will be - is it better? Finally while the criteria for judging how it is better may be sound for comparative purposes, the logic, realism or descriptive use of the statistical model underlying the geophysical process may make the claim presumptious.

The words 'new' or 'improved' most often describe increases in mathematical or statistical complexity unrelated to physical limitations on the process. For example the usual form of the 3-parameter (so-called) Generalised Extreme Value (GEV) distribution, considered as an advance on the 2-parameter Extreme Value(EV) distribution, sets upper or lower limits on the data range depending on whether the introduced third parameter is positive or negative. Usually there is no restriction on parameter sign in the estimation method and in most published examples the estimates of the index k take negative values. Thus by implication the process still has no upper bound which perpetuates the conceptual contradiction in flood studies of 'improved' predictions of mean maxima using GEV and probable **maximum** precipitation or flood (PMP or PMF). Justification for such studies seems to be that it involves more parameters to describe the process so it must be better.

Physical questions concerning the processes underlying rainfall totals or maxima can be built into statistical models for data analysis. After analysis questions can be asked about how well the physically meaningful model parameters represent mean or maximum numbers of events (rates of occurrence) or event sizes for particular regions or locations . Empirical models include:-

Parameters	Extremes	Total Amounts
2	Gumbel (Type I EV) Frechét (Type II EV) Weibull (Type III EV)	Gamma (Γ) Log-normal Kappa (Mielke, 1973)
3	Jenkinson (GEV, 1955) Generalised Pareto (van Montfort & Witter, 1986) Log-logistic (Ahmad *et al*, 1988)	Generalised Gamma Shifted log-normal
4	Two-component EV(TCEV Rossi *et al*,1984)	TC total amount(TCTA)
5	Wakeby (Greenwood *et al*, 1979)	

Assessment of which distribution(s) give better (or best) representations of past data is usually based on goodness of fit or accommodation of 'outliers'. However one should always be aware of the falsity of trying to model a mixture of processes or régimes with an over-simplified model or without some judicious censoring or prior classification (Klemeš, 1986). Eventually the direction, if any, of further generalisation becomes difficult to justify and is usually tempered by problems with parameter estimation. On the other hand there is a quite natural progression in extending simple models based on assumptions about processes underlying rainfall extremes or totals. Some of these process generated models have direct analogues in the empirical distributions while others show up some of the unrealistic expectations of 'improvement' in the empirical search for 'truth'.

Physical models

The simplest 2-parameter physical models of rainfall maxima and totals are well documented in the literature; see Revfeim (1983) for other references. Assuming a Poisson distribution of event occurrence (at rate ρ) and an exponential distribution of event sizes (with mean μ) we get the distribution function for maxima (within a prescribed time interval)

$$G_2(x) = (\exp[-\rho e^{-x/\mu}] - e^{-\rho})/(1 - e^{-\rho}) \tag{1}$$

and density function for totals

$$h_2(x) = x^{-1} e^{-\rho - x/\mu} \sum_{r=1}^{\infty} (\rho x/\mu)^r / r!(r-1)! \tag{2}$$

There are obvious extensions to 3-parameter models by including the more realistic assumption of Gamma or Weibull distributed sizes with non-zero mode i.e. the most frequent amount in a rainfall event is not zero! Relaxation of the point process model can also be made assuming independent exponential distribution of durations (Rodriguez-Iturbe *et al* , 1984; Revfeim, 1985). Various other ways of introducing a third parameter might be tried such as including some stochastic dependence in size or occurrence (Leadbetter *et al*, 1989), or in some negative exponential relationship between size and occurrence.

In the point process model above it is assumed that the size and number of events is unbounded, or at least that the effects in the underlying distribution tails is negligible. Natural 3-parameter generalisations are obtained by including a size limit parameter (representing the concept of probable maximum precipitation PMP) or the maximum number of events that can occur in finite time (the quasi-binomial nature of synoptic events). For example if we retain Poisson occurrence but assume that event sizes have a Beta distribution with $F(x) = 1 - (1 - x/\mu\eta)^{\eta}$ then the distribution of extremes becomes

$$G_{31}(x) = \{\exp[-\rho(1 - x/\mu\eta)^{\eta}] - e^{-\rho}\}/(1 - e^{-\rho})$$

If $e^{-\rho}$ is negligible G_{31} is easily recognised as an analogue of the so-called Generalised Extreme Value distribution (Jenkinson, 1955) but restricted to positive values of η and defined on the range $0 \le x \le \mu\eta$.

On the other hand if we retain exponentially distributed sizes but assume that the number of events have upper limit λ, and occurrences have a binomial distribution with mean rate ρ, then it is easy to show that

$$G_{32}(x) = \{(1 - \rho e^{-x/\mu}/\lambda)^{\lambda} - (1 - \rho/\lambda)^{\lambda}\}/\{1 - (1 - \rho/\lambda)^{\lambda}\}$$

If $(1 - \rho/\lambda)^{\lambda}$ is negligible we have the alternate exponential limit form of the EV which is surely just as general as $G_{31}(x)$. Better still G_{31} and G_{32} have physical interpretations and could be used appropriately depending on whether a bound on the size of event or number of events was the dominant constraint. Further details are given in Revfeim (1989).

Both of the above 3-parameter generalisations can equally be applied to the Compound Poisson distribution of totals h_2 although they do not lead to convenient closed forms; for instance the Beta distribution does not have the additive reproductivity of the Gamma distribution. However expressing the moments of these distributions in terms of the parameters is quite straightforward and can be used to test the realism of estimated bounds if there are feasible solutions to the moment equations.

Additional parameters can be introduced with powers of data values ($x^{\nu}, \nu > 1$ similar to Weibull replacing exponential) to give more realistic non-zero modality of event size, or by adding some form of dependence. However allowing for sensitivity to, and the practical use of, increasingly sophisticated models there is perhaps more purpose in considering a mixture underlying extremes or totals.

Mixtures

Concurrent weather processes or alternate régimes are often recognised by the description of types of events or the nature of seasons (e.g. state of ENSO index). First we need to establish the clear distinction between a distribution arising from a mixture of two (or more) concurrent processes and a mixture of two (or more) alternate régimes. Suppose we have two Poisson processes of events occurring at rates ρ_1, ρ_2 where each event has size distribution F_1, F_2 respectively. Distributions arising from these two types of mixtures are set out below where the probalilities of the alternate régimes are p and $q = 1 - p$.

	Concurrent Processes	Alternate Régimes
All observations	$(\rho_1 F_1 + \rho_2 F_2)/(\rho_1 + \rho_2)$	$(p\rho_1 F_1 + q\rho_2 F_2)/(p\rho_1 + q\rho_2)$
Maxima	$G_1 G_2$	$pG_1 + qG_2$
Totals	$e^{-\rho_2} H_1 + e^{-\rho_1} H_2 + H_1 \otimes H_2$	$pH_1 + qH_2$

In the pdf array G_j, H_j correspond to equations (1), (2) and the convolution $H_1 \otimes H_2$ corresponds to the combined total from joint occurrence of both processes.

The concept of two component processes underlying maxima has been considered by Waylen and Woo(1982; who by classifying floods into rainfall-generated or snowmelt-generated were really monitoring alternate régimes) and Rossi *et al* (1984). In the latter case the TCEV may be written in terms of recurrence rates $\rho \pm \epsilon$ and sizes $\mu \pm \delta$ as

$$\begin{aligned} G_4 &\approx \exp\{-(\rho+\epsilon)e^{-x/(\mu+\delta)} - (\rho-\epsilon)e^{-x/(\mu-\delta)}\} \\ &\approx \exp\{-2\rho e^{-x}[1 - \sigma x/\mu + \tau(x/\mu)^2]\} + O(\delta/\mu)^3 \end{aligned}$$

where $\sigma = (\delta/\mu)(\delta/\mu - \epsilon/\rho)$ and $\tau = (\delta/\mu)^2/2$. While it is possible to derive approximate equations for moment and maximum likelihood (ML) estimates of the parameters they may not provide a feasible solution. It seems more important to question the lack of realism in an implied underlying mixture of **exponentially** distributed event sizes. Unexceptional events with mode near zero might be approximated by the exponential distribution. However one would expect that the alternate component of a mixture would have a significantly non-zero mode; at least if it was expected to be distinguishable from 'ordinary' events. Thus a model with relatively high order gamma or similarly distributed event sizes would seem to be more applicable. Such a model was considered for dealing with the mixture of 'regular' storms and rare tropical cyclone events in Revfeim(1986).

Two-component total amounts(TCTA) could be expressed empirically as the sum of two gamma distributed values but for the parameters to be estimable the two modes need to be readily distinguishable in a histogram. Such observations would seem to be rare in the 'noisy' histograms of real rainfall data although there are exceptions e.g. Landsberg(1975).

Similar to the considerations for maxima above a more realistic approximation might be the sum of a compound Poisson variate and a lower rate alternate Poisson process of non-zero-modal distributed sizes. Of course this introduces a fifth parameter for the modality of the sizes. Assuming that there are conceptually plausible models for two-component processes with tractable methods for estimating parameters then results from analysis of totals should give parameter estimates comparable with the analysis of maxima particularly over typical event duration times such as 1 or 2 days.

Alternate régimes

This class of models does not appear to have received much attention (at least in the literature) but it does pose some of the questions about rainfall data that one might seek an answer to. For instance is there any evidence that in some years (or rainfall seasons) there are greater rainfall amounts from similar numbers of event occurrences? Or are the data representative of régimes with differing rates of occurrence but similar event sizes? At least in the latter case there might be supporting information from data on numbers of days with rain or counted frontal passages.

The case of the same exponentially distributed event sizes with mean μ, and Poisson occurrence with differing rates $\rho \pm \epsilon$ is a 4 parameter estimation problem for régime probabilities p, q with moment solution (if it exists) for total amounts obtained from

$$\begin{aligned} L_2 &= k_2 - 2\mu k_1 &&= 4pq(\epsilon\mu)^2 \\ L_3 &= k_3 - 6\mu(k_2 - \mu k_1) &&= -8pq(p-q)(\epsilon\mu)^3 \\ L_4 &= k_4 - 12\mu(k_3 - \mu(3k_2 - 2\mu k_1)) &&= 16pq(1-6pq)(\epsilon\mu)^4 \end{aligned}$$

where k_1, k_2, k_3, k_4 are the first four cumulants, leading to a quartic in μ, $L_2L_4 - L_3^2 + 2L_2^3 = 0$. If a solution exists then $\hat{p} = \{1 + [1 - 1/(1 + L_3^2/4L_2^3)]^{1/2}\}$, $\hat{\epsilon}$ is obtained from the relationship L_2, and $\hat{\rho}$ from the mean $k_1 = \mu[\rho + \epsilon(p - q)]$.

The complementary case of two régimes with the same rates of occurrence ρ but differing exponentially distributed sizes with means $\mu \pm \delta$ may provide a moment solution from

$$\begin{aligned} L_2 &= \rho a_2/r_1 - a_1^2 &&= 4pq(\delta\rho)^2 \\ L_3 &= \rho a_3 r_1/r_2 - a_1 a_2 &&= 8pq\mu(\delta\rho)^2 r_1 \\ L_4 &= \rho a_4 r_1^2/r_3 - a_2^2 &&= 16pq(\mu\delta\rho r_1)^2 \end{aligned}$$

where a_1, a_2, a_3, a_4 are the first four raw moments and $r_1 = 2 + \rho$, $r_2 = 6 + 6\rho + \rho^2$, $r_3 = 24 + 36\rho + 12\rho^2 + \rho^3$. The resulting equation is of order 7 in ρ and $L_2L_4 - L_3^2 = 0$ has at least one real root but the existence of real solutions for the other parameters p, μ, δ is still not assured.

In a purely empirical setting the right skewed tail would invite a 'normalising' transform. The usual Taylor series expansion shows that a square- root transform of an $h_2(x)$ CP variable has approximate mean $\sqrt{\rho\mu}(1 - 1/4\rho)$ and variance $\mu/4$, and a logarithm transform has approximate mean $\ln(\rho\mu) - 1/\rho$ and variance $2/\rho$. This provides a possible ML solution for both cases of constant μ and constant ρ which translate to an mixture of approximately normal variables with constant variance. Rao's(1948) solution to a mixture of normal variables with different means and constant variance is a simplification of the original 5-parameter (including different variances) problem of Pearson(1894) with its nonic equation solution for moment estimates. The 5 parameter model of a mixture of régimes with different event sizes and rates of occurrence is likely to be as elusive in application as the search for mixtures of normal distributions.

Analyses of maxima from alternate régimes ($pG_1 + qG_2$) for typical event durations such as 1 day should give supporting parameter estimates; moment solutions are tractable but unattractive.

Examples

The clear bimodiality in annual rainfall totals for Dakar(Landsberg, 1975) invites fitting of an alternate régime model to Sahel region data. Data for the period 1896-1983 (kindly supplied by P.D. Jones) were first analysed assuming the simple single process model $h_2(x)$ given by (2) with results as shown in Table 1.

Table 1. Mean recurrence rates $\hat{\rho}$ and mean event sizes $\hat{\mu}$ for Dakar rainfall.

Month	$\hat{\rho}$ (events/month)	$\hat{\mu}$ (size/event)	Mean total (mm)
June	1.5	9.8	14
July	3.6	22.4	80
August	6.7	32.9	219
September	9.3	15.7	146
October	1.9	23.6	44
November	0.3	9.3	2

Initial estimates were then made for the alternate régime model assuming constant ρ or μ. The results in Table 2 show greater consistency for constant μ than constant ρ and would encourage further enquiry as to the mixed model representativeness of the rainfall climate in the Sahel region.

Table 2. Moment (MO) and maximum-likelihood (ML) estimates of alternate régime (probabilities $p, 1-p$) parameters.

Month		same rate/different amounts				different rates/same amount			
		$\hat{p}$	$\hat{\rho}$	$\hat{\mu}$	$\hat{\delta}$	$\hat{p}$	$\hat{\rho}$	$\hat{\epsilon}$	$\hat{\mu}$
June	MO	0.33	5.5	1.6	2.7	0.17	0.3	4.8	4.1
	ML	0.21	2.1	3.9	3.9	0.69	4.3	3.2	4.5
July	MO	0.49	8.1	9.9	5.3	0.25	5.2	5.2	10.3
	ML	0.55	1.1	114.6	4.4	0.67	4.9	1.8	18.8
August	MO	0.40	20.1	10.0	4.5	0.45	18.2	8.0	11.5
	ML	0.41	1.9	146.9	12.3	0.46	6.8	1.0	31.8
September	MO	0.47	17.7	8.1	2.7	0.26	14.9	7.3	7.9
	ML	0.46	11.9	12.1	3.3	0.43	9.7	1.4	14.6

Conclusions

The application of 3, 4 or 5 parameter statistical distributions from the 'standard' repertoire to rainfall data may occasionally show a 'better fit' of a particular distribution under certain comparison criteria. For a different data period for the same station or for different locations it may be found that the distribution is not the best. That is justification for a model may not be universal and the practitioner is unable to identify the problem because the parameters do not have a physical interpretation.

Generated models of rainfall processes can provide as much variety of shape in statistical distribution as the standard repertoire. The nature of the local rainfall climate can be included in the model as interpretable parameters. Limits on the numbers of synoptic rainfall events that might occur can be estimated as well as upper bounds on the size of events. Refinements to these models are an orderly procedure within a natural framework but are restricted for the present by problems of identification and parameter estimability.

References

Ahmad, M.I., Sinclair, C.D. and Werrity, A., 1988: Log-logistic flood frequency analysis. *J. Hydrology* **98**, 205-224.

Greenwood, J.A., Landwehr, J.M., Matalas, N.C. and Wallis, J.R., 1979: Probability weighted moments: definition and relation to parameters of several distributions expressible in inverse form. *Water Resour. Res.* **15**, 1049-1064.

Jenkinson, A.F., 1955: The frequency distribution of the annual maximum (or minimum) values of meteorological elements. *Quart. J.R. Met. Soc.* **81** , 158-171.

Klemeš, V., 1986: Dilettantism in hydrology: transition or destiny? *Water Resour. Res.* **9**, 177-188.

Landsberg, H.E., 1975: Sahel drought: change of climate or part of climate? *Arch. Met. Geoph. Bioklim.* **B 23**, 193-200.

Leadbetter, M.R., Weissman, I., de Haan, L., Rootzén, H., 1989: On clustering of high values in statistically stationary series. *Proc. 4IMSC*(Rotorua), ??

Mielke, P.W., 1973: Another family of distributions for describing and analysing precipitation data. *J. Appl. Met.***12**, 275-279.

Pearson, K., 1894:Contributions to the mathematical theory of evolution. *Phil. Trans.* **A 185**, 71-110.

Rao, C.R., 1948: Problems of bilogical classification. *J. Roy. Stat. Soc.* **B 10**, 159-193.

Revfeim, K.J.A, 1983: Stochastic process analysis rainfall totals and extremes. *Proc. 2IMSC*(Lisbon), 10.2.1-5.

_____, 1984: An initial model of the relationship between rainfall events and daily rainfalls. *J. Hydrol.* **75**, 357-364.

_____, 1986: Proverbial outliers. *Proc. Pacific Stats. Congress* (Elsevier), 296-298.

_____, 1989: Extremes of observations bounded by a limit on size of event or a limited number of events. *(unpublished).*

Rodriguez-Iturbe, I., Gupta, V.K., and Waymire, E., 1984: Scale considerations in the modeling of temporal rainfall. *Water Resour. Res.* **20**, 1611- 1619.

Rossi, F., Fiorentino, M., and Vesace, P., 1984: Two-component extreme value distributions for flood frequency analysis. *Water Resour. Res.* **20**, 847-856.

van Montfort, M.A.J., and Witter, J.V., 1986: The generalized Pareto distribution applied to rainfall depths. *J. Hydrol. Scs.* **31**, 151-161.

Waylen, P., and Woo, M., 1982: Prediction of annual floods generated by mixed processes. *Water Resour. Res.* **18**, 1283-1286.

Statistical problems of climate monitoring

G.V. Gruza
Hydromet Centre, Moscow, USSR

Abstract

Monitoring of changing climate became nowadays a new important task of climatology. The goal of climate monitoring (CM) is: collecting and summarizing of climatic data and determination of characteristics of current Earth climate, probabilistic evaluation of anomaly range of climate system state, revealing of natural and man-induced causes of observed anomalies and maybe also the estimate of scales of probable climate changes in the future. While determining CM a distinction should be made between operative monitoring of climate system parameters and CM as a scientific problem.

On air temperature data a set of statistical parameters is proposed that enables us to characterize anomalies of different scales and purposes in compatible unities. Statistical characteristics of Climate anomality indices for spatial and for different time intervals and methods of visual representation of climatic trends are presented.

References

Angell, J.R., and Gruza, G.V., 1984: Climate variability as estimated from atmospheric observations. In *The Global Climate*(Ed. J.J. Houghton) CUP, 25-36.

Gruza, G.V., and Ran'Kova, E.Ja., 1980: Structure and variability of observed climate: Northern hemisphere air temperature. *Hydrometeoizdat*(in Russian), 72pp.

Gruza, G.V., 1986: Monitoring and probability forecast of monthly and seasonal variations in hemisphere atmospheric processes. In *Long-Range Forecasting Report Series VI* 11, WMO/TD-87, 682-688.

Identification of a time varying transfer function model for the variations of air temperature

H. Madsen
IMSOR Technical University, Lyngby, Denmark

J. Holst
Dept. Math. Stats, Univ. Lund, Sweden

Introduction

Transfer functions models are frequently used for describing relations between climate variables, but, traditionally, only models with constant coefficients (i.e. homogeneous models) are considered. However, it is well known that the dynamical behavior of many climatological phenomena show variations in time. In these cases timevarying (i.e. inhomogeneous) models should be determined and studied in order to get a more adequate process description.

In Madsen et. al. (1987) a homogeneous continuous time model for the variations of air temperature is proposed. The model relates the variation of air temperature to the variations of the ground level net radiation. Thereby the well-known asymmetries of the diurnal variations of air temperature (e.g. Hansen and Driscoll, 1977) are explained as effects of the variation of net radiation. But, physical arguments and data suggest an annual variation of the dynamical characteristics, which is not described by the homogeneous model.

This paper describes the formulation and estimation of a timevarying stochastic transfer function model for the variations of the surface layer air temperature. The net radiation at ground level is exploited as an external input process. The variation in time of the dynamical relation is found by recursive estimation of the parameters in a homogeneous transfer function model. A recursive least squares estimation technique including exponential forgetting is used.

The observed trajectories of the recursively estimated parameters confirm the annual variation of the dynamical relation. It is shown that the variation for some of the parameters is negligible, i.e. they can be regarded as constant, while for the rest of the parameters the annual variation can be described by a few terms in the fourier expansion of the periodic parameter trajectory. Finally, such an inhomogeneous model is identified and its parameters are estimated by a maximum likelihood technique.

The data

In the analysis nearly seven years of hourly observations of both air temperature and net radiation have been used. The observations are taken at the climate and water balance station Højbakkegaard, which is situated about 20 km west of Copenhagen, Denmark. The station is freely exposed and surrounded by ordinary agricultural fields, and the soil at the experimental site is covered by dense and short grass.

The air temperature is measured two meters above the ground by a resistance thermometer in a convective open box. The net radiation is measured by a polyethylene shielded net radiometer constructed at the Royal Danish Veterinary and Agricultural University (Jensen and Aslyng, 1967). The radiometer is mounted one meter above the ground. The signals from the thermometer and the radiometer are measured every 10 minutes. From the measured values hourly averages are constructed, and these hourly values are used in this investigation.

Formulation of a transfer function model

The energy balance at the surface of the earth relates the net radiation R_n to the various heat fluxes as

$$R_n = H + LE + G \tag{1}$$

where H, LE and G are the sensible, latent and soil heat flux, respectively. The sensible heat flux is accomplished by a vertical gradient of the air temperature, and the variations of air temperature just above the ground is thus closely related to the variation of net radiation. The magnitude of the various terms in (1) depends on a variety of factors, as e.g. wind speed, roughness length, humidity deficit in the air, vegetation and the amount of available water in the soil. Virtually all these factors are varying in time. Hence, it is reasonable to conclude that a dynamic model, which describes the variations of air temperature by using the net radiation as explanatory variable, has to be timevarying.

It is well known that the overall averaged diurnal variation of air temperature is asymmetric, the time interval from the minimum to the maximum is less than that from the maximum to the minimum. In stochastic models (e.g. Hansen and Driscoll (1977) and Hittle and Pedersen (1978)) the diurnal variation of air temperature is typically described by harmonics, determined by Fourier analysis, and the deviations from the harmonic functions are considered as noise and typically described by autoregressive models. The asymmetry in the diurnal variation is then accounted for by introducing higher harmonics.

In Madsen et al. (1987) a homogeneous linear second order differential equation in state space form was suggested for the variations of air temperature. The structure of the model was based upon simple assumptions about the most important heat capacities and transfers in the physical system. The net radiation was taken as an exogenous variable. Thereby the asymmetries of the diurnal variations of air temperature are explained as effects of the variation of net radiation, which is almost constant during the night but exhibits the typical 'half cosine' variation at daytime, due to the contribution from the global radiation.

By integrating the differential equation in Madsen et al. (1987) through the sample interval, $[t, t+1[$, a discrete time representation of the state space model can be achieved. The transfer function is then obtained by eliminating the state space variable.

Let $T(t)$ and $R_n(t)$ denote the air temperature and net radiation at time t, respectively. By introducing the back shift operator q^{-1} (defined by $q^{-1}T(t) = T(t-1)$) and polynomials of order n_a, n_b and n_c of the form $P(q^{-1}) = p_0 + p_1 q^{-1} + \cdots + p_{n_p} q^{-n_p}$ where $a_0 = c_0 = 1$, the transfer function can be written

$$A(q^{-1})(T(t) - \overline{T}) = B(q^{-1})(R_n(t) - \overline{R}_n) + C(q^{-1})\epsilon(t) \tag{2}$$

where $\overline{T}$ and $\overline{R}_n$ are the the long term averages of the air temperature and net radiation, respectively. The error term $\epsilon(t)$, which accounts for both measurement disturbances and model approximations, is assumed to be Gaussian distributed white noise with zero mean and variance R.

Variations in time of the dynamical parameters

Due to the previously discussed variation in time of wind speed, soil humidity, vegetation, etc., the parameters in the transfer function model are expected to vary in time. In this section a simple method for tracking or adapting regular and slow changes in the time-dependent dynamical relation is discussed.

Let us write the transfer function (2) in the form

$$A(q^{-1})T(t) = B(q^{-1})R_n(t) + d + C(q^{-1})\epsilon(t) \tag{3}$$

where d is defined as $d = A(1)\overline{T} - B(1)\overline{R}_n$.

The model structure in (3) is linear in the parameters, and the model can be written in the common linear form $T(t) = \phi^T(t)\theta + \epsilon(t)$ where

$$\begin{aligned} \phi(t) &= [-T(t-1)\cdots - T(t-n_a)\, R_n(t)\cdots R_n(t-n_b)\epsilon(t-1)\cdots\epsilon(t-n_c)\, 1\,]^T \\ \theta &= [a_1\cdots a_{n_a}\, b_0\cdots b_{n_b}\, c_1\cdots c_{n_c}\, d\,]^T \end{aligned}$$

In the **recursive least square** (RLS) method the estimate at time t of the constant parameter θ is found as $\hat{\theta}(t) = arg\min_\theta S(\theta, t)$ where

$$S(\theta,t) = \sum^{t}(T(s) - \phi^T(s)\theta)^2 = S(\theta, t-1) + (T(t) - \phi^T(t)\theta)^2 \tag{4}$$

If S is quadratic in θ (which is the case if $n_c = 0$) then the minimum is obtained by a single Newton-Raphson iteration

$$\hat{\theta}(t) = \hat{\theta}(t-1) - H_S(\hat{\theta}(t-1), t)^{-1}\nabla_\theta S(\hat{\theta}(t-1), t)$$

where H_S is a matrix containing the second partial derivatives of $S(\hat{\theta}(t-1), t)$ - the Hessian matrix. If $S(\theta, t)$ is quadratic in θ, the Hessian matrix is independent of θ. Hence it follows from (4), that

$$H_S(t) = H_S(t-1) + 2\phi(t)\phi^T(t)$$

and, since $\hat{\theta}(t-1)$ is the minimum at time $t-1$,

$$\nabla_\theta S(\hat{\theta}(t-1), t) = -2\phi(t)[T(t) - \phi^T(t)\hat{\theta}(t-1)]$$

Now introducing $P^{-1}(t) = H_S(t)/2$ the recursions become

$$\begin{aligned} \hat{\theta}(t) &= \hat{\theta}(t-1) + P(t)\phi(t)\epsilon(t) \\ \epsilon(t) &= T(t) - \phi^T(t)\hat{\theta}(t-1) \\ P^{-1}(t) &= P^{-1}(t-1) + \phi(t)\phi^T(t) \end{aligned} \tag{5}$$

If $n_c > 0$ then $S(\theta, t)$ is not quadratic in θ, and the minimum is not obtained in a single step. The recursions can, however, be used anyhow, and converge in most cases to the true estimates (Ljung and Söderström, 1983). The procedure is then called the recursive extended least square (RELS), and is a kind of recursive pseudo linear regression (RPLR).

In the **exponential forgetting method** for estimation of a timevarying parameter, $\theta(t)$, the criterion includes an exponentially decaying weight of the old observations

$$S(\theta(t), t) = \sum^{t}\lambda^{t-s}(T(s) - \phi^T(s)\theta(t))^2 = \lambda S(\theta(t), t-1) + (T(t) - \phi^T(t)\theta(t))^2$$

where $0 < \lambda < 1$. That is, in every step only a part, λ , of the old information is reused. It is readily seen that the only difference, compared to (5), is in the recursion for $P(t)$, which becomes

$$P^{-1}(t) = \lambda P^{-1}(t-1) + \phi(t)\phi^T(t)$$

The effective number of observations behind the information is constant and equal to $N_\lambda = \sum_{i=0}^{\infty}\lambda^i = 1/(1-\lambda)$.

Different values of the forgetting factor, λ , have been considered, and $\lambda = 0.999$ is found adequate in order to obtain rather insensitive estimates of the long term variations of the dynamics. For the order of the polynomials in the transfer function, the values $n_a = 3$, $n_b = 2$ and $n_c = 0$ have proved

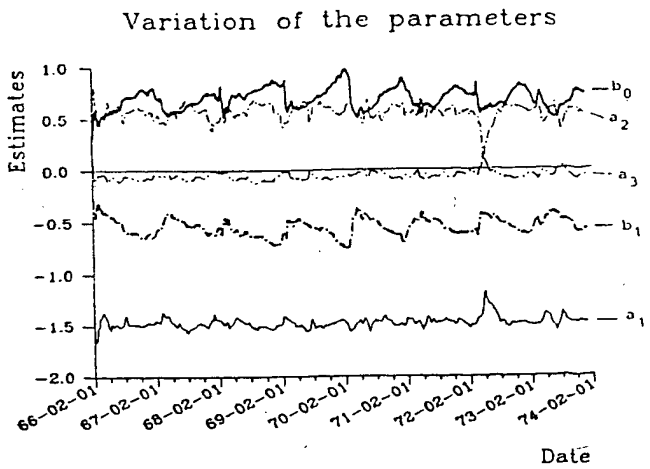

Figure 1: Trajectories of recursive estimates with $\lambda = 0.999$ of the parameters in the transfer function model (3) with $n_a = 3$, $n_b = 2$ and $n_c = 0$.

to be reasonable (Madsen, 1985). The trajectories of the parameters during the almost seven year period used, are shown on Figure 1.

Some variation in the parameters is observed and an annual variation is seen for b_0, b_1 and perhaps a_2. A clear annual variation of the parameters belonging to the A-polynomial is rather difficult to observe in Figure 1; but - as will be shown in the next section - a different parameterization of the polynomial may show a clear annual variation.

The method is readily generalized to variable forgetting, where the idea is to adjust the forgetting, $\lambda(t)$, according to the actual fit of the model. For the actual data an application of the variable forgetting method (Madsen, 1985) has shown almost the same results as for the constant forgetting method. For a description of several recursive estimation methods for timevarying dynamic systems, see Ljung and Söderström (1983).

A parameterization of an inhomogeneous model

It is noticed from Figure 1 that the trajectory for b_1 is very similar to that of b_0, but of opposite sign. This may indicate that the zero of the B-polynomial is constant. For a parameterization of the annual variation of the parameters, the B-polynomial is thus conveniently rewritten as $B(q^{-1}) = b_0(1 + b_1/b_0 q^{-1})$ where the annual variation then is described by b_0, while b_1/b_0 is constant.

An investigation of the variation in time of the poles of the A-polynomial has shown a very clear annual variation for the pole nearest the unit circle in the complex plane. The variation of this pole, called p_1, is shown in Figure 2(a). This pole is obviously large during the winter - especially in January and February - and small in the autumn. Since only the pole p_1 in the A-polynomial exhibits a clear annual variation, it seems natural, in order to obtain a reasonable parameterization, to rewrite the polynomial as $A(q^{-1}) = (1 - p_1 q^{-1})(1 + a_1' q^{-1} + a_2' q^{-2})$ where a_1' and a_2' are fixed in time.

Based on (3) we introduce

$$\gamma = d/A(1) = \bar{T} - \frac{B(1)}{A(1)}\bar{R}_n = \bar{T} - H(1)\bar{R}_n$$

where $H(1)$ is the stationary gain in the transfer function from the net radiation to air temperature. The value of γ is thus a measure of the difference between the stationary value of the air temperature and the stationary temperature induced by the stationary net radiation. If the recursive estimation with exponential forgetting and an appropriate forgetting factor are used, then γ thus expresses that

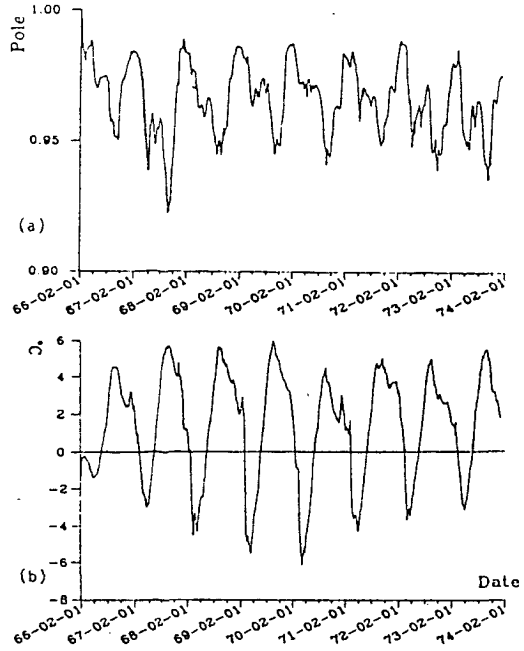

Figure 2: Trajectories of (a): p_1; and (b) γ. Forgetting factor and transfer function as in Figure 1.

part of the long term variation of air temperature, which is not describable by the long term variation of the local net radiation. The variations in time of γ are shown in Figure 2(b).

A very clear annual variation is observed also for γ. The quantity is seen to be negative in spring and positive in autumn. This means, for instance, that the local air temperature in the spring is lower (on average about $4°C$) than expected due to the local net radiation. The reason is most likely that the temperature of the air masses is influenced by the rather cold surrounding sea and oceans.

Although a very clear annual pattern is observed for γ, it is evident that the variations of two different years are not identical. Consider, for instance, the local minimum in Figure 2(b) - the minimum is still decreasing until 1970 and afterwards an increase seems to begin. This pattern is perhaps due to long term climatic variations. It is believed that recursive estimated signals, as γ, can be helpful in tracing or recognizing climate cycles or changes.

In summary, it seems reasonable to consider the following **inhomogeneous transfer function** model

$$(1 - p_1(t)q^{-1})(1 + a_1'q^{-1} + a_2'q^{-2})(T(t) - \gamma(t)) = b_0(t)(1 - z_1q^{-1})R_n(t) + \epsilon(t) \qquad (6)$$

The variation in time is thus limited to a variation of p_1, b_0 and γ. For these parameters a very clear annual variation is found. A fully adequate description of these annual variations must be based on stochastic models for the parameters or parameter models that includes the dependence of external factors. However, it seems natural, as a first approximation, due to the regularity of the observed annual variation, to consider deterministic harmonic functions as a parameterization of the annual variation of p_1 , b_0 and γ. Hence, some terms of a Fourier expansion of the mean annual parameter variation can be used in the parameterization. Estimates for a_1', a_2' and z_1 in the inhomogeneous model (6) can be found by the maximum likelihood method under a Gaussian assumption for $\epsilon(t)$. This is shown and more deeply discussed in Madsen (1985).

Summary

The identification of a timevarying transfer function model for the variation of air temperature is outlined. The model takes the net radiation as an external input process.

As a starting point for the identification the variation in time of the parameters in a homogeneous transfer function model is found using a recursive least square estimation technique including

exponential forgetting. By selecting a reasonable parameterization it turns out that a clear annual variation is obtained for some of the parameters, while others could be considered as constant. The annual variation of the parameters can be approximated by deterministic harmonic functions.

The trajectories of the recursively estimated parameters show, besides the systematical annual variation, also variations of apparently random nature. Future work will concentrate on research, aiming at models which contains a description of both the systematical annual variation and the random variation of the parameters. Models including dynamical models for the variation in time of parameters have previously been discussed by e.g. Young (1984).

The recursive estimation technique including a forgetting structure is frequently used for tracking changes in dynamical systems. In climatology it is believed that this estimation technique will prove as a method for filtering out signals, by which climatic changes and cycles, can be recognized.

References

Hansen, J.E., and D.M. Driscoll, 1977: A mathematical model for the generation of hourly temperatures. *J. Appl. Meteor., 16*, 935-948.

Hittle, D.C., and C.O. Pedersen, 1978: Periodic and stochastic behavior of weather data. *ASHRAE Trans., 85*, 173-194.

Jensen, S.E. and H.C. Aslyng, 1967: Net radiation and net longwave radiation at Copenhagen, 1962-1967. *Arch. Met. Geoph. Biocl., B15.*

Ljung, L., and T.Söderström: 1983: Theory and Practice of Recursive Identification. MIT Press.

Madsen, H., 1985: Statistical Determined Dynamical Models for Climate Processes (Thesis). The Institute of Mathematical Statistics and Operations Research, DK-2800 Lyngby.

Madsen, H., P. Thyregod and J. Holst, 1987: A continuous time model for the variations of air temperature. *Proc. Tenth Conference on Probability and Statistics in Atmospheric Sciences*. 52-58.

Young, P., 1984: Recursive Estimation and Time-Series Analysis. Springer-Verlag.

Wallace, J.M., and P.V. Hobbs, 1977: Atmospheric Science. Academic Press.

Statistical analysis of temperatures in Hong Kong

E. Hui Koo and W.L. Chang
Royal Observatory, Kowloon, Hong Kong

Introduction

Temperature rises have been observed in many cities. Briefly, the main results, summarized from the comprehensive survey given, in Landsberg (1981), are:

1. Dronia (1967) estimated that on average, urban temperatures worldwide increased by 0.008°C per year between 1871 and 1960.
2. Dettwiller (1970) found that between 1891 and 1968, maximum temperatures for Paris rose by 0.011°C per year while minimum temperatures rose at a slightly faster rate of 0.019°C per year.
3. Mitchell (1961) found compatible temperature rises in selected cities in the United States.
4. Fukui (1970) studied temperature rises in Japan and found that for Tokyo, Osaka, and Kyoto the temperature trends were 0.032°C per year, 0.029°C per year, and 0.032°C per year respectively between 1936 and 1965.

Hong Kong has urbanized rapidly in the past forty years. The population has doubled to almost 6 million. There has also been an enormous growth in the number of vehicles, high rise buildings, and industry, all competing for space in the limited area of Hong Kong.

This study is undertaken to examine if temperatures in Hong Kong have trends similar to those in other cities, and to elicit the statistical properties of temperatures in Hong Kong as was done for cities in Greece by Giles and Flocas (1984a, 1984b).

Observations of maximum and minimum temperatures are made at the Royal Observatory Hong Kong since 1885. Except for the period from 1940 to 1946, the records are uninterrupted. The site within the Royal Observatory compound at which temperature readings are made has changed little during the past 100 years. The Royal Observatory is itself an urban station, situated in the heart of the densely populated and commercial centre of Kowloon.

In this paper, analyses were carried out for the following four temperature series: annual mean minimum temperatures 1885-1939 (55 observations), annual mean maximum temperatures 1885-1939 (55 observations); annual mean minimum temperatures 1947-1987 (41 observations), and annual mean maximum temperatures 1947-1987 (41 observations) .

Analysis

Test for normality

Many statistical tests, such as that for randomness below, rest on the assumption that the data are normally distributed. One test for normality is through Fisher's g_1 and g_2 statistics. This test requires the ratio of g_1 and g_2 to their respective standard errors (SE) be less than 1.96 for compliance with normality at the 5% level of significance. Table 1 shows that except for the 1885-1939 minimum temperatures, all the temperature data have g_1/SEg_1 and g_2/SEg_2 which satisfy this criteria. The frequency distributions of these three series are therefore consistent (at the 5% significance level) with the hypothesis that they are normal.

Test for randomness

Table 2 shows the lag 1, lag 2 and lag 3 autocorrelations for the four temperature series. For the three temperature series which are normally distributed, randomness can be tested through their lag 1 autocorrelations r_1 (Mitchell 1966). The test statistic is

$$(r_1)_t = (-1 \pm t_g\sqrt{N-2})/(N-1) \quad (1)$$

where N is the number of observations, and t_g the value of the normal variate corresponding to the required level of significance. Using the one-tail 5% significance level and the positive sign in equation (1), one finds $(r_1)_t = 0.20$ for the 1885-1939 series, and $(r_1)_t = 0.23$ for 1947-1987 series. In all cases r_1 ¿ $(r_1)_t$ so that one can reject at the 5% level of significance the hypothesis that the series are random.

All the lag 1 autocorrelations are positive suggesting that the data contain low frequency variation. Only the 1885-1939 maximum temperatures and the 1947-1987 minimum temperatures have lag 1 autocorrelations which are statistically different from zero (at the 5% level of significance). As r_2 and r_3 for these two series do not fall off exponentially as r_1^2 and r_1^3 respectively, any persistence contained in the data is probably not of the Markov linear type. The other two series with non-significant lag 1 autocorrelations can be regarded as free from persistence.

Trends

Fig.1 shows the time series of the temperature data. For pre-1939 maximum temperatures, linear regression gives a rise of approximately 0.014°C per year (Table 3). The pre-1939 minimum temperatures have a comparable rate of rise. Whether these local temperature rises reflect the general temperature rise in the first part of the century (Gribbin, 1979) is beyond the scope of the present study.

From 1947 onwards, minimum temperatures rose at a rate of approximately 0.024°C per year. This is twice the rate for before 1939. Fig. 2 shows that from the 1970's, the annual mean temperatures at the the rural station of Waglan Island, has been almost constant. This suggests that in the recent couple of decades there is little change in the local climate. One can surmise therefore that the rise in the Royal Observatory's minimum temperature is most probably caused by urbanization. The trend of approximately 0.024°C per year is less than that found for Tokyo from 1946 to 1963, which is 0.047°C per year (Landsberg, 1981).

Linear regression gives no overall trend for maximum temperatures after 1947. But when looked at from the differences between the maximum temperatures between The Royal Observatory and Waglan Island (Fig. 3), the maximum temperatures not only have been rising over the rural values, but in actual fact have been falling from 1971 onwards. At the same time, the minimum temperatures had been rising over their rural counterparts. Decrease in urban solar radiation and sunshine duration in Hong Kong during the period (Fig. 4) could be one of the reasons. The reduction in solar radiation in other cities has been described by Landsberg (1981).

Spectral analysis

Spectral analysis has been used by many investigators to elicit periodicities in temperature data, particularly long term ones such as those associated with the 11-year sunspot or the 22-year double sunspot cycle (Landsberg et al., 1959; Mason 1976). Details of the technique can be found in Mitchell et al. (1966), Blackman and Tukey (1959), and Jenkins and Watts (1968).

Although the temperature series under consideration are too short for proper spectral analysis, it will never the less be interesting to use available data for an experimental analysis to obtain 'rough' indications.

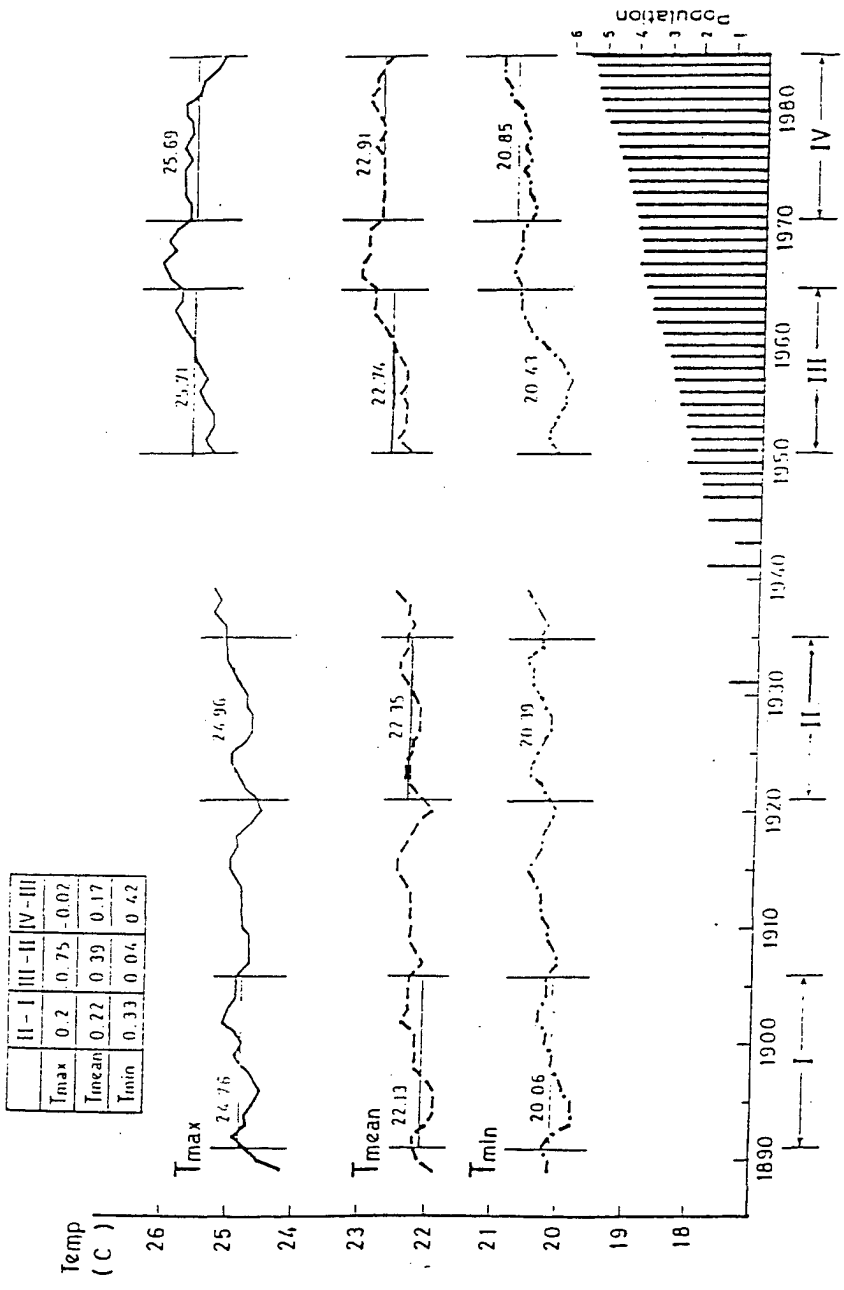

Figure 1: 5-year running mean temperatures at a Hong Kong urban station.

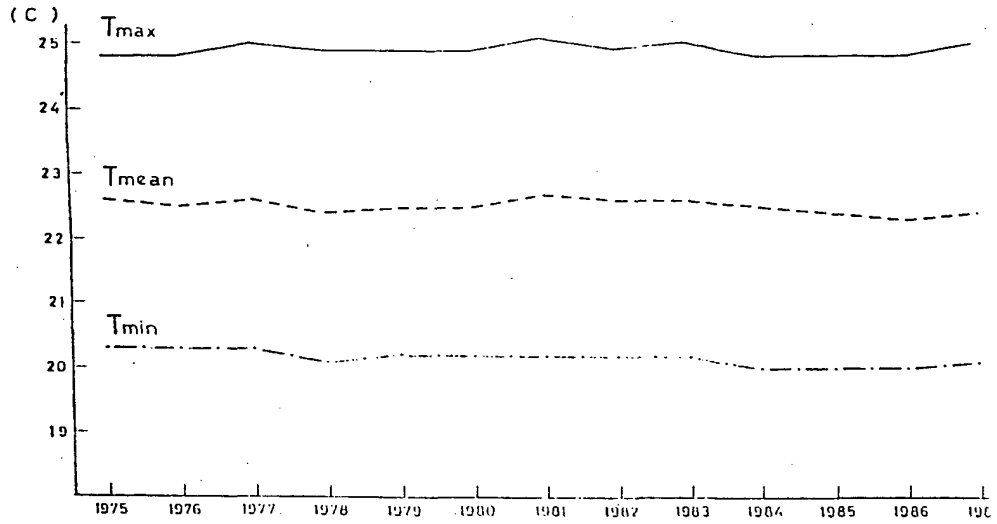

Figure 2: 5-year running mean temperatures at a Hong Kong rural station

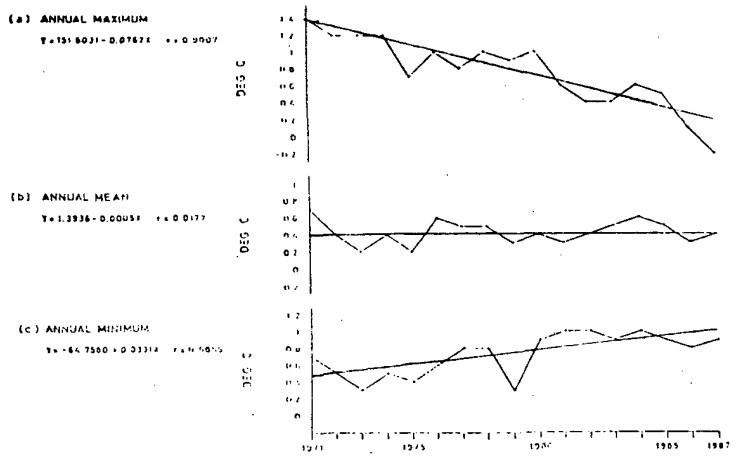

Figure 3: Difference (urban-rural) temperatures.

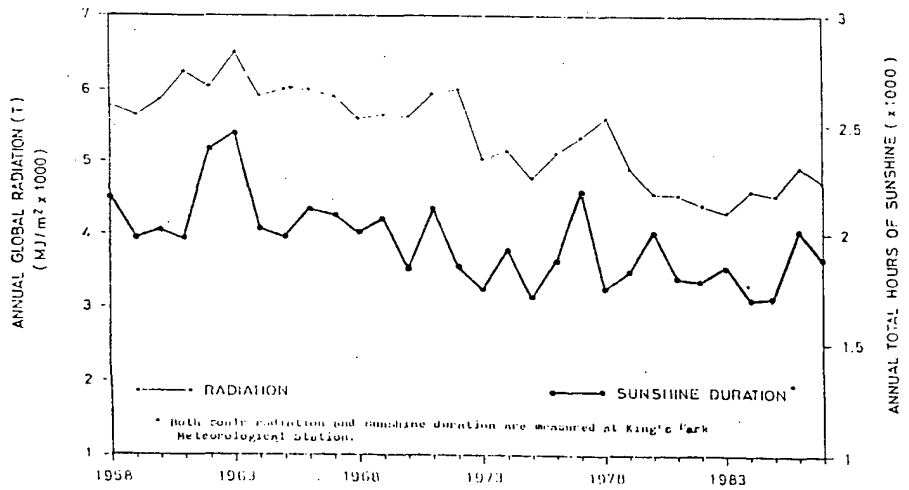

Figure 4: Decreasing global solar radiation (T) and total sunshine hours at a Hong Kong urban station.

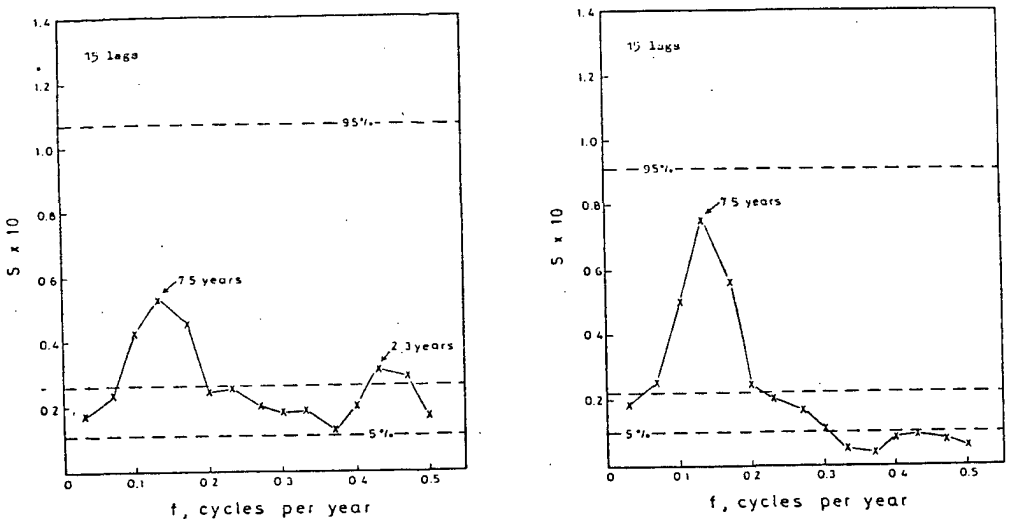

Figure 5: Spectra of the a. mean minimum and b. mean maximum temperatures for 1885-1939. S is the estimated spectral value. The middle dashed line is the average (white) spectrum.

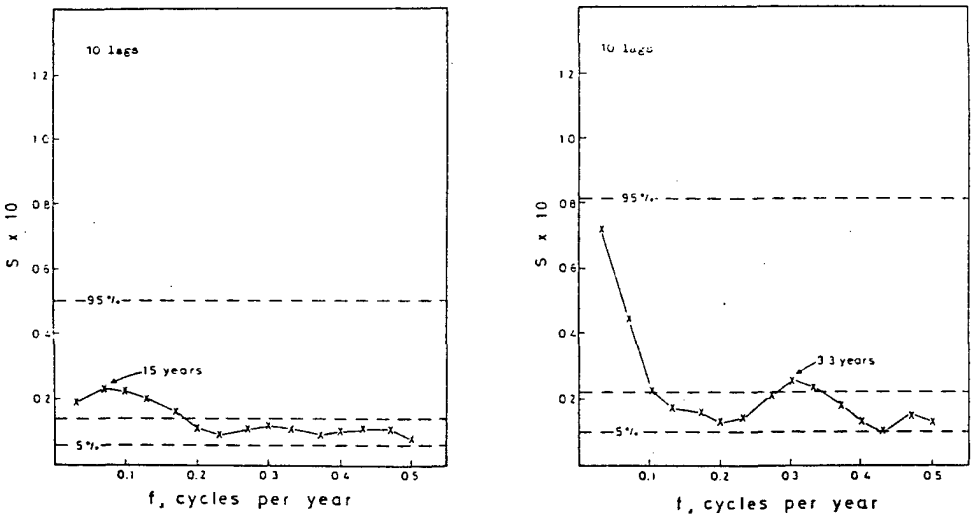

Figure 6: Spectra of the a. mean minimum and b. mean maximum temperatures for 1947-1987. S is the estimated spectral value. The middle dashed line is the average (white) spectrum.

IMSL's subroutine SSWD is used for this purpose. The spectra are computed from Fourier transforms of the autocovariances, and then smoothed by the Tukey-Hamming window. 15 and 10 lags are used for the 1885-1939 and 1947-1987 temperatures respectively, so that the lag number of lags does not exceed one third of the data length in each case. Trends are removed before analysis. As the small lag autocorrelations do not suggest any Markov persistence (Table 2), 5% and 95% confidence limits are computed to the average (white) spectrum.

Fig. 5 shows the spectra for the pre-1939 minimum and maximum temperatures. Most of the variances are found at low frequencies, with peaks at 7.5 years for both series. Additionally there is also a peak at 2.3 years for the minimum temperature. But none of the peaks are statistically significant as they do not exceed the 95% confidence limit of the null (white) spectrum. For the post-1947 series peaks appear at years for the maximum temperature. Again, they are not statistically significant.

Conclusions

The maximum and minimum temperatures recorded at the Royal Observatory, Hong Kong, were analysed for trends and periodicities. It was found that while maximum temperatures before 1939 and minimum temperatures have rising trends, post 1947 maximum temperatures are falling with respect to the maximum temperatures taken at a rural station. The reasons for this are as yet not entirely clear, and need further study. Spectral analyses of these limited temperature data also did not reveal any significant periodicities. It would be interesting to analyse the temperature series as a whole from 1885 to the present, with the data missing between 1940 and 1946 filled. This will be the subject of a further study.

References

Blackman, R.B., and J.W. Tukey 1959: The measurement of power spectra *Dover*

Dettwiller, J. 1970: Evolution seculaire du climat de Paris (Influence de l'urbanisme), *Mem. Meteorol. Natl. Paris No. 53, 83pp*

Dronia, H. 1967: Der Stadteinfluss auf den Temperaturtrend, *Meteorol. Abh., Berlin 74(4). pp 65*

Fukui, E. 1970: The recent rise of temperature in Japan, *Jpn. Prgr. Climatol. Tokyo Univ. Education. 46-65*

Giles, B.D., and A.A. Flocas, 1984a: Air temperature variations in Greece. Part 1. Persistence, trend and fluctuations, *J. Climatol. 4, 531-539*

Giles, B.D., and A.A. Flocas, 1984b: Air temperature variations in Greece. Part 2. Spectral analysis. *J. Climatol. 4, 541-546*

Gribbin John (Ed.), 1979: Climate Change *Cambridge Univ. Press*

Jenkins, G.M., and D.G. Watts, 1968: Spectral analysis and its applications, *Holden-Day*

Landsberg, H.E., Mitchell, J.M. Jnr., and H.L. Crutcher, 1959: Power spectrum analysis of climatological data for Woodstock College, Maryland, *Mon. Wea. Rev. 87, 283-297*

Landsberg, Helmut E., 1981: The urban climate *Academic Press*

Mason, B.J., 1976: Towards the understanding and prediction of climatic variations, *Q. J. R. Met. Soc. 102, 473-498*

Mitchell, J.M. Jnr., et al., 1966: Climate change *Tech. Note No. 79, WMO-No 195. TP-100*

Mitchell, J.M. Jnr., 1961: The thermal climate of cities. *Symp. Air over cities. U.S. Public Health Serv. Publ., SEC Tech Rept. A62-5, 131-143*

Table 1: g_1 and g_2 statistics for testing normality in the four temperature series. SE stands for standard error. TMIN and TMAX denote minimum and maximum temperatures respectively. * Value exceeds that (1.96) consistent with the hypothesis of a normal distribution at the 5% significance level.

	1885-1939		1947-1987	
	TMIN	TMAX	TMIN	TMAX
g_1	1.93	-0.46	-0.17	0.25
SEg_1	0.33	0.33	0.38	0.38
g_1/SEg_1	5.84*	-1.39	-0.45	0.66
g_2	7.68	1.18	-0.17	0.82
SEg_2	0.66	0.66	0.77	0.76
g_2/SEg_2	11.60*	1.78	-0.22	1.07

Table 2: Lag 1, lag 2 and lag 3 autocorrelation coefficients for the four temperature series. * Correlation value statistically different from zero at 5% significance level. † Value exceeds the $(r_1)_t$ value consistent with the hypothesis of randomness at the 5% significance level. *$(r_1)_t$ test not applicable as distribution not normal (at the 5% significance level).

	1885-1939		1947-1987	
	TMIN	TMAX	TMIN	TMAX
r_1	0.20*	0.51*†	0.48*†	0.29†
r_1^2	0.04	0.26	0.23	0.08
r_1^3	0.01	0.13	0.11	0.02
r_2	0.13	0.12	0.41	0.25
r_3	-0.11	-0.11	0.33	0.26

Table 3: Intercepts, slopes and 95% confidence intervals of the slopes of temperature regression lines.

	1885-1939		1947-1987	
	TMIN	TMAX	TMIN	TMAX
Intercept	19.95	24.44	20.16	25.7
Slope	0.012	0.014	0.024	0.0
95% CI	±0.007	±0.007	±0.008	.

Interannual climate variability in the global tropics

C.F. Ropelewski[1], M.S. Halpert[1], E.M. Rasmusson[2]
[1] Climate Analysis Center/NMC/NOAA, Washington DC,USA
[2] Dept. of Meteorology, University of Maryland, College Park MD, USA

Introduction

In previous studies (Ropelewski et al,. 1988a, 1988b) we investigated interannual variability in the principal indices of the Southern Oscillation (SO). These indices include the sea level pressure (SLP) at Tahiti, Darwin, Hobart, and Chatham and the sea surface temperature (SST) for the central and eastern Pacific equatorial ship tracks (Rasmusson and Carpenter, 1982) as well as the SST at Puerto Chicama, Peru. These previous studies and work by other researchers (e.g., Lau and Sheu, 1988, Barnett, 1989) suggest that the SO has significant variability in the biennial range (from 18 to 32 months) and that biennial variability is particularly pronounced in the central Pacific SST. In this paper we describe interannual SST variability in the context of biennial and longer term variations. The analysis is based on the examination of filtered time-longitude SST cross sections in comparison to the un- filtered cross sections for the Pacific basin.

Filtering

An analysis of various SO indices shows that the SST variance in the biennial range is significantly greater than that at higher frequencies and comparable to the variance at lower frequencies (Table 1), where high and low frequencies are defined here with respect to the biennial temporal scale. As a practical matter we designed high pass and low pass time series filters to be compatible with the bandpass biennial filter. The high pass filter has a half power point at 18 months while the low pass filter has a half power point at 32 months corresponding to the half-power points of the biennial bandpass filter. In this framework, SST interannual variability can be viewed as biennial variations modulated by low frequency variations. The high frequency is taken to be a "noise" component in this discussion and is excluded from further analysis.

Table 1: Anomaly variance for selected Southern Oscillation indices.

Index	Variance (percent variance)							
	Total		Biennial		Low pass		High pass	
Ship 1 SST (Eastern Pacific)	1.4	(100)	.36	(26%)	.61	(44%)	.22	(16%)
Ship 6 SST (Central Pacific)	0.5	(100)	.15	(30%)	.20	(40%)	.07	(14%)
Darwin SLP	1.1	(100)	.16	(15%)	.27	(25%)	.52	(47%)
	200 hPa Zonal winds							
Pacific Basin	16.6	(100)	4.7	(28%)	4.4	(27%)	5.7	(34%)
Atlantic Sector	15.8	(100)	1.6	(10%)	3.7	(23%)	4.3	(27%)
Indian Ocean	12.5	(100)	1.2	(10%)	5.7	(46%)	3.9	(31%)

Figure 1: Equatorial time-longitude cross sections of sea surface temperature across the Pacific basin: Left hand panel - unfiltered, central panel - biennially filtered, right hand panel - low pass filtered.

Analysis

The analysis is carried out through comparisons of filtered and un-filtered time-longitude cross sections of equatorial SST for the 1950 to 1979 period. The SSTs were derived from the Comprehensive Ocean Atmosphere Data Set (COADS, Woodruff et al, 1987). Three equatorial time-longitude cross sections of SST across the Pacific basin are compared (Fig. 1). The left hand panel of this figure represents the SST cross section with no filtering applied. The dark shading corresponds to SSTs of 28 degrees Celsius and warmer. The El Nino/Southern Oscillation (ENSO) episodes (1951, 1953, 1957, 1965, 1972, and 1976/77) are clearly identified with eastward extension of the warm water to the east of 150 degrees west longitude. Conversely, the "high index" episodes of the SO (1950, 1955, 1964, 1970, 1973, 1975) are associated with the retreat of the 28 degree Celsius isotherm to near and west of the date line. Also evident in this cross section is the well defined high amplitude annual SST cycle in the eastern side of the basin and almost complete absence of an annual cycle in the vicinity of the date line and westward.

The central panel of Fig. 1 shows a time-longitude cross section of the biennially filtered SST. We employ a sharp cutoff, 55-weight, bandpass filter (after Landsberg et al., 1963) and thus the leading and trailing 27 months are lost from the biennial cross sections. Like the annual cycle, biennial variability appears to be most consistent in the eastern Pacific. Unlike the annual cycle, however, the biennial component of the SST tends to maintain fairly large amplitude across the bulk of the Pacific basin and extends, not significantly diminished, to the date line. This is consistent with the large values of the coherence between the central and eastern Pacific SST at biennial temporal scales found by Ropelewski et al., 1989. Since the amplitude of the annual cycle is relatively small in the central Pacific, the biennial component in this part of the ocean basin is relatively more important than it is elsewhere in the equatorial Pacific and, in fact, accounts for 30the total SST variance for Ship track 6, which crosses the equator near 170 degrees west longitude. Both the cold and warm extremes of the

SO appear to be associated with the relatively high amplitude excursions of the biennial component. The biennial SST component appears to be modulated on relatively large time scales with relatively small amplitude for the periods 1959 to 1962 and 1967 to 1971.

The right-hand panel of Fig. 1 shows the time-longitude cross section of the low pass filtered SST data. Just as in the the biennial bandpass cross section analysis the leading and trailing 27 months of these cross sections are missing because of the filter employed (55 weights). In general, each of the six major positive excursions of the low amplitude SST component illustrated in these cross sections is associated with a warm episode in the 1952 to 1977 period. Thus, ENSO episodes are associated with the positive phases of both the biennial and low frequency components of the SST. The weak 1963 warm episode was associated with a strong positive phase in the biennial component but was not supported by similar warming in the low frequency component of SST variation. The strong positive SSTs in the biennial component from mid-1974 to 1975 did not result in a warm episode, perhaps, because for these years the biennial pulse appears to be riding on a relatively cold low frequency component.

Discussions

A strong biennial component to the SO is illustrated in the cross sections of Pacific SSTs presented above. This biennial tendency is further reflected in the relatively high percentage of biennial scale variance in other SO related indices in the Pacific basin (Table 1). High amplitude biennial variability, however, does not seem to be a sufficient condition for the occurrence of either warm or cold episodes. These episodes appear to occur only when both the biennial and low frequency components are in phase. This strongly suggests that if these temporal components are out of phase no warmings may occur ,as in 1974, or at best only weak warmings may occur, as in 1963. In 1973 and 1975, however, the high amplitude negative excursions of SST anomaly, associated with the biennial component, appear to have acted in concert with the low frequency cool phase to produce "high index" or cold episodes in each of these years.

While the biennial variability may have its origins in temporal scales inherent in large scale ocean-atmosphere dynamics, as is suggested by some numerical models, the origins of the low frequency variability are not as evident. The sources of the low frequency component of variability are, however, most likely tied to large scale ocean processes. In the context of the analysis presented here we might view the ocean/atmosphere/climate system as having three temporal components, an annual cycle - dominated by the atmosphere, biennial variability - dominated by ocean/atmosphere interactions, and low frequency variability - dominated by large scale ocean dynamics.

References

Barnett T. P., 1989: ENSO and QBO: Their interaction and causes. *Proc. of the 13th Annual Climate Diagnostics Workshop, Oct 31-Nov 3, Cambridge, MA.*

Landsberg, H. E., J. M. Mitchell, Jr., H. L. Crutcher and F. T. Quinlan, 1963: Surface Signs of the Biennial Atmospheric Pulse, *Mon. Wea. Rev., 91, 549-556.*

Lau K.-M. and P.J. Sheu, 1988: Annual cycle, quasi-biennial oscillation, and Southern Oscillation in global precipitation, *Jour. Geophys. Res. 93, 10,975-10988.*

Rasmusson E.M., and T.H. Carpenter, 1982: Variations in tropical sea surface temperature and surface wind fields associated with the Southern Oscillation. *Mon. Wea. Rev., 111, 517-528.*

Ropelewski C.F., M.S. Halpert, and E.M. Rasmusson, 1988a: Interannual variability in the tropical belt., *Proc. 7th Conf. on Ocean-Atmosphere Interaction, Jan 31 - Feb 5, 1988, Anaheim CA.*

————————, ————————, and ————————, 1988b: Tropospheric biennial variability and its relationship to the Southern Oscillation. *Proc. of the 12th Annual Climate Diagnostics Workshop, Oct 12-16, Salt Lake City, UT.*

————————, ————————, and ————————, 1989: Climatological aspects of the tropical annual cycle, *Proc. of the 13th Annual Climate Diagnostics Workshop, Oct 31-Nov 3, Cambridge, MA.*

Woodruff S.D., R.J. Slutz, R.L. Jenne, and P.M. Steurer, 1987: A comprehensive ocean-atmosphere data set. *Bull. Amer. Meteor. Soc., 68, 1239-1250.*

Climatology of low frequency tropical convective disturbances

Bin Wang
Dept of Meteorology, University of Hawaii, Honolulu HA, USA

Abstract

Mean behavior of planetary scale tropical convective disturbances with time scale of a month is investigated using ten-year pentad mean OLR data. Preliminary results are summarized as:

(1) Disturbances are usually originated in tropical convergence zone over Africa or western Indian Ocean and strongly intensified over the central and eastern Indian Ocean, moving dominantly eastward into central Pacific where they are dissipated. There are indications of weakening over maritime continent due to poleward splitting and reenhancement over western Pacific. The entire life-cycle suggests that rapid development is related to diabatic instability process and Indian and western Pacific Oceans are preferred geographic locations for the development.

(2) Convective disturbances exhibit clear annual variation: strong eastward propagating equatorial disturbances occur most frequently during December to May, while weak activity is observed during June through September. This annual variation tends to be positively related to the variation of SST in equatorial regions.

(3) Dominant poleward propagation of low frequency tropical convective disturbances is mainly observed over two sectors: 70°-90°E, 0°-25°N and 130-150°E, 0°-30°N. They are closely related to summer monsoon activities over these regions. Northward propagation is not always associated with zonal propagation, suggesting that the mechanism responsible for meridional propagation may differ from that for eastward propagation.

Evaluating a composite climatology of mesoscale rainfall

E. Tollerud
CIRES, Univ.Colorado, USA

Xiao-Ping Zhong
RIPM, Chengdu, PRC

B. G. Brown
NCAR, Boulder, USA

Introduction

After more than a decade of satellite observations, it is clear that a significant fraction of convective precipitation over the globe falls in weather systems organized on the mid- to large mesoscales (100–500 km in extent, 6–18 hours in duration). This realization is important both from a dynamical viewpoint, because of requirements to understand precipation processes and to parameterize them in climate models, and from a practical climatological viewpoint, since the estimation of global precipitation demands the ability to identify mesoscale structures and follow their evolution in satellite data. In particular, mesoscale organization of convection seriously challenges notions of rainfall as a random process involving independent cumulonimbus-scale cells.

Although much vital information about mesoscale convective sytems can be gained from studies of individual cases, large inter-system variability of the extent and spatial distribution of precipitation recommends a composite approach whereby common features can be isolated and investigated. With this, we present results from a climatological study of a class of large summertime mesoscale systems (mesoscale convective complexes, or MCCs; see Maddox, 1980) that produce substantial precipitation over the central United States. Compositing techniques play an important role in this study. As Kane et al. (1987) and others have shown, composite methods can be applied very usefully to study the precipitation in mesoscale systems such as MCCs. A short description of methodology and the principal results are included in Section 2.

Two questions of a statistical nature arise from this study, namely, the suitability of the network of hourly rainfall observations, and the representativeness of the compositing methodology. In Sections 3 and 4, respectively, we address these questions. Their implications for composite studies of the type employed here are discussed in a concluding section.

Methodology and composite results

Hourly precipitation data from the network of observing sites over the central U.S. are our primary source of observed precipitation. Locations of stations used in this study are shown on Fig. 1.

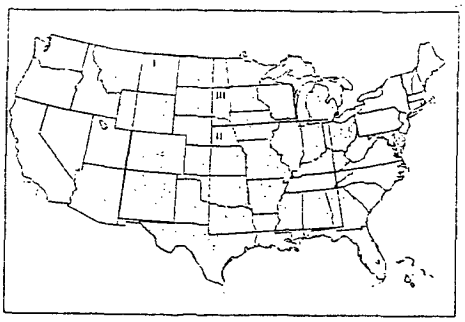

Figure 1: Locations of precipitation-observing stations in December, 1985, for the states included in this study. Rectangular regions identified by Roman numerals are tested seperately for uniformity (see text for explanation)

Using times and locations of MCCs reported between 1978 and 1985, we divide the life cycle of each MCC into three stages: initiating, between first storms and the time of initiation; developing, between initiation and the time of maximum storm size; and mature, between maximum size and termination (see Maddox, 1980, and Rodgers et al., 1983, for definitions and criteria for MCCs). By approximating the anvil size and location during each stage of the MCCs, we identify precipitation assumed to be associated with each MCC and composite that precipitation relative to the system center. In all, 240 MCCs with suitable rainfall observations were identified from available yearly MCC summaries and included in the analysis. A description of the locations, times, and other general characteristics of these MCCs is presented in Tollerud et al. (1987).

The temporal distribution of precipitation during the life cycle of the composite MCC is shown in Fig. 2.

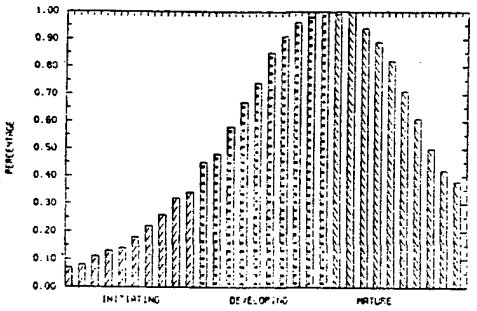

Figure 2: Precipitation in percent of maximum for subperiods of the composite MCC. Each subperiod represents approximately one-half hour

The peak of precipitation intensity occurs late in the developing stage, just before the maximum size is attained. Although the amount of precipitation during the developing and mature stages is approximately equal, other results (not shown) reveal that rainfall during the mature stage is typically less intense but more widespread. This corroborates previous findings and speculation that the character of precipitation evolves from individual cumulonimbus clouds (more intense but widely scattered) in the earlier stages to more widespread but lighter precipitation falling presumably from the extensive anvil of the MCC during the mature stage.

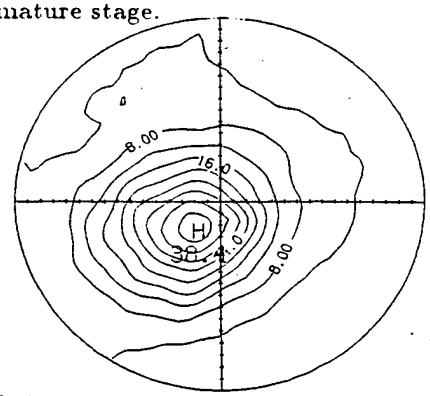

Figure 3: Total rainfall in the composite MCC, in mm. Marks along the axes indicate 25 km increments in distance from the MCC center

Figure 3 shows the horizontal pattern of precipitation during the life cycle of the composite MCC.

plotted relative to the center of the MCC anvils and contoured. Heaviest rainfall is found in the right-rear quadrant (relative to the direction of motion, which is typically from west to east). Some of the displacement from the MCC center is due to the wind shear between the mid- and upper troposphere, with increasing westerlies at upper levels; this shearing effect means that the tops of the anvils viewed by satellite photos will tend to be somewhat downstream from the convective centers at lower levels. In addition, the preponderance of rainfall in the lower (typically, southern) quadrants is likely related to the low-level transport of moisture into the MCC from the Gulf of Mexico to the south.

Evaluating the composite fields: Distribution of rainfall observations

For compositing techniques where observations from many different geographic locations are overlaid, the most critical attribute of the precipitation observations (besides, of course, their accuracy) is their uniformity. If observations from some MCCs are made in regions where the observing stations are much more dense than those from other MCCs, then the former set will be more heavily represented in the final composite results. Ideally, a completely uniform distribution of observations would be desired. In practice, this will almost never be the case; as Fig. 1 suggests, eastern states have denser networks, on average, than their western counterparts.

We would like to assess the sensitivity of our composite results to inhomogeneities in station distribution. To do so, we divide the central U.S. into three rectangular regions as shown on Fig. 1, and apply a chi-squared test to the station densities observed in one-degree squares in each of the regions (see Davis, 1973). Results show that the stations in each region are uniform at a 95% confidence level. Potential problems introduced by MCCs that move between regions or are primarily sampled in different regions are minor, since the great majority of MCC rainfall is found in region II (see Fig. 4).

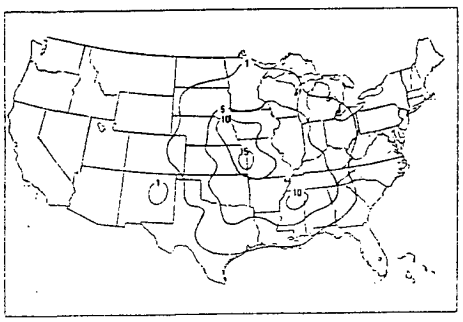

Figure 4: Total number of MCC rainfall observations, in hundreds, from 1978 to 1985

When we investigate the station distribution in more detail, however, significant intra-state non-uniformities appear. To demonstrate this, we compute the set of nearest-neighbor distances separately for the observing stations in Colorado and Missouri. Edge effects at the state boundaries are mitigated by use of the procedure suggested by Dacey (1963).

As Fig. 5 shows, Missouri exhibits a normal-looking distribution around a nearest-neighbor distance that is roughly what would be expected from a uniformly-distributed set of stations in a state the size of Missouri. In Colorado, however, a bimodal distribution is indicated, with one frequency maximum at smaller distances representative of the cluster of stations around Denver, and another frequency maximum representative of the larger distances between the stations in the rest of Colorado.

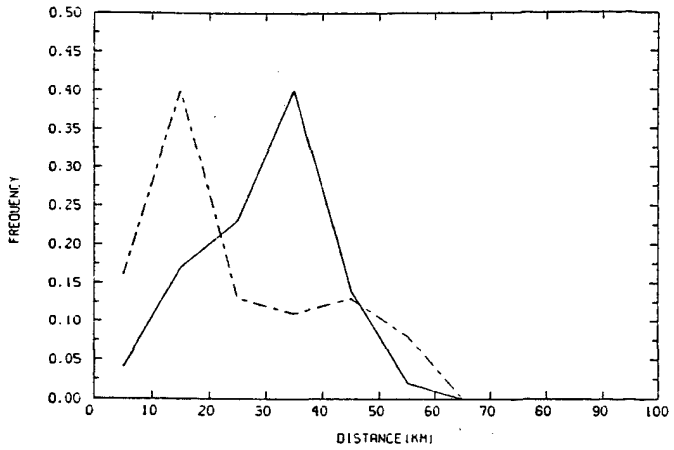

Figure 5: Frequency distributions of nearest neighbor distances for Colorado (dashed line) and Missouri (solid line)

Coincidentally, the average nearest-neighbor distances in Colorado is approximately that expected for a uniform distribution of stations, demonstrating the importance of examining the variance of nearest-neighbor distance in addition to their average values. This set of results suggests that composite studies in which Colorado observations play a major role (unlike the present one) should be interpreted with care.

Evaluating the composite fields: Sampling characteristics

Another set of questions concerns the compositing procedure itself, in particular its sampling characteristics. For instance, what assurance have we that the number of MCCs sampled is enough to provide a stable composite field? More seriously, is it possible that the procedure cannot produce a stable result at all? It is difficult, given the inexact nature of the compositing methodology, to provide an answer to this question analytically. With a large sample set available, however, we do have statistical tools that may be applied.

To answer the first question, we randomly order the MCCs in the total sample set and successively add groups of ten to the composite. At each step we compute the pattern correlation coefficient between the partial composite and the composite that includes all MCCs.

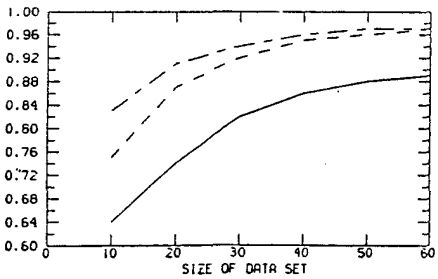

Figure 6: Pattern correlation coefficients between subsets and the full set of MCCs for subset sizes between 10 and 60. Solid, short-and-long dashed, and dashed lines denote results for, respectively, the initiating, developing, and mature stages

Fig. 6 shows that after a sample size of approximately 40 is reached, the composites for each

stage (except perhaps for the initiating stage, when relatively little precipitation falls) have attained essentially the same spatial pattern as the full composite (an example of the latter is the field shown in Fig. 3).

On the strength of this result, we compute composites consisting of 60 randomly-selected MCCs and compare them by again using pattern correlation coefficients. To assess their similarity (or non-similarity), we also compute pattern correlation coefficients between the different stages of the subset composites, where we expect to find discernible differences. The distributions of coefficients between the various possible pairs are shown in Fig. 7.

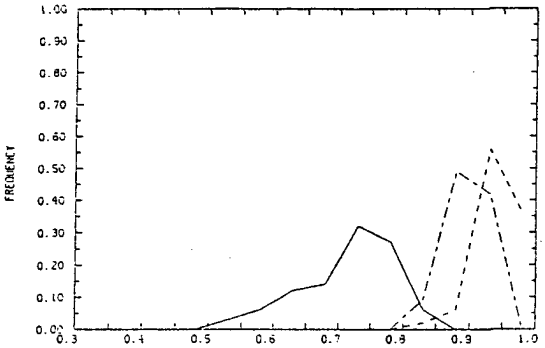

Figure 7: Frequency distributions of pattern correlation coefficients between the rainfall patterns of pairs of successive stages of the MCC composite subsets (solid line: initiating and developing stages; short-and-long dashed line: developing and mature stages) and between mature-stage rainfall patterns of pairs of composite subsets (dashed line)

Those between the same stage of different subsets are consistently between 0.9 and 1.0, while those between successive stages are significantly smaller. Intra- subset differences (which can be attributed to sampling variations) are thus almost unanimously smaller than inter-stage differences (which we interpret to be due to physical evolution of the MCCs).

Conclusions

We have investigated the validity of system-relative composite representations of the precipitation in MCCs from two viewpoints: the adequacy of the station distribution, and the consistency of composites of different samples of MCCs. Concerning the first, we conclude that the uniformity of stations in the region in which most of the precipitation occurs indicates that no significant effect on the composite results should be expected. Although we cannot prove, relative to the question of sampling, that the composites produced are physically realistic descriptions of a "real" MCC, that possibility is strongly supported by the coherent and stable patterns produced by randomly-selected subsets as well as by the rational evolution of the fields during the course of MCC development.

References

Dacey, M.F., 1963: Order neighbour statistics for a class of random patterns in multidimensional space. *Annal. Amer. Assoc. Geogr.*, **53**, 505–515.

Davis, J.C., 1973: *Statistics and Data Analysis in Geology.* John Wiley & Sons, New York, 550 pp.

Kane, R.J., C.R. Chelius, and J.M. Fritsch, 1987: Precipitation characteristics of mesoscale convective weather systems. *J. Clim. Appl. Met.*, **26**, 1345–1357.

Maddox, R.A., 1980: Mesoscale convective complexes. *Bull. Amer. Meteor. Soc.*, **61**, 1374–1387.

Rodgers, D.M., K.W. Howard, and E.C. Johnston, 1983: Mesoscale convective complexes over the United States during 1982 - annual summary. *Mon. Wea. Rev.*, **113**, 888-901.

Tollerud, E.I., D.M. Rodgers, and K.W. Howard, 1987: Seasonal, diurnal, and geographic variations in the characteristics of heavy-rain-producing mesoscale convective complexes: A synthesis of eight years of MCC summaries. *Preprint Volume, Seventh Conference on Hydrometeorology*, Oct. 6–8, Edmonton, Alta., Canada, pp. 143–146.

A comparison between multiple regression and factor analysis for climatological predictions

Oskar Essenwanger
Environmental Science, University of Alabama, Huntsville, Alabama, USA

Introduction

Most scientists use multiple linear regression models for the prediction of parameters based on statistical data collections, e.g. climatological records. Most of them consider factor analysis as a diagnostic tool. Both methods base their calculations on the same (linear) correlation matrix as data input (the elements, i.e. predictors, are not limited to their first order exponent.)

In this article factor analysis as a prediction tool will be discussed. Klein (1983, 1985) found that empirical polynomials (and as such factor analysis) were inferior to linear regression models. It will be illustrated that factor models may have some place in (climatological) predictions, e.g. where the predictand changes for extremes with reference to the mean within the prediction interval, or where correlations between predictands and predictors are low but a contemporary predictor may have a higher correlation.

The factor model

The widespread employment of multiple linear models may have three major reasons. Most scientists are familiar with the technique, and the coefficients are easily calculated. "Canned" programs for electronic data processing are readily available. Finally, the number of elements to be included in the model is virtually unlimited, restricted only be the storage capacity of the electronic data processing system and the choice by the scientist.

Factor analysis is based on the calculation of eigenvalues and eigenvectors of a correlation matrix (Cattell, 1952; Essenwanger, 1976). This is equivalent to the calculation of empirical polynomials (Lorenz, 1956). Since the factors are orthogonal a smaller number of factors than elements in a regression model leads virtually to the same magnitude of the residual variance (Essenwanger, 1986a, b). This alone may not be an attractive feature for using a factor model because electronic data processing for multiple regression models is fast and the savings in time for fewer components may not be essential.

It is well known that regression models tend to underpredict extreme values. This is especially the case when the predictand switches sides for extremes with reference to the mean value within the prediction interval, e.g. from clear to overcast sky. If these cases comprise a considerable fraction of the data, the factor analysis model may fare better. In these cases the factors are considerably different from the others, and a frequency distribution of the factors will readily disclose the number of switches (Table 1; Essenwanger, 1988).

Since prediction is based on factor, contemporary predictors with the predictand can be included into the model. This is not customary for the multiple linear regression.

It may seem an advantage that the coefficients for the prediction of several elements (predictands) can be obtained from one single "factor load matrix" (Essenwanger, 1986a,b, 1987b, 1988) because contemporary predictors can be included. Factors can be added or deleted without going through new calculation of coefficients such as would be necessary for the regression scheme. Although the rotation may increase the weight of the first factor, rotation of factors does not further reduce the residual variance, i.e. the system has an optimum reduction which cannot be changed by rotation (Essenwanger, 1987a; Kaiser, 1958).

One other feature of the factor model may be important. The coefficients in the "factor load matrix" permit us to estimate the residual variance without calculation of the predicted value such as it is required in multiple regression schemes. The estimates of the residual variance is precise for the unrotated factors. This enables us to evaluate readily the potential of a particular factor model. It can aid in the decision to add or delete elements or factors.

It is usually advantageous for predictions to perform a "principal components" analysis. If this statistical estimation method is unsatisfactory, several other estimation methods for the communalities based on statistical principles are available (Jöreskog, 1967; Essenwanger 1987a; Guttman, 1956).

Examples

Ceiling prediction

Predictions of cloud amount, cloud ceiling and visibility by employing factor analysis have been previously discussed by the author (1986a, b, 1987b, 1988). For predicting changes in cloud ceiling the frequency distribution of the numerical value of the first factors is given in Table 1 for the ceiling group 999.

Table 1: First factor for January data, Stuttgart (1956-1963) when ceiling is 999 at 08LST. A refers to when the ceiling changes 3 hours later from 999 to < 200, while class B refers to ceiling remaining at 999.

Factor	< -4	-4	> -4
A	0	2	6
B	25	1	0

Table 1 illustrates that a distinct separation boundary exists (in this case -4). Counting -4 into class A would make only one wrong prediction in 34 cases. Thus the frequency distribution of factors can aid in the development of a model and a decision tree. More details have been discussed by Essenwanger (1987b, 1988).

Prediction of snow days

In the previously mentioned articles by the author (1987b, 1988) factor analysis disclosed some advantages over a regression model where extreme values switched sides with reference to the mean value. Now an example is illustrated where factor analysis leads to a lower residual variance than a regression model without the switch of sides of extremes. It is a case where the predictand has a high correlation with a contemporary element while association with past records is weak.

Table 2 displays the factor load matrix which is based on the same correlation matrix as the regression model. The last column exhibits the linear correlation coefficients, which are most weak.

Table 3 displays the residual variance (fractions of total variance) for predicting NS(Mar). The first column represents the prediction by persistence from NS(Feb). Since persistence is very weak (r = 0.38 in Table 2), and the sample size is relatively small, a simple assumption NS(Mar) = NS(Feb) would cause an increase of the variance to 3.94 times the predictand's variance. Hence a one term linear regression model was chosen for persistence, ultilizing NS(Feb), rendering 0.85.

Table 3 provides the results for the residual variance for the factor and the regression model in the first line (A). The difference between the regression model (.41) and the factor model (.16) is caused

by inclusion of NS(Mar) in the calculation of factors. The number .16 provides also for the optimum reduction of the variance with four factors. Since NS cannot assume negative values, this fact was included into the prediction scheme which renders the second line values (B). This fact benefited the regression model more than the factor model.

Line C and D are based on estimation of factors. It is apparent that estimation will lead to a somewhat higher residual variance than with the correct factors. However, in this estimation a predicted temperature T(Mar) was included for factor estimation. The correlation (r) between T(Mar) and NS(Mar) is -0.76.

It was attempted to include this same estimate of T(Mar) into a regression model, calculating a new set of coefficients and eliminating T(Jan). Since a predicted value of the temperature was used instead of the correct value, the regression model reduced the variance only to 0.53. Hence this value was not used in the comparison. Apparently the deviations from the true March temperature played a lesser role in the factor model.

The last line of Table 3 displays the ratio of the residual variances: regression/factor. The ratio 1.74 for two factors is statistically significant at the 95% level for 35 years of data (F-test). In our case two factors may be sufficient for a good prediction.

It is unfortunate that the model could not be tested on independent data since the data sample is too small for separation. It may serve however, to demonstrate that factor analysis has some potential even in the specific cases where no switches of the extreme occur. Furthermore, the chosen example is not the best case to show the advantages of a factor model but was readily available.

Conclusion

The potential for employing factor analysis for prediction in particular cases was discussed. As previously pointed out by the author (1987b, 1988) if the predictand has extreme values which switch sides with reference to the mean during the prediction interval, it may be worthwhile to look into a factor model. The author previously discussed these cases, such as changes from an unlimited ceiling to a low ceiling, or clear to overcast sky (1987b, 1988).

Another case was illustrated here where the correlation with the available past elements (predictors) is weak but a contemporary correlation (such as the temperature in March) was much stronger. In this case the factor model was less sensitive to a prediction of a contemporary element which was included into factor estimation.

Several authors have found that empirical polynomials may not be of value for predictions, every individual case needs examination. We may not be able to determine *a priori* the advantages of factor analysis for a particular case.

References

Cattell, R.B., 1952: *Factor analysis* Harper and Row (New York) 462pp.

Essenwanger, O.M., 1976: *Applied statistics in atmospheric sciences*, Elsevier(Amsterdam), 412pp.

Essenwanger, O.M., 1986a: A comparison of methods for factor analysis of visibility. Army Research Office Rept 86-2, 39-59. *Proc. 31st. Conf. on the Design of experiments in Army research, development and testing.*

Essenwanger, O.M., 1986b: Comparison of principal components and factor analysis methods for climatological parameters. *Proc. 3rd Int. Conf. on Statistical Climatology*, Vienna, 23-27.

Essenwanger, O.M., 1987a: On rotation in factor analysis of atmospheric parameters. Army Research Office Rept 87-2, 59-76. *Proc. 32nd. Conf. on the Design of experiments in Army research, development and testing.*

Essenwanger, O.M., 1987b: Prediction of cloud parameters by using factor analysis. *Preprints 10th Conf. on Probability and Statistics*, Edmonton, 43-46.

Essenwanger, O.M., 1988: On the use of factor analysis as a prediction tool. Army Research Office Rept 88-2, 145-156. *Proc. 33rd Conf. on the Design of experiments in Army research, development and testing.*

Guttman, L., 1956: "Best possible" systematic estimates of communalities, *Psychrometrika*.**21**, 273-285.

Jöreskog, K.G., 1967: Some contributions to maximum likelihood factor analysis, *Psychrometrika*,**32**, 443-482.

Kaiser, H.F., 1958: The VARIMAX criterion for analytical rotation in factor analysis. *Psychrometrika*.**23**, 187-260.

Klein, W.H., 1983: Objective specification of monthly mean surface temperature from mean 700mb heights in winter, *Mon. Wea. Rev.*,**111**, 674-691.

Klein, W.H., 1985: Space and time variance in specifying mean surface temperature from the 700mb height fields, *Mon. Wea. Rev.*,**113**, 277-290.

Lorenz, E., 1956: Empirical orthogonal functions and statistical weather prediction. Scientific Rept. # 1. *Stat. Forecasting Proj.*, M. I. T., Dept. Meteorol., Cambridge, Mass., 49pp.

Table 2: Factor load matrix and correlation, Stuttgart (1953-1988)

Element	F(1)	F(2)	F(3)	F(4)	r(NS)
T(Nov)	-.67	-.26	-.54	.07	.57
S(Nov)	-.43	-.52	-.11	-.28	.08
T^2(Dec)	-.36	.23	-.53	-.45	.27
T(Jan)	.26	.18	-.23	.76	-.01
S^2(Jan)	.34	.68	.09	-.16	.13
T^2(Feb)	.31	.25	.35	-.38	-.17
R(Feb)	-.52	-.11	.31	.43	.25
NS(Feb)	-.30	.44	.62	-.01	.38
S(Feb)	.63	.22	-.56	.06	-.29
NS(Mar)	-.71	.55	-.05	.09	1.00
Variance	2.31	1.51	1.58	1.24	

T = temperature; T^2 = temperature squared; S = sunshine hours; S^2 = sunshine hours squared; R = precipitation; NS = number of snow days; r(NS) = linear correlation coefficient with NS(Mar).

Table 3: Fraction of the residual variance for three prediction models prediction the number of snow days in March at Stuttgart, FRG.

	Pers.	F(1)	F(2)	F(3)	F(4)	Regr.
A	.85	.48	.18	.17	.16	.41
B	.85	.48	.17	.17	.16	.41
C	.85	.56	.24	.24	.21	.41
D	.85	.55	.21	.21	.19	.37
Ratio	-	-	1.74	1.78	1.92	-

A: Factor model; B: Setting negative NS to zero; C: Estimation of factors; D: Estimation of factors and setting negative NS to zero.

Time series modelling based on mean generation function and its application to long term climate prediction

Hongxing Cao and Fengying Wei
State Meteorological Academy, Beijing, China

Introduction

The two major purposes of time series analyses are to abstract periods existing implicitly in the series and to build a mathematical model for forecasting. The periodogram based on harmonic analysis and analyses of both the power spectrum and the maximum entropy spectrum are very useful to detect the periods. But they cannot be used for making a forecast. The autoregressive (AR) model and the autoregressive moving average (ARMA) model are able to be used to predict but only a few steps for the series. A so-called periodic extrapolation using variance analysis was suggested by both meteorologists and mathematicians and employed widely in long range weather forecast practice in China. A series of works on the periodic extrapolation has been done fruitfully (Cao and Lu, 1983; Tian, 1981; Wei et al. 1983).

In this paper, a mean generation function (MGF) of a time series $x(t)$ is defined and a normalization calculation for MGF is made with the Gram-Schmidt procedure. For the normalized variables, we relate them with $x(t)$ in a linear model and the variables of the model are selected by using a so-called couple(d) score criterion (Cao et al. 1988). This model not only can be used to detect periods existing in $x(t)$ but also is suitable for multiple-step forecasts.

Mean Generation Function

Consider a time series

$$x(t) : x(1), x(2), x(3), \ldots, x(N) \tag{1}$$

where N is the sample size. Constitute a MGF

$$\bar{x}_l(i) = \frac{1}{n_l} \sum x(i + jl) \tag{2}$$

where i= 1, ..., l and l= N/2. n_l is the largest integer required by $n_l \leq N/l$, $L = max l$ if N is even, $L = N/2$; if N is odd, $L = (N-1)/2$.

When l = 1

$$\bar{x}(1) \equiv \bar{x} = \frac{1}{N} \sum_{i=1}^{N} x(i)$$

When l = 2

$$\begin{aligned} \bar{x}_2(1) &= \frac{1}{n_2} \sum_{j=0}^{n_2-1} x(1 + 2j) \\ &= \frac{1}{n_2} [x(1) + x(3) + \ldots + x(1 + 2k) + \ldots + x(1 + 2(n_2 - 1))] \end{aligned}$$

$$\begin{aligned} \bar{x}_2(2) &= \frac{1}{n_2} \sum_{j=0}^{n_2-1} x(2 + 2j) \\ &= \frac{1}{n_2} [x(2) + x(4) + \ldots + x(2 + 2k) + \ldots + x(2 + 2(n_2 - 1))] \end{aligned}$$

$\bar{x}_2(i)$ is called a MGF with the length 2. Similarly $\bar{x}_3(i)$, $\bar{x}_4(i), \ldots, \bar{x}_l(i)$ are obtained.

Define the MGF matrix with order L

$$H = \begin{pmatrix} \bar{x}_1(1) & & & \\ \bar{x}_2(1) & \bar{x}_2(2) & & \\ \vdots & \vdots & & \\ \bar{x}_L(1) & \bar{x}_L(2) & \ldots & \bar{x}_L(L) \end{pmatrix} \tag{3}$$

and an extended MGF matrix

$$\begin{aligned} \tilde{F} &= (\tilde{f}_{ij})_{DimNxL} \\ \tilde{f}_{ij} &\equiv \tilde{f}_l(t) \end{aligned} \tag{4}$$

where $\tilde{f}_l(t) = \bar{x}_l(i), t = imod(l)$ and $t = 1, 2, ..., N$.

Thus

$$\tilde{F}^T = \begin{pmatrix} \bar{x} & \bar{x} & \bar{x} & \bar{x} & \ldots & \ldots & \bar{x} \\ \bar{x}_2(1) & \bar{x}_2(2) & \bar{x}_2(1) & \bar{x}_2(2) & \ldots & \ldots & \bar{x}_2(i_2) \\ \bar{x}_3(1) & \bar{x}_3(2) & \bar{x}_3(3) & \bar{x}_3(1) & \ldots & \ldots & \bar{x}_3(i_3) \\ \vdots & \vdots & \vdots & \vdots & \vdots & \vdots & \vdots \\ \bar{x}_L(1) & \bar{x}_L(2) & \vdots & \bar{x}_L(L) & \bar{x}_L(1) & \ldots & \bar{x}_L(i_L) \end{pmatrix} \tag{5}$$

where $\bar{x}_2(i_2)$ shows one of $\bar{x}_2(1)$ and $\bar{x}_2(2)$; $\bar{x}_3(i_3)$ shows one of $\bar{x}_3(1)$, $\bar{x}_3(2)$, and $\bar{x}_3(3)$. The others are similar.

Whole modelling of time series $x(t)$ proceeds on $\tilde{F}$ and every column of which is looked upon as one independent variable.

Modelling procedure

In order to build a model based on the MGF, the following procedure is suggested.

1. Normalize the original series $x(t)$ with

$$x'(t) = (x(t) - \bar{x})/s \tag{6}$$

   where $\bar{x}$ and s are the average and standard deviation of $x(t)$ respectively.

2. Construct the MGF of $x'(t)$ with (2) and the extended MGF matrix $\tilde{F}$ with (4).

3. Regarding f as a primary vector of the Gram-Schmidt procedure, we obtain a normalized MGF, which is denoted as $f_2, f_3, \ldots, f_L$.

4. Assume a linear model between the variables $f_l; l = 2, \ldots, L$ and $x(t)$ given by

$$x(t) = \sum_{i=2}^{L} b_i f_i(t) + \varepsilon \tag{7}$$

   The matrix form is $X_{DimNx1} = F_{DimNx(L-1)} B_{Dim(L-1)x1}$

5. Using the least square estimation technique, the coefficient vector B is obtained by

$$B = (F^T F)^{-1} F^T X \tag{8}$$

Since vector f_l is normalized, the covariance matrix is a symmetric triangular matrix

$$F^T F = \begin{pmatrix} f_{22} & & & 0 \\ & f_{33} & & \\ & & \ddots & \\ 0 & & & f_{LL} \end{pmatrix}$$

where $f_{ii} = \| f_i \|^2$, and the inverse matrix $G = (F^T F)^{-1}$ is also a symmetric triangular matrix. Its elements are $g_{ii} = f_{ii}^{-1}$. It is clear that the inverse operation is very easy to be done by this method.

6. Selecting variables.
According to (8), coefficients of the linear model are represented by

$$\varphi_i = g_{ii} \sum_{t=1}^{N} f_i(t) x(t) \tag{9}$$

where $i = 2, 3, \ldots, L$. The variables f_i are put into the equation one by one according to their absolute value of φ from large to small. We employ the couple(d ed?) score criterion

$$\begin{aligned} CSC_k &= \frac{S_k^2}{S_x^2} + \frac{\lambda N}{N_k} \\ S_k^2 &= \sum_{t=1}^{N} [x(t) - \hat{x}(t)]^2 \\ S_x^2 &= \sum_{t=1}^{N} [x(t) - \bar{x}]^2 \end{aligned} \tag{10}$$

to select the variable number admitted to input into the equation. When k is the number of variables in the model, N_k is the trend score of a forecast, λ is an adjustment coefficient ranging from about 1.0 to 1.5, through which the second term in (10) will play an appropriate role in the CSC_k. Denoting the number of trend category as I, we make the transformation

$$\begin{aligned} \varphi(x(t+1) - x(t)) &= C_i(t) \\ \varphi(\hat{x}(t+1) - x(t)) &= \hat{C}_i(t) \end{aligned} \tag{11}$$

The trend score is defined as

$$N_k = \sum_{t=2}^{N} [1 - |C_i(t) - \hat{C}_i(t)|/(I-1)]$$

If only three categories of trend are taken into account for a forecast, namely, the rise, the stable, and the fall, $C_i(t)$ in (11) is taken as

$$C_u(\Delta x_t) = \begin{cases} 1 & \Delta x_t > U \\ 0 & |\Delta x_t| \le U \quad U > 0 \\ -1 & \Delta x_t < -U \end{cases} \tag{12}$$

where $\Delta x_t = x(t+1) - x(t)$, U is calculated simply by $U = \frac{1}{N-1} \sum_{t=1}^{N-1} \Delta x_t$ or is determined according to the requirements for prediction. The trend scores become $N_k = \sum_{t=2}^{N} [1 - \frac{1}{2} |C_u(\Delta x_t) - C_u(\Delta \hat{x}_t)|]$ where $\Delta \hat{x}_t = \hat{x}(t+1) - x(t)$. Obviously, when a minimum CSC_k and a maximum N_k appear, the number of variables in the model are finally determined.

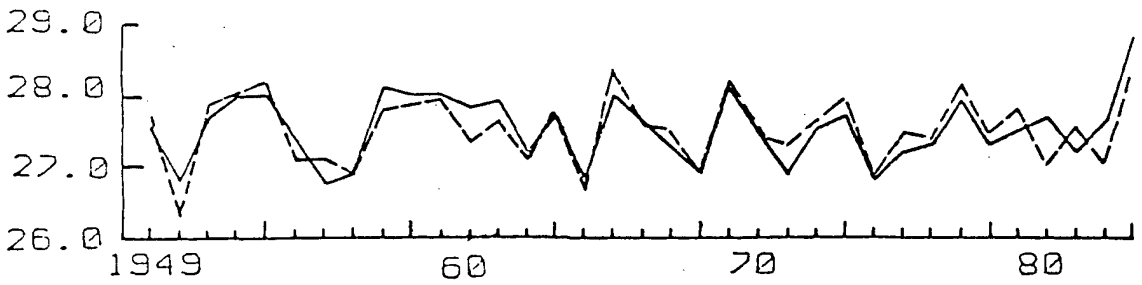

Figure 1: 1949-1983 SST curves of fitting (dashed line) and observation (solid line).

7. Making a forecast
As soon as the coefficients are calculated with normalized variables f_i, we should calculate the coefficients with the original variables $\tilde{f}_i$. Letting k_0, as the number of variables selected by the above procedure, we relate f_i with $x(t)$ in a linear model

$$x(t) = \tilde{\varphi}_0 + \sum_{i=1}^{k_0} \tilde{\varphi}_i \tilde{f}_i(t) \tag{13}$$

where $\tilde{\varphi}_i$ are called original coefficients.

If making the q-step period extension for $\tilde{f}_i$ with

$$\tilde{f}_l(t) \equiv \bar{x}_l(i) \tag{14}$$

where $t = imod(l), t = 1, 2, \ldots, N, N+1, N+2, \ldots$, we will be able a q-step forecast with $\hat{x}(N+q) = \tilde{\varphi}_0 + \sum_{i=1}^{k_0} \tilde{\varphi}_i \tilde{f}_i(N+q), q = 1, 2, \ldots$

Computational example

As everyone knows, monitoring and forecasting the change of the sea surface temperature (SST) in the equatorial Eastern Pacific area (0-10°S, 180-90 °W) is of great importance for climatic prediction over the most parts of the world. The above procedure is applied in the analysis of the SST series (1949-1983) during the austral spring time (March to May), with N=35, and L=17. For this case, six period variables are used in the equation. The prediction equation is given below

$$\hat{x}(t) = 0.00005448 + \tilde{f}_7(t) + 0.9948\tilde{f}_4(t) - 0.2349\tilde{f}_2(t) + 0.9565\tilde{f}_5(t) + 0.9085\tilde{f}_6(t) + 0.1032\tilde{f}_9(t) \tag{15}$$

Here $\tilde{f}_7(t)$ denotes a MGF of the SST series with the length 7, the others have the same meaning.

The root mean square error of fitting for the series calculated with (15) is 0.27°C. From Fig.1, it is shown that the predicted temperatures (dashed line) are very consistent with observed temperatures (solid line).

Extending five-step MGF's with (14) and putting MGF's into (15), a five-step forecast for 1984-1988 has been made; the results are shown in Table 1. From Table 1, it is easily found that both the quantitative and the qualitative score of forecast are quite high.(i.e. observed and predicted temperatures are similar. ed?)

References

Cao Hongxing, and Z. Lu, 1983: An adaptative method of periodic analysis and its application to climate prediction, *Second International Meeting on Statistical Climatology Sep. 1983, Lisbon*

Table 1: Forecasts and observed SST values in spring during 1984-1988

Year	1984	1985	1986	1987	1988
Forecast	27.3	27.2	27.0	28.0	27.5
Observed	27.4	27.2	27.4	28.4	27.7

Cao Hongxing et al. 1988: Couple score criterion for selection of Statistical model, *to appear in Mathematica Statistics and Applied Probability, Beijing, 1988.*

Tian, C.J. 1981: Convergence of periodic extrapolation with variance analysis, *Kexue Tongbao, 26. 140-142.*

Wei Fengying et al.1983: A method of analysing implied periods of climatological data using step-wise regression, *Second International Meeting on Statistical Climatology Sep. 1983, Lisbon*

The analysis of pentad precipitation vibration and the features of the space distribution of summer precipitation in Eastern China

Yafang Liu
Institute of Meteorology, Nanjing, Peoples Republic of China

Introduction

Harmonic analysis of pentad precipitation is applied to data from 51 stations in Eastern China during the period 1961-1979 and the annual precipitation vibrations are established. Then we study features of the spatial distribution of Summer(4-8 month) precipitation with the principal component analysis method during the period 1970-1979. This shows that the annual precipitation vibrations of Eastern China are divided into 12 types and the summer(4-8 month) precipitation anomaly field is divided into five main types.

Analysis of yearly change of precipitation in China

The area of China is large with the complex and different climates. Because of the year-to-year changes of circulation over large areas, the precipitation in every area changes greatly and droughts and floods frequently occur. Hence the study of yearly vibration features and time and space distribution of precipitation has significant meaning for agriculture and the national economy. Precipitation is a climatic element with large stochastic vibration, it's essential nature of yearly oscillation is different, and it's yearly change law is also different. Based on several laws of yearly change for precipitation, this paper uses objective analysis of the harmonic components, with an aim to provide better precipitation forecasting and serve the national economy. We selected the accumulation pentad precipitation data of 51 stations with recompular(regular?) distribution during the period of 1961-1979 in Eastern China.

Harmonic analysis of the mean pentad precipitation series

The time series of meteorological elements is known as the complex period phenomena, it consists of many different periods. If the mean pentad precipitation series is $y_0, y_1, \ldots\ldots y_{71}$ then by formula of Fuliye (refce?) we get

$$y_t = a_0 + a_1 \cos \omega t + b_1 \sin \omega t + a_2 \cos \omega t + b_2 \sin 2\omega t \ldots\ldots + a_n \cos n\omega t + b_n \sin n\omega t \qquad (1)$$

where a_0 is the arithmetical mean of series $y_0, y_1, \ldots y_{71}$ and $a_1, b_1, a_2, b_2 \ldots\ldots$ are the coefficients of the harmonic wave.

Because the yearly period, half-year period and dry/wet period of precipitation can best show the law of yearly variation, we only take the sum of the first, second and third harmonic wave terms i.e. $n = 3$ in (1).

$a_0, a_1, a_2, a_3, b_1, b_2, b_3$ are respectively given by the formula $a_0 = (1/72)\sum_{t=0}^{71} y_t$, and $a_k = (1/72)\sum_{t=0}^{71} y_t \cos k\omega t$, $b_k = (1/72)\sum_{t=0}^{71} y_t \sin k\omega t$, $k = 1, 2, 3$ where $\omega = 2\pi/72$.

The formula of the amplitude and phase for harmonic wave are amplitude $C_k = \sqrt{a_k^2 + b_k^2}$ and phase $D_k = \arctan(a_k/b_k)$ for $k = 1, 2, 3$.

We analyse the accumulated pentad precipitation series at 51 stations in Eastern China using the above method, and obtain the amplitude C_1, C_2, C_3 and phase D_1, D_2, D_3 for the first three harmonic waves, then examine the principal pattern of precipitation oscillation using the systematic clustering method with indicies of seven coefficients $C_1, C_2, C_3, D_1 D_2, D_3$ and a_0.

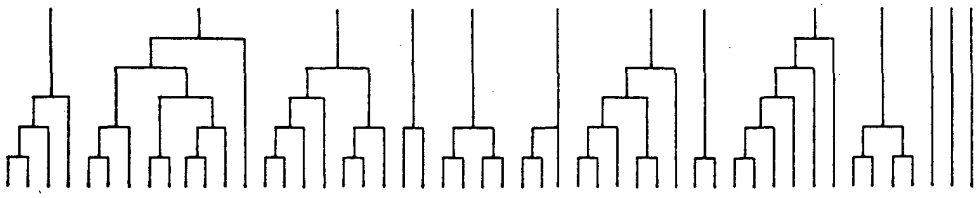

Figure 1: Map of precipitation cluster

Essential precipitation vibration patterns

Based on the above seven indicies, first we rank the 51 stations , then compute their similarity coefficient matrix $\mathbf{R} = (r_{ij})$. where $r_{ij} = \cos\phi_{ij} + 1/(D_{ij}+1)$ is the similarity coefficient.

$$\cos\phi_{ij} = \sum_{k=1}^{7} x_{ik}x_{jk} / \sqrt{\sum_{k=1}^{7} x_{ik}^2 \sum_{k=1}^{7} x_{jk}^2}, \quad D_{ij} = \sqrt{\sum_{k=1}^{7}(x_{ik}-x_{jk})^2}/51$$

Selecting two generas G_p and G_q with the largest similarity coefficient, we construct one new genera G_r with weight-centred vector $\bar{X}_r$ given by $\bar{X}_r = (n_p\bar{X}_p + n_q\bar{X}_q)/n_r$

$$\bar{X}_p = \begin{pmatrix} \bar{X}_{p1} \\ \bar{X}_{p2} \\ \vdots \\ \bar{X}_{pm} \end{pmatrix} \qquad \bar{X}_q = \begin{pmatrix} \bar{X}_{q1} \\ \bar{X}_{q2} \\ \vdots \\ \bar{X}_{qm} \end{pmatrix}$$

$$\bar{X}_{pk} = \sum_{i\in G_p} X_{ik} \qquad \bar{X}_{qk} = \sum_{i\in G_q} X_{ik}$$

The distance between two sorts is defined as $D_{pq} = d\bar{X}_p\bar{X}_q$ The distance between new sort G_r and other sorts is computed by the formula

$$D_{rk}^2 = n_pD_{kp}^2/n_r + n_qD_{kq}^2/n_r - n_pn_qD_{pq}^2/n_r^2 \tag{2}$$

where $n_r = n_p + n_q$ and n_p, n_q, n_r are respectivly sample numbers of G_p, G_q, G_r. Based on the principal of the systematic clustering, we may select two sorts with the biggest similarity coefficient and make them one new sort, compute the distances between new sort and the other sorts, this process did not finish until all sorts make one sort. The pentad precipitation yearly vibration is divided to 13 types on given distance criterion.

Since the precipitation yearly variation curve and the pentad precipitation cent ratio between Nicha,Gueya are similar, their precipitation yearly vibration has to belong to a similar sort.

Table 1: The ratio of season to year in precipitation.

	Spring	Summer	Autumn	Winter
Nicha	25.6	45.5	22.6	6.3
Gueya	28.6	44.2	22.1	5.1

Therefore, the precipitation yearly vibration can be combined into 12 types. If we can make the right analysis of representativeness of station precipitation into 12 types, the the essential situation of the precipitation vibration can be decided over whole country.

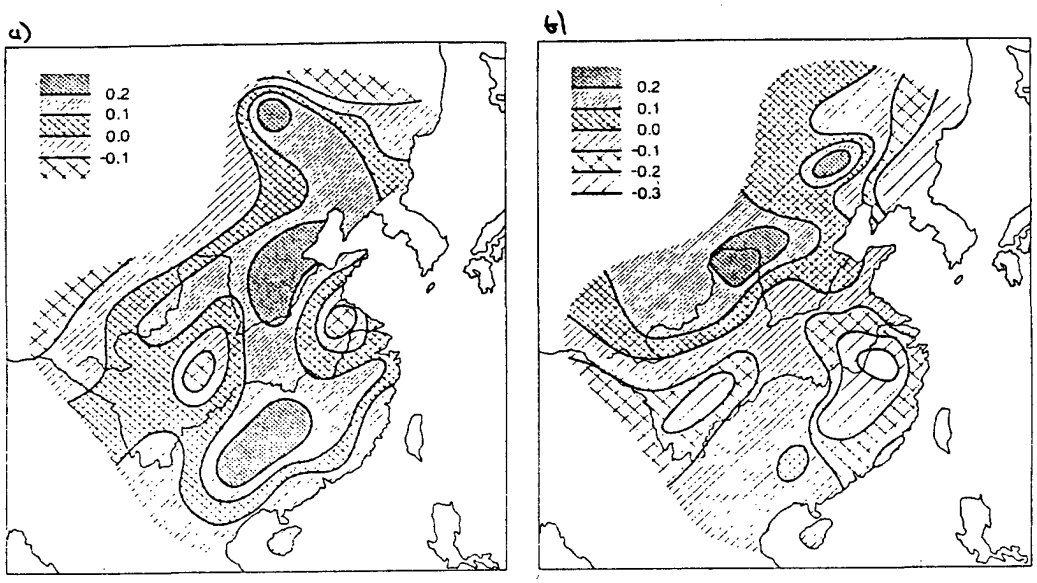

Figure 2: Principal fields of summer(4-8month) precipitation, a. first, b. second.

The space distribution features of summer precipitation

The summer precipitation field series (4-8month) selected above 51 stations of geographic uniform distribution is computed along with the EOF decomposi tion of the field series, ordering

$$F_{ij} = \begin{pmatrix} X_{11} & X_{12} & \cdots & X_{1n} \\ X_{21} & X_{22} & \cdots & X_{2n} \\ \vdots & \vdots & \vdots & \vdots \\ X_{n1} & X_{n2} & \cdots & X_{nn} \end{pmatrix} \tag{3}$$

X_{ij} is precipitation anomaly of rain spell at station j in year i.

Fig.2 shows five principal fields of (4-8month) precipitation field, Each principal field respectively expresses different precipitation distribution, the variance is 75.8%. For example the precipitation distribution with the first principal field is plus anomaly on Hua Bki, Hua Nan, the precipitation is more,the area in Jiang Huai, Han Zhong basin is negative anomaly, the precipitation is less. The second principal field is opposite anomaly in North and South area(Yellow river is bound line), North is plus anomaly, South is negative anomaly.

Table(2) shows the former five principal fields coefficients T_1, T_2, T_3, T_4, T_5 for summer (4-8month) precipitation field using EOF decompsition. Because the principal field coefficient shows variance, of the principal field to real anomaly field, the summer (4-8month) precipitation field is divided several types based on the principal field coefficient value in Table 2.

Table 2: The coefficients of summer (4-8month) precipitation field with EOF decomposition and anomoly type (absolute extreme).

Year	T_1	T_2	T_3	T_4	T_5	Type
1970	0.559	-0.020	-0.007	0.712	-1.837	5-
1971	-0.100	-0.117	0.060	0.772	0.403	4+
1972	1.856	-1.365	-0.270	0.287	0.208	1+
1973	-1.977	-1.054	-0.633	1.234	0.312	1-
1974	0.193	-0.847	-1.132	-0.510	1.227	5+
1975	1.296	-0.475	0.205	-0.236	-1.885	5-
1976	-0.759	1.374	0.840	0.625	-0.239	2+
1977	-0.348	-1.585	-0.050	-2.160	-0.604	4-
1978	-0.350	0.620	1.714	0.772	1.843	5+
1979	-0.372	2.459	-0.720	-1.304	0.572	2+

The types of yearly anomaly field are shown in Table 2. We see that only seven types appear; in 10 years type 3 did not appear .

Conclusions

The annual precipitation vibrations are divided into 12 types using the harmonic analysis method for the accumulation pentad precipitation series at 51 stations in Eastern China. The Summer(4-8month) precipitation anomaly field can be divided into five main types, each type relating to certain weather.

References

Jones, P.D., Kelly, P.M. 1982: Principal component analysis of the Lamb Catalogue of daily weather types, *Journal of Climatology*, **2**, ??.

Cooley, W.W., Lohnse, P.R. 19??: Multivariate Data Analysis. Wiley, ???pp.

Kidson, J.W., 1975: Eigenvector analysis of monthly mean surface data, *Mon. Weather Rev.*, **103**, ???.

Tu Qipu, 1981: Features of the time and space distribution of winter temperatures in China, *Journal of Nanjing Institute of Meterology*, ???.

On the modes of growing-season precipitation over central North America

P.J. Lamb and M.B. Richman
Climate and Meteorology Section, State Water Survey, Champaign IL. USA

Abstract

This presentation will summarize the results of principal component and correlation analyses of growing season precipitation over central North America for time scales of 3- through 61-days (Richman and Lamb, 1988, Proceedings of the Eleventh Annual Climate Diagnostics Workshop). Analyses were performed on a recently developed and quality-controlled set of 557 stations which form a nearly grid-like distribution extending from the Gulf of Mexico to the northern limit of North American agriculture and from the eastern edge of the Rocky Mountains to the western edge of the Appalachian Mountains.

Results which will be highlighted are:

(i) Analysis of how the modes of rainfall variation change with respect to time integration interval (i.e., 3-day totals, 7-day totals, ...) to provide insight into how weather integrates into climate and the associated changes in scale.

(ii) Analyses of the intra-seasonal evolution of the regions from the early growing season (May) through later phases (August) for 8 discrete 15-day periods within each season. The changes in the relative importance of specific regions, as the growing season progress, will be shown. Furthermore, the anisotrophic nature of certain patterns will be examined as this provides insight into the mechanisms of rain production.

(iii) The year-to-year variability of rainfall modes will also be shown to help determine to representativeness of the patterns.

The statistical character of decadal climate in China

You-tang Liu
Lin Fen Area Observatory, Shanxi Province, China

Abstract

100 years of data. respresenting 100 stations. of dryness and wetness durations. have been statistical analyzed.

The smoothed EOF (empirical orthogonal functions) method. was used to calculate between dryness and wetness distributions and their changes for 100 years. The distribution of duration show spatial and temporal components. The spatial component mainly respresenting differences between northern and southern .eastern and western regions which are related to the time scale.

Otherwise. for temporal components.by time series method.forecasting future climatic change for 10 years in dryness and wetness.

According to the rainfall. relating to temperature . forecasting future climatic change for 10 years in coldness and warmness.

Rainfall as a fractal process

Tom Beer
CSIRO Division of Atmospheric Research, Mordialloc, Australia

Introduction

Total rainfall R_τ over a time period τ is the sum of the amount of water carried by discrete drops of varying size falling into an enclosure at varying times. Modern tipping-bucket raingauges, however, produce a somewhat different result. These gauges have two equal sized small buckets, which typically hold either 0.5 mm or 1 mm, on a see-saw arrangement. The higher bucket collects rainwater until it is full whence it drops at which time the other bucket raises, and a signal is recorded to mark the time at which the tip occurred. Thus a tipping bucket raingauge can measure the time interval between constant amounts of rainfall.

Lovejoy and Mandelbrot (1985), Lovejoy and Schertzer (1985) and Skoda (1987) used radar data from a variety of locations to estimate the probability of changes in rainflux (i.e. rainfall in m^3/s) and have shown this to be consistent with a fractal model of rainfall. By contrast, theoretical arguments (Kedem and Chiu, 1987) supported by tipping-bucket rain gauge data (Zawadski, 1987) have been used to show that rain rate processes are not self-similar and do not scale. This paper argues in favour of rainfall having a fractal structure somewhat different to that postulated earlier and it is shown that this structure is consistent with tipping-bucket rain gauge observations.

Lovejoy-Mandelbrot fractal model

Identification of rainfall as a fractal process relies on the concept of scaling in which a random fluctuation $X(t)$ is scaling if the statistical distribution of $X(\lambda t)$ is the same as the statistical distribution of $\lambda^H X(t)$ where H is a scaling exponent. The graphs of scaling functions represent fractal sets characterised by a fractional dimension that is a non-integer quantity related to H. The existence of a hyperbolically distributed random variable guarantees scaling, and thus serves to identify the fractal nature of the quantity.

Lovejoy and Mandelbrot (1985) used their radar derived rainflux results to confirm that the probability distribution of rainflux asymptotes to a hyperbolic distribution and is therefore scaling. They found that

$$P(R_f > r_f) \propto (r_f/r_f^*)^{-\alpha} \tag{1}$$

where the random rainflux variable is denoted by R_f and its measured value by r_f. The quantity r_f^* converts the right hand side to non-dimensional form and represents the width, or amplitude, of R_f. Lovejoy and Mandelbrot derived a value of $\alpha = 1.660 \pm 0.05$. They also used their rainflux results to argue that the rainfield is scaling in time so that the amplitude of R_f is measured by

$$r_f^* \propto t^{H_L} \tag{2}$$

where they obtained $H_L = 0.64 \pm 0.05$. The subscript L emphasises that their method produced a 'Lagrangian' scaling in which rainfall fluctuations were tracked within the overall flow. In this report the scaling in time of rainfall is directly tested by using tipping-bucket raingauge data, in which t represents the time between tips and r the rainfall rate. In this case, because the rain gauges are fixed in location the resulting scaling parameter produces an 'Eulerian' scaling.

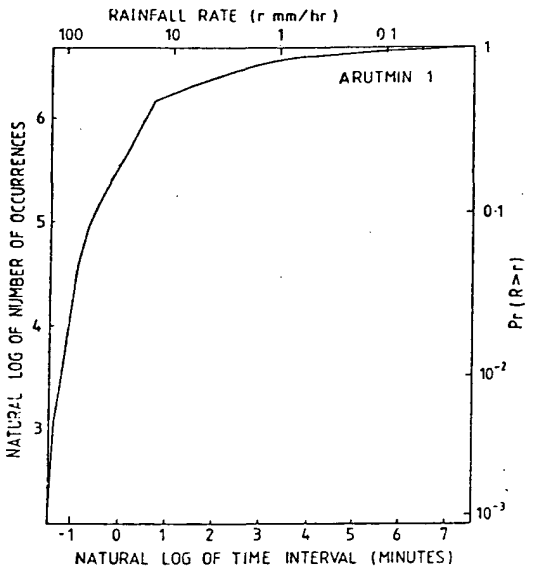

Figure 1: Cumulative probability distribution that rainfall rates measured by a tipping bucket raingauge exceed the value on the upper abscissa

Rainfall data

The rainfall data used in this study were obtained from a high rainfall area in Indonesia. A Mace/Rimco tipping bucket pluviometer with 0.5mm buckets was used. It recorded its information on an Eprom chip that was returned to Australia and deciphered in the laboratory. The pluviometer was installed at 2000 on 10 June 1984 and ran for 40 days. The chip was then replaced and the instrument recorded for a further 16 days.

Figure 1 follows Lovejoy and Mandelbrot (1985) in plotting the cumulative probability that the rainfall rate exceeds the value given on the upper abscissa. This probability is denoted $P(R > r)$ and is plotted on double logarithmic paper. When their results were plotted on double logarithmic paper, Lovejoy and Mandelbrot found a straight line portion over a factor of 10 in their rain flux. The pluviometer data do not exhibit the same behaviour when $P(R > r)$ is plotted. This has also been independently noted by Zawadzki (1987) who argued against the existence of scaling of rain rate increments in time (and hence against a fractal structure for rain) on the basis of his result. However it appears that rain rates do exhibit scaling in time because, as illustrated in Figures 2 and 3, when $P(R < r) = 1 - P(R > r)$ is plotted then both the 40 day data set (Figure 2) and the 16 day data set (Figure 3) exhibit straight lines over four decades of rain rate.

Estimating scaling parameters

Figures 2 and 3 provide evidence for hyperbolic distributions in that the tail probability

$$P(R < r) \propto t^{-\beta} \tag{3}$$

Estimation of the numeric value of β is subjective to the extent that one only wishes to fit a straight line to the tail section of the curves of Figures 2 and 3. If this is done by eye then $\beta = 0.44$

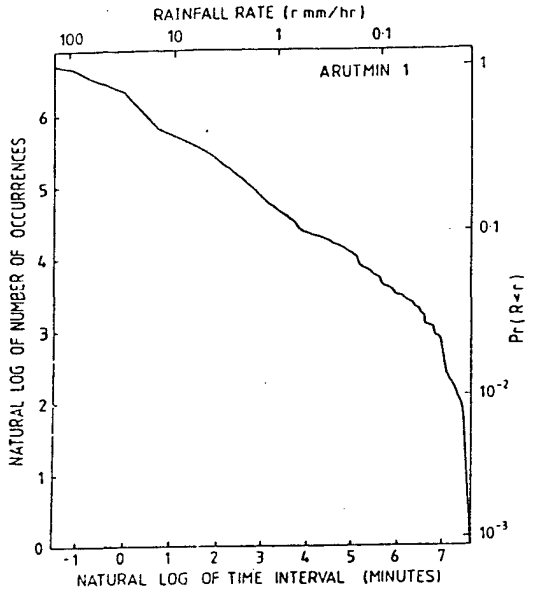

Figure 2: Cumulative probability distribution that rainfall rates measured by a tipping bucket raingauge are less than the value on the upper abscissa. Results based on a 40-day raingauge deployment in Indonesia

in Figure 2 and $\beta = 0.59$ in Figure 3.

Fitting data by eye is a subjective procedure. The most obvious objective procedure that utilises all the available data, namely a linear regression of $\log[P(R < r)]$ on $\log t$, though adequate will produce an estimate for β that is too high because of the influence of the data points that depart from the hyperbolic distribution at large values of t. In devising a procedure that does not suffer from these problems it was noted that the fourth and fortieth percentiles of both graphs produce results that were close to the curves fitted by eye, and it is thus suggested that

$$\beta = \frac{\log 10}{\log(t_4/t_{40})} \tag{4}$$

where t_4 and t_{40} are the fourth and fortieth percentile values respectively. This produces β values of 0.44 and 0.64 respectively for the data of Figures 2 and 3.

Discussion

The results presented here, which confirm the fractal description of rainfall at a single raingauge, raise a number of serious issues in practical meteorology in relation to the traditional description of rainfall as a point process. At first sight it would appear that common usage has interchanged dependent and independent variables and rather than making a statement such as 'the mean annual rainfall of Sydney is 1190mm' one should phrase it as 'the mean time for 1190mm of rain to fall in Sydney is one year'. In fact, the fractal description indicates that neither statement is likely to be valid because the mean is not a well defined quantity for our hyperbolic distribution. Neither is the variance.

Mandelbrot (1977, p.320) jokes that life without variance is hard, but life without expectation demands psychological adjustment. This is especially so as other measures of central tendency also

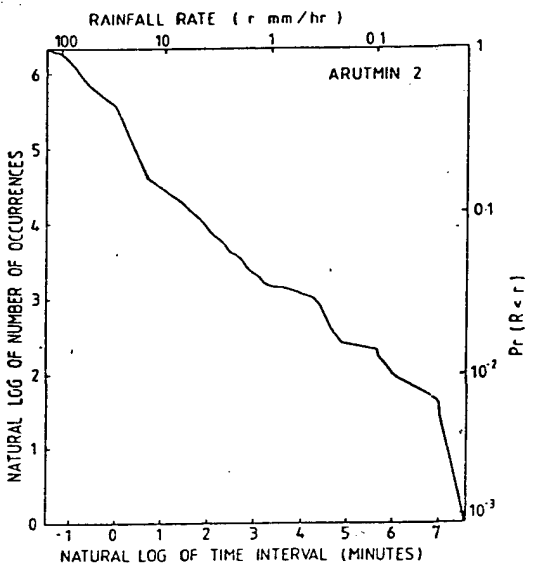

Figure 3: As for Figure 2 based on a 16-day raingauge deployment at the same location

fail to produce values that coincide with standard meteorological conventions. The median is zero and there is no mode.

Notwithstanding the theoretical arguments given above, the practicing meteorologist or hydrologist is able to extract means and medians from the data of Figures 2 and 3. In the case of Figure 2, the data has a median time interval of 1.60 minutes between 0.5mm of rain and a mean time interval of 71.6 minutes between 0.5mm of rain. The corresponding figures for Figure 3 are 0.71 minutes and 41.24 minutes. These values can be calculated because of the existence of finite cutoffs at both low and high time intervals. Denoting these by η and p respectively one finds that the median is close to $(2^{1/\beta})\eta$ providing p is sufficiently large. The mean, however, depends on both cutoffs and approximates

$$< t >= \left(\frac{\beta}{1-\beta}\right)\left(\frac{p^{1-\beta}}{\eta^{-\beta}}\right) \tag{5}$$

in the divergent case of $\beta < 1$.

The quantity p is the longest time interval between rainfall events (i.e. the drought period) whose practical value will, in turn, be dependent on the length of time for which the raingauge was deployed. The quantity η is a measure of the maximum rainfall rate (0.44 minutes per mm in this case) whose value will depend on (i) a sufficient length of deployment to ensure large rainfall events are recorded and (ii) the mechanical attributes of the tipping bucket which will determine the minimum time between tips. The data depicted in Figures 1 to 3 were obtained during a tropical rainy season in an attempt to ensure that the record would incorporate large rainfall events.

Simulation

The statistics that the fractal model generates for daily rainfall were examined using a Monte-Carlo simulation of forty sets of forty day rainfall simulations. The values of t, corresponding to time intervals obeying the hyperbolic distribution, were randomly generated until the sum of the time

intervals equals T, chosen as 40 days in this case. This interval is broken up into durations τ of 24 hours and the number of draws occuring in each duration is noted, each draw is assigned a rainfall of 0.5mm, and the total rainfall is $(N/2)$mm.

Table 1 gives the simulation statistics. For the 40 simulations, the maximum value of the simulated daily rainfall was 107mm and its mean value was 62.20 mm. This is compared with the daily rainfalls calculated from the 40 day data set used to construct Figs. 1 and 2 which had a maximum value of 59mm. These values in Table 1 appear reasonable.

Table 1. Comparison of the statistics of daily rainfalls from 40 simulations of 40-days rainfall

	Data	Simulations			
Rainfall class		Median	Mean	Maximum	Minimum
Maximum (mm)	59	63.5	62.20	107	4.5
Minimum (mm)	0	0	0	0	0
Mean (mm)	10.2	6.74	7.19	21.3	0.1
Median (mm)	3.0	0	0.6	11.5	0

Conclusion

The preliminary results presented above confirm an identification of rainfall as a fractal process, with the time interval between successive rainfall amounts possessing the fractal structure. Such processes are self-similar, in contrast to the traditional specifications of rain rate processes which do not appear to be self-similar (Kedem and Chiu, 1987). They also asymptote to a hyperbolic distribution.

The fractal model is unable to simulate the seasonality of rainfall occurrence, presumably because a purely random choice of t is unable to reproduce seasonal constraints on the choice of t. Given that a single choice of a high t value represents the end of the rainy season, the likelihood of this choice being made should range from almost zero at the start of the rainy season to almost one at the end of the rainy season.

These considerations raise doubts as to the 'universality' of the fractal description during dry periods. Rainfall seems to possess a fractal structure during convective periods, but do drought periods also exhibit fractal structure? It is unclear whether a universal hyperbolic distribution, with a choice of t governed by seasonal constraints produces results that are the same or different to random choices of t made from a distribution that deviates from the hyperbolic at high values of t. Given these provisos it would appear that the fractal model is of relevance during rainy periods, but that its performance during rainless periods remains uncertain.

References

Kedem, B. and L.S. Chiu, 1987: Are rain rate processes self-similar? *Water Resources Res., 23, 1816-1818.*

Lovejoy, S. and B.B. Mandelbrot, 1985: Fractal properties of rain, and a fractal model. *Tellus. 37A. 209-232.*

Lovejoy, S. and D. Schertzer, 1986: Generalized scale invariance in the atmosphere and fractal models of rain. *Water Resources Res., 21, 1233- 1250.*

Mandelbrot, B.B., 1977: Fractals: form, chance and dimension. *W.H. Freeman and Company, San Francisco.*

Skoda, G. 1987: Fractal dimension of rainbands over hilly terrain, *Meteorol. Atmos. Phys., 36, 74-82.*

Zawadzki, I. 1987:Fractal structure and exponential decorrelation in rain, *J. Geophys. Res., 92, 9586-9590.*

Generation of daily rainfall for Jamaica using a self-adjusting distribution function

M. Molina, C. Gray, Y. Nishimura
National Meteorological Service, Jamaica WMO

Abstract

Daily rainfall is a useful data for water resources planning such as in irrigation and flood potential evaluation, particularly when transformed into streamflow data.

A first order Markov chain model can be used to extend daily rainfall for locations with a short record. A transition probalility matrix (TPM) that shows the likelihood that a rainfall of a given magnitude will preceed another one is calculated and smoothed to produce several marginal discrete distribution functions. These functions and a given initial condition makes possible to generate, by a Montecarlo method, a sequence of daily rainfall values.

The soothing process is done using harmonic and generating function techniques and allows for filling up of gaps the recorded data may produce in the TPM.

The data generation includes sampling from bounded normally-distributed random numbers and transformation of the extended daily rainfall from integer to real.

A station with 110 year of record is used to generate daily rainfall at four stations in the Kingston area.

A computer programme written in Fortran 77 for a micro-computer IBM PC/AT, perform all the computations.

A precipitation climatology based on the frequency of wet days

E.S. Epstein, A.G. Barnston, D.L. Gilman
Climate Analysis Center, NMC/NWS, Camp Springs MD, USA

Abstract

We have developed an approach to describing the climatology of precipitation in terms of the frequencies of 0, 1, or more days with measurable precipitation in five day sequences. A plotting diagram has been devised on which one can display the annual course of these frequencies at a station. By assuming a Markov chain model for the occurrence of daily precipitation events, this diagram allows one to infer, within the limitations of the model and the data, the unconditional daily probabilities of precipitation and the conditional probabilities of precipitation following a wet day. Precipitation amounts are described in terms of distributions conditional on there being one, or more than one wet day in five. The procedure used to derive, from daily station data, the values of the various climatological parameters will be described. The precipitation climatologies, in these terms, of a diverse group of stations, and the geographical distribution across the United States of the various frequencies and conditional amounts will also be presented.

Analysis of regional precipitation patterns in West Africa based on the law of leaks

L. Le Barbe, T. Lebel
Labatoire d'hydrologie, Montpellier, France

Introduction

Regional rainfall frequency analysis is increasingly used to describe climatic patterns, and as a basis for water resource management studies. In contrast to point rainfall frequency analysis, the spatial coherence required by regional analysis leads to put less emphasis on the best possible fit for a given series and requires a distribution model valid for the whole area of study, with parameters varying only to account for the differences between measurement stations. While it may be relatively easy to find such a model by any numerical optimization (e.g. a 3 parameter gamma or beta function), the physical significance of the obtained parameters is often unclear. The problem is further complicated if a model fitted to data for a given period of accumulation (e.g. one month), is to be extended to other periods of accumulation (e.g. one day).

This is of special interest in Sahelian countrys where monthly data are generally reliable, which is not the case for daily data. However in terms of climatic knowledge and agricultural needs, it is the frequency analysis of one to fifteen day data which is the most relevant. It is thus a major concern to be able to derive the distribution of rainfall for periods smaller than one month from monthly distributions.

Deeply involved in the study of West African rainfall regimes, ORSTOM scientists were thus led to develop a distribution model allowing extrapolation both in space and in time (period of accumulation) : this distribution is the law of leaks, named after its utilisation in the study of the distribution of gas leakage from gaz pipes by Morlat (cited in Babusiaux, 1969).

The law of leaks: a versatile rainfall distribution model

Presentation of the law of leaks.

The law of leaks originates from the renewal theory (e.g. Cox, 1964), the purpose of which is to study the statistical distribution of the values of chronological events, the duration of the events and the time between two consecutive events being considered as random variables (R.V). To our knowledge it first appeared in the literature in a publication by Einstein(1937) as a special case of Compound Poisson Processes.

Let Y be an exponentially distributed R.V. :

$$f(Y) = (1/s)e^{-Y/s} \tag{1}$$

where f is the probability density function (pdf) and s the expected value of Y (i.e. $E(Y) = s$ and $VAR(Y) = s^2$).

Let N be the number of occurrences of Y over a given period T. N is a R.V. which is assumed Poisson distributed:

$$P(N) = e^{\lambda}\lambda^N/N! \tag{2}$$

where λ is the mean number of occurrences.

We are now interested in studying the distribution of Y_T , which is obtained by accumulating all the realizations of Y over the period T. For a given number of realizations, n, the scaled variable:

$$U = Y_T/s$$

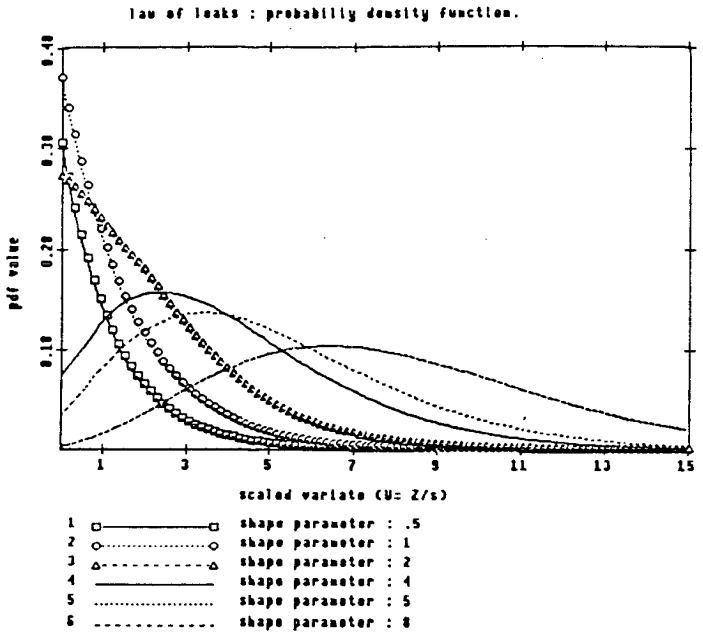

Figure 1: Probability density function of the leak distribution for various shape parameters.

is Pearson III distributed, with pdf

$$f(U) = e^{-U}U^{n-1}/[s(n-1)!]$$

The marginal distribution of U, letting n vary from one to infinity is then

$$f(U) = \sum_{n=1}^{\infty} e^{-\lambda}\lambda^n/[(n!)(n-1)!]U^{n-1}e^{-U)}$$

$$\text{or } f(U) = e^{-\lambda}\lambda e^{-u}\sum_{n=0}^{\infty}[\lambda u]^n/[n!(n+1)!]$$

Let $J = \sum_{n=0}^{\infty}[\lambda u]^n/[n!(n+1)!]$ then J may be written

$$J = I_1(2\sqrt{\lambda U})/[\sqrt{\lambda U}]$$

where $I_1 2\sqrt{\lambda U}$is the modified first order Bessel function. The distribution of Y_T is thus given by :

$$f(U) = e^{-\lambda}\lambda e^{-U}I_1(2\sqrt{\lambda U})/[\sqrt{\lambda U}] \tag{3}$$

for $U > 0$ and $F(0) = F_0 = e^{-\lambda}$ with $U = Y_T/s$.

As can be seen in Fig. 1, this pdf is J-shaped for < 1, and tends towards a Gaussian pdf as it approaches infinity.

Using the characterizing function

$$\Phi(t) = F_0 e^{it0} + \int_0^{\infty} e^{itx}f(x)dx$$

Babusiaux(1969) has shown that the first three moments of the law of leaks are

$$K_1 = E(Y) = \lambda s$$
$$K_2 = E[(Y - E(y))^2] = 2\lambda s^2$$
$$K_3 = E[(Y - E(y))^3] = 6\lambda s^3$$

and thus the coefficient of variation (CV) and the skewness coefficient (γ_1) are

$$CV = \sqrt{K_2}/K_1 = \sqrt{2/\lambda}$$
$$\gamma_1 = K_3/K_2^{1.5} = 3/\sqrt{2\lambda}$$

It is easy to see that for a given CV, the leak distribution is more symmetrical ($\gamma_1/\mathrm{CV} = 3/2$) than the Pearson III distribution ($\gamma_1/\mathrm{CV} = 2$).

Several methods were developed by Babusiaux(1969) to fit the leak distribution. The maximum likelihood method was derived later by Ribstein (1983) and proved more effective.

Application to rainfall distributions

It is widely acknowledged that the distribution of individual events is approximately exponential (Lebel and Guillot,1983), the difficulty being to identify what an individual rainfall event is. Denoting this elementary rainfall event as Y, its pdf is given by equation (1). Further assuming that for a large duration of accumulation (T= one month for instance), the total rainfall depth results from the sum of N independent realizations of Y, and that N is a Poisson distributed R.V., the total rainfall has a leak distribution, its scale parameter being the average amount of rainfall produced by an elementary event and its shape parameter N being the average number of elementary events over the period .

It is then theoretically easy to deduce the distribution of rainfall over a period T' from the leak distribution fitted to the period data: the scale parameter remains constant while the shape parameter may be computed as

$$N_{T'} = N_T T'/T \tag{4}$$

This may prove useful when daily data are unfit for processing due to missing observations which are subsequently accumulated over a longer period.

Furthermore the fitting of a leak distribution to the time series available over a whole region gives physical significance to the spatial variations of the parameters : an increase (or decrease) in average total precipitation can be explained either by an increase (or decrease) in the average number of events or by an increase (or decrease) of the average rainfall depth delivered by an elementary event.

Rainfall related characteristics of the West African climate

In the early days of the science of meteorology tropical meteorology was the most advanced branch. The first general circulation model designed by Hadley in 1735 was anchored in a description of the trade winds regime. During the first half of our century, on the initial impetus of the Norwegian school, the meteorology (and thus its associated science, climatology) of temperate regions saw remarkable progress, while the meteorology of tropical regions stagnated. Insufficient knowledge in these regions has been since recognized as a major impediment to further improvement of General Circulation Models and climatology in general (e.g. Newell and Kidson, 1979), leading the Global Atmospheric Research Programme (GARP) of the WMO to instigate several experiments in tropical countries (GATE and WAMEX among others). These experiments have provided the scientific community with a better understanding of the synoptic, mesoscale and local meteorological processes associated with the wet season precipitations in West Africa(June to September).

It was first confirmed (e.g. Barnes and Sieckman, 1984) that the most significant phenomenon associated withw rainfall production was the squall line. Squall lines are westward travelling disturbances with very active convection. They appear as large and dark cloud fronts to ground observers and can remain organized for more than 3000 km and travel at an average speed of 40 to 70 km/h (ASECNA, 1976). They display a discontinuous activity, the cells of maximum rainfall being separated by zones of very low or even zero rainfall. It seems that the travelling speed of the squall lines

must be related to the maximum rainfall intensities rather than to the total amount of rainfall. Even though there is not yet any satisfactory description of their interaction with the general circulation, the PREGATE-ASECNA experiment of 1973, followed by numerous studies of cloud clusters using satellite imagery allowed Desbois et al.(1988) to give a fairly 'objective' definition of a squall line as viewed by satellite as: (1) a sharp edge on the west side; (2) persistence during at least 12 hours; (3) independence from the cloudy environment (clear area ahead of the line).

Ground measurements show that at a given station the rainfall lasts a few hours. The most significant rainfalls over West Africa, north of the 1200 mm yearly rainfall isoline thus display a marked intermittent character at the daily scale, and thus fall in the category of random process described in section 2.

Nowhere is a good statistical modelling of rainfall distributions more needed than in Sahelian Africa. This region is highly dependent on surface water for its agricultural development but a large number of streams are not perennial. The crops are thus grown during the rainy season and are very sensitive to any variation of the climate, whether in space or in time.

The Benin case study

As a first test of the applicability of the leak distribution as a model of monthly rainfall distribution, the rainfall of Benin was chosen. This country is not representative of the region, since the south is under the influence of the ocean and a mountain range is present in the center. The variations of the yearly rainfall are thus not as meridionally organized as they are further north (for more details see Le Barbe and Ale, 1989).

Forty three stations are available over the period 1950-1985. The calendar months were chosen to define twelve different populations, each represented by a sample of 36 values. The lengths of a few series are much longer (up to 60 years for Cotonou). The study of these series showed no major differences in the average distribution between the period 1950-1985 and the longer periods. This may be related to the fact that the fifty's were wetter than normal, while since 1968, the drought has been severe.

The leak distribution generally fits the experimental distribution well, especially in the middle of the rainy season (July, August and September), as can be seen from Fig. 2. The parameters of the leak distribution were therefore mapped. The maps shown in Fig. 3, display a spatial organisation of these parameters, in agreement with prior knowledge. In particular the specific behavior of the stations bordering the Gulf of Guinea is striking. Over the rest of the country, the shape parameter isolines are roughly organised along latitudes. The organisation of the scale parameter isolines reveals two regions: (1) the south where its value decreases northward, which corresponds to the decreasing influence of the ocean and, (2) the north where no organisation is apparent, which seems to mean that the average magnitude of an elementary event is roughly constant. In addition, the variations of the mean monthly rainfall from March to October are correlated with the variations of the shape parameter (number of events), while the scale parameter remains roughly constant.

For a few stations the parameters of the five and ten day rainfall distribution were computed from the monthly parameters, the scale parameter remaining constant ($s_5 = s_10 = s_30$) and the shape parameter being obtained using equation 4 with T= 30 and T'= 5 or 10. The leak distributions so obtained were plotted along with the corresponding experimental distributions and Fig. 4 shows that, using this procedure, one is able to compute a theoretical distribution that fits the experimental distribution relatively well.

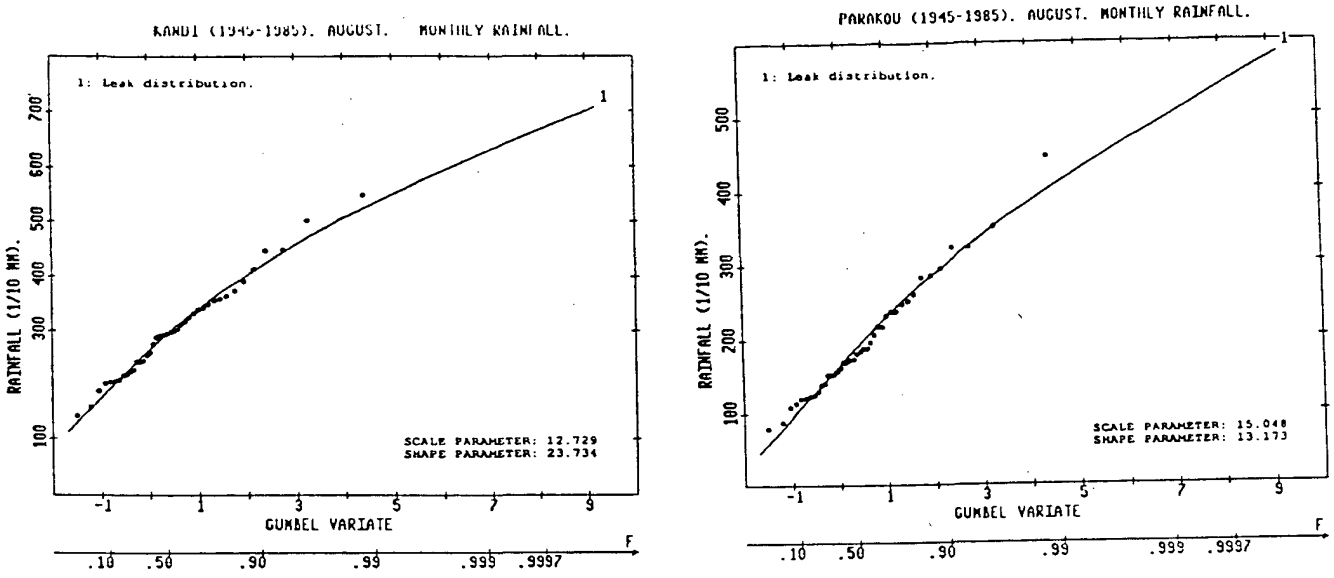

Figure 2: The leak distribution fitted to monthly data.

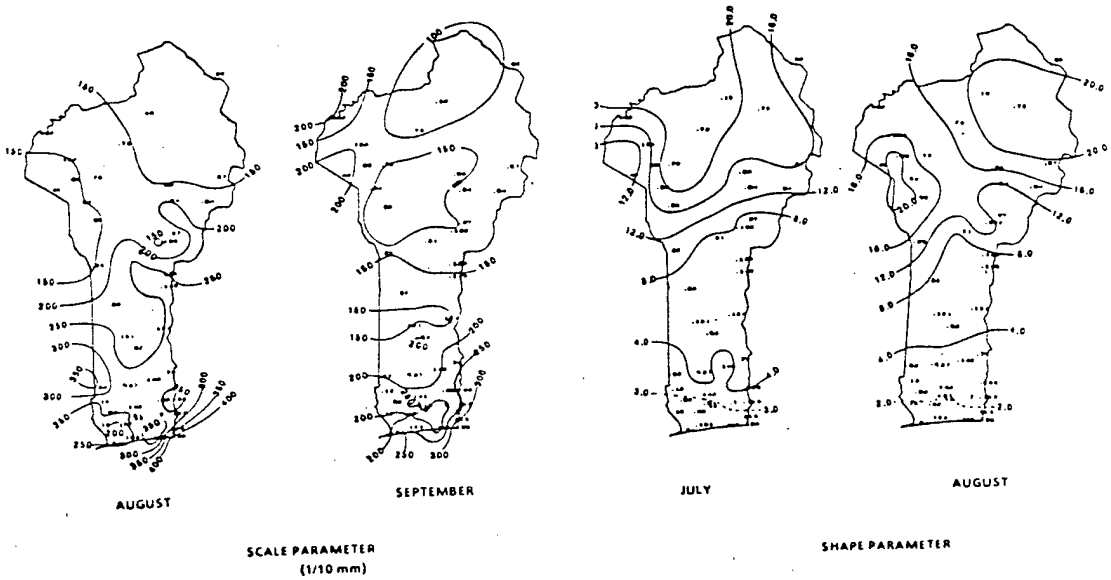

Figure 3: Maps of the scale and shape parameters over Benin.

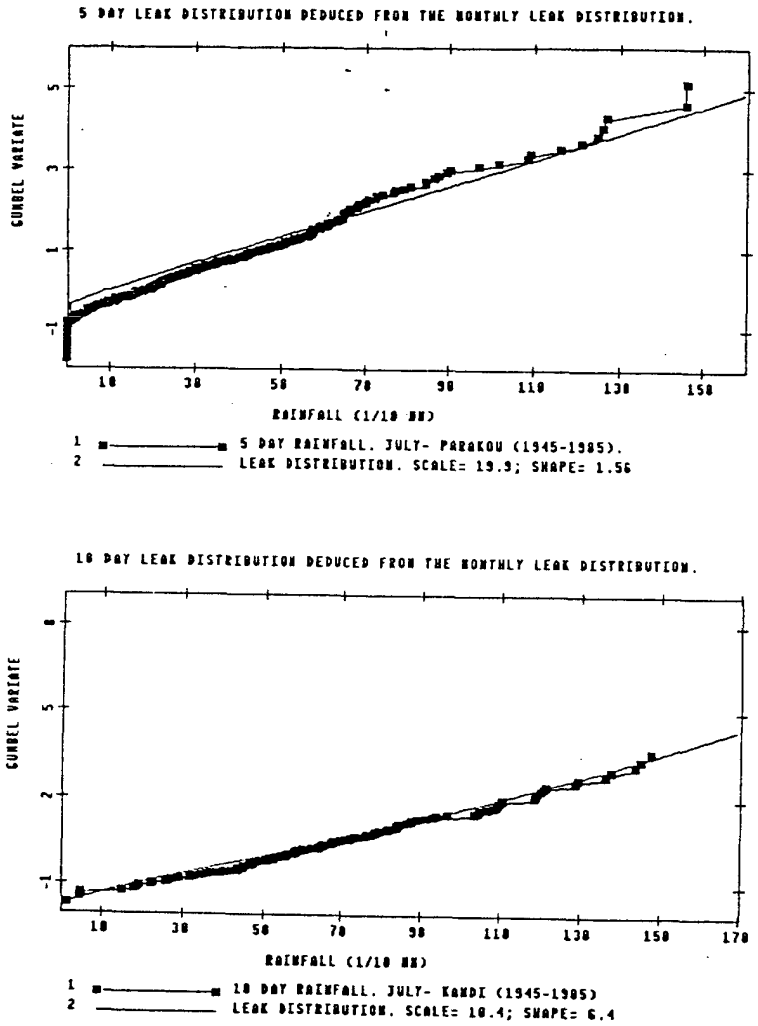

Figure 4: Five day leak distribution deduced from the monthly leak distribution.

Conclusion

Regional rainfall frequency analysis is a cornerstone of water resource management in West Africa, and especially in the assessment of its agricultural potentatial. The leak distribution, one parameter of which (the scale parameter s) is the average rainfall depth of the elementary rainfall event and the other (the shape parameter N) is the average number of events over a given period, provides a good fit for the 43 experimental point monthly distributions available over the period 1950-1985 in Benin. The physical significance of the parameters of the leak distribution allows an interpretation of their spatial variations from a climatological point of view. The main points resulting from this analysis are the following:

- the average number of events increases regularly from the south to the north, for all four months of the rainy season.
- the spatial organisation of the scale parameter allows to divide the area into two regions: 1) the south, under the influence of the Gulf of Guinea with a progressive decrease of the scale parameter from the south to the north; 2) the north, where the scale parameter varies more or less randomly, showing that the meridional rainfall gradient is primarily caused by a variation of the number of events rather than that of the average depth of the rainfall events.
- the end of the rainy season in the north is related to a sharp decrease of the number of rainfall events in October, the average depth of the rainfall events remaining almost constant from March to October.
- the leak distribution allows direct computation of the parameters of the five and ten day rainfall distributions, using the parameters of the leak distribution fitted to monthly data. This is of particular interest when monthly data are available and data over smaller durations are of questionable reliability.

This work is the first step of a larger study of the regional precipitation patterns over West Africa. The suitability of the leak distribution for such a purpose has been established for Benin and will have to be confirmed on a broader scale. This second phase is in progress and has already produced some interesting results.

References

ASECNA (B.E), 1976: Analyse de lignes de grains dans la boucle du Niger. *La meteorologie. VIeme serie.***6**, 183-189.

Babusiaux C., 1969: Etude statistique de la loi des fuites. Thesis prepared at the Paris University of Science.

Barnes G.M., and K. Siekman, 1984: The environment of fast and slow moving tropical mesoscale convective cloud lines. *Mon. Wea. Rev.*,**104**,1029-1035.

Cox D.R., 1964: *Renewal theory* Ed. Methuen. French edition : Dunod(Paris).

Desbois M, T. Kayiranga, B. Gnamien, S. Guessous, and L. Picon, 1988: Characterization of some elements of the sahelian climate and their interannual variations for July 83, 84 and 85 from the analysis of Meteostat ISCCP data. *J. Appl. Meteor.*(to appear).

Einstein H.A., 1937: Der geschiebetrieb als wahrscheinlichkeitsproblem, mitteilung der verschsanstalt fur wasserbau,an der Eidgenossische Technische Hochschule in Zurich. Verlag Rascher & Co., 110 ppp (Translation into English by W. W. Sayre(1972); Bed load transport as a probability problem, *Sedimentation*, H.W. Shen ed.. Fort Collins, Colorado.

Le Barbe L., and Ale, G., 1989: Monographie des ressources en eau de surface du Benin. *Direction de l'Hydraulique du Benin*, ORSTOM, Paris.

Lebel T., and Guillot, P., 1983: Statistical analysis of point and areal hourly rainfalls. *Proceedings 7th International Conference on Hydrometeorology*, AMS , 17-25.

Newell R.E., and Kidson, J.W., 1979: The tropospheric circulation over Africa and its relations to the global tropospheric circulation. *Saharan Dust*, C. Morales, Ed., Wiley 133-169.

Ribstein P., 1983: Loi des fuites. *Cahiers ORSTOM, serie hydrologique*.**20**, 117-145.

Some analytically derived distribution functions for rainfall totals

Van-Than-Van Nguyen[1], Huynh-Ngoc Phien[2]
[1]Dept. Civil Engineering and Applied Mechanics, McGill University, Montreal, Canada; [2]Div. Computer Science, Asian Institute of Technology, Bangkok, Thailand

Introduction

Several statistical models have been presented in the literature for describing the distribution of rainfall accumulations over an n-day period. One common approach is to select a probability distribution function which may appear to fit the observed frequencies of the data (see,e.g., Dingens and Steyaert, 1971; Öztürk, 1981). Parameters of such empirical distribution functions are properties of the sample and, usually, have no physical interpretation. The type of distribution selected depends upon the length n of the period considered and may vary at different locations. The alternative approach is to derive analytically a distribution function for rainfall totals by taking into account some stochastic properties of the underlying rainfall process. This analytical approach should be valid for whatever the length of the period considered and applicable to all locations where the assumed model structure is adequately obeyed. The analytical method has been used in some previous studies to describe the distribution of n-day rainfall totals (Todorovic and Woolhiser, 1975; Stern and Coe, 1984; Nguyen and In-na, 1987).

In a previous paper (Nguyen, 1984) a general stochastic model was proposed for characterizing the temporal distribution of rainfalls within each individual rainfall event or the temporal pattern of each rainfall event. An event was defined as an unbroken sequence of consecutive rainfall depths. The model was applied to daily rainfall process in which the daily rainfall depths were assumed to be independent and identically exponentially distributed random variables while the sequences of wet days were represented by a first-order stationary Markov chain. Hence, the model did only account for the dependence of rainy day occurences through the first-order Markov chain. The present paper, a continuation of the previous one, suggests more general models which can take into account either both the persistence in daily rainfall occurences and the dependence between successive daily rainfall depths or the correlation between cumulative rainfall depths and rainfall durations.

The objective of this paper is to determine analytically the probability distribution of cumulative rainfall amounts in a given rainfall event. In this study, we will use an analytical methodology similar to that proposed in the earlier cited work (Nguyen and In-na, 1987) for characterizing the distribution of rainfall totals within a fixed calendar-time period (e.g., the first ten days in May, etc.). In such an application, only a portion of a rainfall event or some of the events that have occurred within the fixed period selected have been considered. Various modifications, therefore, will be needed to use this analytical method in the estimation of the distribution function for the total rainfall event depths. The use of an analytical solution seems to have several advantages over the use of empirical fitting approaches because it can take explicitly into account some observed random properties of an actual daily rainfall record.

Theoretical development

In view of the objective stated above, a rainfall event in this study will be defined as an uninterrupted sequences of consecutive daily rainfalls. Consider now an interval of time which consists of n days. In order to consider the total depths of all complete rainfall events that have occurred, all events are arranged to begin with the first day of the n-day period, and the length of the n-day time interval considered must be at least equal to the longest observed rainfall event duration (or the longest observed wet period).

Let ε_ν denote the daily rainfall depth in the ν-th day. Let D_n represent the total duration of a rainfall event (or the total number of consecutive rainy days). The total rainfall depth or the accumulated amount of rainfall $V(n)$ during D_n consecutive rainy days of the n-day period can be defined as

$$V(n) = \sum_{\nu=1}^{D_n} \varepsilon_\nu \tag{1}$$

Then the distribution function $F_n(x)$ of $V(n)$can be written as follows (Todorovic and Woolhiser, 1975 or Nguyen, 1984):

$$F_n(x) = P\{V(n) \leq x\} = \sum_{k=1}^{n} P\{X_k \leq x, D_n = k\} \tag{2}$$

in which $P\{.\}$ denotes the probability, and $X_k = \sum_{\nu=1}^{k} \varepsilon_\nu$ for $k = 1, 2, \ldots, n$.

In the above theoretical development, the equation (2) was restricted to daily rainfall process. However, it is readily seen that this restriction is not necessary. The general model, equation (2), might be used for rainfall data of any time interval. In the following for daily rainfall process, we consider the following particular cases:

(A) The cumulative rainfall depth X_k and the rainfall duration D_n are independent

In this case we can write:

$$F_n(x) = \sum_{k=1}^{n} P\{X_k \leq x\}.P\{D_n = k\} \tag{3}$$

Hence, to determine the distribution function $F_n(x)$, it is necessary to compute the probabilities $P\{X_k < x\}$ and $P\{Dn = k\}$. In this paper, the probabilities $P\{Dn = k\}$ for $k = 1, 2, \ldots, n$ is assumed to be approximated by a first-order stationary Markov chain (Nguyen, 1984), and the distribution function $P\{X_k \leq x\}$ are analytically derived as shown in the work by Nguyen and In-na (1987).

More specifically, if the successive daily rainfall depths $\varepsilon_1, \varepsilon_2, \ldots, \varepsilon_n$ are independent and identically exponentially distributed random variables, it can be readily shown that (e.g., Todorovic and Woolhiser, 1975):

$$F_n(x) = \sum_{k=1}^{n} \left(\frac{\alpha^k}{\Gamma(k)} \int_0^x u^{k-1} e^{-\alpha u}\, du \right) .P\{D_n = k\} \tag{4}$$

in which $\Gamma(k) = (k-1)!$ for $k = 1, 2, \ldots, n$, and α is the parameter of the exponential distribution of daily rainfalls. Furthermore, if there exists a significant correlation between successive daily rainfall amounts, the probability $F_n(x)$ can be written as follows (Nguyen and In-na, 1987):

$$F_n(x) = \sum_{k=1}^{n} \left\{ (-1)^{k-1} \sum_{i=1}^{k} \left[\prod_{j \neq i} \left(\frac{\lambda_j}{\lambda_i} - 1 \right)^{-1} . \left(1 - e^{-\frac{\alpha}{\lambda_i} x} \right) \right] \right\} .P\{D_n = k\} \tag{5}$$

where the λ's are the eigenvalues of the correlation matrix of successive daily rainfalls, and $\prod_{j \neq i} (\lambda_j / \lambda i - 1)^{-1}$ is the product of the $(\lambda_j / \lambda_i - 1)^{-1}$'s for $i, j = 1, 2, \ldots, k$ and $j \neq i$. The parameters α and λ's in equations (4) and (5) will be estimated from the observed data.

(B) The cumulative depth X_k and the rainfall duration D_n are dependent

Under this hypothesis we can write

$$F_n(x) = \sum_{k=1}^{n} P\{X_k \neq x | D_n = k\}.P\{D_n = k\} \tag{6}$$

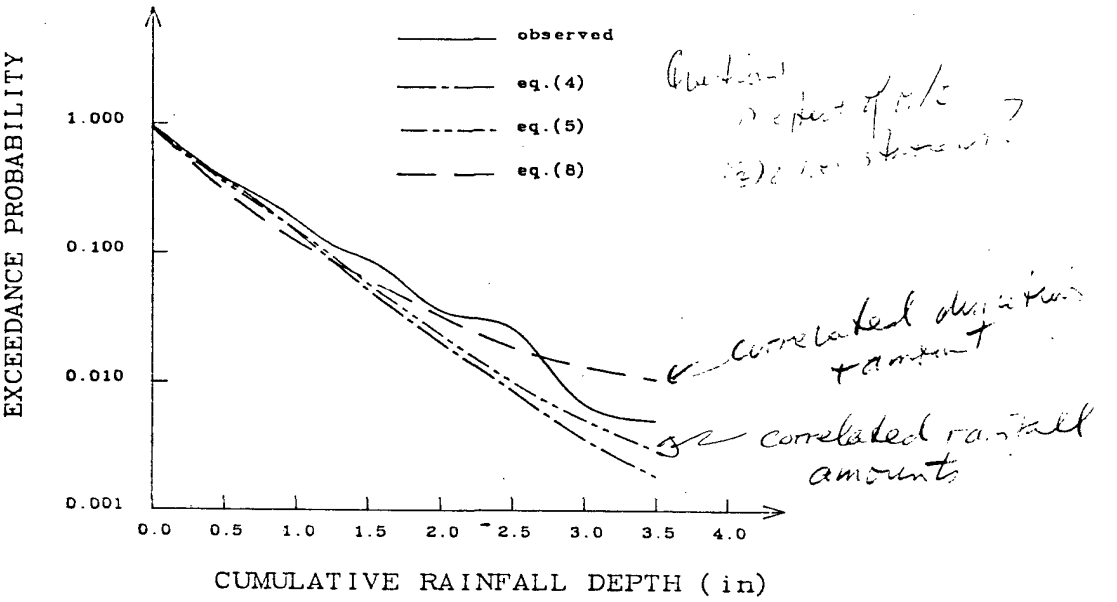

Figure 1: Observed and theoretical distributions of rainfall totals

Furthermore, in this paper we will assume that X_k and D_n are linearly dependent. That is,

$$X_k = (aD_n + b)\frac{\epsilon_k}{100} \tag{7}$$

where a and b are constant coefficients, and ϵ_k is the random transformed percent residuals. If the distribution of ϵ_k can be adequately described by a simple exponential distribution with parameter β, hence equation (6) can be written as follows (Nguyen and In-na, 1987):

$$F_n(x) = \sum_{k=1}^{n} \left[1 - exp\left(-\frac{100\beta}{ak+b}x\right)\right] .P\{D_n = k\} \tag{8}$$

The parameters a, b and β will be estimated from the observed data.

Numerical application

In the following, to test the descriptive capabilities of the theoretical distribution functions, equations (4), (5) and (8), an illustrative application will be presented using daily rainfall data in summer seasons (June–September) for the 1943-1974 period at Dorval Airport in Canada. According to the definition of a rainfall event in this study, a total of 768 events having durations of from 1 to 12 days have been selected from the 32-year record.

Figure 1 shows a comparison between observed and theoretical distributions of total rainfall event depths. It is noted that the model with serial correlation between daily rainfall amounts, eq. (5), gives a small improvement as compared to the model without serial correlation, eq. (4), probably due to the weak correlation inherent in the observed daily rainfall record considered. However, by taking into account the dependence between cumulative rainfall depth and duration, the model (8) provides the best fit to the observations. This indicates that, in determining the distribution of total rainfall in a given event, the effect of serial correlation of daily rainfalls seems to be negligible as compared to that due to the correlation between total rainfall depth and duration.

Conclusion

An analytical method that can explicitly take into account some observed stochastic properties of an actual rainfall record has been suggested in this study for determining the probability distribution of total rainfall depths in a given wet period. It can be concluded that the proposed method is more general and more flexible than the empirical fitting approaches that have been used in most previous investigations. The use of an analytical solution is a convenient feature of the suggested method because, with this method, it is not necessary to guess which theoretical distribution best fits to the observed frequency distribution of rainfall totals. Further studies with a more extensive data base are planned to compare the performance of different models proposed.

References

Dingens, P. and H. Steyaert (1971). Distribution for k-day rainfall totals. *Bull. of the International Association of Scientific Hydrology, 16(3), pp.19-24.*

Nguyen, V-T-V. (1984). A Stochastic Description of Temporal Daily Rainfall Patterns, *Canadian Journal of Civil Engineering, 11(2), pp. 234-238.*

Nguyen, V-T-V. and N. In-na (1987). On probability distribution of n-day rainfall totals, *Proc. of the Tenth Conference on Probability and Statistics in Atmospheric Sciences, Edmonton, Alberta, October 6-8, 1987, American Meteorological Society, pp. 146-148.*

Öztürk, A. (1981). On the study of a probability distribution for precipitation totals, *J. of Appl. Meteor., 20, pp.1499-1505.*

Stern, R.D. and R. Coe(1984). A model fitting analysis of daily rainfall data, *J.R. Statist. Soc. A. 147, pp. 1-34.*

Todorovic, P. and D.A. Woolhiser (1975). A stochastic model of n-day precipitation, *J. of Appl. Meteor., 14, pp. 17-24.*

On Clustering of high values in statistically stationary series

Ross Leadbetter, Ishay Weissman, Laurens de Hann, Holger Rootzén
University of North Carolina, Chapel Hill NC, USA; The Technion, Haifa, Israel; Erasmus University Rotterdam, Netherlands; University of Lund, Sweden

Introduction

The statistical properties of high values of observed (e.g. meteorological) series leave traditionally been discussed by application of classical extreme value theory, assuming that the observations are well modelled as a sequence of statistically independent and identically distributed (i.i.d.) values. One finds that under such a model very high values tend to occur singly - i.e. are typically preceded and followed by 'moderate' values. On the other hand when observations are serially dependent a high value will tend to induce further high values, so that these high values occur in clusters (cf. Figure 1).

A study of the cluster structure has two important purposes:

1. To model statistically the duration of 'episodes' of high values of series of interest (such as wind speed, leading to storms; rainfall, leading to floods. etc.)

2. To provide appropriate modifications to the classical theory of extreme values to deal with dependence among the observations in discussing the largest and other high values in long time periods.

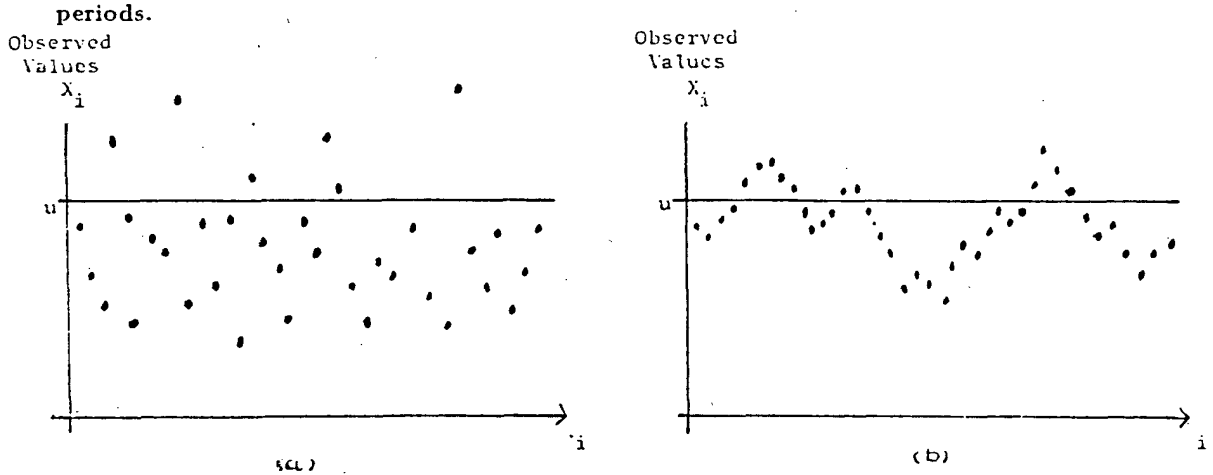

Figure 1: (a) Independence - no clustering (b) Clustering under dependence

The question of precisely defining a 'cluster' of high values will be taken up in Section 3. For the moment however we simply regard cluster of 'exceedances' as the groups of consecutive observed values above a high level u (cf. Fig. 1).

The statistical properties of the lengths of the clusters are of course basic to the discussion of cluster structure. In particular it turns out that under wide conditions, the mean cluster length (i.e. the average cluster size above a high level in a long time period) is an important parameter. We denote this parameter by $1/\theta$ and refer to θ as the 'extremal index' of the observed series (cf. [5] [6]).

It may be shown ([6]) that the value of θ lies between zero and one. In the 'classical' case for i.i.d. observations the high values tend to be isolated as noted so that clusters have size 1 and correspondingly $\theta = 1$. This is true also under serial dependence in a number of cases (e.g. many Gaussian models). On the other hand for highly dependent series the mean cluster size will exceed

one and correspondingly one then has $\theta < 1$. Thus in understanding the clustering phenomenon it is important to estimate the value of θ - a topic considered in Section 3 using theory of [3], illustrated by practical examples in Section 4.

In addition to its relevance to cluster structure, the extremal index θ has important bearing on the extreme value theory for dependent observations. Specifically if the values observed are $X_1, X_2, ...$ and

$$M_n = max(X_1, X_2, ..., X_n)$$

then the classical theory discusses the possible limit laws for M_n of the form

$$P\{a_n(M_n - b_n) \leq x\} \rightarrow G(x), \text{ as } n \rightarrow \infty \tag{9}$$

under the assumption that the terms X_i are i.i.d. In particular the theory shows that G must (aside from linear normalisations) then be one of the three so-called 'extreme value types' $G(x) = exp(-e^{-x}), G(x) = exp(-x^{-\alpha}), \alpha > 0, x > 0$, or $G(x) = exp(-(-x)^{\alpha}), \alpha > 0, x < 0$.

If on the other hand observations X_i are allowed to be statistically **dependent** but keep the same (marginal) distribution function, more recent theory (cf. [6])shows that then under wide conditions the only change to (1) is the replacement of G by G^{θ}. It is readily shown that G^{θ} is of the same extreme value type as G itself, so that the classical criteria for the type of limit may be used, just as if the observations were i.i.d.

Thus knowledge of the value of the extremal index is all that is necessary in modifying the classical limiting distribution of the maximum to deal with a wide class of (stationary) series of dependent observations. For other 'order statistics' (e.g. second, third largest values etc.) the modification depends more intimately on the detailed statistical properties of the cluster sizes but θ still plays an important role.

Thus estimation of θ is also important for extreme value theory applications. It is perhaps of interest to note that the classical i.i.d. - based theory has been traditionally used in applications where the data is clearly dependent. In fact this would perhaps be so for most naturally occurring phenomena , such as meteorological series. The success of extreme value theory in such cases stems from the fact noted above that the type of the limit law is unchanged by the introduction of dependence, though the constants may change.

Since the constants are estimated, the dependence in the data is not necessarily apparent from the estimation process. Of course, an estimation of θ is really involved implicitly in such an analysis even if not carried out explicitly.

In Section 2 the specific theory surrounding the extremal index θ briefly indicated, and Section 3 discusses estimation procedures for θ. This is illustrated in Section 4 from measurements of acid levels in periods of rain, obtained from the acid deposition study [2], and by tide level series from the port of Den Helder, Holland.

The extremal Index

A detailed theory regarding the clustering of high values may be found in [6] [4] and here we indicate only some main features.

If $X_1, X_2, ...$ are i.i.d. random variables with common distribution function (d.f.) F, and $\tau > 0$, let $u_n = u_n(\tau)$ be a family of 'levels' such that

$$n(1 - F(u_n)) \rightarrow \tau \tag{10}$$

It is easily shown (since the d.f. for M_n is F^n) that (1) is entirely equivalent to

$$P\{M_n \leq u_n\} \rightarrow e^{-\tau} \tag{11}$$

This simple equivalence underlies much of classical extreme value theory - for example (1) may be put in the form (3) by writing $u_n = x/a_n + b_n$, $G(x) = e^{-\tau}$. Further, use of the equivalence yields so-called 'domain of attraction' criteria in terms of the tail $1 - F(x)$ to determine which type of extreme value limit occurs in particular cases.

Typically $u_n(\tau)$ increases as n increases and 'high values' of the observations X_i are interpreted as being those which exceed the level $u_n(\tau)$. As n increases these 'exceedances' of time scale) occur at points of time which become like a Poisson Process. The points of this Poisson Process are of course isolated and do not occur in clusters.

Assume now that $X_1, X_2, ...$ can be dependent, forming a statistical stationary sequence. Then under a mild dependence decay condition at large separations (cf. [6]) it may be shown that if (1) holds then

$$P\{M_n \leq u_n\} \to e^{-\theta\tau} \tag{12}$$

for a parameter θ, $0 < \theta < 1$ which does not depend on τ. The parameter θ is in fact the extremal index and it follows simply that

$$P\{a_n(M_n - b_n) \leq x\} \to (G(x))^\theta \tag{13}$$

For the dependent sequence, exceedances of the level $u_n(\tau)$ now occur in clusters (Fig. 1) which, after time scale change, are situated at (approximately) Poisson points when the level is high. The exceedances then approximate more and more closely a so-called 'Compound Poisson Process' where the Poisson positions of the clusters (occurring at the rate $\theta\tau$)are 'compounded' or 'marked' by the cluster sizes. As noted above the mean cluster size tends to $1/\theta$ as the level u_n increases.

Finally in this sketch of basic concepts we note that the distribution of the rth largest value $M_n^{(r)}$ (rth 'order statistic') may be obtained from that for $M_n (= M_n^1)$ in either i.i.d. or dependent contexts. This is done by a simple consideration of the limiting Poisson (or Compound Poisson) nature of the exceedances by noting that the event $\{M_n^{(r)} \leq u_n\}$ occurs precisely when there are less than r exceedances of u_n among $X_1, X_2, ..., X_n$. In the i.i.d. case this leads to the limiting distribution

$$P\{a_n(M_n^{(r)} - b_n) \leq x\} \to G(x) \sum_{s=0}^{r-1} (-logG(x))^s/s! \tag{14}$$

when M_n has limiting distribution given by (1). In the dependent case this must be modified to read

$$P\{a_n(M_n^{(r)} - b_n) \leq x\} \to G^\theta(x) \sum_{s=0}^{r-1} \sum_{j=s}^{r-1} (-logG^\theta(x)^s/s!)\pi_{s,j} \tag{15}$$

where π_s, j are constants - specifically being for each s, the sth convolution probabilities of the limiting cluster size distribution.

A comparison of (6) and (7) highlights the fact that the introduction of dependence makes much more of a difference for rth largest values (for r=2, 3,....) than for r=1 when G is simply replaced by G^θ. This is especially important to note in applications where e.g. the second (or rth for $r \geq 2$) largest values are periodically reported, rather than the maximum itself.

Estimation of θ

In view of the interpretation of θ^{-1} as limiting size of an exceedance cluster it is natural to estimate θ simply as the reciprocal of the average cluster size in the given observations. That is one estimates θ by

$$\hat{\theta} = Z/\sum_{i=1}^{Z} Y_i$$

where Y_i is the size of the ith cluster and Z is the total number of clusters. But the sum of cluster sizes is simply the total number N of exceedances of the level u_n so that

$$\hat{\theta} = Z/N \tag{16}$$

Two practical questions arise, the first concerning the precise definition of a cluster. A natural definition would be that any group of consecutive exceedances forms a cluster. This 'exceedance run' definition is simple but difficult to deal with theoretically and has the disadvantage that two or more nearby but separated groups should perhaps be regarded as just one cluster. Another definition is obtained by dividing the n observation times into smaller blocks of specified size and regarding all exceedances (if any) in any one block as forming a cluster (cf. [4]). Of course this can split single clusters and combine two or more into one. However it is simple to deal with theoretically, does not depend critically on the block size, and is asymptotically equivalent to the first definition under general conditions ([7]). In Section 4 we use both definitions, and vary the block sizes for the latter 'block based' definition.

The second practical question is philosophically more serious but provides guidance concerning the proper procedure to be used. When the level u_n satisfies (2) there are insufficient exceedances to give statistical 'consistency' for the estimate $\hat{\theta}$. That is as n increases the value of $\hat{\theta}$ does not necessarily converge appropriately to the value θ. It has, however, been shown ([3] for the block-based estimator and [8] for the runs estimator) that consistency can be achieved by the use of somewhat lower levels - replacing (2) by

$$1 - F(u_n) = \gamma_n \to 0,\ n\gamma_n \to \infty \tag{17}$$

F is typically unknown but γ_n is approximately the proportion of observations exceeding u_n. Thus (9) suggests selecting a small value for γ_n and choosing u_n so that the proportion of observations exceeding u_n is γ_n (i.e. u_n is the (1 - γ_n) percentile of the data). If possible γ_n should be selected so that $n\gamma_n$ (approximately the number of values exceeding u_n) is large. For the first application in the next section we have (for n = 504) taken γ_n = .05 and 0.1 so that $n\gamma_n$ = 25 and 50. Of course 'consistency' is concerned with increasing values of n rather than fixed sample sizes. However the guidance provided in the choice of u_n does seem valuable.

It has also been shown in [3] under appropriate conditions, when u_n is chosen by (9), that a block-based estimator $\hat{\theta}$ is approximately normal with mean and variance

$$\hat{\theta}(\hat{\theta}^2 V - 1)/(n\gamma_n) \tag{18}$$

where (using the previous notation)

$$V = \sum_1^Z Y_i^2/Z \tag{19}$$

V is simply the average of squares of cluster sizes. This result applies when n is large and $0 < \theta < 1$. Similar properties for the runs estimator are considered in [8].

This result enables one to provide confidence intervals or a hypothesis test regarding θ, i.e. to determine the extent of clustering of high values in the observed data.

Applications

Our first example comes from acid levels ([2]) in periods of rain measured in Pennsylvania, USA. In the study one measurement of each quantity of interest was made in each of a series of 504 consecutive 'rain events' and these are here taken as the basic data - focusing specifically on sulphur dioxide (SO_2). An excerpt from the data is shown in Table 1 in which the observed values greater than 93 μ mole/L are reported together with the numbers (in time sequence) of the rain periods in which they occurred.

Table 1: Rain periods and sulphate values (μ mole/L) exceeding 93 μ mole/L.

Rain														
Period	55	60	*64*	*65*	*73*	*74*	*75*	77	83	85	102	129	150	160
Sulphate	140	95	150	110	99	130	120	110	110	120	130	98	110	95
Rain														
Period	168	*176*	*177*	184	*187*	*188*	*228*	*229*	237	242	247	253	315	317
Sulphate	110	130	130	150	110	110	280	160	96	96	98	150	94	110
Rain														
Period	324	334	353	*374*	*375*	*376*	*377*	*397*	*398*	402	*404*	*405*	415	439
Sulphate	200	330	100	110	110	95	99	340	99	140	95	100	150	100
Rain														
Period	*452*	*453*	*455*	*469*	470	476	480	485						
Sulphate	100	100	190	130	130	105	110	150						

Three choices were made for the level u_n (viz. 93, 99, 110 μ mole/L) corresponding approximately to the 90%, 92.5% and 95% percentiles of the data, the numbers of exceedance values being respectively N=50, 34, 22. The observed distributions of cluster sizes are given in Table 2 along with the estimate $\hat{\theta}$ and its estimated standard deviation (s.d.) $\hat{\sigma}$.

In this table runs occur where two or more rain periods with consecutive index values appear. These are indicated by italicizing.

Confidence intervals for θ are complicated by the dependence of the variance of $\hat{\theta}$ on θ and the fact that θ is only approximately unbiased. However calculations show that e.g. the classical 95% interval $(\hat{\theta} \pm 2\hat{\sigma})$ is likely to give a reasonable approximation to the true interval (and will be conservative in cases where the bias is small). For example for the runs estimate based on the $u_n = 99$ level, this 95% confidence interval for θ is (.68, .90).

Such elementary comparisons of differences between the estimated values with standard deviations show no statistically significant differences between the different procedures but all estimates $\hat{\theta}$ are significantly less than one, so that it may be safely concluded that $\theta < 1$ i.e. clustering is present. This is confirmed by a test of the null hypothesis that the data is i.i.d. (which implies $\theta = 1$) based on the number of runs one then expects to find in the data. This avoids the bias problem referred to above. Specifically under the hypothesis of i.i.d. data one has ([1])

$$E(\hat{\theta}) = E(Z/N) = [\frac{1}{2} + n^{-1}N(n-N]/N$$

$$\sigma^2 = var\hat{\theta} = \frac{1}{2}(n-N)[2N(n-N) - n]/(n^3N)$$

For the three levels considered the estimated values, means and variances are:

	Estimated value	Expected value under independence	s.d. under independence
u_n	$\hat{\theta}$	$E(\hat{\theta})$	σ
93	.74	.91	.040
99	.79	.94	.040
110	.82	.98	.042

Since the estimated values differ from the expected values for i.i.d. values by approximately four standard deviations one can clearly reject the i.i.d. hypothesis - again providing strong evidence that $\theta < 1$, i.e. clustering is present.

Table 2: Cluster size and estimates ($\hat{\theta}$) for the extremal index (θ) with estimated standard deviation ($\hat{\sigma}$). (* Number in parenthesis indicates block length.)

Cluster Definition	u_n	N	Frequency of cluster sizes 1	2	3	4	Z	$\hat{\theta}$	V	s.d. $\hat{\sigma}$
Runs	93	50	27	8	1	1	37	.74	2.27	.060
Runs	99	38	22	8	-	-	30	.79	1.80	.051
Runs	110	22	14	4	-	-	18	.82	1.67	.067
Block (5)*	93	50	21	10	3	-	34	.68	2.59	0.52
Block (5)	99	38	15	10	1	-	26	.68	2.46	.050
Block (5)	110	22	12	5	-	-	17	.77	1.88	.064
Block (10)*	93	50	11	11	3	2	27	.54	4.22	.050
Block (10)	99	38	13	8	3	-	24	.63	3.00	.056
Block (10)	110	22	12	5	-	-	17	.77	1.88	.064

One cautionary (and instructive) note concerns the increase of the estimates $\hat{\theta}$ as the level increases which is apparent (even if not statistically significant) in all three procedures. For dependent, but non-clustering data ($\theta = 1$) one would certainly expect the clusters of size greater than one to become 'thinned out' more and more as the level increases,leading to higher values of$\hat{\theta}$. Hence some modest caution needs to be attached to our (statistically highly significant) conclusion $\theta < 1$. The observed consistent increase in $\hat{\theta}$ with level suggests that one's procedure in practice should be to try higher levels until the value of $\hat{\theta}$ either stabilises at some value less than one, or else tends to one, or until the level is so high that exceedances are very few, and the estimated standard deviation $\hat{\sigma}$ of $\hat{\theta}$ thus shows a substantial increase. That point appears to have been reached in the above table with an increase in $|sigma$ of between 11% and 28% from the 93 to the 110 level.

The final point to be made regarding this data is that the block based estimates tend to be somewhat smaller than for runs, and the larger block size gives the smaller estimates (as would be expected). For 'smoothly varying' observations the runs definition seems preferable but a choice should be made from a visual inspection of the data. As noted the estimators are asymptotically equivalent [(8)] so that their closeness to each other is another indication as to whether the level being used is sufficiently high for the given data set.

The second study concerns the heights of tides measured at Den Helder, Holland in winter periods from 1932-1985.

Four levels were selected - corresponding to the 90%, 92.5%, 95%, 97% percentiles (actual levels 106, 114, 128, 149 cm). The estimates of θ and their standard deviations are given in Table 3 for estimators based on runs and on block lengths of 4, 5, 10.

Again in this data there is clear evidence that $\theta < 1$, indeed some values of $\hat{\theta}$ differ from 1 by as much as fourteen standard deviations. Again also the estimates $\hat{\theta}$ are increasing with increasing level and do not show signs of stabilising with the levels used. However the more than 60% increase in standard deviation for $\hat{\theta}$ from low to high levels suggests that one may not wish to use yet higher levels in view of the attrition of exceedances. In this application the shortest block size used actually gives estimates which are larger than (and quite close to) those for runs. Again, unless the observations tend to oscillate rapidly when above a high level, the use of the runs estimator seems preferable in

Table 3: Estimates ($\hat{\theta}$) for the extremal index (θ) with estimated standard deviation ($\hat{\sigma}$). (* Number in parenthesis indicates block length.)

Cluster Definition	u_n (cm)	N	Z	$\hat{\theta}$	s.d. $\hat{\sigma}$
Runs	106	947	602	.64	.028
Runs	114	722	465	.64	.032
Runs	128	470	324	.69	.036
Runs	149	233	167	.72	.046
Block (4)*	106	947	616	.65	.025
Block (4)	114	722	483	.67	.028
Block (4)	128	470	335	.71	.033
Block (4)	149	233	175	.75	.043
Block (5)*	106	447	572	.60	.027
Block (5)	114	722	456	.63	.030
Block (5)	128	470	317	.67	.035
Block (5)	149	233	173	.74	.044
Block (10)*	106	947	440	.46	.032
Block (10)	114	722	361	.50	.036
Block (10)	128	470	258	.55	.041
Block (10)	149	233	147	.63	.055

avoiding the ambiguity of block size choices.

In summary, the two data sets analysed both have extremal index estimates which are significantly less than one, demonstrating the presence of clustering of high values in each case. The differences between the 'runs' and 'block based' estimators are not statistically significant; the former may be preferred in practice because of its unambiguous definition, especially for 'smoothly varying' observed series, though the latter is theoretically more tractable. Finally we note that it is possible in principle to estimate the limiting cluster size distribution by similar means, but this requires yet larger amounts of data to obtain satisfactory statistical properties for the estimates.

References

[1] Brownlee, KA., 1960: Statistical theory and methodology in Science and Engineering, *Wiley, New York*

[2] Gentleman, Zidek and Olson, 19XX: MAP3S/PCN Acid rain precipitation data base, *Tech. Rept. 19, Statistics Department, University of British Columbia*

[3] Hsing, T., 1988: Estimating the parameters of rare events, *Preprint, Texas A & M University, submitted for publication*

[4] Hsing. T., J. Husler, and M.R. Leadbetter, 19: On the exceedance point process for a stationary sequence, *Probab. Th. Rail. Fields, 78, 97-112*

[5] Leadbetter. M.R., 1976: Extremes and local dependence in stationary sequences, *Z. Wahr. Verw. Geb., 34, 11-15*

[6] Leadbetter, M.R., J. Lindgren, H. Rootzén, 1983: Extreme and related properties of random sequences and processes, *Springer, New York*

[7] Leadbetter, M.R., and S. Nandagopalan, 1988: On exceedance point processes for stationary sequences under mild oscillation restrictions, *University of North Carolina Center for Stochastic Processes Tech. Rept, 23*

[8] Nandagopalan, S., 19XX: *Ph.D thesis, University of North Carolina Center for Stochastic Processes, in preparation*

CLIMPROB- A computer program to develop probabilities for different types of agricultural weather situations

R.E. Neild and Y-H. Xu
Center for Agricultural Meteorology and Climatology
University of Nebraska, Lincoln NE, USA

Abstract

. Daily weather histories of maximum-minimum temperature and precipitation approaching 100 years or more have been recorded for many locations in the U.S.A. as well as in other nations. Reported here is a completely flexible program for small computers that can generate a chronology of different types of agweather situations that have happened and develop their probabilities from a ranked frequency of the incidence in the long term history.

. The program is flexible and allows users to open historic daily weather files for any time period considered as critical and select a type of analysis from a menu of 21 different items which, with user input values for thresholds, accumulations or extreme limits for temperature or precipitation, define an agroclimatic situation of interest. Data are presented comparing CLIMPROB results with more sophisticated Markov Chain and incomplete gamma analysis of precipitation. CLIMPROB has been used for analysis of possible trends and seasonal interrelationships between commonly discussed weather changes. Example applications of CLIMPROB menu items to agriculture are also presented and discussed.

Neild, R.E., Seeley, M.W., and Richman, N.H., 1978: The computation of agriculturally oriented *normals* from monthly climate summaries. *Agric. Meteorol.*, **19**, 181-187.

Feyerherm, A.H., Bark, L.D., and Burrows, W.C., 1966: Probabilities of sequences of wet and dry days. *Kansas Tech. Bull.*, **139**, Kansas State University, Manhattan, Kansas.

PARTICIPANTS

Superscript on name indicates previous IMSC's attended

Dr. Ian Andrew
Forest Research Institute
Private Bag
Rotorua
NEW ZEALAND

Prof. Craig F. Ansley
Dept. Accounting & Finance
Univ. Auckland
PB Auckland

Dr. Robert C. Balling[3]
Lab. Climatology
Arizona State Univ.
Tempe AZ 85287
USA

Dr. L. le Barbe
Lab. d'Hydrologie ORSTOM
20501 Ave du Val de Montferrand
34032 Montpellier CEDEX
FRANCE

Dr. Tom Beer
Div. Atmos. Res. CSIRO
PB No. 1 Mordialloc
Vic 3195
AUSTRALIA

Dr. Thomas L. Bell
NASA/Goddard Space Flight C
Greenbelt MD 20771
USA

Prof. Susana A. Bischoff
Fac. Ciencias Exactas y Natur.
Univ. de Buenos Aires
1428 Buenos Aires
ARGENTINA

Dr. Albert R. Boehm[123]
ST Systems Corporation
109 Massachusetts Ave
Lexington MA 02173
USA

Dr. A. Brett Mullan
Meteorol. Service
PO Box 722
Wellington
NEW ZEALAND

Dr. Barbara G. Brown
E & S Impacts Group NCAR
PO Box 3000 Boulder CO 80307
USA

Dr. Robert F. Cahalan[23]
Lab. Atmospheres
NASA/Goddard Space Flight C
Greenbelt MD 20771
USA

Dr. Hongxing Cao
Academy Meteorol. Sc.
46 Baishiqiaolu Rd
Beijing
PEOPLES REPUBLIC CHINA

Prof. Pao-Shin Chu
Dept. Meteorol Univ. Hawaii
2525 Correa Road
Honolulu HA 96822
HAWAII

Dr. Rosa H. Compagnucci
Fac. Ciencias Exactas y Natur.
Univ. de Buenos Aires
1428 Buenos Aires
ARGENTINA

Dr. A.(Hans) J. Coops[23]
Inst. Met..Rijksuniv. Utrecht
Princetonplein 5
NL-2506 Utrecht
THE NETHERLANDS

Prof. Arnold Court[23]
Dept. Geography
California State Univ.
Northridge CA 91330
USA

Dr Bengt Dahlstrom
SMHI Fack
S-60176 Norrkoping
SWEDEN

Dr. Edward Epstein[23]
Climate Analysis Center
W/NMC51
Washington DC 20233
USA

Prof. Oskar Essenwanger[23]
610 Mountain Gap Drive.
Huntsville AL 35803
USA

Ms. Zhi-fang Fang
Inst. of Meteorol
Chengdu Sichuan
PEOPLES REP. OF CHINA

Dr. Tibor Farago[2]
Meteorol. Service
114 PO Box 38
H-1525 Budapest
HUNGARY

Dr T. K. Fernando
Dept. Meteorol.
Bauddhaloka Mawatha
Colombo 7
SRI LANKA

Dr. Eugene A. Fitzpatrick
RMB 'Danellen'
Hume Highway
Moss Vale NSW 2577
AUSTRALIA

Dr. Heribert Fleer
Zentralamt DWD
Postfach 100465
D-6050 Offenbach am Main
FRG

Dr. Klaus Fraedrich
Inst Meteorol Freie Univ. Berlin
Dietrich Schafer Weg 6-8
D-1000 Berlin 41
FRG

Dr. Neil D. Gordon
Meteorol. Service
PO Box 722
Wellington
NEW ZEALAND

Dr. Malcolm G. Grant
Meteorological Service
PO Box 722
Wellington
NEW ZEALAND

Dr. Jan Holst[2]
Dept. Mathematical Stats.
Univ. Lund
Box 118 S-22100 Lund
SWEDEN

Dr. Philipe D. Jones[2]
Climatic Res. Unit
Univ. of East Anglia
Norwich NR4 7TJ
UNITED KINGDOM

Dr. Felix N. Kogan[2]
NOAA NESDIS AISC
1825 Connecticut Ave NW
Washington DC 20235
USA

Dr. O.S.R.U. Bhanu Kumar
Dept. Meteorology
Univ. Nairobi
PO Box 30197 Nairobi
KENYA

Dr. Karl K. Leiker
Dept. Geography
Westfield State College
Westfield MA 01086
USA

Dr. Robert E. Livezey[23]
Natl. Meteorol. Center
Washington DC 20233
USA

Dr. Francis M. Fujioka[3]
Pacific SW Forest Exp. Stn.
4955 Canyon Crest Drive
Riverside CA 92507
USA

Mr. Allister J. Gorman
Inst. Geophys. Victoria Univ.
PO Box 600 Wellington
NEW ZEALAND

Dr. Donald D. Grantham[3]
Geophysics Lab.
Hanscom Airforce Base
MA 01731
USA

Mr J. David Jasper
S&TS Branch Bureau of Met.
PO Box 1289K
Melbourne Vic 3001
AUSTRALIA

Dr. Richard W. Katz[23]
National Center Atmos. Res.
PO Box 3000
Boulder CO 80307
USA

Dr. Elaine H. Koo
Res. & Records Divn.
Royal Observatory
134A Nathan Rd Kowloon
HONG KONG

Dr. Peter J. Lamb[2]
State Water Survey Div.
2204 Griffith Drive
Champaign IL 61820
USA

Dr. Yafang Liu
Inst. of Meteorol.
Nanjing
PEOPLES REP. OF CHINA

Dr. Janice M. Lough
Inst. Marine Science
PMB No. 3 Townsville Qld 4810
AUSTRALIA

Prof. K. Ruben Gabriel[2]
Univ. of Rochester
Rochester NY 14627
USA

Mr. Stephen W. Goulter
Meteorol. Service
PO Box 722 Wellington
NEW ZEALAND

Mr. John S. Hickman
49 Anne St
Wellington
NEW ZEALAND

Prof. Shi Jiuen[3]
Inst. Meteorol.
46 Baishiqiao Rd.
Western Suburb Beijing
CHINA

Dr. John W. Kidson
Meteorol. Service
PO Box 722
Wellington
NEW ZEALAND

Dr. Ramesh H. Kripalani
Inst. Tropical Meteorol.
PO Box 913 Shivajinager
Pune 411 005
INDIA

Prof. M. Ross Leadbetter
Dept. Statistics
Univ. North Carolina
Chapel Hill NC 27599-3260
USA

Dr. You-tang Liu
Area Observatory
Lin Fen
CHINA

Dr. P.K. Love
Inst. of Geophysics RSES
Victoria Univ.
PO Box 600 Wellington
NEW ZEALAND

Dr. Henning Madsen[23]
Meteorol. Inst.
100 Lyngbyvej
DK-2100 Copenhagen
DENMARK

Dr. Henrik Madsen[23]
Inst. Maths. Stats. and OR
Technical University
DK-2800 Lyngby
DENMARK

Dr. James McGregor
Inst. of Geophysics RSES
Victoria Univ.
PO Box 600 Wellington
NEW ZEALAND

Dr. Alistair McKerchar
Hydrology Centre DSIR
P.O.Box 1479
Christchurch
NEW ZEALAND

Dr. Neil D. Mitchell
Botany Dept.
Univ. Auckland
PB Auckland

Dr. Medardo Molina
Flood Plain Mapping Project UNDP
PO Box 280 Kingston
JAMAICA WI

Dr. Edward C. Monahan[2]
Marine Scs Inst.
Univ. Connecticut Avery Point
Groton CO 06340
USA

Prof Allan H. Murphy[123]
Dept. Atmos. Scs.
Oregon State Univ.
Corvallis OR 97331
USA

Prof. Van-Thanh-Van Nguyen
Dept. Civil Eng. McGill Univ
817 Sherbrooke St West
Montreal QC H3A 2K6
CANADA

Dr. Neville Nicholls[2]
BMRC
GPO Box 1289K
Melbourne Vic 3001
AUSTRALIA

Prof. R.E. Nield
Center Agric. Met./Climatology
377N Plant Science Bldg
Univ. Nebraska-Lincoln NE 68583
USA

Prof. Iognaid G. O'Muirheartaigh[2]
Dept. Mathematics
University College
Galway
IRELAND

Prof. Huynh-Ngoc Phien
Div. Computer Sc.
Asian Inst. Technology
PO Box 2754 Bangkok
THAILAND

Dr. V.T. Radiuhin[3]
State Committee Hydromet.
6 Korolev Street
Obninsk Kaluga 249 020
USSR

Dr. B.P. Ratnam
Univ. Agricultural Scs.
Krishinagar Dharwad 580 005
INDIA

Dr. Stephen J. Reid
Meteorological Service
PO Box 722 Wellington
NEW ZEALAND

Mr. Jim Renwick
Meteorol. Service
PO Box 722
Wellington
NEW ZEALAND

Mr Cliff G. Revell
16 Wairere Grove
Paraparaumu
NEW ZEALAND

Dr. K. John A. Revfeim[23]
Meteorol. Service
PO Box 722
Wellington
NEW ZEALAND

Dr. Michael B. Richman[23]
State Water Survey Div.
2204 Griffith Drive
Champaign IL 61820
USA

Dr. Chester F. Ropelewski
Climate Analysis Center W/NMC52
Washington DC 20233
USA

Mr. John Sansom
Meteorol. Service
PO Box 722
Wellington
NEW ZEALAND

Prof. Christian-D Schonwiese[3]
Inst. Met. Geoph. Univ.Frankfurt
Feldbergstrasse 47
D-6000 Frankfurt 1
FRG

Prof. Alastair J. Scott
Dept. Maths & Stats
Univ. Auckland
PB Auckland

Dr. A. Mary Selvam
Inst. Tropical Meteorology
PO Box 913 Shivajinager
Pune 411 005
INDIA

Dr. Boris Sevruk
Federal Inst. Technology
ETH Zentrum
CH-8092 Zurich
SWITZERLAND

Dr. Dennis J. Shea
National Center Atmos. Res.
PO Box 3000
Boulder CO 80307
USA

Dr. Shyam V. Singh[2]
Inst. Tropical Meteorology
PO Box 913 Shivajinager
Pune 411 005
INDIA

Dr. Hans von Storch[2]
Max Planck Inst. fur Meteorol.
Bundestrasse 55
D-2000 Hamburg 13
FRG

Dr. Peter J. Thomson
ISOR
Victoria Univ.
PB Wellington
NEW ZEALAND

Dr. Tai-Houn Tsou
Dept. Statistics
Univ. California
Riverside CA
USA

Dr. Martin A.J. van Montfort[3]
Dept. Maths. Agric. Univ.
De Dreijen 8 POB 8003
NL-6700 EB Wageningen
THE NETHERLANDS

Prof. Bin Wang
Dept. Meteorol. Univ. Hawaii
2525 Correa Road
Honolulu HA 96822
HAWAII

Dr. David Wratt
Meteorol. Service
PO Box 722
Wellington
NEW ZEALAND

Dr. E.E. Zhukovsky
Agrophys. Res. Inst.
Leningrad
USSR

Dr. Raymonde Sneyers[123]
IRMB
3 Ave Circulaire
B-1180 Bruxelles
BELGIUM

Dr. Tim Swartz
Dept. of Statistics
Simon Fraser Univ.
Vancouver BC
CANADA

Dr. Edward Tollerud
Weather Res. Programme
Env. Res. Lab. NOAA
325 Broadway Boulder CO 80303
USA

Dr. Tatsuo Ueno
Forecast Divn. Meteorol. Agency
1-3-4 Oote-machi Chiyoda-ku
Tokyo 100
JAPAN

Dr. Walter M. Vargas[2]
Dept. Meteorol. Ciudad Univ.
Pabellon 2 1428 Nunez
Pcia. Buenos Aires
ARGENTINA

Prof. Peter Whittle
Stats Lab Univ. Cambridge
16 Mill Lane
Cambridge CB2 1SB
UK

Dr. Jin-Song Xu[2]
Max Planck Inst. fur Meteorol.
Bundestrasse 55
D-2000 Hamburg 13
FRG

Dr. Francis W. Zwiers
CCC Atmos. Env. Service
4905 Dufferin Street
Downsview Ontario M3H 5T4
CANADA

Dr. Steven T. Sonka
Dept. Agric. Economics
Univ. Illinois
Urbana IL 61801
USA

Dr. Stephen M. Thompson
Hydrology Centre DSIR
P.O.Box 1479
Christchurch
NEW ZEALAND

Dr. Kevin E. Trenberth
Climate Analysis Section NCAR
PO Box 3000 Boulder CO 80307
USA

Dr. Jelko Urbancic[3]
Hydromet. Inst.
Jamova 39/p.p. 100
YU-61111 Ljubljana
YUGOSLAVIA

Prof. David Vere-Jones
ISOR
Victoria Univ.
PB Wellington
NEW ZEALAND

Dr. Klaus Wolter
CIRES Univ. Colorado
Campus Box 449
Boulder CO 80309-0449
USA

Dr. Xiao-Ping Zhong
Res. Inst. Plateau Meteorol.
Chengdu Sichuan
PEOPLES REPUBLIC CHINA